SYNTHESIS AND CHARACTERIZATION OF POROUS POLYMERS AND METAL-ORGANIC FRAMEWORKS/POLYMER COMPOSITES FOR CARBON CAPTURE

BY

MAHMOUD M. ABDELNABY

A Dissertation Presented to the

DEANSHIP OF GRADUATE STUDIES

KING FAHD UNIVERSITY OF PETROLEUM & MINERALS

DHAHRAN, SAUDI ARABIA

In Partial Fulfillment of the
Requirements for the Degree of

DOCTOR OF PHILOSOPHY

In

CHEMISTRY

DECEMBER 2018

KING FAHD UNIVERSITY OF PETROLEUM & MINERALS

DHAHRAN- 31261, SAUDI ARABIA

DEANSHIP OF GRADUATE STUDIES

This thesis, written by **Mahmoud M. Abdelnaby** under the direction of his thesis advisor and approved by his thesis committee, has been presented and accepted by the Dean of Graduate Studies, in partial fulfillment of the requirements for the degree of **DOCTOR OF PHILOSOPHY IN CHEMISTRY**.

Dr. Omar M. Yaghi

(Advisor)

Dr. Khalid R. Alhooshani

Department Chairman

Dr. Othman C. Al Hamouz
(Co-Advisor)

Dr. Salam A. Zummo
Dean of Graduate Studies

Dr. Bassam M. El-Ali
(Member)

21/1/09

Date

Dr. Anvarhusein A. Isab
(Member)

Dr. Mazen M. Khaled
(Member)

To my parents, dear beloved wife and kids, my brothers

& all my friends who gave me inspiration, encouragement and valuable support

toward the success of this study.

ACKNOWLEDGMENTS

All praise is to ALLAH Almighty who made it possible for me to accomplish this research work successfully.

First, I would like to thank my advisor Professor Omar M. Yaghi for his guidance and support and for giving me the opportunity to work in his group at KFUPM, his encouragement and insights enabled me to build my academic and scientific career. I would like to thank my co-advisor Dr. Othman Al Hamouz for his guidance and patience during the thesis work. Dr. Othman's patience and support enabled me to achieve wonderful results and to overcome the problems along the way.

I would also like to thank all the committee members Dr. Bassam Al-Ali, Dr. Isab A., Dr. Mazen Khaled for their interest and valuable suggestions and support for this work. I would also like to express my gratitude to Dr. Zain Yamani for his continuous support by using CENT labs and facilities from the first day I joined KFUPM. Also, I would like to thank all the faculty members of the Chemistry Department. To all of them, I appreciate what they have done to help me in my scholastic and professional growth.

I would also like to thank Mr. Kyle E. Cordova for his heroic efforts with me and continuous support during this research. I acknowledge my friend Ahmad Alloush, Dr. Bassem Almythalony and Dr. Naef Qasem for their cooperation. Thanks to my research Yaghi team members: Dr. Aasif Helal, Dr. M. Usman, Dr. H. Nguyen, Mr. Mostafa Zeama, and Mr. Abduhadi Al-Zahrani. I am deeply grateful to those I have not mentioned above and whose best wishes have always encouraged me, in no order: Dr. M. Abdrubuhseen, Dr. A Attia, Dr. Ahmed Nada, Dr. Husein Attia and Dr. M. Ali Hassan. Finally, my heartfelt gratitude is extended to my family who always supported me throughout my whole life.

TABLE OF CONTENTS

LIST OF TABLES

LIST OF FIGURES

LIST OF ABBREVIATIONS

DMF	:	*N*,*N*-dimethylformamide
HCl	:	Hydrochloric acid
$FeCl_3$	:	Anhydrous ferric chloride
CuCl	:	Copper (I) chloride
CO_2	:	Carbon dioxide
H_2S	:	Hydrogen sulphide
Q_{st}	:	Enthalpy of Adsorption
BT	:	Breakthrough
DA	:	1,4-benzenediamine
Phz	:	Phenothiazine
Py	:	Pyrrole
MPy	:	Melamine-Pyrrole copolymer
TriPy	:	1,3,5-triaminobenzene-Pyrrole copolymer
TMTPy	:	2,4,6-Trimethyl-1,3,5-triaminobenzene-pyrrole copolymer

ABSTRACT

Full Name : [Mahmoud Mohamed Abdelnaby]

Thesis Title : [SYNTHESIS AND CHARACTERIZATION OF POROUS POLYMERS AND METAL-ORGANIC FRAMEWORKS/POLYMER COMPOSITES FOR CARBON CAPTURE]

Major Field : [Chemistry]

Date of Degree : [December 2018]

The aim of this work firstly, the synthesis and characterization of Metal Organic Frameworks (MOFs) with open metal sites (MOF-74 analogs) then test the synthesized MOF for selective CO_2 capture. second main part is the design, synthesis and characterization of a novel class of hypercrosslinked porous polymers with excellent physiochemical properties via one step polycondensation reaction to produce efficient, selective and chemically stable porous polymer networks for the capture of carbon dioxide in presence of water. These polymers were then characterized by ^{13}C-NMR, FTIR, and CHN elemental analysis for structure elucidation and powder XRD was used for determination of amorphous nature of the materials. Thermal properties were investigated using thermal gravimetric analysis. The polymer networks will go through different reaction conditions in order to achieve best textural features that will consist of the high surface area, microporosity, and high adsorption capacity of carbon dioxide with high CO_2 selectivity compared to methane and nitrogen. The different functionalities ($-NH_2$, -NH-, and -S-) present in the polymer backbone are expected to contribute to the efficacy of the

adsorption process. The rigid aromatic-heteroaromatic functionalized repeating units linked with methylene units should provide the textural features, a high surface area with amine adsorption sites specific for carbon dioxide. Once synthesized and characterized, the porous polymeric networks were evaluated for their efficacy in the selective adsorption of carbon dioxide. Furthermore, Dynamic breakthrough measurements were then performed, in which the synthesized new copolymers were demonstrated capable of separating CO_2 from both dry and wet (91% relative humidity) gas mixtures – mixtures whose composition mimicked those found in a flue gas stream. Finally, the outcome of the work is evaluated by a comparison of the related organic polymers reported before to identify the efficiency of the synthesized polymers in this study.

ملخص الرسالة

الاسم الكامل: محمود محمد محمد عبد النبي

عنوان الرسالة: تحضير وتوصيف بوليمرات و خليط البوليميرات و الأطر المعدنية العضوية لاحتجاز غاز ثاني أكسيد الكربون

التخصص: : كيمياء

تاريخ الدرجة العلمية: ديسمبر 2018

تهدف هذه الدراسه الي تحضير و توصيف أولا أطر معدنيع عضويه ذان معادن بها اوربتال فارع و تطبيق هذة المواد واختبارها لمتصاص و تخزين غاز ثاني أكسيد الكربون. الاجزء الاخر في هذه الدراسه يهدف الي تحضير مجموعة بوليميرات جديدة ذات كثافه عاليه من النيتروجين القلوي المعروف بقابليته علي زياده اختيارية المواد لمنصاص و فصل غاز ثاني أكسيد الكربون. ثم توصيف هذه المواد بطرق مختلفة لتوضيح طبيعة وكيفية ارتباط الوحدات المكونة لهذه البوليمرات بعضها ببعض حيث تم استخدام جهاز الرنين المغناطيسي النووي والأشعة تحت الحمراء وتحليل العناصر الأساسية. وتم أيضاً دراسة الصفات الحرارية للبوليمرات عن طريق جهاز التحليل الوزني الحراري. بعد الانتهاء من توصيف المواد بالأجهزة المذكورة وغيرها تم اختبار قدرة المواد على امتصاص غاز ثاني أكسيد الكربون بالإضافة إلى غازات أخرى وهي الميثان والنيتروجين. و لقياس قدرة المادة على الامتصاص الاختياري لغاز ثاني أكسيد الكربون من الخليط الذي يحتوي علي النيتروجين و بخار الماء (الطبقا للظروف المماثلة في الصناعه) تم اختبار البوليميرات الجديده للفصل الحركي لغاز ثاني أكسيد الكربون من هذا الخليط باستخدام تقنية البريك ثروbreakthrough measurements. في النهاية تم مقارنة النتائج مع مواد أخرى تم نشرها في أعمال بحثية مختلفة لتقييم قدرة المواد التي تم تحضيرها في هذا العمل. و اظهرت هذة المقارنه أن المواد المحضره في هذة الدراسه تتفوق علي معظم المواد العضويه التي تم نشرها في هذا المجال

CHAPTER ONE

INTRODUCTION

1.1 Carbon Dioxide Capture: A Global Challenge

Carbon dioxide has attracted a great deal of scientific interest owing to its contribution as a greenhouse gas and its profound impact on global climate change[1,2]. It is noted that global warming, due to the emissions of greenhouse gases, is considered to be the most important environmental problem currently facing the world. With that, approximately 35 billion tons of CO_2 are generated from the combustion of fossil fuels (source of energy), which has led to an increase, since 2010, in the atmospheric CO_2 concentration to levels exceeding 390 ppm and these emissions are expected to rise further for the next several decades. The effect of greenhouse gases on climate change is assessed by the International Panel on Climate Change (IPCC)[3]. Based on the IPPC 2007 report, a rise in the average global temperature is expected from 1.8 to 6.4 ℃ by the end of 21^{st} century. Therefore, halting, or even slowing, the emissions of CO_2 requires an urgent practical solution in order to address this environmental issue[4,5].

1.1.1 Carbon Capture Materials and Technologies

Carbon capture and sequestration (CCS) is an effective method for reducing CO_2 emissions into the atmosphere. CCS deals with two main processes pre-combustion of CO_2 from fuel gas and gasification of the coal prior to combustion producing high-pressure flue gas and post-combustion from flue gas in which removing CO_2 produced from the combustion of fuel gas. The materials used for capturing CO_2 from post-combustion processes must fit

the requirements for their general conditions which are a total pressure of 1 bar; and gas stream containing a mixture of N_2 (70-75%), CO_2 (15-16%) and H_2O (5-7%) by volume[6].

Table 1 Typical Post-Combustion Flue Gas Composition for a Coal-Fired Power Plant

molecule	concentration (by volume)
N_2	73-77%
CO_2	15-16%
H_2O	5-7%
O_2	3- 4%
SO_2	800 ppm
NO_x	500 ppm
Others	10-100 ppm

The oldest and most widely employed technology makes use of liquid amines for industrial CO_2 capture from post-combustion gases and is based almost exclusively on commercially available monoethanolamine (MEA) solutions[7]. The MEA is usually dissolved in water in a concentration of 20-30 wt% and the capturing technology works by chemisorption, in which CO_2 reacts with the alkyl amine functional group to form carbamates through a Zwitterion mechanism (Scheme 1)[5]. Although selective, these solutions have several outstanding drawbacks: (i) the total working capacity is between 2.1 and 5.5 wt%, based on a 30 wt% MEA solution, which is low compared to many solid sorbents[5,8]; (ii) a high energy process is required for regeneration of these solutions, which is attributed to the solutions' high heat capacity; (iii) the corrosive nature of the solutions requires costly engineering designs; and (iv) volatility problems are inherent to the MEA solutions[8].

Therefore, it is essential to study and develop new materials/technology for use in overcoming these challenges.

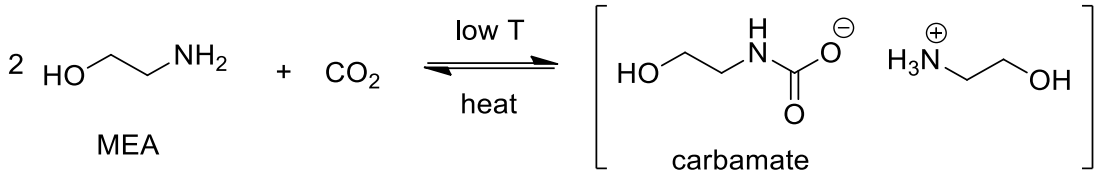

Scheme 1 General reaction schemes for the chemical adsorption (chemisorption) of CO_2 by primary and secondary amines.

Synthesis of solid porous materials that can separate CO_2 from flue gas is particularly important for post-combustion CO_2 capture. To capture post-combustion CO_2, the material used must fit the requirements for this condition which is a total pressure of 1 bar; gas streams contain a mixture of N_2 (70-75%), CO_2 (15-16%), and H_2O (5-7%) by volume. CCS using solid sorbents has attracted great attention from both academic and industrial fields in the last decade. Compared to the aqueous amine solutions, these solid adsorbents usually require a lower cost for regeneration because of the CO_2 adsorption is mainly physical adsorption, lower pressure for gas recovery, and less energy for regeneration in addition to being environmentally friendly. A variety of porous materials were successfully synthesized such as zeolites[9], porous organic polymers (POPs)[10–12], MOFs[13], [14] and mesoporous silica modified by different functional groups[15,16].

In order to deem a solid sorbent material viable for carbon capture, *seven criteria must be considered*[17]*:* (i) relatively high CO_2 adsorption capacity. Since CO_2 represents 15-16% *v*/*v* concentration of a flue gas stream, adsorption capacity must be relatively high at low partial pressures (<0.2 bar) [18,19]; (ii) high selectivity toward CO_2. Selectivity governs the purity of the CO_2 obtained, which plays a critical role in the economics of the process[17,19]; (iii) fast adsorption kinetics. The adsorption kinetics are sufficiently fast to

realize practical implementation. This means that the equilibrium capacity, obtained from thermodynamic isotherms, is similar to the working capacity found in dynamic adsorption[20]; (iv) mild regeneration conditions. The majority of the energy penalty in current post-combustion capture technologies lies in the fact that a substantial energy input is required to regenerate the adsorbent material[21]; (v) long-term stability over the course of extensive use. The material must retain its performance over many adsorption-desorption cycles; (vi) tolerance to other components in a flue gas stream, including and most importantly, water. The majority of conventional porous adsorbent materials (*e.g.* zeolites and porous carbon) suffer from water poisoning. Materials based on reticular chemistry (*i.e.* metal-organic frameworks) have only recently demonstrated their effectiveness in mitigating contaminants, such as water, in flue gas streams[22,23]; and, finally, (vii) low production cost.

Given these criteria, the development of a new porous adsorbent material represents a target worth pursuing. Accordingly, we turned our attention to porous organic polymers, which are viewed as strong candidates to replace current technologies due to their demonstrable high and selective CO_2 uptake in conjunction with their structural diversity and exceptional physicochemical stabilities[24]. A variety of porous organic polymers have been explored[11,25,26] and several of these materials standout as particularly noteworthy in the context of the aforementioned seven criteria[27–29]; however, there have only been few notable reports, in which such materials were shown to have met most of these criteria.

1.2 Literature Review of materials for CO_2 Capture.

A variety of porous materials were successfully synthesized such as zeolites[9], porous organic polymers (POPs)[10–12], MOFs[13,14], and mesoporous silica modified by different functional groups[15,16].

1.2.1 Metal-Organic Frameworks: Designable Materials with Practical Limitations

MOFs have received great interest as solid porous materials due to their high surface areas, tunable pore sizes, exceptional thermal stability, robustness, and crystal structures. Due to the high surface area of the most MOFs, they show excellent capability of gas storage and application technology[30]. These porous crystalline solids are constructed from organic building blocks that coordinates to metal nodes forming one or two- or three-dimensional extended networks. The nodes consist of one or more metal ions or cluster of ions (e.g. Zn^{2+}, Co^{2+},Ni^{2+} Al^{3+}, and others) bonded to the organic linkers through terminal functional groups mainly carboxylates (Figure 1). The systematic long-range order of the structures is a key characteristic of the MOFs system over other porous materials (e.g. polymers, mesoporous silica and porous carbons, etc.). Their synthetic methods, properties and applications have been reported in several reviews[13,62–67].

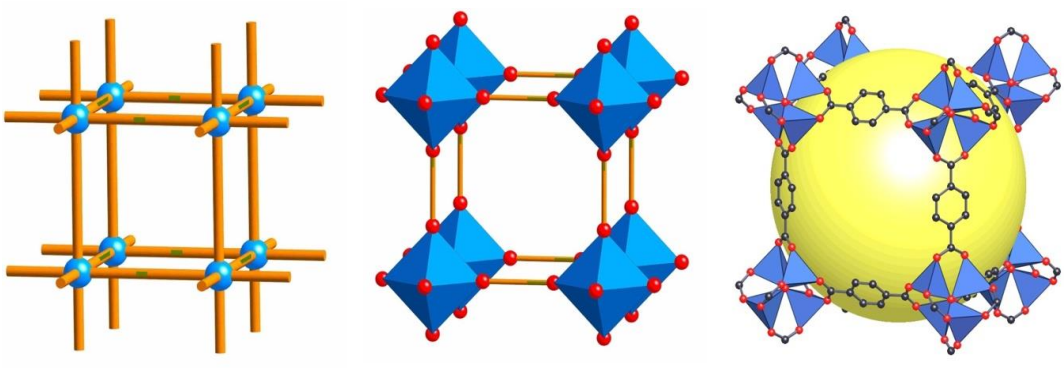

Figure 1 The right figure structure representation of MOF-5 as a prototype structure represented ZnO4 polyhedral blue clusters joined by ditopic 1,4-benzene dicarboxylic acid as organic linkers (O, red and C, black) to form 3D cubic extended structure with large pore (yellow sphere- pore space filling without including the van der Waals size of the structure). The figure in the left shows the topology of the structure shown as a ball-and-stick model, and the one in the middle represent the tetrahedral Metal topology with rode linkers[31].

Great achievements have been done in the field of MOF-based CO_2 capture during the last decads[14,37–40]. The design and structure of the MOFs, some unique properties of the MOFs is considered the key points to be effective for CO_2 capture. From the synthetic point of view after activation of the MOF by heating or purging with gas, the occluded solvent molecules are removed from the pore to yield accessible pores with active sites for CO_2 molecules. Another advantage of MOFs compared to other porous solids is the tenability of the pore wall modification of polar functional groups present on the aromatic linker, maintaining the whole framework connectivity[41].

Another alternative strategy for synthesizing MOF for gas adsorption application is generation the MOF with unsaturated open metal active site within the pores, such sites can facilitate the selective adsorption for specific gas molecule, for instance Mg-MOF-74 [Mg_2(DOT); DOT: 2,5-dioxidoterephthalate], in which CO_2 capture and selectivity is enhanced by removing the terminal coordinated solvent molecules leaving a metal center coordinately unsaturated and available to bind with CO_2.[42] Mg-MOF-74, an example,

consists of one-dimensional hexagonal channels with five magnesium(II) ions coordinated decorate the edges of each channel (Figure 2). CO_2 uptake of Mg-MOF-74 was found to be 23.6 wt% at 0.15 bar (the partial pressure of CO_2) and 296K and 35.2 wt% CO_2 at 1 bar and 296K. Although Mg-MOF-74 exhibits the greatest CO_2 capacities at 0.15 bar of all reported MOFs[42], but unfortunately, after exposition of relative humidity of 70% this high CO_2 uptake is decrease sharply at low pressure to 16% of its original uptake this is due to the strong binding of the water with the unsaturated metal active site, that will prohibit the application of this MOF under humid conditions this drawback obstacle its industrial application[43].

1.2.2 Covalent Organic Frameworks (COFs)

Covalent organic frameworks (COFs) are crystalline highly order organic networks firstly discovered by the Yaghi group. These materials are constructed from precisely defined and covalently linked organic moieties. The pore sizes and the surface area of COFs can be tuned by varying the linker length to form two-dimension or three-dimension networks[44]. COF exhibit good ability to capture CO_2 (COF-1: 51.9 $cm^3 g^{-1}$, COF-5: 29.9 $cm^3 g^{-1}$, COF-8: 32.0 $cm^3 g^{-1}$, and COF-10: 27.0 $cm^3 g^{-1}$)[45]. As these COFs have the same functionality, its clearly noticed that the CO_2 uptakes do not correlate with the surface area but correspond to their pore size with smaller pores having higher affinity to CO_2.

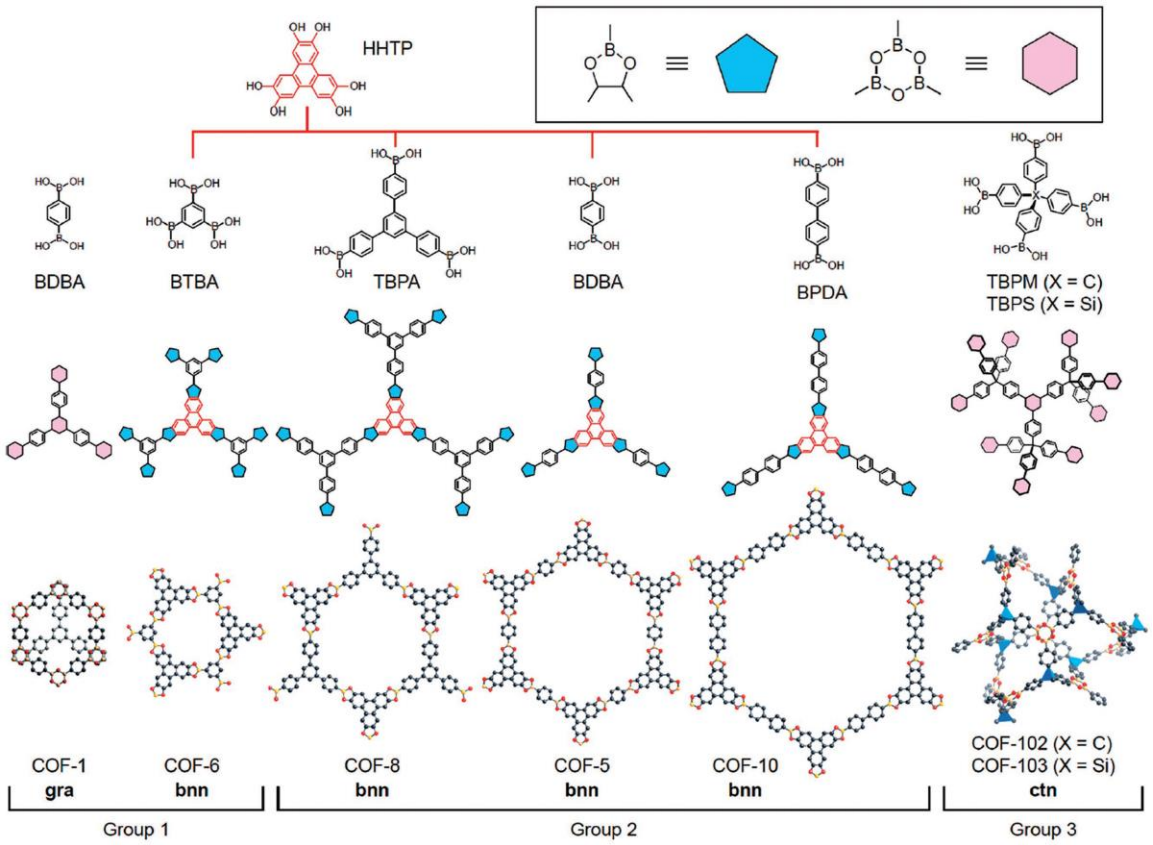

Figure 2 A representative structure of some COFs with their controlled Pore size. (Figure from: Adv. Mater., Feb. 2016)[46].

Functionalization of 2D COF channel-walls was developed as an effective strategy to convert the low porosity COFs into an exceptional platform for CO_2 capture (Figure 3)[47]. Post-synthetic functionalization channel walls of $[HO]_{100\%}$-H_2P-COF with carboxylic acid groups triggered a dipole interaction with CO_2. Therefore, the CO_2 capacity increased from 15.7 $cm^3 g^{-1}$ for $[HO]_{100\%}$-H_2P-COF to 38.7 $cm^3 g^{-1}$ for $[HO_2C]_{100\%}$-H_2P-COF at 298 K and 1 bar.

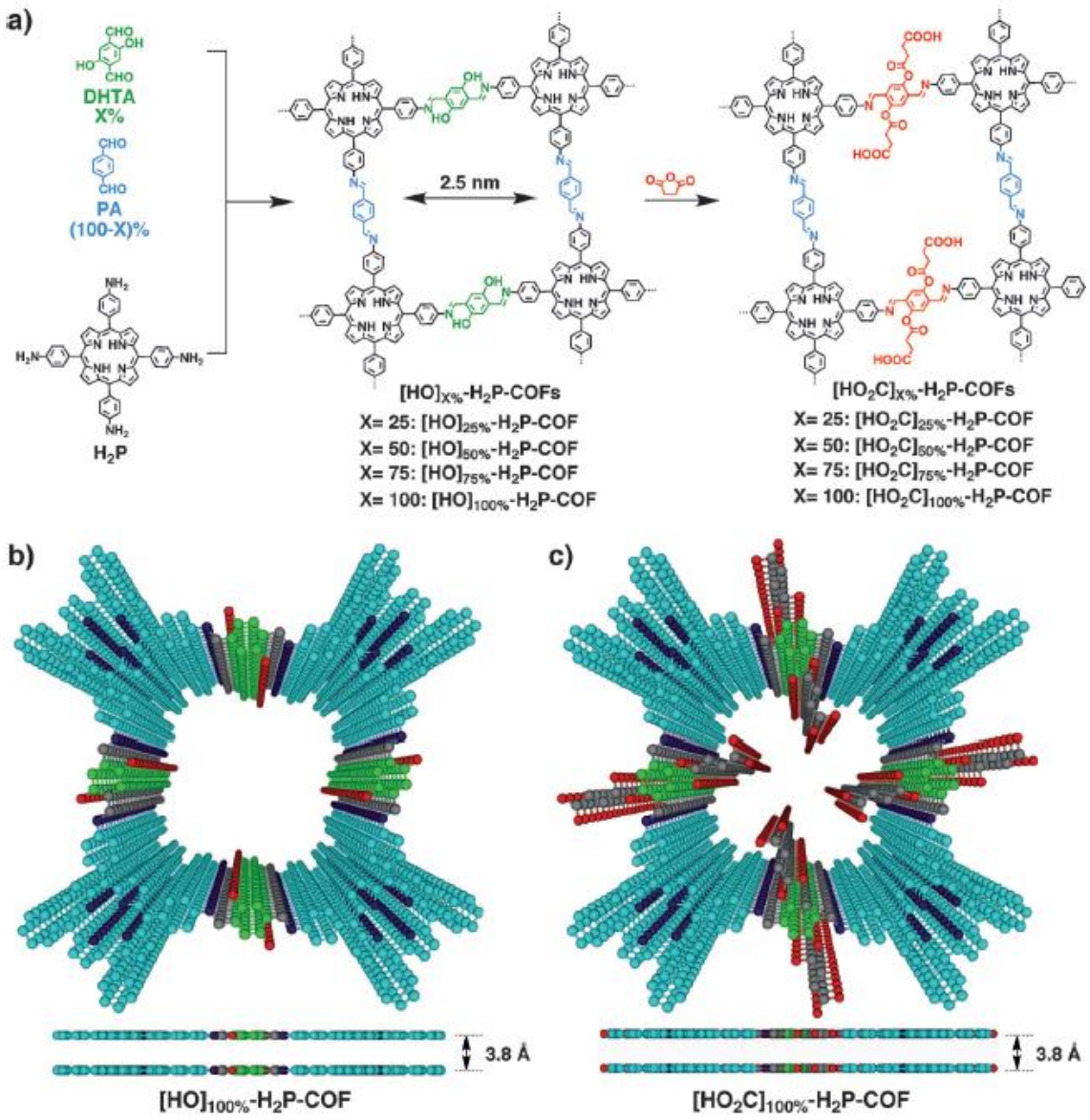

Figure 3 a) Synthesis of $[HO_2C]_{X\%}$-H_2P-COFs with channel walls functionalized with carboxylic acid groups through the ring opening reaction of $[OH]_{X\%}$-H_2P-COFs with succinic anhydride. Top views of b) $[HO]_{100\%}$-H_2P-COF and c) $[HO_2C]_{100\%}$-H_2P-COF (Figure from: *Angew. Chem. Int. Ed.*, *54*, 2986–90, 2015.)[47].

Porous organic polymer (POPs)[10,48,49] are regarded as promising candidates for selective CO_2 capture, due to their high uptake and selective CO_2 capture in combination with their good water and chemical stability, and synthetic diversity alongside the presence of multifunctional active groups[25,50,51]. A wide range of porous organic networks had been explored in the last few decades including covalent organic frameworks

(COFs)[45,46,52], hyper-crosslinked polymers (HCPs)[53–55], crystalline triazine frameworks (CTFs)[26,56], porous aromatic frameworks (PAFs)[57], and conjugated microporous polymers (CMPs)[48].

1.2.3 Covalent Triazine Frameworks (CTFs

Covalent triazine frameworks (CTFs) are another class of ordered porous organic polymers, discovered by the Thomas group in 2008[58]. Their bonding connectivity is based on the triazine ring formation, which is constructed from the acid-catalyzed condensation of aromatic nitriles (Scheme 2). Recently, the incorporation of fluorine groups in the CTFs' structure was reported to play a significant role in the enhancement of the CO_2 capture and separation (Scheme 3)[28]. The strongly polar C-F bonds enhance the CO_2 adsorption due to increased electrostatic interaction. FCTF-1 exhibited a CO_2 uptake of 39.4 $cm^3 g^{-1}$ at 273 K and 0.1 bar with a high CO_2/N_2 selectivity of 77 under kinetic flow condition (31 calculated from single isotherms). Furthermore, FCTF-1 retained its capacities in presence of moisture.

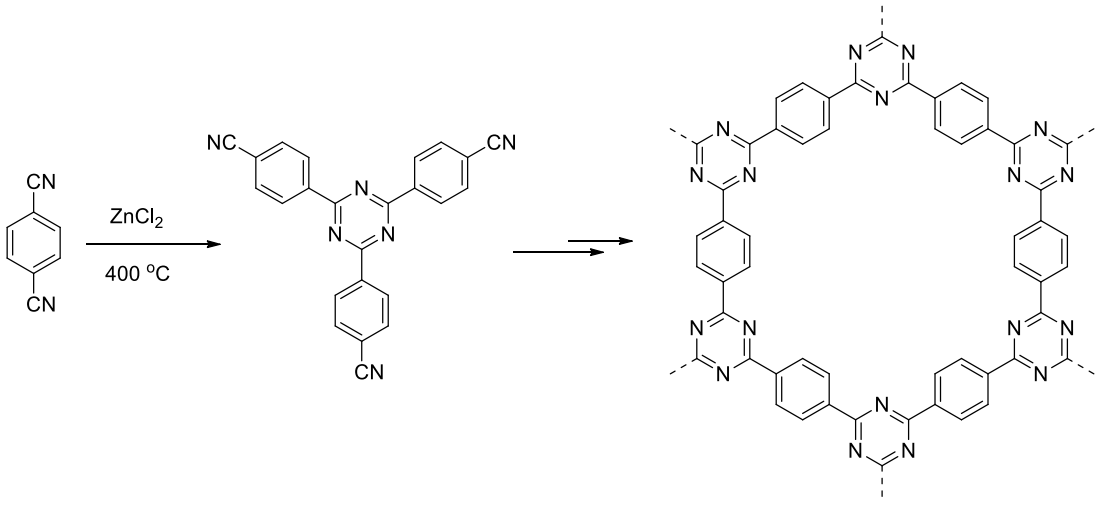

Scheme 2 Reaction scheme and structure of Covalent triazine frameworks (CTFs) synthesized using Lewis acid catalyst at elevated temperature.

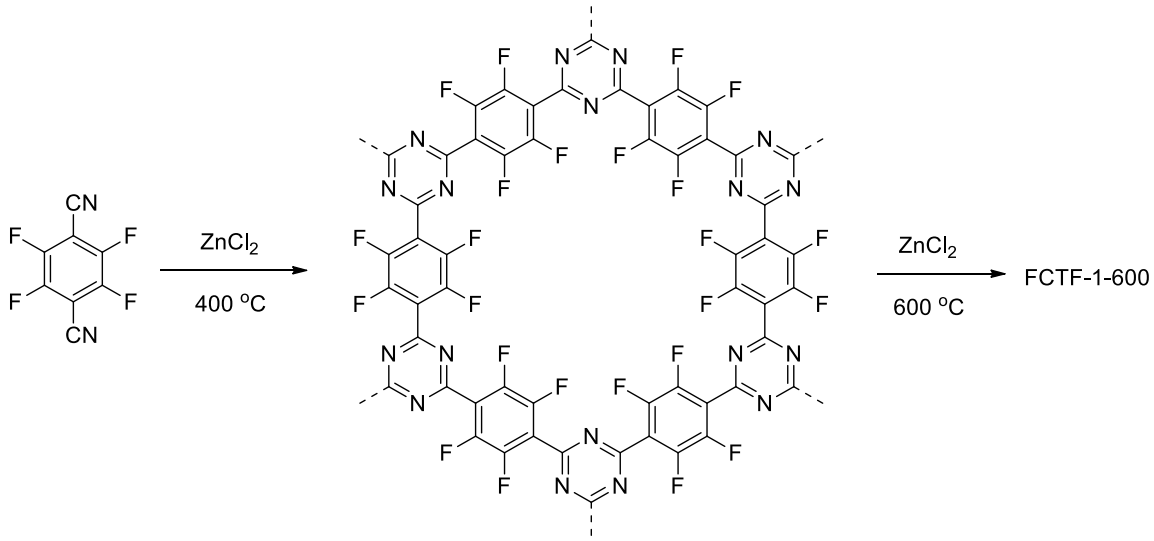

Scheme 3 Reaction scheme for the synthesis and structure of FCTF-1.

1.2.4 Hypercrosslinked polymers (HCPs)

Hypercrosslinked polymers (HCPs), among the above-mentioned networks, are not novel porous organic polymers, but they have showed rapid development in the last decade. They are robust microporous organic networks synthesized mainly by Friedel-Crafts chemistry using methylene linkages to link aromatic moieties in a nonpolar solvent (mainly dichloroethane) producing rigid highly crosslinked networks with permanent porosity[55,59,60], $FeCl_3$ was used extensively as a catalyst for HCPs synthesis with an equimolar ratio to the linker (Scheme 4).

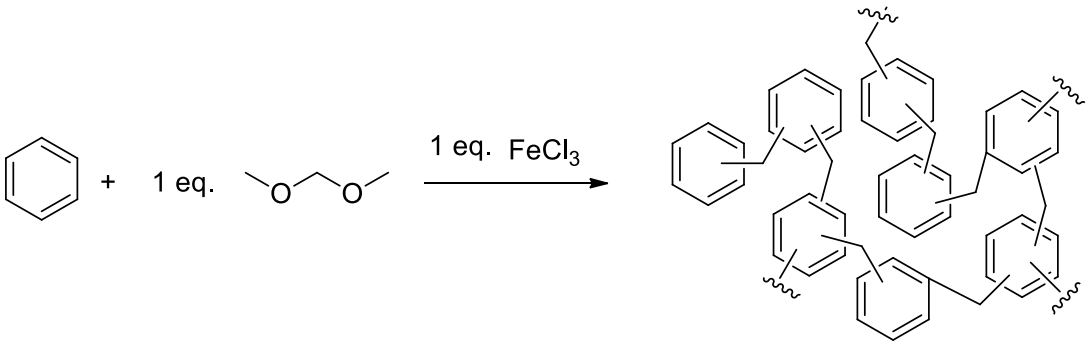

Scheme 4 General synthesis strategy for the synthesis of benzene HCPs.

Self-condensation polymerization. Self-polymerization of simple functional monomers has been carried out to produce porous crosslinked polymers. Crosslinking of polystyrene chains in a strong solvating media have been used to synthesis hyper-crosslinked polystyrene networks, but unfortunately, the resulting surface area was low[61]. Further investigation for done by Cooper group in order to achieve more rigid Hypercrosslinked porous structures, based on one-pot condensation of bis(chloromethyl) aromatic building blocks including 1,4-bis(chloromethyl)benzene compound, 4,4'-bis(chloromethyl)-1,1'-biphenyl and 9,10-bis(chloromethyl)anthracene (1:1:1) (Figure 4).

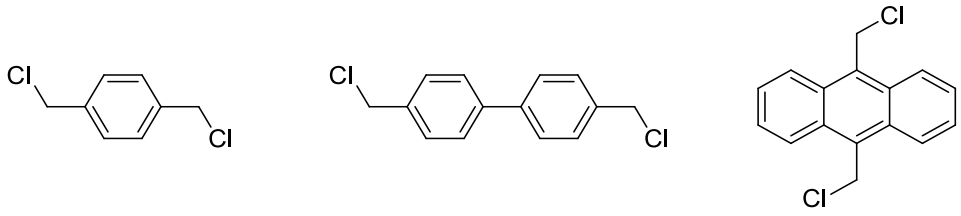

Figure 4 Functional monomers used for the self-polycondensation synthesis of HCPs.

External crosslinking. A versatile strategy using an external linking agent for preparing hyper-crosslinked polymers from a broad variety of available aromatic building blocks has been explored in the literature[55]. Formaldehyde dimethyl acetal (FDA) was extensively used as an external crosslinker to harvest simple aromatic compounds with rigid methylene linkage via Friedel‑Crafts reaction. The proposed mechanism for this reaction was based on the formation of carbocation intermediates as a result of complexing the methoxymethyl group with a Lewis acid catalyst and weakening the methoxy group from the central carbon of the linker. As the reaction proceeds, a large number of carbocation intermediates attack the aromatic ring to add multi-methoxy methyl groups that further react with another aromatic ring producing methanol as byproduct (Scheme 5).

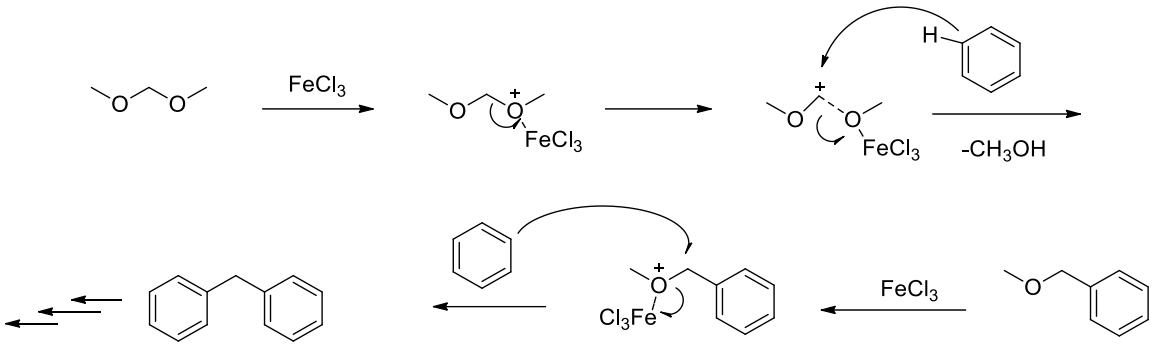

Scheme 5 Proposed mechanism of HCPs formation using external crosslinker and Friedel-Crafts catalyst.

Several aromatic moieties are used as building blocks for knitting hyper-crosslinked polymers with permanent microporosity and high surface areas, such as benzene, biphenyl, methylbenzene, poly-benzene, and other fused benzene rings. Moreover, the functionality of the polymer networks can be tuned by using aromatic building units with different functional groups (Table 2). Due to the resulting high surface areas and microporous nature of the resulting hyper-crosslinked polymers, the CO_2 adsorption properties were investigated and proved the capability of such materials as a suitable candidate for CO_2 capture and separation.

Table 2 Some selected aromatic monomers used for the synthesis porous HCPs with their surface areas and CO_2 adsorption capacities of the resulting polymer networks.

Aromatic monomer unit	Surface area (m^2 g^{-1})	CO_2 capacity (cm^3 g^{-1})[a]	Reference
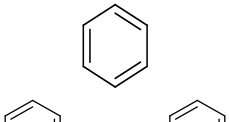	1391	68.7	[62]
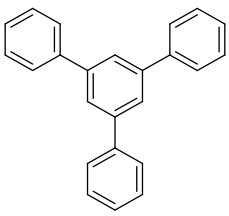	1059	103.8[b]	[62]
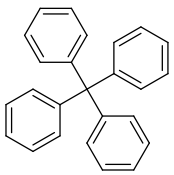	1470	66.4	[10]

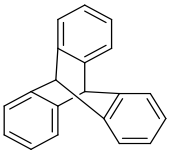	1426	79.9	[63]
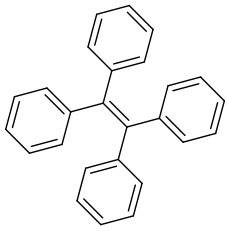	1980	81.4	[64]
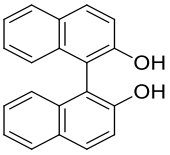	1015	88.6	[59]
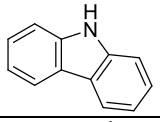	563	67.2	[65]

[a]at 273 K and 1 bar, [b]at 273 K and 1.13 bar.

Introducing amine functionalities within HCP frameworks has been used for the design and synthesis of HCPs for selective CO_2 capture application. For instance, the CO_2 selectivity of hyper-crosslinked benzene networks was significantly increased by incorporation of aniline as a monomer, but led to a sharp decrease in the surface area of the final copolymer[66].

Aniline formaldehyde condensates were reported with coated silica gel for metal removal applications, specifically, removal of hexavalent chromium[67]. The synthesis of this condensate was performed in acidic conditions using concentrated hydrochloric acid at high temperature up to 100 ^{o}C[68]. The synthesized crosslinked polyaniline polymer was obtained via two-step reaction, firstly, polycondensation of aniline with paraformaldehyde and then the product was crosslinked with new aniline monomers via the free amine groups.

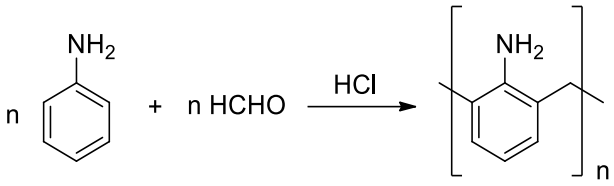

Figure 5 Polycondensation of aniline with paraformaldehyde.

Fabrication of new polymeric networks from two simple monomers; 2,4,6-tris(chloromethyl)mesitylene and ethylenediamine, through the direct and simple nucleophilic substitution reaction under mild conditions in a *catalyst-free reaction* has been reported (Scheme 6)[69]. The reaction was carried out in three different solvents, tetrahydrofuran, 1,4-dioxane, and ethyl acetate and the produced polymers were found to be of good efficiency for CO_2 capture and demonstrated high selectivity over both N_2 and CH_4 gases with uptake capacities of 57.6 mg g^{-1} (5.52 wt%). A porous polymer synthesized from divinylbenzene and 4-vinyl benzyl chloride was synthesized using free radical polymerization (Scheme 7), upon chemical modification by ethylenediamine, diethylenetriamine, triethlenetetramine, and tetraethylenepentamine resulted in significant uptake capacities of 1.49, 1.86, 1.86 and 1.82 mmol g^{-1} (6.27, 7.84, 7.84, 7.67 wt%) respectively at 1 bar and 273 K.

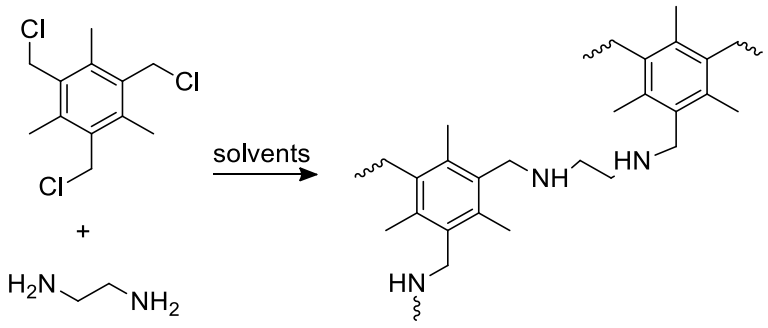

Scheme 6. Fabrication of polymeric networks out of two simple monomers; 2,4,6-tris(chloromethyl)mesitylene and ethylenediamine

Polyethyleneimine (PEI) - Impregnated divinylbenzene and 4-vinyl benzyl chloride with 36% PEI achieved a CO_2 capacity of 7.1 wt% (1.7 mmol g^{-1}) at 0.15 bar under dry CO_2 capture[70]. Although the CO_2 adsorption decreases significantly with increased temperature, the CO_2/N_2 selectivity of the polymers was enhanced at higher temperatures. The polymers showed fast CO_2 adsorption and the sorption equilibrium (10 wt%) was recorded during 5 min at 313 K for the simulated gas mixture streams.

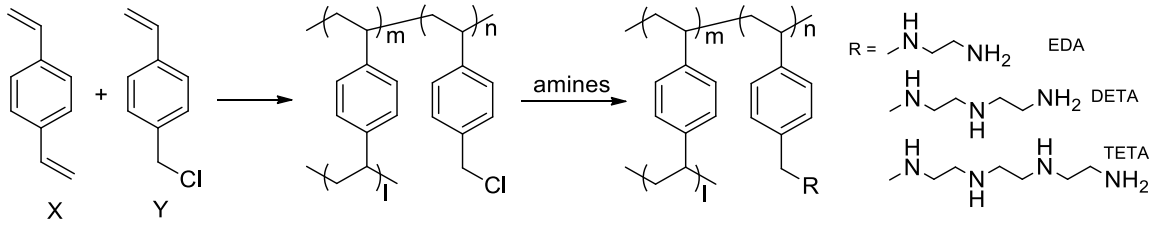

Scheme 7 Porous polymer synthesized from divinylbenzene and 4-vinyl benzyl chloride and its functionalization with aliphatic amine for CO_2 capture.

Recently hyper-crosslinked polymers constructed from the heteroaromatic monomers: pyrrole, thiophene, and furan were synthesized with formaldehyde dimethyl acetal (FDA) as a cross-linker using Friedel-Crafts alkylation (Scheme 8)[53]. This report demonstrated an easy synthetic route for the synthesis of heterocyclic microporous polymers with BET surface areas of up to 720 m^2 g^{-1}. These polymers showed a satisfactory CO_2 capacity of 12.7, 11.9, and 9.7 wt% of CO_2 near 1 bar. The polymers have high CO_2/N_2 selectivity especially for the pyrrole (Py-1) 117:1 using the initial slope selectivity method.

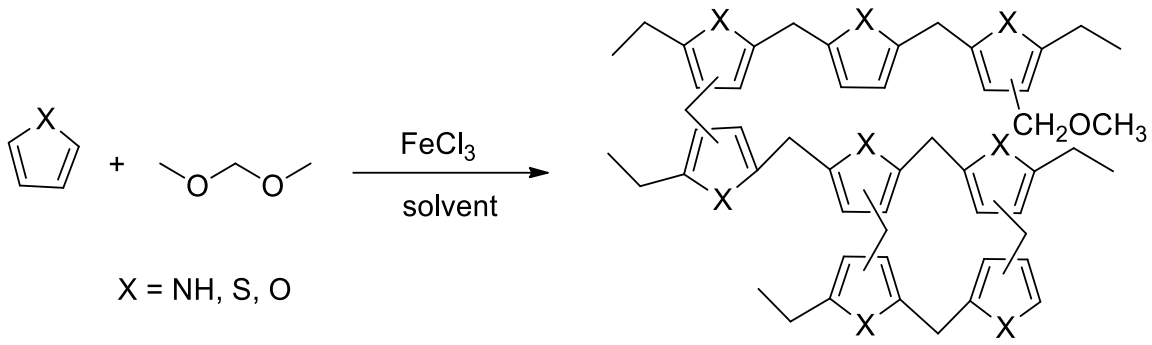

Scheme 8 Hypercrosslinked polymers of the heteroaromatic monomers.

The above-synthesized materials showing good CO_2 uptake correlates with the special characteristics of CO_2 gas such as the large quadrupole moment of the CO_2 molecule (2.85). This means that it can be used to design new CO_2-philic porous materials with amino groups to create significant adsorptive sites with high selectivity[48,70].

Objectives

- Synthesis and characterization of M-MOF-74 analogs from modified linker.
- Synthesis and characterization of novel class of hyper cross-linked porous polymers via one step polycondensation reaction. Figure 6 shows the aromatic-heteroaromatic monomers used to design new porous polymers with amine functionality decorating the porous networks.

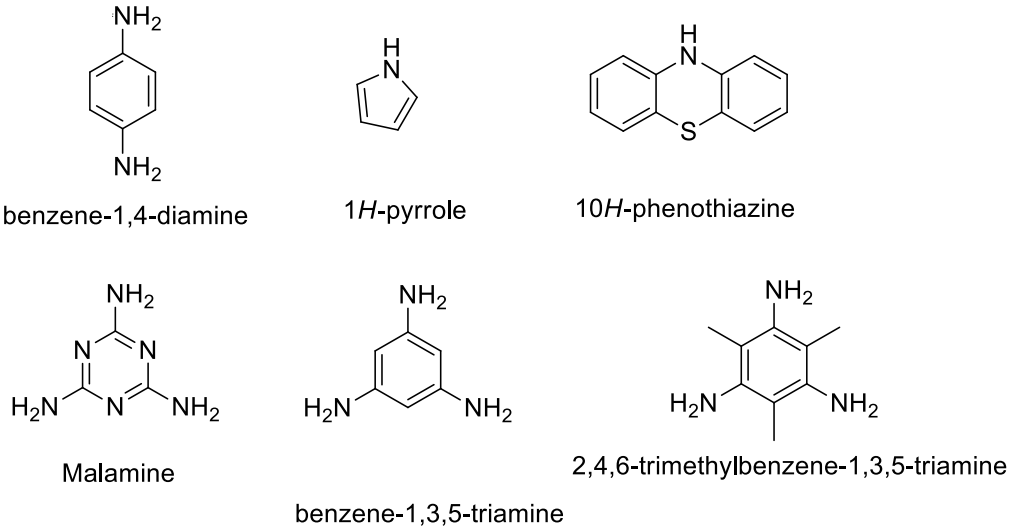

Figure 6 Monomers selected for designing new amine-based copolymers in this work.

- Investigate the CO_2 capture properties of synthesized porous materials through the single gas adsorption measurements and the estimated coverage dependent heat of enthalpy (Q_{st}) and its relationship with the amine functionality with the polymer networks.
- Discuss the role of nitrogen functionalities and pore size in the adsorption of the CO_2 in the synthesized porous polymers.
- Investigate the dynamic separation of CO_2 from gas mixture in dry and wet condition for the synthesized porous materials.

1.3 Carbon Dioxide Evaluation and Measurements

1.3.1 Coverage Dependent Enthalpy of Adsorption (Q_{st}) and Gas Selectivity Calculations

The Q_{st} estimates the enthalpy of specific gas molecules upon adsorption to an adsorbent material. This property is intrinsic for a material and independent of the temperature. A virial-type expression comprising temperature independent parameters a_i and b_j was used in order to establish relationships between two different single component isotherms of CO_2 gas at two different temperatures (273 K and 298 K). The virial-type equation used is [72]:

$$\mathrm{Ln}(p) = \ln(v) + \frac{1}{T}\sum_{i=0}^{m}(a_i\, v_i) + \sum_{i=0}^{n}(b_i\, v_i) \qquad (1.1)$$

where P is pressure (Pa), υ is the adsorbed amount (mol g^{-1}), a_i and b_j are the virial coefficient, T is temperature, and m and n represent the number of coefficients required to describe the isotherms, the iteration will be applied until reaching the minimum values of these constants.

- Isosteric Heat of Adsorption equation*:*

$$Qst(v) = -R\sum_{i=0}^{m}(aivi) \qquad (1.2)$$

- Henry's Law equation:

$$Q_o = -Ra_o \qquad (1.3)$$

where Q_o Isosteric Heat of Adsorption at zero coverage.

Henry's Law Selectivity

The selectivity of the sorbent material toward a specific gas (CO_2 or CH_4) is estimated using Henry's model since it describes the gas adsorption on a solid as a linear relation. The Henry's isotherm equation is [73]:

$$q = KP \qquad (1.4)$$

where q is the adsorbed amount of gas per unit weight of the material (cc g^{-1}), P is the adsorbate gas pressure (torr), and k is the Henry's law constant (cc g^{-1} $torr^{-1}$).

$$K = e^{(-b0)} . e^{(-a0/T)} \qquad (1.5)$$

IAST Selectivity

The Ideal Adsorbed Solution Theory (IAST) is used to calculate the composition of the adsorbed phase from pure component isotherms and predicting the selectivity of the binary mixture CO_2/N_2. IAST assumes an ideal behavior to represent the relationship between the bulk gas phase and adsorbed phase as:

$$y_i \, P_t = \, x_i \, P_i \quad (1.6)$$

where P_t is the total pressure of gas mixture in the bulk phase, P_i is the standard state pressure of pure component i which yields the same spreading pressure as that of the mixture at the same temperature, y is the molar fraction of the bulk phase, and x is the molar fraction of the adsorbed phase.

For two components (a and b), the equilibrium obtained from the spreading pressure results in:

$$\int_0^{P_a} \frac{q_a}{P} \, dP = \int_0^{P_b} \frac{q_b}{P} \, dP \qquad (1.7)$$

Combining Eq. (6) and (7) resulting in:

$$\int_0^{\frac{y_a P_t}{x_a}} \frac{q_b}{P}\, dP = \int_0^{\frac{y_b P_t}{x_b}} \frac{q_b}{P}\, dP \quad (1.8)$$

The molar fraction of a mixture should be unity.

$$y_a + y_b = 1 \quad (1.9)$$

$$x_a + x_b = 1 \quad (1.10)$$

Here, q_a and q_b are the adsorption isotherms of components a and b; they can be fitted from experimental data by using dual-site Langmuir method as:

$$q_i = \frac{q_{max1,i}\ K1_i\ y_i\ P_t}{1+ K1_i\ y_i\ P_t} + \frac{q_{max2,i}\ K2_i\ y_i\ P_t}{1+ K2_i\ y_i\ P_t} \quad (1.11)$$

where $q_{max1,i}$ and $q_{max2,i}$ are the saturation capacity of component *i* (a or b) and *K1 and K2* is the affinity constant.

Given P_t, y, q_{max} and K, there is only one unknown variable quantity x which can be solved by MATLAB software. The selectivity can, then, be estimated as:

$$S = \frac{x_a/y_a}{x_b/y_b} \quad (1.12)$$

1.3.2 Breakthrough Experiments

A dynamic breakthrough setup as shown in Figure 7was used to separate CO_2 from different gas mixtures with concentrations representing industrial flue gas stream. The required gas mixture can be controlled by the mass flow controllers, which will mix the gases through the mixing loop before passing through a fixed bed packed with a polymer material. The home-made system is composed of a fixed adsorbent bed column that is filled with the polymer. The breakthrough system also has inlet gas cylinders, H_2O humidifier, two gas regulators with dual pressure gauges and output control valves, two mass flow controllers (one calibrated for CO_2 flow and the other calibrated for N_2), two check valves,

bypass line (for calibrating the mass spectrometer from the input feed gas), bourdon absolute pressure, mass spectrometer (to analyze the output concentration of effluent gases from the bed), heater jacket and vacuum pump (for regeneration purpose), and interconnecting stainless steel valves and tubes to control and regulate the flow of carrier gas within the system.

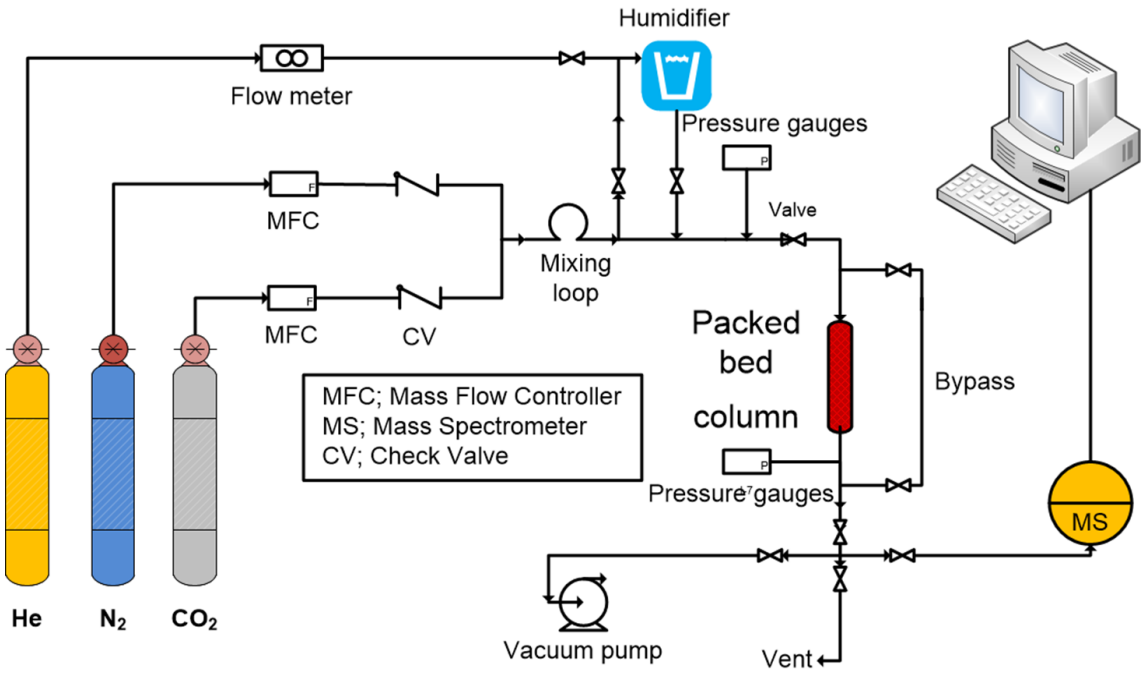

Figure 7 Schematic representation of the column breakthrough experiment.

The first step in the operation of breakthrough setup involves the degassing of the sample at 373 K under vacuum for 24 hours to remove any guest molecules trapped inside the pores. The breakthrough experiments were conducted under ambient conditions (298 K and 1 bar). The flow rate of the feed gas, which was a mixture of 20% CO_2 and 80% N_2, was kept constant at 10 sccm. For the humid mixture, the gases (20% CO_2 and 80% N_2) were wet by passing through a water humidifier. In order to control the relative humidity, we first pass dry N_2 gas through a water humidifier at a constant flow rate (10 sccm) and at constant temperature (298 K) until H_2O percentage reaches equilibrium in the mass

spectrometer. This condition generating ~2.73% (*v*/*v*) of moisture, which is equivalent to 91% relative humidity. The full breakthrough capacity of CO_2 and N_2 was measured by evaluating the ratio of compositions of the downstream gas and the feed gas.

The dynamic CO_2 adsorption capacity of the polymer sample is evaluated using the expression [74].

$$q_{co_2} = \frac{1}{m} F\ C\ t \qquad (1.13)$$

where q_{co_2} represents the CO_2 capacity, *m* mass of adsorbent (g), *F* is the input flow rate ($cm^3\ min^{-1}$), *C* is influent CO_2 concentrations (*v*%), *t* is the time (min).

CHAPTER TWO SYNTHESIS AND CHARACTERIZATION OF METAL ORGANIC FRAMEWORK (MOF-74) FOR CARBON CAPTURE

2.1 Introduction

Unlike mesoporous silica, and porous carbon that usually have very large pore opening hundred nanometers, the formation of MOFs is consists of organic linker with the metal atoms to build up the secondary building unit (SBUs). These characteristics, combine both the tenability of MOFs' composition with the variation in the structure dimensions , make the MOFs highly eligible for precise inclusion processes and indeed distinguish them from other porous materials[75].

Here, we discuss the synthesis of the organic linkers used for the MOF synthesis starting from available raw materials. The organic linkers synthesized in this chapter used for the MOF-74 analogue synthesis with large scale.

2.2 Experimental section

Materials and Methods.

Resorcinol (98% purity), potassium bicarbonates ($KHCO_3$, 98% purity), $Ni(NO_3)_2.6H_2O$, 98% purity), methanol (99.9% purity), N,N-dimethylformamide (99% purity), were purchased from Alfa Aser .All the chemicals were used with-out further purification. For gas sorption measurements, ultrahigh purity grade nitrogen (99.999%), helium (99.999%), and high purity CO_2 (99.9%) were obtained from Abdullah Hashem Industrial Co., Dammam, Saudi Arabia.

Synthesis of meta-dihydroxy isophthalic acid (mdobdc)

Meta-dihydroxy-benzene-dicarboxylic acid (mdobdc) was synthesized by modified Method[76]. Resorcinol (3.0 g, 27.3 mmol) was mixed with $KHCO_3$ (8.4 g, 84 mmol) in 125 mL Teflon lined Autoclave. Then Dry ice (17.88 g) was added to the reactants mixture at this point the bomb was sealed and placed in heating oven at 220 °C for 17 h. the resulting pale-yellow solid mixture was washed with 50 mL diethyl ether by stirring for 15 min at 300 rpm and collected by filtration on filter paper. Then the solid was dissolved in 500 mL deionized water under stirring at room temperature for 15 min. Concentrated hydrochloric acid was added to the solution dropwise until the pH reaches 1-2. The precipitate was collected by filtration and washed with 300 ml water. The pale-yellow solid was obtained and dried in vacuum oven at 65°C for 12 h. ^{1}H NMR (DMSO, 300 MHz): 6.38 (s, 1H) and 7.8

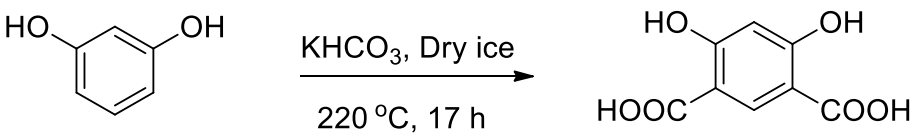

Scheme 9 Synthesis of meta-dihydroxy benzene dicarboxylic acid (H_2mdobdc).

Synthesis of Ni-MOF-74 from the meta-linker H4(mdobdc) by solvothermal method

Ni $(NO_3)_2$.6 H_2O (870 mg, 3 mmol) and H_4(mdobdc) (240 mg, 1.2 mmol) were dissolved in 80 mL mixed solvent (52 mL DMF and 28 mL Methanol) by sonication for 5 minutes. Then the solution is transferred equally into eight 20 mL scintillation vials, which were sealed and heated at 120 °C in oven for 20 h. After cooling to room temperature, the precipitated pale green solid was collected after sonication for 1 min. The combined suspension was centrifuged, and the supernatant was exchanged by fresh DMF. Then the DMF was exchanged three times per days for 3 days then by Methanol for additional 3

days. Then the product was activated by heating at 130 °C under vacuum (< 0.1 bar) for 20 h. FT-IR (KBr, cm^{-1}) 3386 (br), 1601 (s), 1558 (s), 1462 (m), 1392 (s), 1284 (s), 1184 (m), 1092 (m), 741 (w).

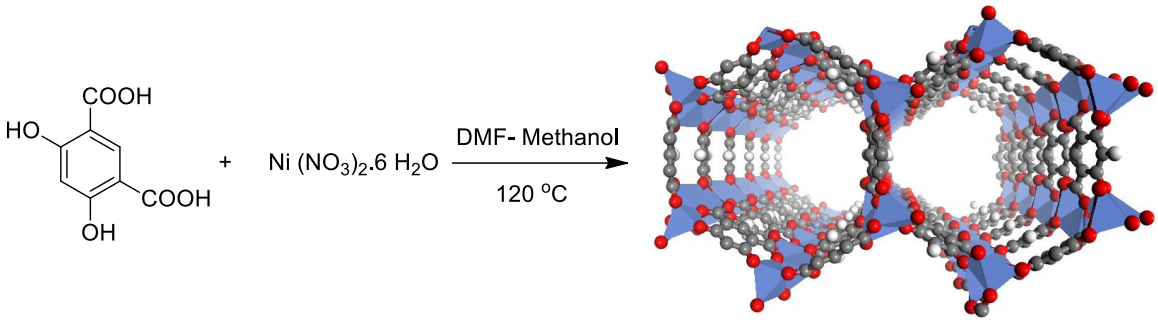

Scheme 10 General synthesis scheme of Ni-MOF-74m.

Synthesis of Co-MOF-74m,

Same procedure as Ni-MOF-74m but using Co $(NO_3)_2$.4 H_2O (3 mmol) and H_4(mdobdc) (240 mg, 1.2 mmol).

2.3 Characterization

Powder X-ray diffraction (PXRD) measurements were recorded on a Rigaku MiniFlex II X-ray diffractometer with Cu K_α radiation (λ = 1.54178 Å). Fourier transform infrared (FT-IR) spectroscopy measurements were performed on a PerkinElmer 16 PC spectrometer from KBr pellets. The spectra were recorded over 4000 – 600 cm^{-1} in transmission mode and the output signals were described as follows: s, strong; m, medium; w, weak; and br, broad. Thermal gravimetric analysis (TGA) was run on a TA Q-500 instrument with a platinum pan sample holder under. About 10 mg of smaple were heated under air flow with heating rate 10 °C per min. Field emission scanning electron microscope (FE-SEM) images were taken on a

Tescan LYRA3 Dual Beam microscope at an acceleration voltage of 10 kV. Low pressure nitrogen sorption isotherms were undertaken using a Quantachrome QUADRASOROB *evo* instrument. A liquid nitrogen bath was used for the measurements at 77 K. CO_2 sorption isotherms were measured on an Autosorb iQ2 volumetric gas adsorption analyser. The measurement temperatures at 273 and 298 K were controlled with a water circulator.

2.4 Results and Discussion

2.4.1 Synthesis strategy

The aim of this study was to synthesize MOF-74 analog from cheap linker delivered from row material. As such gram scale meta dihydroxy benzene dicarboxylic acid (mdobdc) was synthesized by solvent free carboxylation of resorcinol (Scheme 16), which then used for the synthesis of the MOF. Ni-MOF-74m was synthesized in large scale in round flask.

2.4.2 Structural characterization.

Structure characterization of the organic linkers, a pure compound of the synthesized mdopdc linker was clearly elucidated from the Nuclear Magnetic Resonance (^{1}H and ^{13}C-NMR), as shown in **Error! Reference source not found.** Figure 8 and Figure 9 respectively.

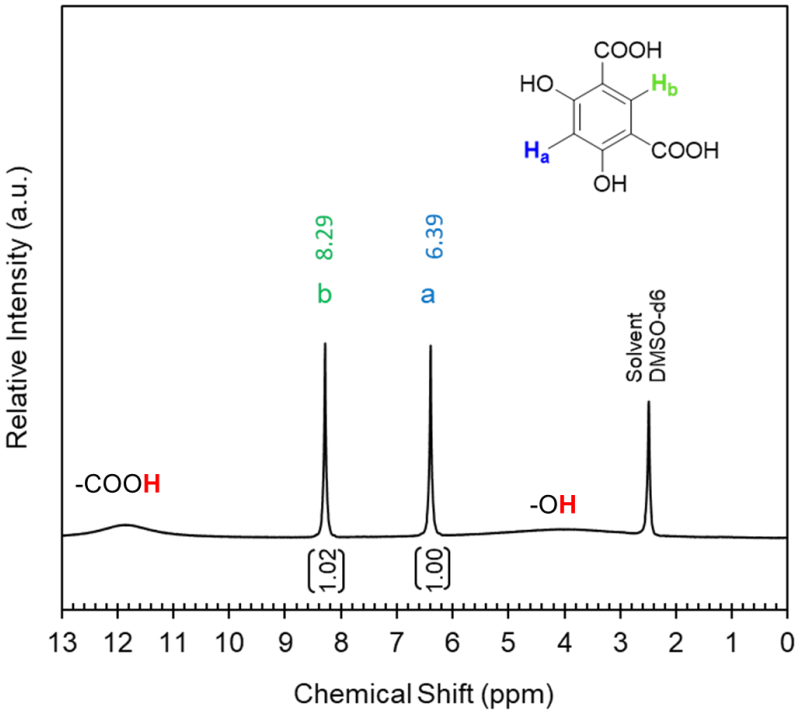

Figure 8 ^{1}H NMR (DMSO-d^{6}, 300 MHz) of mdopdc, inset of the structure with assigned peeks in the NMR.

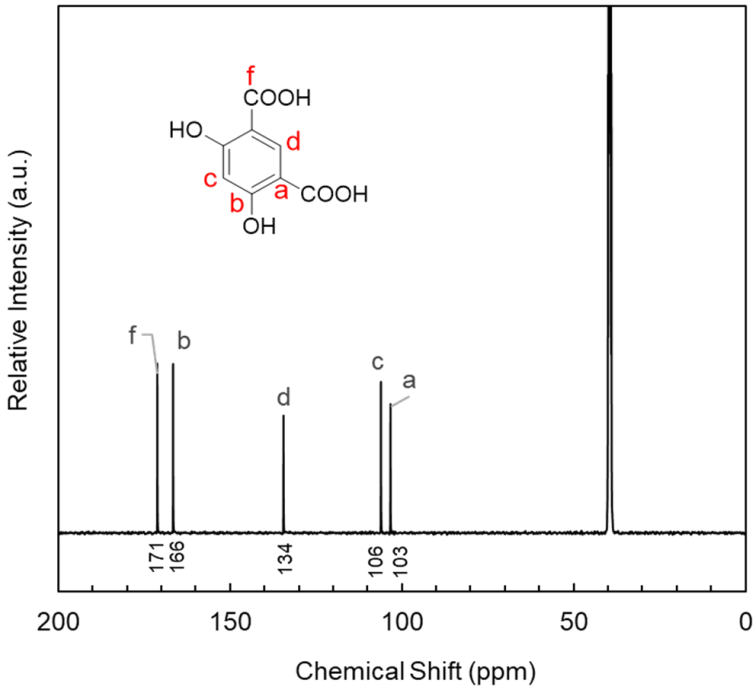

Figure 9 ^{13}C NMR (DMSO-d^6, 300 MHz) of mdopdc, inset of the structure with assigned peeks in the NMR.

Powder X-ray Diffraction (PXRD)

Powder X-Ray Diffraction was done for all the synthesized MOF samples to evaluate the crystallinity of the materials. The data was obtained in the range of 5 to 40 degrees with a rate of 2 degrees/min. For Ni-MOF-74m, from the data obtained and presented in (Figure 10) it can be clearly stated that all the synthesized Ni-MOF-74m is crystalline and peak position is matching the calculated powder pattern the reported single crystal data. Figure 11 also prove the successful synthesis of Co-MOF-74m(M) using microwave method as the peaks are matching the calculated powder pattern.

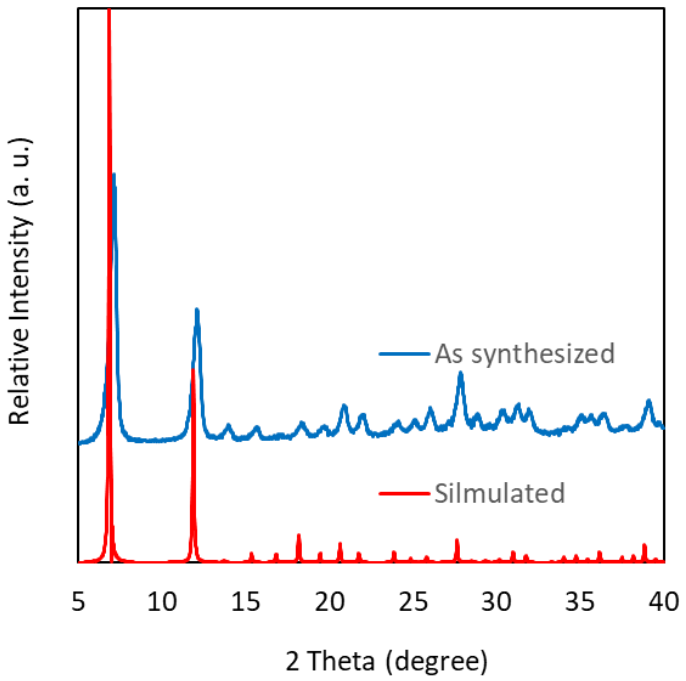

Figure 10 PXRD of the synthesized Ni-MOF-74m (blue), matched with the simulated Powder pattern from reported single crystal data (red).

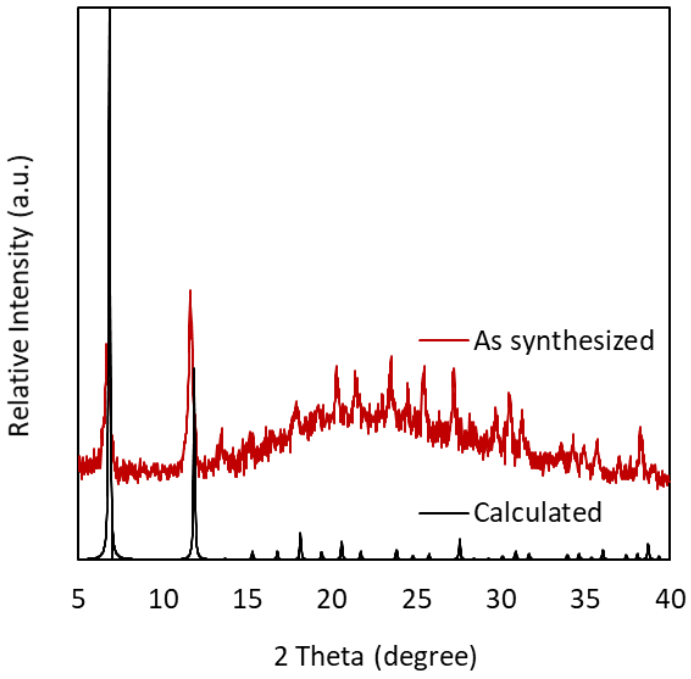

Figure 11 PXRD of the synthesized Co-MOF-74m(M) (red), matched with the simulated Powder pattern from reported single crystal data (black).

Fourier Transform Infrared Spectroscopy (FTIR)

FT-IR spectra of the Ni-MOF-74m(solv) (Figure 12) is supporting the formation of the MOF. The spectral band at 3386 cm^{-1} can be assigned to the stretching vibration of the water molecules bind to the open metal sites of the MOF. The band at 1601 cm^{-1} assigned to the stretching vibration of C=C bond in the linker. The band at 1558 cm^{-1} can be assigned to the phenyl ring C=C vibration mode.

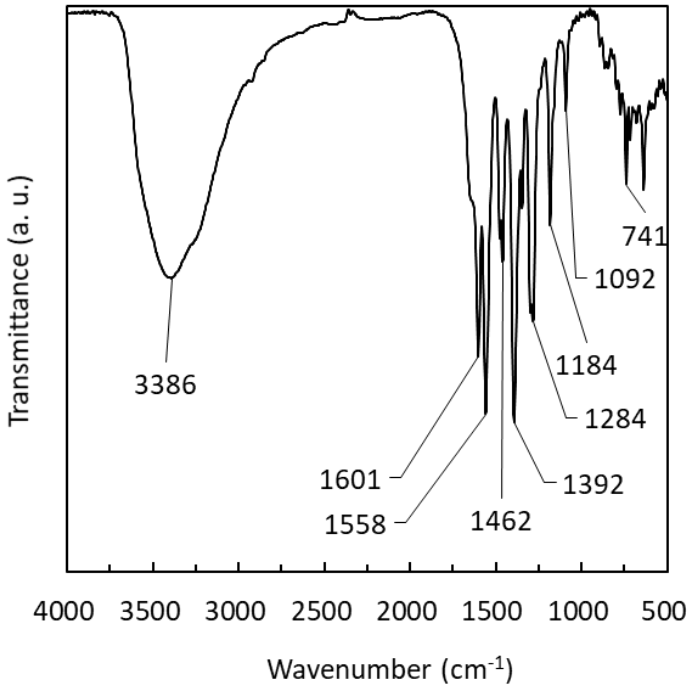

Figure 12 Fourier transform-infrared spectroscopy (FT-IR) spectrum of Ni-MOF-74m(solv.)

Thermal Gravimetric Analysis (TGA)

TGA analysis (Figure 13) demonstrates the thermal stability of the synthesized MOFs up to 250 °C. with water molecules were released prior to structural decomposition.

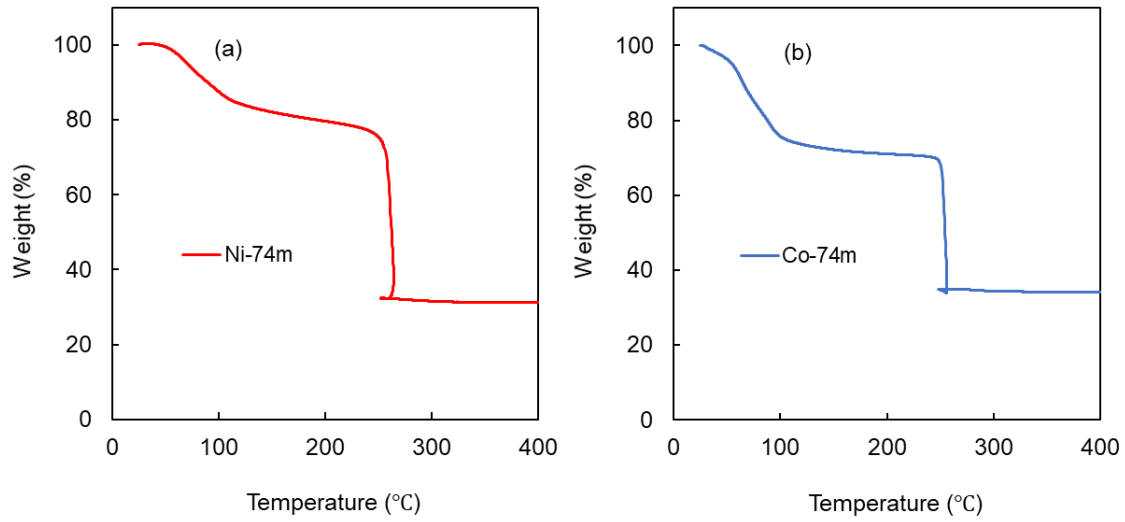

Figure 13 Thermogravimetric analysis of the Ni-MOF-74m (red), and Co-MOF-74m (blue) measured under air.

Scanning Electron Microscope imaging (SEM)

Field emission scanning electron microscope (FE-SEM) images were taken on a Tescan LYRA3 Dual Beam microscope at an acceleration voltage of 10 kV. The materials were coated using a gold coating of thickness 10 nm directly before being introduced to the machine. Figure 23 reveals the flower shape crystals of Ni-MOF-74m and needle shape Co-MOF-74m with nanoscale (50-100 nm) cross section.

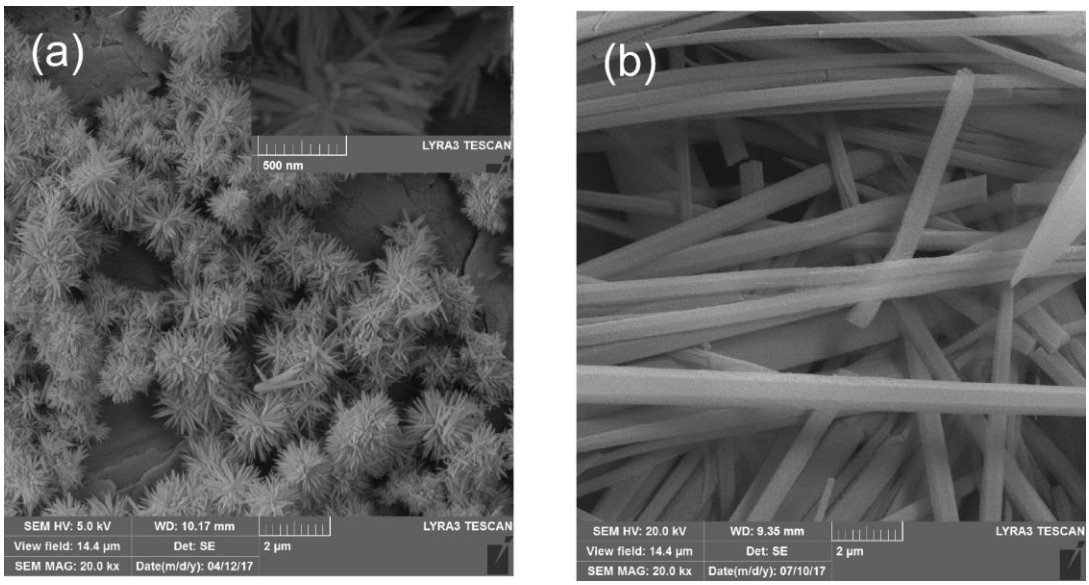

Figure 14 SEM of Ni-MOF-74m crystals (a) and Co-MOF-74m.

2.4.3 Textural properties and Porosity characterization

The textural and surface properties of Ni-MOF-74m(solv) and Co-MOF-74m(solv) were determined by N_2 sorption measurements at 77 K (Figure 15). From the figure, a sharp uptake at low relative pressure ($P/P_0 < 0.001$) indicates the predominance of a microporous nature of type I isotherm according to the IUPAC classification[26,76]. The BET surface area (at P/P_0 = 0.01-0.3) of Ni-MOF-74m(solv) was found to be 1080 $m^2 g^{-1}$ while for Co-MOF-74m(solv) found to be 1000 $m^2 g^{-1}$ these values are comparable with the reported structures in the literature. The pore size distribution was calculated using NLDFT models (**Error! Reference source not found.**) confirms the micropore nature of both MOFs.

Figure 15 N_2 adsorption isotherm at 77 K for Ni-MOF-74m(solv). Filled and open symbols represent adsorption and desorption branches, respectively. The connecting lines serve as a guide to the eye.

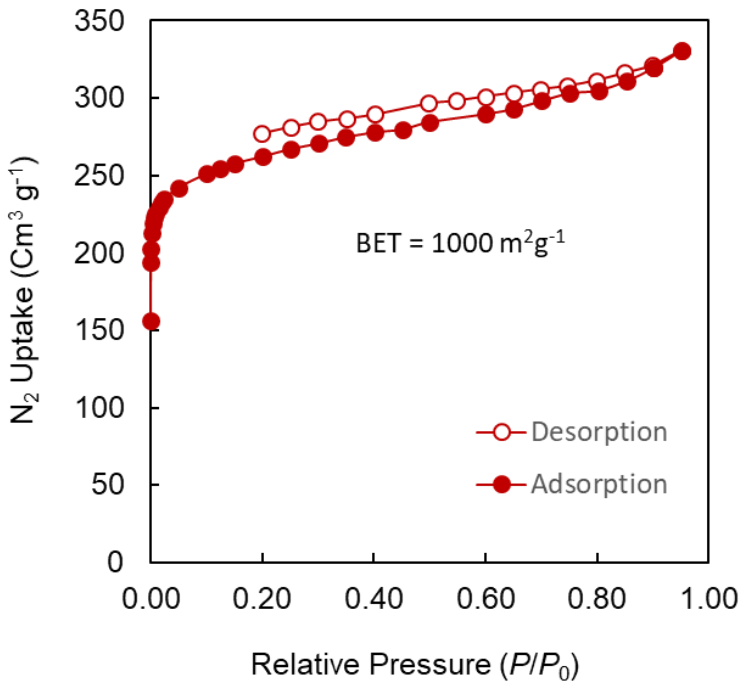

Figure 16 N_2 adsorption isotherm at 77 K for Co-MOF-74m(M). Filled and open symbols represent adsorption and desorption branches, respectively. The connecting lines serve as a guide to the eye.

2.4.4 Gas Adsorption Studies

The thermodynamic gas adsorption properties were assessed for the synthesized MOFs at 273 and 298 K (Figure 35). The isotherms exhibit a reversible adsorption and desorption reflecting the physisorption mechanism of the MOF with the CO_2 gas. Co-MOF-74m exhibited high CO_2 uptake capacity of 171 $cm^3\ g^{-1}$ at 298K and 760 Torr. While low N_2 uptake capacities was found under the same conditions (21 $cm^3\ g^{-1}$ 298 K and 760 Torr). Ni-MOF-74m exhibited similar CO_2 uptake of 116 $cm^3\ g^{-1}$ at 298K and 760 Torr. While low N_2 uptake capacities was found under the same conditions (18.5 $cm^3\ g^{-1}$ 298 K and 760 Torr). It clearly seen that the CO_2 isotherms were steeper than that of the N_2, reflecting the higher affinity of the materials toward CO_2 compared to the N_2, which advance the potential use of both MOFs as an adsorbent for selective CO_2 capture from flue gas.

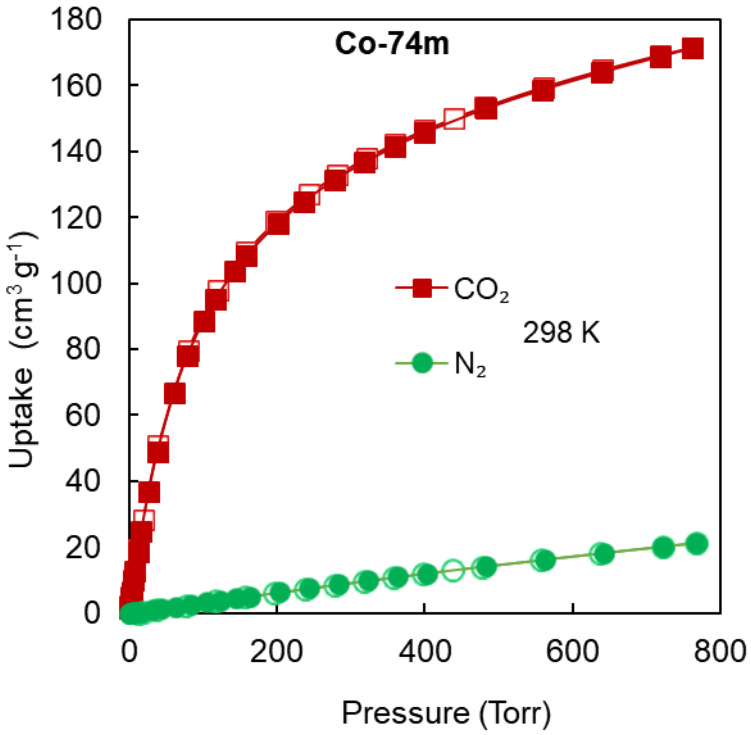

Figure 17 Gas adsorption properties of Co-MOF-74m. CO_2 (red cube) and N_2 (green circle) adsorption isotherms for Co-MOF-74m at 298 K. Filled and open symbols represent adsorption and desorption branches, respectively. The connecting lines serve as a guide to the eye.

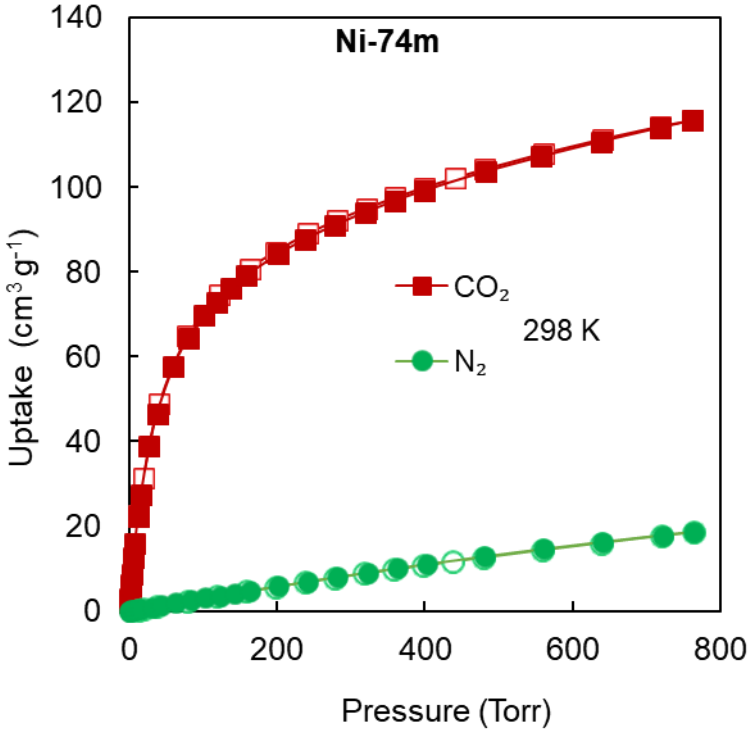

Figure 18 Gas adsorption properties of Ni-MOF-74m. CO_2 (red cube) and N_2 (green circle) adsorption isotherms for Co-MOF-74m at 298 K. Filled and open symbols represent adsorption and desorption branches, respectively. The connecting lines serve as a guide to the eye.

CHAPTER THREE

CARBON DIOXIDE CAPTURE IN THE PRESENCE OF WATER BY AN AMINE-BASED CROSSLINKED POROUS POLYMER

3.1 Introduction

As discussed in the introduction chapter, the development of a new porous adsorbent material represents a target worth pursuing. Accordingly, we turned our attention to porous organic polymers, which are viewed as strong candidates to replace current technologies due to their demonstrable high and selective CO_2 uptake in conjunction with their structural diversity and exceptional physicochemical stabilities[24]. A variety of porous organic polymers have been explored and several of these materials standout as particularly noteworthy in the context of the seven criteria needed for any material to be effectively separate CO_2 [27,28,77]; however, there have been few, if any, notable reports, in which such materials were shown to have met all of the criteria. In this contribution, we describe the development of a new porous polymer, termed KFUPM-1 (where KFUPM = King Fahd University of Petroleum and Minerals), that was synthesized via acid catalyzed polycondensation of the inexpensive, CO_2-philic monomers pyrrole and 1,4-benzenediamine with *p*-formaldehyde as the linking agent (Figure 19; criteria #7). The synthetic design strategy was founded upon increasing the density of polar aromatic amines within the backbone of the resulting polymer in order to increase the material's affinity to CO2. KFUPM-1 was proven permanently porous with relatively high CO2 uptake capacity at relevant partial pressures (criterion #1) and ultrahigh CO_2/N_2 selectivity (criterion #2).

Dynamic breakthrough measurements were then performed, in which KFUPM-1 was demonstrated capable of separating CO_2 from both dry and wet (91% relative humidity) gas mixtures – mixtures whose composition mimicked those found in a flue gas stream (criteria #3 and #6). Following this, continuous multicycle breakthrough experiments (>45 cycles) were carried out under wet conditions. These measurements proved that the dynamic CO_2 uptake capacity in the presence of water remained relatively unchanged over 45 cycles (criterion #5). Finally, the ease of regeneration between each cycle was accomplished under mild conditions (criterion #4).

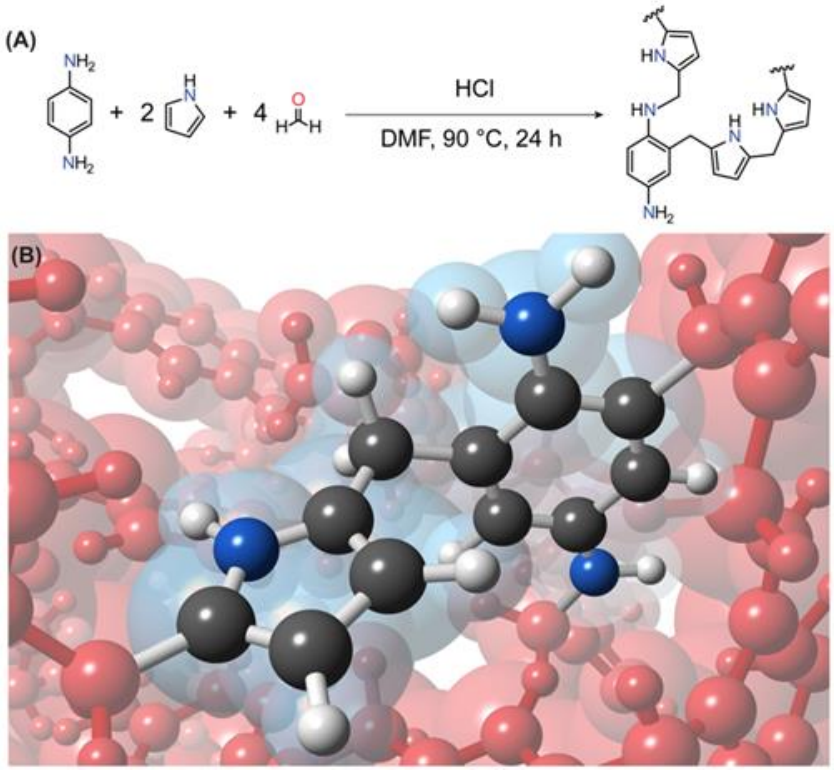

Figure 19 Important structural features found within the backbone of the crosslinked, porous polymer, KFUPM-1. (A) The synthesis of KFUPM-1 was carried out by linking 1,4-benzenediamine and pyrrole with *p*-formaldehyde in the presence of a hydrochloric acid catalyst. (B) The structural features are a pyrrole monomer linked to 1,4-benzenediamine monomer by a methylene unit that is derived from *p*-formaldehyde. Atom colors: C, black; N, blue; and H, white. The surrounding backbone structure of KFUPM-1 is depicted in red.

3.2 Experimental section

Materials and Methods.

Pyrrole (98% purity), 1,4-benzenediamine (98% purity), methanol (99.9% purity), *N*,*N*-dimethylformamide (DMF, 99% purity), and hydrochloric acid (37 wt%) were purchased from Sigma Aldrich Co. Anhydrous iron(III) chloride (≥99.99% purity) was acquired from Alpha Chemika. Paraformaldehyde (≥99% purity) was obtained from Fluka. Ammonium hydroxide (28-30% *w*/*w*) was purchased from Fisher Scientific. Pyrrole was distilled under N_2 flow at 418 K and stored under an N_2 environment at 269 K prior to use. All other chemicals were used without further purification. For gas sorption measurements, ultrahigh purity grade nitrogen (99.999%), helium (99.999%), and high purity CO_2 (99.9%) were obtained from Abdullah Hashem Industrial Co., Dammam, Saudi Arabia.

Synthetic Procedures

Different parameters were applied in order to synthesize the KFUPM-1 polymer, in all the trials the monomer 1,4-benzenediamine and pyrrole were used by (1:2) molar ratios respectively.

Synthesis of KFUPM-1.

1,4-Benzenediamine (1.08 g, 10.0 mmol) and paraformaldehyde (1.20 g, 40.0 mmol) were combined with 70 mL DMF to a 100 mL round bottom flask and stirred at room temperature for 5 min. Pyrrole (1.34 g, 20.0 mmol) was then added into the reaction mixture and stirred for an additional 5 min. After this, 1.6 mL conc. HCl (12 M) was added dropwise into the reaction mixture and the flask was sealed with a rubber septum and purged with N_2 for 2-3 min. The mixture was subsequently heated at 363 K in an oil bath for 24 h with continuous stirring at a rate of 200 rpm. After this time elapsed, a black solid was isolated by filtration. The solid was washed with 40 mL of methanol followed by sonication for 30 min. The solid was filtered and immersed in an ammonia solution (25% *w*/*w*) for 24 h, 40 mL distilled water for 24 h, and 60 mL of methanol per d for 3 d with stirring, at which time a clear filtrate solution was obtained. Finally, the product was dried at 348 K under vacuum (<0.1 bar) for 20 h. The final yield (2.56 g) was 88% based on the monomers weights. FT-IR (KBr, cm^{-1}) 3413 (br), 3240 (br), 2918 (w), 2852 (w), 1618 (m), 1510 (w), 1423 (w), 1024 (w), 671 (m).

Yield calculation:

% yield = (experimental weight/(total monomers weights-weight of the H_2O)) * 100

= 2.56 / (1.08 + 1.34 + 1.2 – (0.04 mol * 18)) = 2.56/ 2.9 = 88%

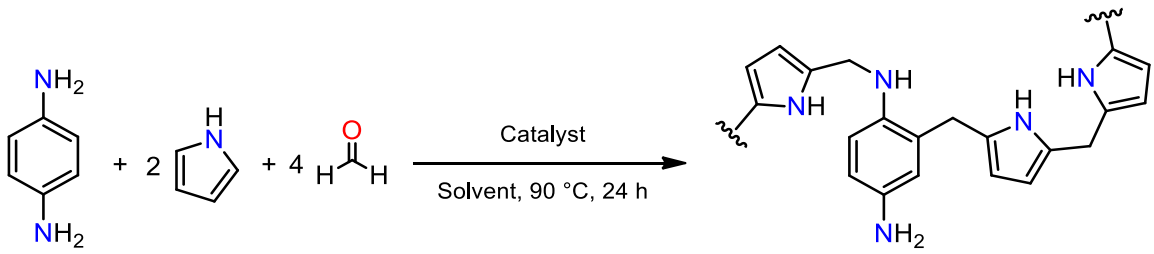

Scheme 11 General synthetic scheme of KFUPM-1 polymer.

Breakthrough measurements.

The schematic for the homemade breakthrough system set-up is shown in Figure 7. The bed was packed with KFUPM-1 powder (1.12 g) and the sample was activated at 373 K under vacuum for 24 hours prior to carrying out the breakthrough measurements. The breakthrough experiments were conducted under ambient conditions (298 K and 1 bar) with a 10 sccm flowrate of CO_2:N_2 (20:80 *v*/*v*) feed mixture. For the measurements under humid conditions, the sample bed was subjected to a stream of wet N_2 gas (91% relative humidity, RH), in which the water level in the gas stream was monitored until saturation was obtained as detected by mass spectrometry. At this point, dry CO_2 was introduced into the wet N_2 stream with the same flowrate as the dry conditions noted above. The full breakthrough capacity of CO_2 was measured by evaluating the ratio of compositions of the downstream gas and the feed gas.

3.3 Characterization

^{13}C solid-state nuclear magnetic resonance (NMR) spectroscopy measurements were performed on a Bruker 400 MHz spectrometer operating at 125.65 MHz (11.74 T) and at ambient temperature (298 K). Samples were packed into 4 mm ZrO_2 rotors and cross-polarization magic angle spinning (CP-MAS) was employed with a pulse delay of 5.0 s and a magic angle spinning rate of 10 kHz for the 1,4-benzenediamine monomer or 14 kHz for the polymer. Fourier transform infrared (FT-IR) spectroscopy measurements were performed from KBr pellets using a PerkinElmer 16 PC spectrometer. The spectra were recorded over 4000 – 400 cm^{-1} in transmission mode and the output signals were described as follows: s, strong; m, medium; w,

weak; and br, broad. Thermal gravimetric analysis (TGA) was run on a TA Q-500 instrument with the sample held in a platinum pan under air flow with a 10 °C per min heating rate. To identify the type of gases trapped within the pores, TGA-mass spectrometry (TGA-MS) analysis was performed using a QMS 403 C Aëolos with STA 449 F1 Jupiter instrument. Powder X-ray diffraction (PXRD) measurements were carried out using a Rigaku MiniFlex II X-ray diffractometer with Cu K_α radiation (λ = 1.54178 Å). Field emission scanning electron microscope (FE-SEM) images were taken on a Tescan LYRA3 Dual Beam microscope at an acceleration voltage of 10 kV. Low-pressure nitrogen sorption isotherms were collected on a Micromeritics ASAP 2020. A liquid nitrogen bath was used for the measurements at 77 K. CO_2 sorption isotherms were carried out on an Autosorb iQ2 volumetric gas adsorption analyser. The measurement temperatures at 273 and 298 K were controlled with a water circulator. Water adsorption measurements were performed on a DVS Vacuum, Surface Measurement Systems Ltd, London, UK. Prior to these measurements, KFUPM-1 was pre-treated by heating (383 K) under vacuum for 10 h using the Dynamic Vapor Sorption Analyzer Desorption.

3.4 Results and Discussion

3.4.1 Synthesis strategy

The underlying objective for this research program was to synthesize a porous polymer based on inexpensive monomers, which contain accessible CO_2-philic functional groups. As such, pyrrole and 1,4-benzenediamine were identified as the monomers since they have integrated polar aromatic amine moieties (known for inducing strong interactions with CO_2) within their molecular structures[53].The

synthetic strategy used to crosslink these CO_2-philic monomers was based on an acid catalyzed polycondensation reaction whereby *p*-formaldehyde would serve as a linking agent. In the quest to optimize the reaction conditions, the solvent (dichloroethane, DMF, or dimethylsulfoxide) and the catalyst (conc. HCl, $FeCl_3$, or CuCl) were varied (Appendix A, Table 8). Conventional Lewis acid catalyzed polycondensation reactions typically make use of $FeCl_3$ as the catalyst, in equimolar amounts, in order to activate the linking agent[55]; however, our findings demonstrated that the optimized conditions relied on using a catalytic amount of conc. HCl (27 mol% of monomers) with DMF as the solvent. Indeed, these conditions produced the crosslinked, porous polymer product, KFUPM-1, in 88% yield. It is noted that KFUPM-1 could be synthesized using the other catalysts or solvents, but those products suffered drawbacks resulting from either lower yield, trapped catalyst (Fe) or unreacted species, lower surface area, or lower CO_2 sorption uptake. The proposed mechanisms for the reaction are shown in Scheme 12 in which the catalyst activates the formaldehyde. It's worth to mention that these mechanisms were not proposed depending on kinetic study, and there is no proof whether the reaction goes via SN^1 or SN^2 mechanism, but the free carbocation was introduced here as a transition state because generally bulky material are less likely to undergo bimolecular reaction.

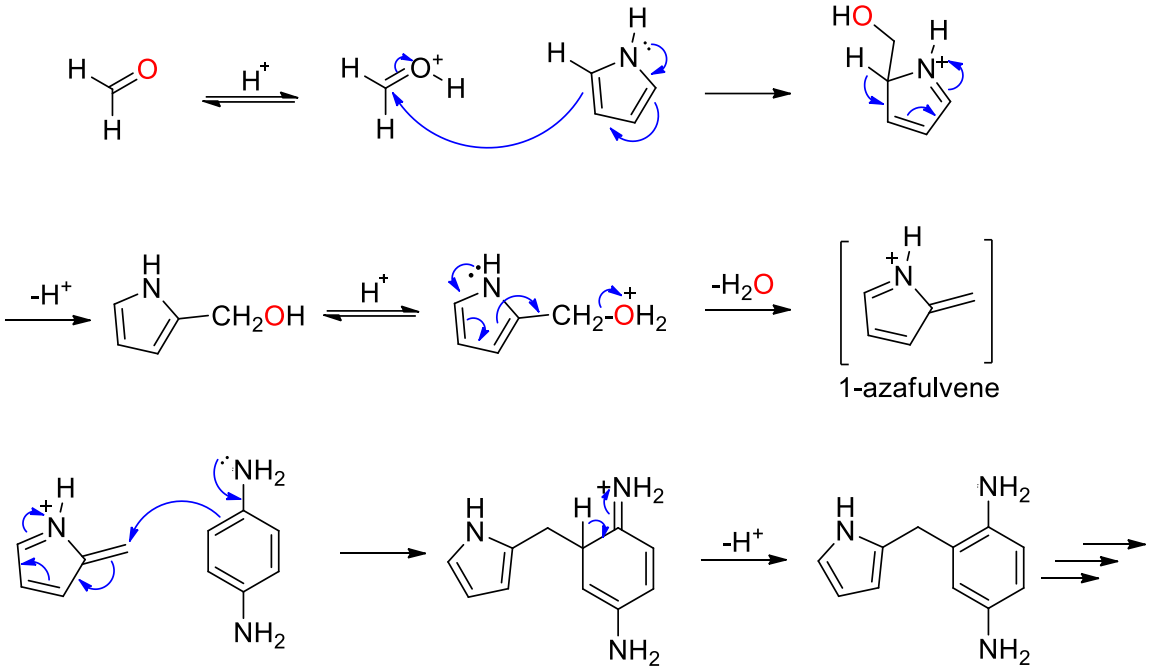

Scheme 12 Proposed polycondensation reaction mechanism of the synthesized KFUPM-1 copolymer.

After synthesis, KFUPM-1 was thoroughly washed with water and methanol followed by a solution of ammonium hydroxide in order to remove any unreacted starting materials and to neutralize any residual acid, respectively. It is noted that in order to prove the complete removal of Cl^- ions, we added $AgNO_3$ to the filtrate, in which no precipitate was found to have formed. Prior to use in further characterization, KFUPM-1 was activated at 348 K under dynamic vacuum for 20 h.

3.4.2 Structural characterization.

Solid-state Nuclear Magnetic Resonance (^{13}C-NMR)

Due to the amorphous nature of KFUPM-1, as evidenced by PXRD, the connectivity of the constituents was assessed using a combination of cross polarization-magic angle spinning (CP-MAS) ^{13}C NMR and FT-IR spectroscopies. Accordingly, the ^{13}C NMR spectra of KFUPM-1 revealed two resonances corresponding to CH_2

species: (i) a broad peak centered at δ = 24 ppm, which was assigned to a chemical shift for a CH_2 that links aromatic C atoms from either monomer; and (ii) a lower intensity peak at δ = 40 ppm, which was assigned to a CH_2 linked to the N atom in 1,4-benzenediamine (Figure 20A). An additional broad resonance, centered at δ = 129 ppm, was assigned to the chemical shifts of aromatic C atoms. The spectral data agree with that in previous reports [26,53,78]. A shoulder peak at δ = 140 ppm was also noted and attributed to the aromatic C atom to which the amine functionality is located. Further support for these assignments came from observing similar resonances in the ^{13}C NMR spectrum for a model polymer based on the polycondensation of 1,4-benzenediamine with *p*-formaldehyde (Figure 20B, C).

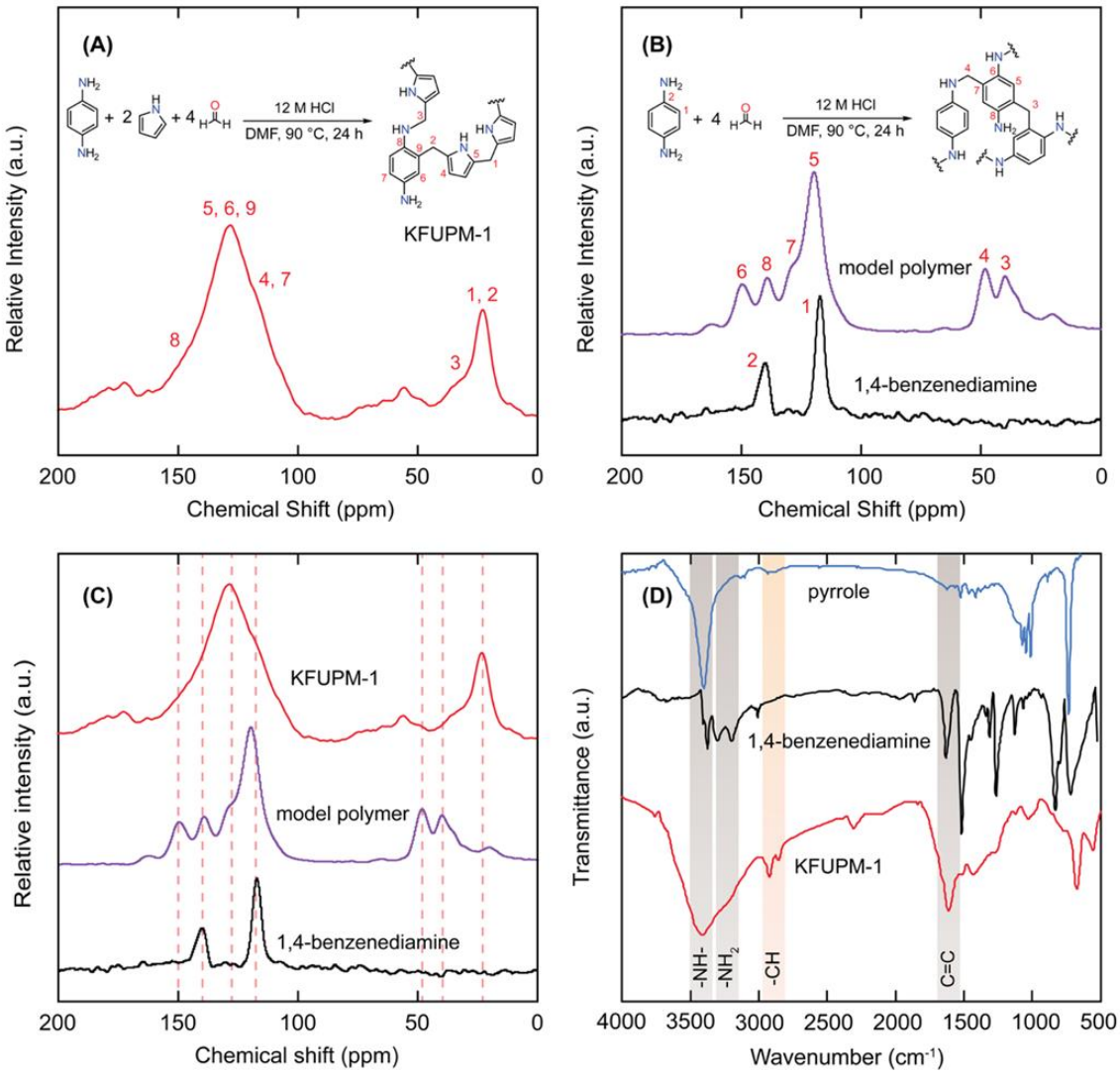

Figure 20 Structural characterizations and solution of KFUPM-1. (A) CP-MAS ^{13}C NMR spectrum of KFUPM-1, with the corresponding core structure of KFUPM-1, provided in the inset for peak assignment. (B) CP-MAS ^{13}C NMR spectra of the model polymer (purple; polycondensation of 1,4-benzenediamine with *p*-formaldehyde) and the 1,4-benzenediamine monomer (black). The corresponding core structure of the model polymer is provided in the inset for peak assignment. (C) Stacked CP-MAS ^{13}C NMR spectra for comparing KFUPM-1 (red), the model polymer (purple), and the 1,4-benzenediamine monomer (black). (D) Fourier transform-infrared spectroscopy (FT-IR) analysis of KFUPM-1 (red) in comparison to pure 1,4-benzenediamine (black) and pure pyrrole (blue). Those absorption bands directly related to the characteristic functionalities of KFUPM-1 are highlighted. The new methylene linkage is highlighted in orange.

Fourier Transform Infrared Spectroscopy (FTIR)

To further support the ^{13}C NMR data, FT-IR spectra were collected for the pure pyrrole and 1,4-benzenediamine monomers as well as for KFUPM-1 (Figure 20D, Appendix, Table 15). The FT-IR spectra for KFUPM-1 exhibited a broad absorption band centered at 3413 cm^{-1}, which is characteristic of the ν_{N-H} stretching frequency. This absorption band is confirmed by the spectrum for the pure pyrrole. Evidence for free amine moieties in KFUPM-1 was provided by the appearance of a shoulder absorption band at ~3240 cm^{-1}, which is also present in the spectrum for the pure 1,4-benzenediamine. The broadening of this band was attributed to trapped water molecules (ν_{O-H} stretching) as evidenced by TGA-MS analysis, which demonstrated that only water molecules were released prior to structural decomposition occurring at 220 °C (Figure 21)[51,79]. Noteworthy in the FT-IR spectra of KFUPM-1 was the appearance of a new absorption band at 2918 cm^{-1} for methylene ν_{C-H} stretching modes (Figure 20D). This band was distinctly absent in the spectra for both pure monomers. Finally, the aromatic $\nu_{C=C}$ vibrational mode, situated at 1515 cm^{-1}, for the 1,4-benzenediamine was present in the spectrum of KFUPM-1, which lends strong support for the incorporation of this monomer within the polymer.

Thermal Gravimetric Analysis (TGA)

TGA-MS analysis (Figure 21) demonstrates that only water molecules were released prior to structural decomposition occurring at 220 °C.

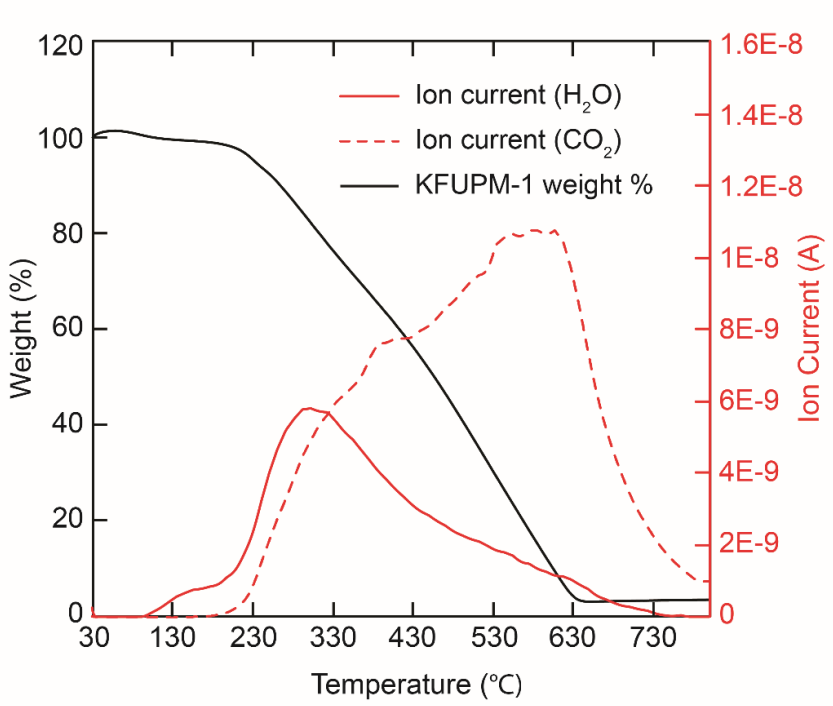

Figure 21 TGA-MS of the KFUPM-1 activated sample under air, the solid red line represents the H_2O molecules emitted from the sample, while the dashed red line represents the CO_2.

Powder X-Ray Diffraction (PXRD)

Powder X-ray diffraction was done for all the polymers to evaluate the crystallinity of the materials. The data was obtained in the range of 5 to 40 degrees with a rate of 2 degrees min^{-1}. From the data obtained and presented in (Figure 22), it can be clearly stated that all the synthesized polymers are amorphous in nature.

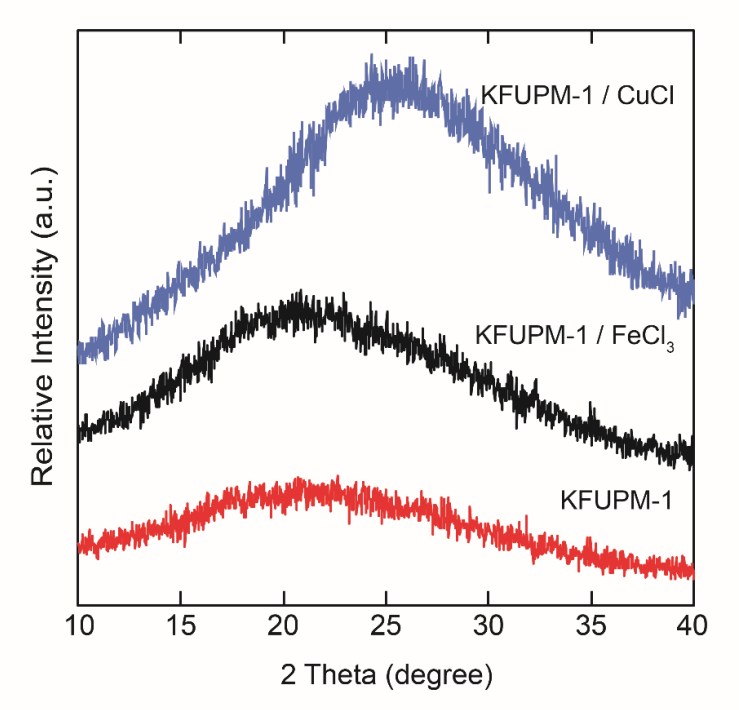

Figure 22 Powder X-ray diffraction of KFUPM-1 (red), KFUPM-1/$FeCl_3$ (black) and KFUPM-1/CuCl (blue).

Scanning Electron Microscope imaging (SEM)

Field emission scanning electron microscope (FE-SEM) images were taken on a Tescan LYRA3 Dual Beam microscope at an acceleration voltage of 10 kV. All the materials were coated using a gold coating of thickness 10 nm directly before being introduced to the machine. Figure 23 reveals the amorphous nature of the synthesized polymers.

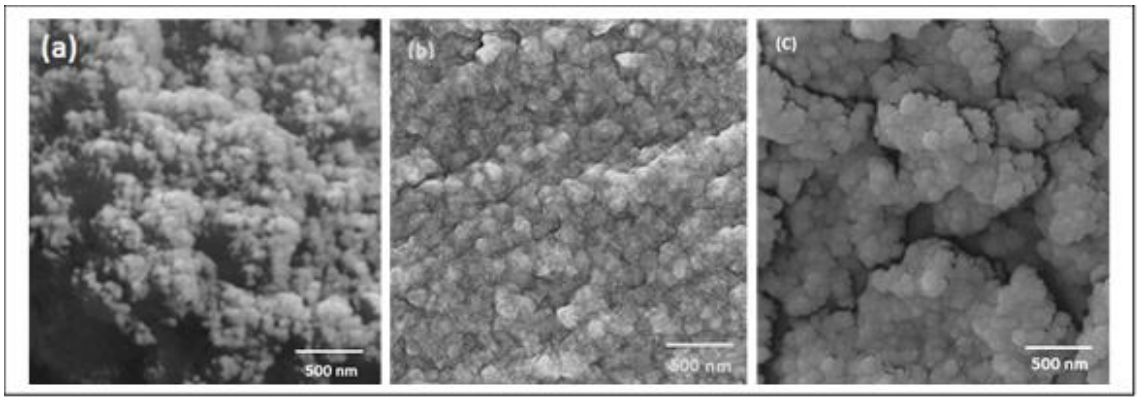

Figure 23**. SEM Images the of the polymers (a) KFUPM-1, (b) KFUPM-1/$FeCl_3$, (c) KFUPM-1/CuCl.**

3.4.3 Textural properties and Porosity characterization

The architectural stability and permanent porosity of KFUPM-1 were then investigated by N_2 adsorption isotherm at 77 K (Figure 24). At low relative pressures ($P/P_0 < 0.6$), KFUPM-1 exhibited a Type-I profile. At $P/P_0 > 0.6$, a sharp uptake was observed indicating that inter-particle condensation was occurring (*i.e.* the presence of meso-/macropores between particles). Upon desorption, a small hysteresis was noted likely as a result of elastic deformation or swelling[81]. The Brunauer-Emmett-Teller (BET) model was applied over the $P/P_0 = 0.01$-0.3 range to yield a calculated surface area of 305 $m^2 g^{-1}$. It is important to note that a relatively uniform pore size distribution indicating mesoporosity was found for KFUPM-1 (Figure 25). In terms of practical applicability, the stability of this material toward water was then examined by carrying out water adsorption measurements. Accordingly, the water adsorption isotherm at 298 K for KFUPM-1 displayed a Type-II profile, which indicates that the material is capable of adsorbing 33.5 wt% water at $P/P_0 > 0.9$ (90% RH) (Appendix A, Figure 71). To assess the long-term stability of KFUPM-1 toward water, a multicycle continuous water isotherm at 313 K (>20 cycles) was carried out, which demonstrated that KFUPM-1 was able to retain its water adsorption properties over long periods of time and use.

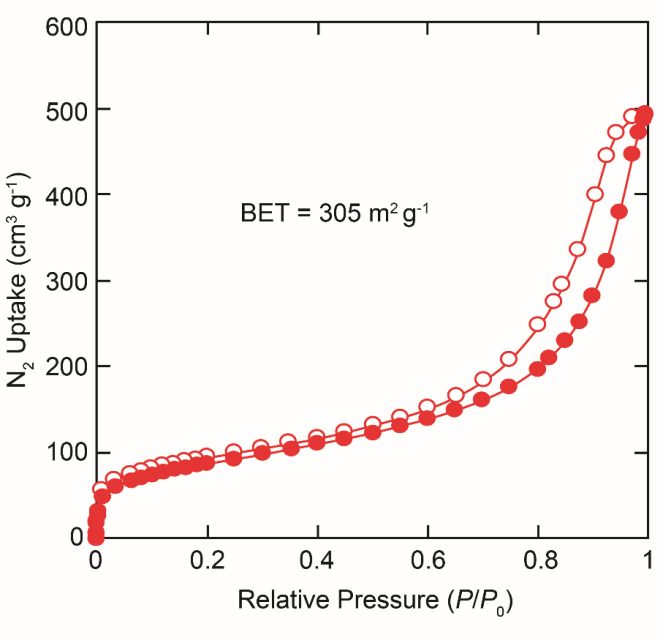

Figure 24 N_2 adsorption isotherm at 77 K. Filled and open symbols represent adsorption and desorption branches, respectively. The connecting lines serve as guides for the eye.

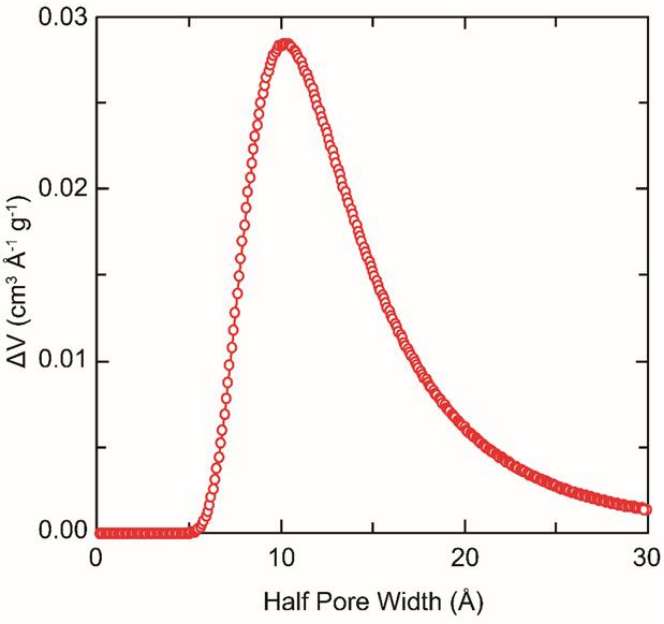

Figure 25 Differential pore size distribution (PSD) as calculated by Dubinin Astakhov (DA) method.

3.4.4 Gas Adsorption Studies

Thermodynamic uptake capacity. On the basis of the aromatic amine-rich structure and KFUPM-1's permanent porosity and water stability, we sought to assess the material's thermodynamic gas adsorption properties. Accordingly, low-pressure, single-component gas adsorption isotherms for CO_2 and N_2 were measured at 273 and 298 K up to 760 Torr (Figure 26). KFUPM-1 exhibits moderate CO_2 uptake capacities of 34.0 $cm^3\ g^{-1}$ at 273 K and 760 Torr and 23.4 $cm^3\ g^{-1}$ at 298 K and 760 Torr. This is in contrast to the N_2 uptake capacities under the same experimental conditions (1.2 and 1.0 $cm^3\ g^{-1}$ at 273 and 298 K, respectively, and 760 Torr). Interestingly, as depicted in Figure 26, KFUPM-1 displays a much steeper CO_2 uptake in the low-pressure region at 298 K when compared to the N_2 uptake. This observation is indicative of stronger polymer-CO_2 interactions (*i.e.* higher affinity) than that found for N_2, which lends credence to the potential of KFUPM-1 to serve as an adsorbent for selective CO_2 capture from flue gas.

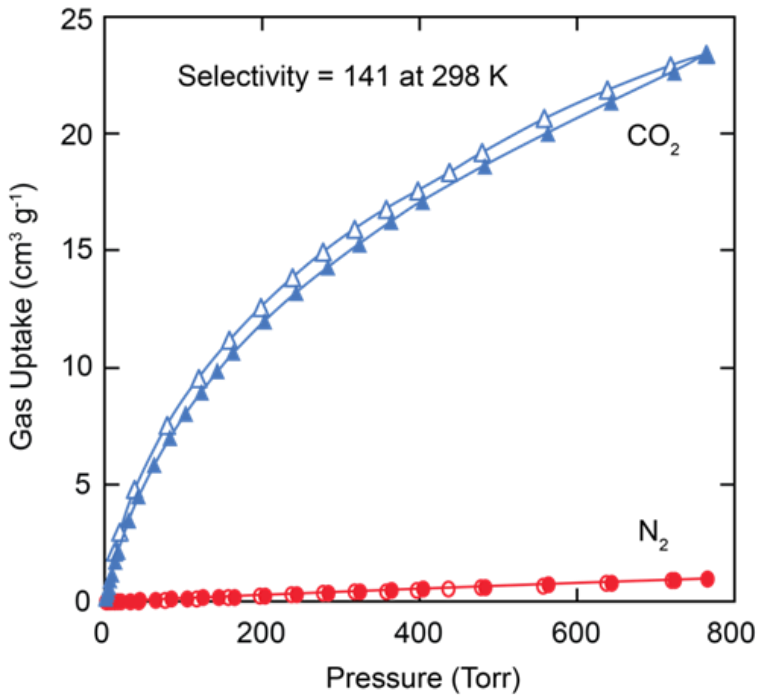

Figure 26 Gas adsorption properties of KFUPM-1. CO_2 (blue triangle) and N_2 (red circle) adsorption isotherms for KFUPM-1 at 298 K. Filled and open symbols represent adsorption and desorption branches, respectively. The connecting lines serve as a guide to the eye.

3.4.5 Coverage Dependent Enthalpy of Adsorption (Q_{st}) and CO_2/N_2 selectivity.

Coverage Dependent Enthalpy of Adsorption (Q_{st}). Due to the thermodynamic gas adsorption measurement results, we were encouraged to pursue a deeper understanding of KFUPM-1's relationship with CO_2. Accordingly, the coverage-dependent enthalpy of adsorption (Q_{st}) for CO_2 was estimated by fitting the isotherms collected at 273 and 298 K with a virial-type expansion equation. The resulting initial Q_{st} value was calculated to be 34 kJ mol^{-1}, which quantifiably demonstrates the material's strong binding affinity to CO_2. It is noted that the Q_{st} remained relatively constant, thus, reflecting the homogeneous binding strengths over multiple sites at low coverage. The Q_{st} value is moderately high for physisorption-driven materials as compared to the related materials: BILP-1 (26.5 kJ mol^{-1})[82], Azo-COP-1 (29.3 kJ mol^{-1})[71], and PAF-1 (15.6 kJ mol^{-1})[83]. With these results,

the CO_2/N_2 selectivity was then estimated based on Henry's law. KFUPM-1 demonstrated a remarkably high CO_2/N_2 selectivity of 249 and 141 at 273 and 298 K, respectively. These values were corroborated by applying Ideal Adsorbed Solution Theory (IAST), which provided information about selectivity with pressure as a consideration (Figure 27). These selectivities are among the highest values reported for crosslinked, porous polymers to date.

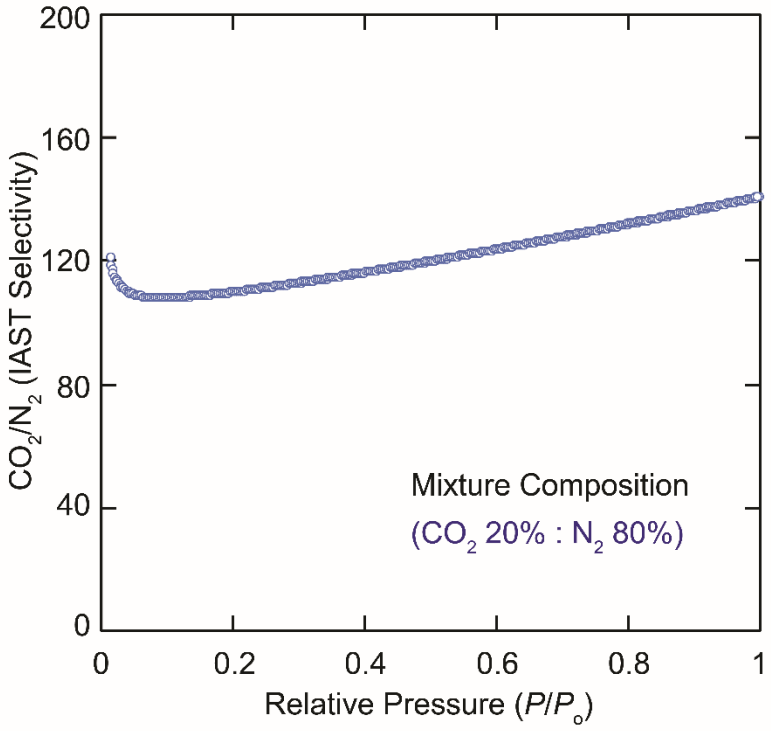

Figure 27 Ideal Adsorption Solution Theory (IAST) selectivity of CO_2/N_2 at 298 K for KFUPM-1.

3.4.6 Dynamic CO_2 Capture by Breakthrough Experiments

In order to evaluate the performance of KFUPM-1 in effectively and selectively capturing CO_2 under practical flue gas conditions, dynamic breakthrough experiments were implemented. In a typical experiment, an activated sample of KFUPM-1 was loaded into a bed and exposed to a gaseous mixture of 20% (*v*/*v*) CO_2 and 80% (*v*/*v*) N_2 (volumetric percentages closely resembling flue gas

composition). The effluent was monitored for the breakthrough time (the time in which adsorbed CO_2 'breakthroughs' the bed) by an online mass spectrometer. As seen in Figure 28, N_2 (red filled triangles) is solely present in the effluent for 4.79 min, at which point the CO_2 (blue filled diamonds) breakthrough point is observed. Clearly, CO_2 is selectively retained by KFUPM-1 for a significant period of time while N_2 passes freely through the material. The corresponding dynamic CO_2 uptake capacity of KFUPM-1, calculated from the breakthrough time, was 8.6 $cm^3\ g^{-1}$. As shown in Table 3, the capacity of KFUPM-1 is comparable to other porous polymers, such as CTF-FUM-350 and CTF-DCN-500 (11.4 and 8.3 $cm^3\ g^{-1}$, respectively)[84], as well as covalent organic frameworks (*e.g.* LZU-301 and $[HO_2C]_{100\%}$-H_2P-COF: 4.9 and 16.4 $cm^3\ g^{-1}$, respectively)[84,85].

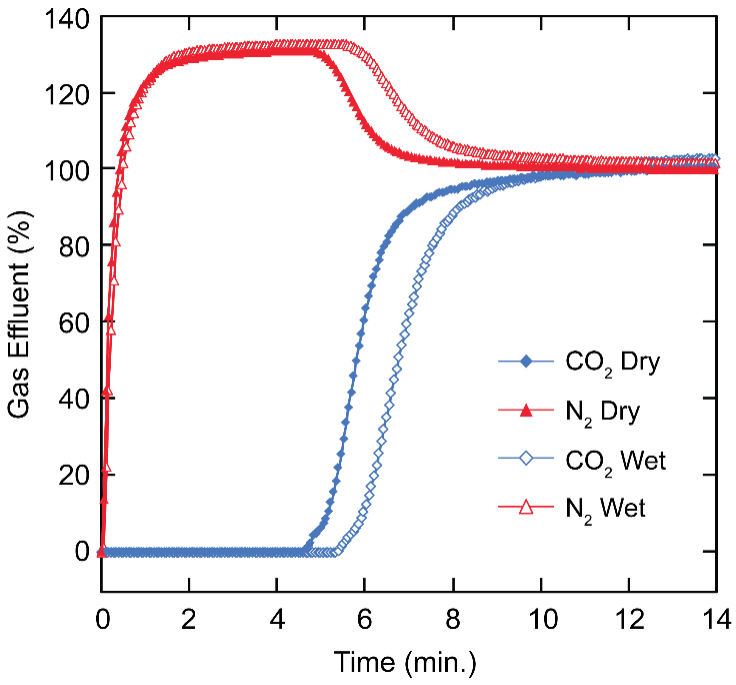

Figure 28 Dynamic breakthrough measurements demonstrating the ability of KFUPM-1 to separate CO_2 from N_2 under both wet and dry conditions. A 20:80 (*v*/*v*) gas mixture containing CO_2 and N_2, respectively, under dry (closed symbols) or wet (91% RH, open symbols) conditions was flown through a fixed bed of KFUPM-1 at 298 K and 1 bar.

Although these results represent initial promise for KFUPM-1, a critical parameter remains untested. In flue gas, water is the third major component by volumetric concentration (5-7%)[19]. As such, porous materials typically experience difficulty in selectively capturing CO_2 in the presence of water since competitive adsorption readily occurs[87]. This results in decreased CO_2 uptake capacity and/or a lack of long-term stability and recyclability of the material. Porous materials such as MOFs[88], zeolitic imidazolate frameworks (ZIFs)[89], and copper silicates[90] have made great strides in capturing CO_2 in the presence of water; however, there remain very few reports of porous polymers that have been investigated for this property[27–29], [59]. Given KFUPM-1's initial breakthrough results under dry conditions in conjunction with its water stability, we examined the material's ability to separate CO_2 from N_2 in the presence of water. Accordingly, KFUPM-1 was exposed to a ternary gas mixture containing CO_2 (20% *v*/*v*), N_2 (80% *v*/*v*), and H_2O (91% RH).

As shown in Figure 28, KFUPM-1 was again able to selectively retain CO_2 (blue open diamonds) while N_2 (red open triangles) passed through unencumbered. The longer CO_2 retention time (5.29 min) under wet conditions was not unexpected as KFUPM-1 adsorbs ~33.5 wt% water at 91% RH, which leads to stronger interactions with CO_2. Indeed, this longer retention time has been observed in other systems[88, 90].

The resulting dynamic CO_2 uptake capacity from the ternary gas mixture ($CO_2/N_2/H_2O$) was calculated to be 9.5 $cm^3\ g^{-1}$. For implementation in an industrial setting, an adsorbent material's long-term use and recyclability, without loss in performance, is a critical factor that must be considered. Accordingly, we carried out a multicycle continuous breakthrough

measurement (>45 cycles) at 298 K (Figure 5). For each cycle of this experiment, KFUPM-1 was first exposed to a wet N_2 stream (91% RH) until water saturation was detected. At the point of saturation, a dry stream of CO_2 (20% *v*/*v*) was then added to the wet N_2 stream and the effluent was monitored for the breakthrough time. KFUPM-1 exhibited an exceptional stability and recyclability over the course of the multicycle measurements. Although the breakthrough time exhibited non-negligible fluctuation over the course of these cycles, the performance (*i.e.* dynamic CO_2 uptake capacity as measured by breakthrough time) remained relatively unchanged (15 cm^3 g^{-1}) when comparing the 2nd and the 45th cycles (Figure 29).

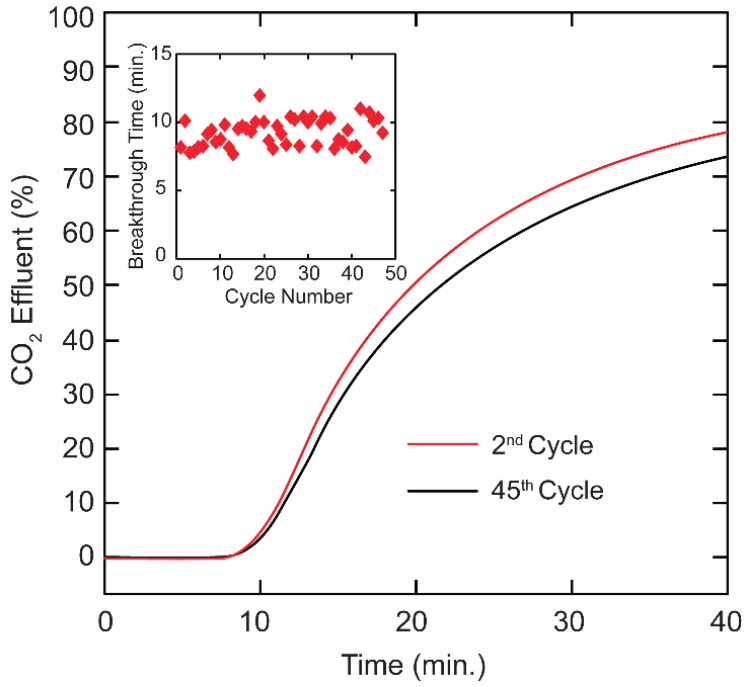

Figure 29 Long-term recyclability performance of KFUPM-1 as demonstrated by CO_2 breakthrough measurements under wet conditions. There is no loss in dynamic adsorption capacity over 45 consecutive breakthrough measurements. Inset: The breakthrough time as a function of the cycle number.

It is important to note that between each cycle, KFUPM-1 was regenerated by simply flowing a wet N_2 stream through the material at 298 K. From an energy cost standpoint,

this regeneration procedure represents a remarkably attractive feature for using KFUPM-1 as an adsorbent for the selective capture of CO_2 from real flue gas mixtures.

Table 3 Surface area, CO_2 capture properties, and CO_2/N_2 selectivity for KFUPM-1 in comparison with high performing, similarly related polymeric materials. KFUPM-1 represents one of the highest performing materials among all porous organic materials applied toward the selective capture of CO_2 in the presence of water.

Material	A_{BET} ($m^2\ g^{-1}$)	CO_2 Uptake ($cm^3\ g^{-1}$)[a]	CO_2/N_2 Selectivity[b]	Dynamic CO_2 Uptake Capacity - **Wet** ($cm^3\ g^{-1}$)[c]	Regeneration Temperature (K)	Ref.
KFUPM-1	305	23.4	141	15.1	298	This work
CTF-FUM-350	230	57.2	102	—	—	[84]
CTF-DCN-500	735	38.4	37	—	—	[84]
LZU-301	654	35.6	—	8.2	373	[86]
$[HO_2C]_{100\%}$-H_2P-COF	364	76	77[d]	—	353[e]	[47]
FCTF-1	662	72	31[d]	14.2	298[f]	[28]
TB-COP-1	1340	70.7	68[d]	—	—	[92]
BPL Carbon	1210	47	—	4.2	—	[89]
Azo-COP-1	635	32	96[d]	—	298	[71]
NUT-6	1138	83.5	338[d]	—	333	[93]
NUT-10	100[g]	40.2	159[d]	—	333	[94]
PPN-6-SO_3NH_4	593	81	196	25.8[h]	363	[95]

[a]At 298 K and 760 Torr. [b]Calculated from single component isotherms by Henry's law. [c]Calculated from dynamic breakthrough experiments. [d]Calculated by Ideal Adsorbed Solution Theory at 298 K and 1 bar. [e]Regeneration temperature needed for dry breakthrough experiment. [f]Regenerated under vacuum. [g]measured by CO_2 adsorption at 273 K. [f]At 313 K. Those properties that were not reported are identified with '—'.

CHAPTER FOUR

PHENOTHIAZINE-PYRROLE CROSSLINKED POLYMER

4.1 Introduction

Defining the problems that are faced in the CO_2 capture and treatment industry, the most dramatic effect in losing the adsorption properties is contamination by water; as it binds effectively to the active sites in the adsorbing material. In our endeavor to solve this problem we synthesized a porous organic polymer (KFUPM-1) that showed stability under humid conditions (91% relative humidity) and the polymeric material was stable and recyclable for several times without the loss of activity; but satisfactory results in the dynamic capacity under humid conditions of 15.1 cm^3 g^{-1}[96]. In order to enhance the effectiveness of the dynamic capacity; a new porous cross-linked polymer termed KFUPM-2 was synthesized. The new porous organic polymer was synthesized by a one-pot in situ polymerization of phenothiazine, pyrrole and p-formaldehyde as a linker in the presences of iron (III) chloride as a catalyst.

4.2 Experimental section

Materials and Methods.

Pyrrole (98% purity), methanol (99.9% purity), *N,N'*-dimethylformamide (99% purity), were purchased from Sigma Aldrich Co. Anhydrous iron(III) chloride (≥99.99% purity) was obtained from Alpha Chemika. Phenothiazine (98% purity), and Paraformaldehyde (≥99% purity) were purchased from Fluka. Ammonium hydroxide (28-30 *w*/*w*%) was

purchased from Fisher Scientific. All the chemicals were used without further purification unless pyrrole was distilled under N_2 flow at 145 °C prior to use. For gas sorption measurements, ultrahigh purity grade nitrogen (99.999%), helium (99.999%), and high purity CO_2 (99.9%) were obtained from Abdullah Hashem Industrial Co., Dammam, Saudi Arabia.

Synthesis of KFUPM-2.

Phenothiazine (0.40 g, 2.00 mmol) and p-formaldehyde (0.36 g, 12.0 mmol) were dissolved in 20 mL DMF in a 50 mL round bottom flask and stirred at room temperature for 5 min. Then, pyrrole (0.40 g, 6.00 mmol) was added and the reaction mixture was stirred for an additional 5 min. and purged with N_2 for 2-3 min. At this time, ferric chloride ($FeCl_3$, 0.194 g, 1.20 mmol) was added under inert atmosphere and the flask was sealed with a rubber septum. The reaction was heated by a preheated oil bath at 90 °C and continuously stirred for 24 h with a rate of 500 rpm (a black solid was formed after 10 min). The resulting solid was washed with 20 mL of methanol followed by sonication for 30 min. The solid was then rigorously washed with 30 mL of methanol two times per day for 5 days with stirring until a clear filtrate solution was obtained. Finally, the product was dried at 80 °C in an oven for 12 h. The final yield (0.87 g) was 92% based on the monomer weights (after excluding the equivalent amount of water as a by-product). EA: Found C, 51.47, H 3.24, N 10.07, S 1.79; FT-IR (KBr, cm-1) 3430 (br), 2920 (w), 2860 (w), 1620 (w), 1410 (w), 1020 (w) and 747 (w).

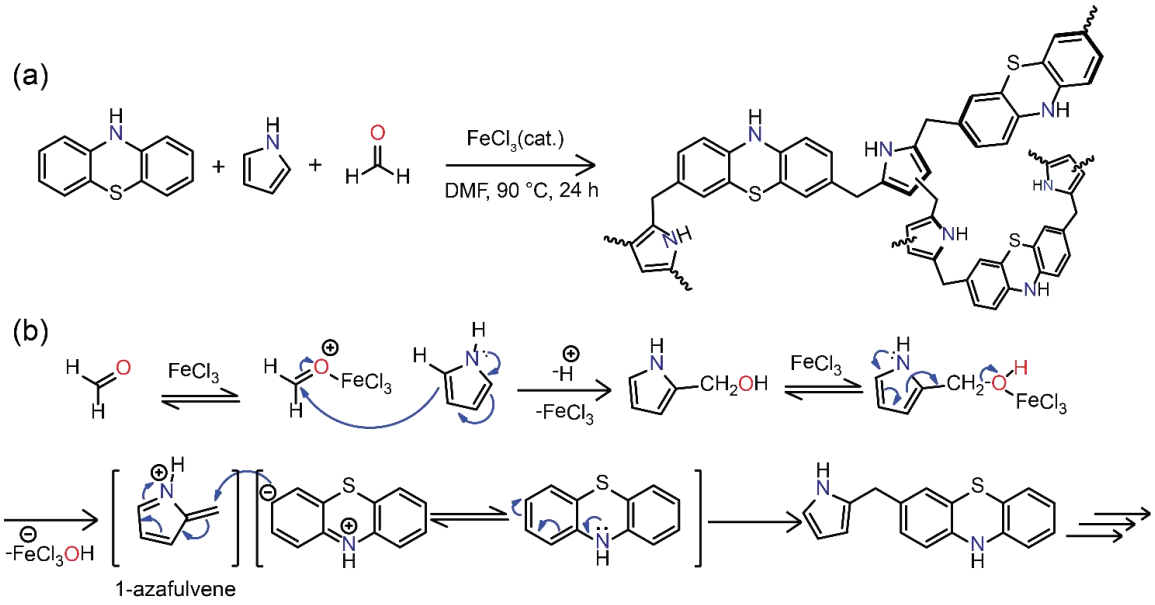

Scheme 13 (a) Synthesis of KFUPM-2. (b) Proposed mechanism of Phenothiazine-pyrrole methylene linkage formation.

Breakthrough measurements.

The schematic for the homemade breakthrough system set-up is shown in Figure 7. The bed was packed with KFUPM-2 powder (0.63 g) and the sample was activated at 373 K under vacuum for 24 hours prior to carrying out the breakthrough measurements. The breakthrough experiments were conducted under ambient conditions (298 K and 1 bar) with a 10 sccm flowrate of CO_2:N_2 (20:80 *v*/*v*) feed mixture. For the measurements under humid conditions, the sample bed was subjected to a stream of wet N_2 gas (91% relative humidity, RH), in which the water level in the gas stream was monitored until saturation was obtained as detected by mass spectrometry. At this point, dry CO_2 was introduced into the wet N_2 stream with the same flow rate as the dry conditions noted above. The full breakthrough capacity of CO_2 was measured by evaluating the ratio of compositions of the

downstream gas and the feed gas. The regeneration of the sample was done by the flow of pure wet N_2 through the sample bed at room temperature for 5-6 h.

4.3 Characterization

Solid state ^{13}C nuclear magnetic resonance (NMR) spectroscopy measurements were measured on a Bruker 400 MHz spectrometer operating at 125.65 MHz (11.74 T) and at ambient temperature (298 K). Samples were packed into 4 mm ZrO_2 rotors and cross-polarization magic angle spinning (CP-MAS) was employed with a magic angle spinning rate of 14 kHz. Fourier transform infrared (FT-IR) spectroscopy measurements were performed on a PerkinElmer 16 PC spectrometer from KBr pellets. The spectra were recorded over 4000 – 600 cm^{-1} in transmission mode and the output signals were described as follows: s, strong; m, medium; w, weak; and br, broad. CHN analysis was carried out at PerkinElmer (EA-2400) elemental analyzer. Thermal gravimetric analysis (TGA) was run on a TA Q-500 instrument with a platinum pan sample holder under. About 10 mg of sample were heated under air flow with heating rate 10 °C per min. Powder X-ray diffraction (PXRD) measurements were recorded on a Rigaku MiniFlex II X-ray diffractometer with Cu K_α radiation (λ = 1.54178 Å). Low-pressure nitrogen sorption isotherms were undertaken using a Quantachrome QUADRASOROB *evo* instrument. A liquid nitrogen bath was used for the measurements at 77 K. CO_2 sorption isotherms were measured on an Autosorb iQ2 volumetric gas adsorption analyser. The measurement temperatures at 273 and 298 K were controlled with a water circulator.

4.4 Results and Discussion

4.4.1 Synthesis strategy

The synthetic approach for synthesizing a new, CO_2-philic, microporous polymer relied on a modified Friedel-Crafts alkylation polymerization[55]. Phenothiazine and pyrrole were chosen as monomers due to their polar structures – an important consideration for increasing the affinity of CO_2 to the backbone of the resulting polymer. For the polymerization reaction, phenothiazine and pyrrole were dissolved in *N*,*N*'-dimethylformamide (DMF) in a molar ratio of 1:3. The molar ratio of these monomers was initially varied and, ultimately, it was found that the 1:3 ratio was optimal for producing the polymer with the highest surface area. DMF was chosen due to its high boiling point (153 °C) and its solvation ability, both of which proved important for this polymerization. An excess of crosslinking agent, *p*-formaldehyde, was also added together with $FeCl_3$ catalyst (chosen for its strong Lewis acidity). The reaction mixture was stirred and heated to 90 °C under an inert atmosphere for 24 h. It is noted that the polymerization occurred very rapidly with a black, insoluble solid precipitating within 10 min, however, we found that allowing the reaction to proceed for a longer period of time led to consistently higher yields and higher resulting surface areas, presumably due to thermal rearrangement of the polymer. After 24 h, the resulting polymer, termed KFUPM-2, was obtained in a 92% yield (Figure 1a). To ensure reproducibility, the synthesis of KFUPM-2 was repeated over four separate batches, in which case, each batch produced the same yield, surface area, and CO_2 uptake capacity. The formation of KFUPM-2 occurs via the following proposed mechanism: *p*-formaldehyde is first activated by the $FeCl_3$ catalyst, which, in turn, leads to an electrophilic aromatic substitution with the α-carbon of a pyrrole monomer. This forms

a primary alcohol that serves as the precursor to the eventual methylene crosslinking unit (Figure 1b). Upon activation, the primary alcohol leaves to yield the resonance-stabilized 1-azafulvene intermediate. Through a second electrophilic aromatic substitution process, the intermediate is added to a phenothiazine monomer at the γ-carbon closest to sulfur (this is due to the electron-donating nature of the nitrogen atom in phenothiazine). Indeed, this step is critical in that the two monomers are now crosslinked together. The overall addition-elimination reaction then proceeds until all of the monomers are essentially consumed.

4.4.2 Structural characterization.

Solid-State Nuclear Magnetic Resonance (^{13}C-NMR)

The resulting polymer product were structurally characterized using the combined data from solid state ^{13}C NMR, FT-IR a s well as elemental analysis. Elemental analysis of the KFUPM-2 polymer showed a deviation from the expected values which is can be attributed to incomplete combustion during the analysis, trapped adsorbate species (*i.e.* gases and water vapors), as well as irregularities of the polymer structure itself and this behavior are found in other reported porous polymers[53,96,97].

The ^{13}C NMR spectra Figure 30 shows the characteristic peaks that elucidate the connectivity between the phenothiazine and pyrrole moieties and as a direct prove for formation of the copolymer. Peak at 25 ppm assigned to the CH_2 (aliphatic C 1, 2&3) connected to the pyrrole rings and the pyrrole and phenothiazine rings respectively, peaks at 108 ppm assigned to aromatic carbons (4, 5 & 6) while characteristic peak centered at 120 ppm assigned for the aromatic C atom 7 of the phenothiazine. Peak centered at 130 ppm assigned for the aromatic C atoms (8, 9,

10 &11) form the alpha position of the N atom for the pyrrole, while shoulder peak at 140 ppm assigned for the aromatic C atom 13 of the phenothiazine, this considered as an evidence for incorporating of the two monomers into the final polymer networks.

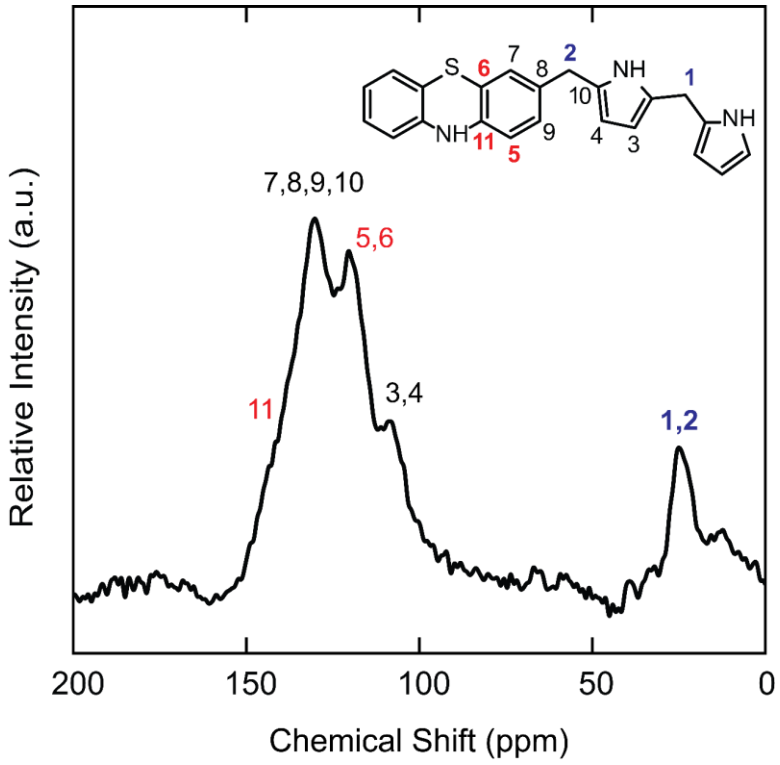

Figure 30. Cross polarization-magic angle spinning solid state nuclear magnetic resonance (CP-MAS ^{13}C-NMR) spectrum at 14 KHz, with the corresponding peak assignments. Inset: The core structure of KFUPM-2 fragment is provided for peak assignment.

Fourier Transform Infrared Spectroscopy (FTIR)

To further support the ^{13}C NMR data, FT-IR spectra were collected for the pure pyrrole and phenothiazine monomers as well as for KFUPM-2 (Figure 31). The FT-IR spectra of KFUPM-2 show absorption bands ~3413 cm^{-1} attributed to the –NH- stretching vibration present in pyrrole and phenothiazine. The absorption bands ~ 2918 cm^{-1} assigned to the methylene -CH stretch specific for CH_2 linkage between the pyrrole and phenothiazine moieties. The -C=C- absorption bands ~1600 cm^{-1} are

assigned to the aromatic rings present in pyrrole and phenothiazine moieties. The –C-S-C- absorption band ~690 cm^{-1} found in the phenothiazine moiety.

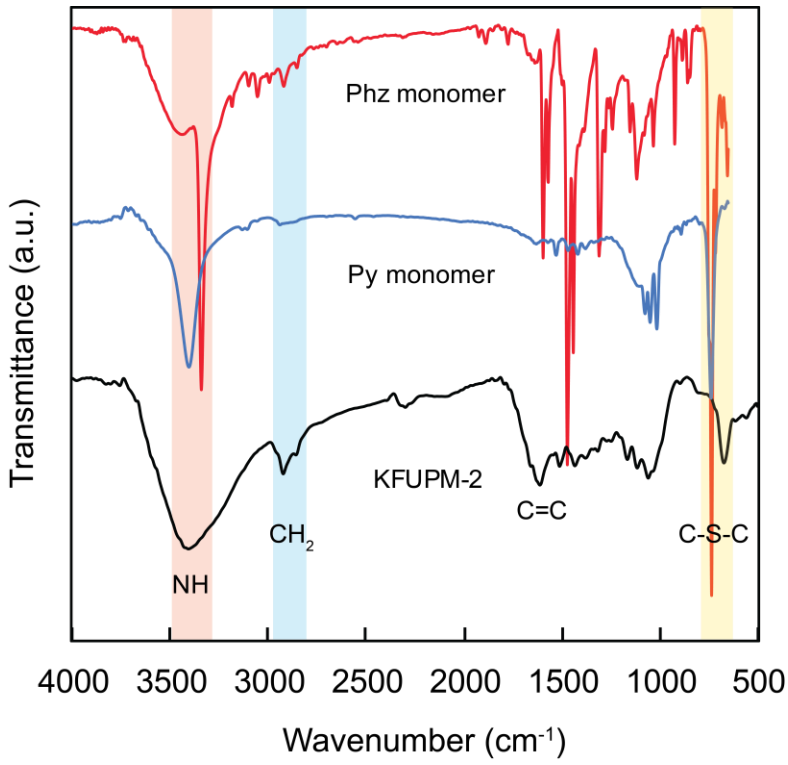

Figure 31 Fourier transform-infrared spectroscopy (FT-IR) analysis of KFUPM-2 (black) in comparison to pure phenothiazine (red) and pure pyrrole (blue). Those absorption bands directly related to the characteristic functionalities of KFUPM-1 are highlighted.

Elemental composition

Elemental analysis of the KFUPM-2 polymer was carried out in order to support the structural composition of the polymers. Its noted that chemical formulation of porous polymers by elemental analysis is notoriously difficult. The deviation between theoretical and experimental values are observed in our samples, and this can be attributed to incomplete combustion during analysis, trapped adsorbate species (*i.e.* gases and water vapors), as well as irregularity of the polymer structure itself and this behavior, is found in other reported porous polymers[53,96,97].

Thermal Gravimetric Analysis (TGA)

The thermal stability of KFUPM-2 polymer was examined by TGA measurement in air. The TGA of the polymer (Figure 32) reveals that the KFUPM-2 show a sharp weight loss around 500 °C, indicating high thermal stability of the polymer networks. The first derivative of weight loss with the temperature confirms that the polymer has one decomposition peak around 500 °C, that also may reflect the homogeneity of the structural connectivity between the two monomers (C-C bond is the main connection between the monomers and no or very less connection through the NH of the phenothiazine).

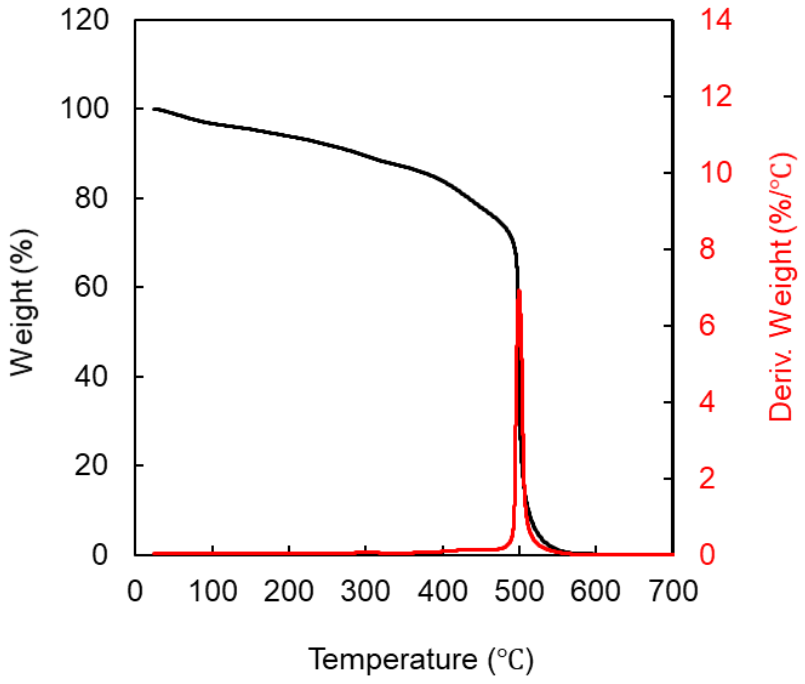

Figure 32 Thermogravimetric analysis of the KFUPM-2 polymer network, measured under air (black) and first derivative with the temperature (red).

Powder X-Ray Diffraction (PXRD)

Powder X-Ray Diffraction was done for all the polymers to evaluate the crystallinity of the materials. The data was obtained in the range of 5 to 40 degrees with a rate of 2 degrees/min. From the data obtained and presented in (Figure 33), it can be clearly stated that all the synthesized polymer is amorphous in nature.

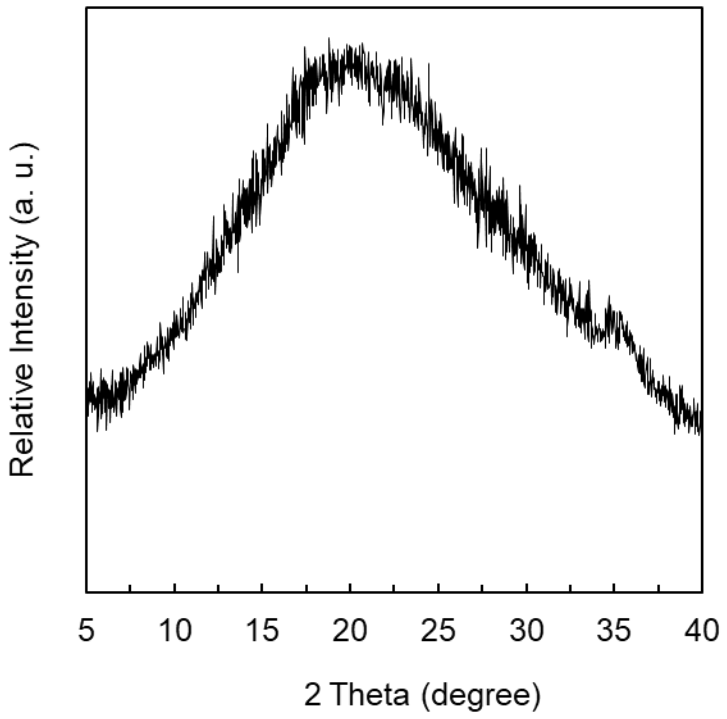

Figure 33 Powder X-ray diffraction of KFUPM-2.

4.4.3 Textural properties and Porosity characterization

The textural and surface properties of KFUPM-2 were determined by N_2 sorption measurements at 77 K (Figure 34A). From the figure, a sharp uptake at low relative pressure (P/P_0 < 0.001) indicates the predominance of a microporous nature of Type I isotherm according to the IUPAC classification[26,76]. The isotherm for KFUPM-2 showed hysteresis during the desorption which could be attributed to the elastic

deformation or swelling of the polymeric network[81]. The BET surface area (at P/P_0 = 0.01-0.3) of KFUPM-2 was found to be 352 $m^2 g^{-1}$. The pore size distribution was calculated using QSDFT models (Figure 34B) confirms the micropore nature of the KFUPM-2.

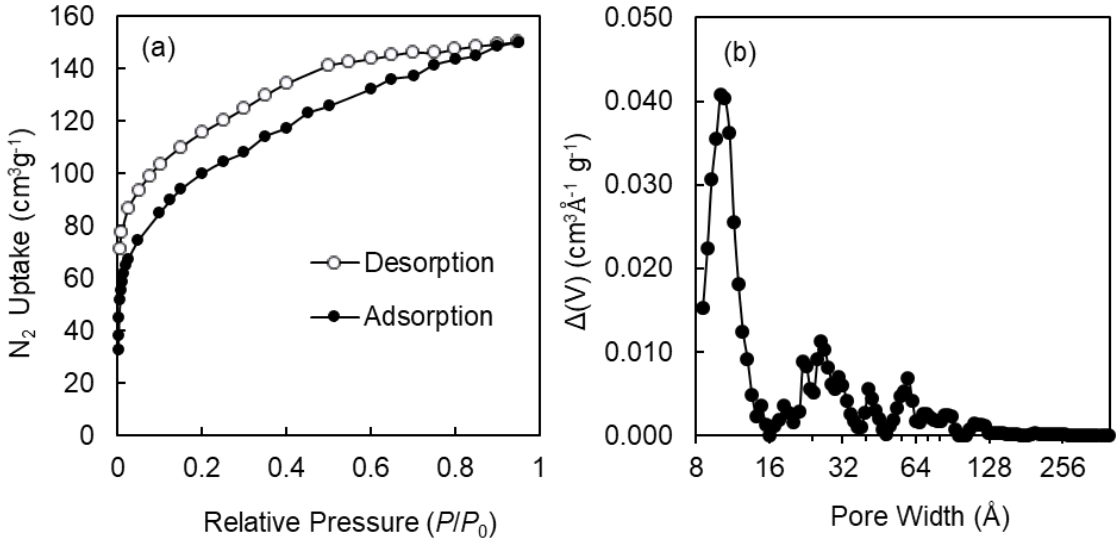

Figure 34 (a) N_2 isotherms measured at 77 K, Full symbols characterize adsorption isotherms, hollow symbols the corresponding desorption curve, (b) pore size distributions calculated by QSDFT adsorption branch kernel for slit, cylindrical, and sphere pores in carbon-based materials.

4.4.4 Gas Adsorption Studies

Our strategy for evaluating KFUPM-2 for use in post-combustion CO_2 capture centered on understanding four key properties: (i) thermodynamic CO_2 uptake capacity; (ii) coverage-dependent enthalpy of adsorption to understand the material's affinity toward CO_2; (iii) selectivity of KFUPM-2 towards CO_2 over N_2; and (iv) dynamic adsorption capacity, via breakthrough measurements, under both dry and wet conditions.

Thermodynamic Uptake Capacity. It is well understood through previous reports, that the ability of a material to capture CO_2 effectively depends not only on the surface area or pore nature, but also the internal pore environment through its density of polarizable sites. The

CO_2 capture properties of many microporous organic polymers were investigated[11,64,98–101]. Thus, the combination of advantageous properties found in KFUPM-2 (*e.g.* intrinsic microporosity and nitrogen-enriched backbone) provided justification for testing this material's CO_2 adsorption properties. Accordingly, the thermodynamic gas adsorption properties were assessed for the KFUPM-2 polymer at 273 and 298 K (Figure 35). The isotherms exhibit a reversible adsorption and desorption with small hysteresis indicating larger interaction of the CO_2 with material. KFUPM-2 exhibited high CO_2 uptake capacity of 39.1 $cm^3\ g^{-1}$ at 273 K and 760 Torr and 23.3 $cm^3\ g^{-1}$ at 298K and 760 Torr. While low N_2 uptake capacities was found under the same conditions (5.1 and 1.0 $cm^3\ g^{-1}$ at 273 and 298 K, respectively, and 760 Torr). It clearly seen that the initial slopes of the CO_2 isotherms were sharper than that of the N_2, reflecting the higher affinity of the material toward CO_2 compared to the N_2, which advance the potential use of KFUPM-2 as an adsorbent for selective CO_2 capture from flue gas. The CO_2 uptake capacity of KFUPM-2 at 273 K is comparable of or higher than those of reported crystalline covalent frameworks COFs (COF-1 51.9 $cm^3\ g^{-1}$, COF-5 29.9 $cm^3\ g^{-1}$, COF-8 32.0 $cm^3\ g^{-1}$,and COF-10 27.0 $cm^3\ g^{-1}$)[45] and comparable with other porous organic polymers such as NUT-1 (36.8 $cm^3\ g^{-1}$)[94], CMP-1 (29.6 $cm^3\ g^{-1}$)[10], and PPN-6-CH_2Cl (28.6 $cm^3\ g^{-1}$)[83].

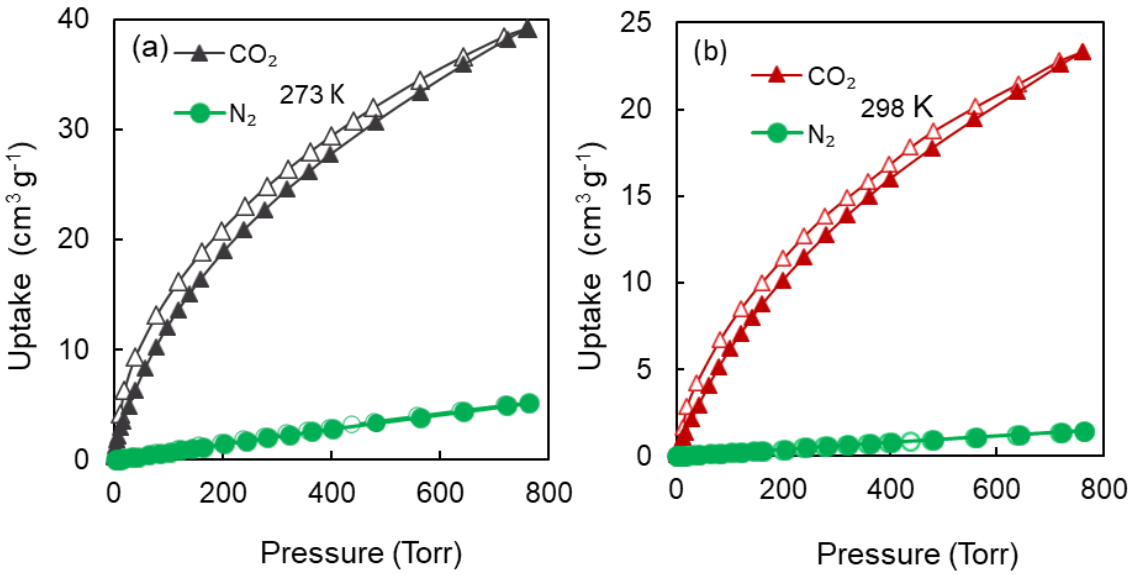

Figure 35 (a) and (b) Gas adsorption properties, CO_2 (green triangle) and N_2 (red circle) adsorption isotherms for KFUPM-2 at 273 and 298 K respectively. Filled and open symbols represent adsorption and desorption branches, respectively. The connecting lines serve as a guide to the eye.

4.4.5 Coverage Dependent Enthalpy of Adsorption (Q_{st}) and CO_2/N_2 selectivity.

Coverage Dependent Enthalpy of Adsorption (Q_{st})

Coverage-Dependent Enthalpy of Adsorption and CO_2/N_2 Selectivity. With the thermodynamic uptake capacities in hand, we were encouraged to further pursue and understand the relationship of KFUPM-2 with CO_2. Accordingly, a virial-type expansion equation was employed to fit the CO_2 isotherms at 273 and 298 K in order to estimate the coverage-dependent enthalpy of adsorption (Q_{st}) (Figure 36). The resulting initial Q_{st} value was calculated to be 34 kJ mol^{-1}, which quantifiably reflects the strong binding affinity of KFUPM-2 material to CO_2. It is observed that the Q_{st} decreases as the CO_2 uptake increases due to the occupying of the CO_2 active sites. The Q_{st} value is moderately high for physisorption-driven materials as compared to the related materials: BILP-1 (26.5 kJ mol^{-1})[82], Azo-COP-1 (29.3 kJ mol^{-1})[71], and PAF-1 (15.6 kJ mol^{-1})[79]. With these results, the high Q_{st} values comes in the favorable range for strong enough and reversible adsorption-desorption for efficient CO_2 separation, which lands squarely in the physisorption range.[24],[74] This clearly indicates that KFUPM-2 works as physisorption material and can be simply regenerated at mild conditions. The CO_2/N_2 selectivity of the KFUPM-2 was then estimated using Ideal Adsorption Solution Theory (IAST) model. KFUPM-2 shows remarkably good CO_2/N_2 of 64 for the mixture 20% CO_2 and 80% N_2 at pressures varying from 0 to 1 atm (Figure 37), that is comparable with other porous organic polymers (Table 5).

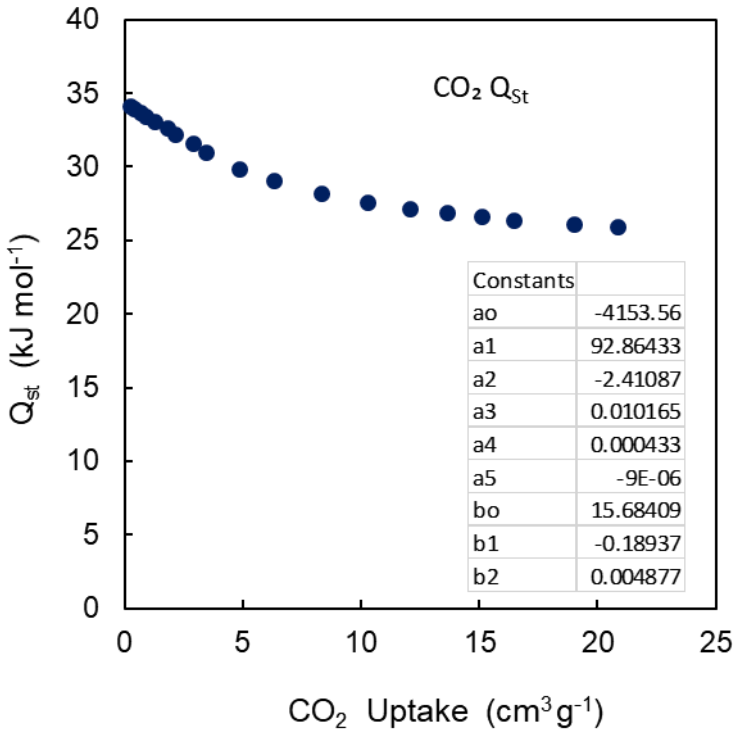

Figure 36 Calculated enthalpy of adsorption (Q_{st}) of CO_2 gas for KFUPM-2. Inset provides the constants used for the fitting of 273 K and 298 K CO_2 adsorption isotherms using virial-type equation.

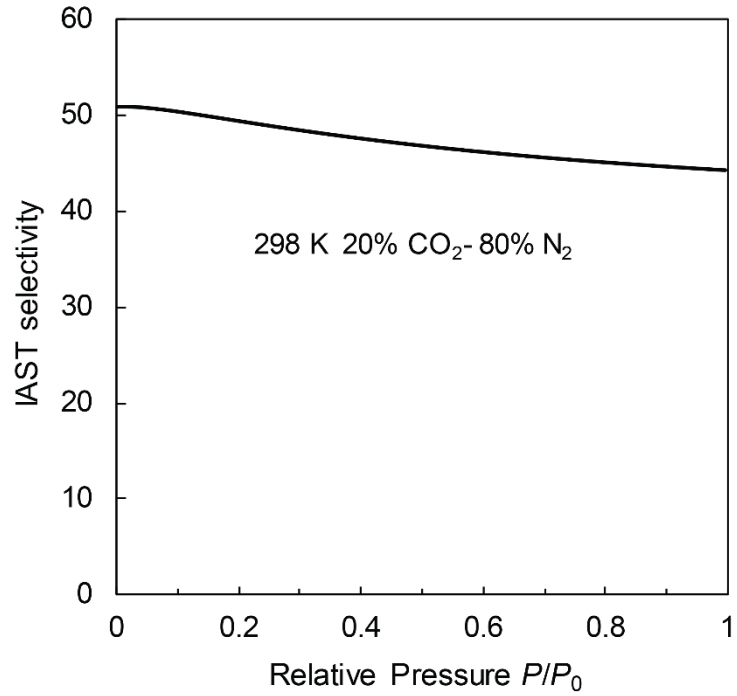

Figure 37 Ideal adsorption solution theory (IAST) calculated selectivity for KFUPM-2 at 298 K of binary mixture of 20% CO_2 and 80 % N_2.

4.4.6 Dynamic CO_2 Capture by Breakthrough Experiments

Given the thermodynamic (static) gas adsorption properties of KFUPM-2, we sought to assess the practical capability of this material for selectively capturing CO_2 from N_2 under both dry and wet conditions in a dynamic environment. The gold standard for assessing this is through a dynamic breakthrough measurement, in which an adsorbent material is exposed to a gaseous mixture and the effluent is monitored by mass spectrometry. Firstly, the activated dry sample of KFUPM-2 was subjected to dry gas mixture stream of 20% (*v*/*v*) CO_2 and 80% (*v*/*v*) N_2. The experimental breakthrough curves (Figure 38a) shows that CO_2 was retained while N_2 passed through the bed that clearly indicating the selectivity and affinity of KFUPM-2 polymer for CO_2 over N_2. The CO_2 capacity calculated from the respective breakthrough curve was estimated to be about 9.7 $cm^3\ g^{-1}$ for dry CO_2/N_2 mixture and this value are comparable with other porous polymers with higher surface area (CTF-FUM-350 & CTF-DCN-500 are 11.4 and 8.3 $cm^3\ g^{-1}$ respectively)[84] and greater than some other COFs (LZU-301, 4.9 $cm^3\ g^{-1}$)[86], and commercially BPL Carbon (6.0 $cm^3\ g^{-1}$)[103].

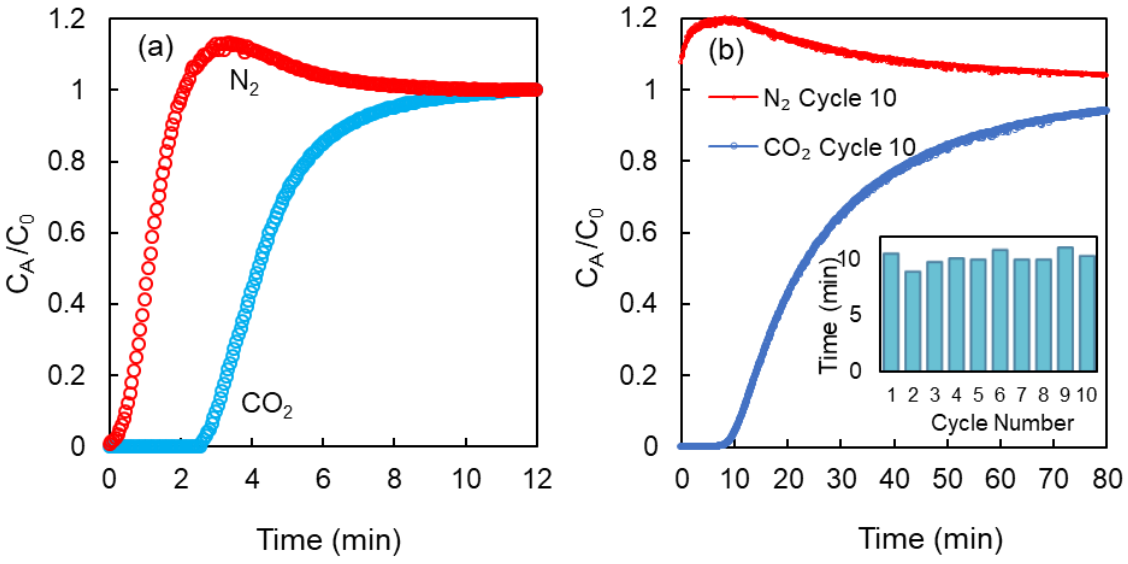

Figure 38 A 20:80 gas mixture containing CO_2 and N_2, respectively, was flown through a fixed bed of KFUPM-2 at 298 K and 1 bar (a) under dry conditions (b) under wet conditions (91% relative humidity). There is no loss in dynamic adsorption capacity over 10 consecutive breakthrough measurements (b and c).

Tanking in consideration that industrial flue gas contains significant amount of moisture (5-7%)[18], the sorbent materials should demonstrate their effectiveness to mitigate the effect of water. Accordingly, we tested the KFUPM-2 material for its stability and recyclability for separating CO_2 in presence of water through multicycle continuous breakthrough experiments (10 cycles) at 298 K. The KFUPM-2 material is exposed firstly to N_2 stream with 91% relative humidity (2.7 wt% as detected by the mass spectrometry) until saturation of the KFUPM-2 bed. At this point, a dry CO_2 stream is passed with the dual mixture (N_2 and H_2O) and this process was repeated for 10 cycles through which, the material showed an excellent recycling stability with the interesting improvement in CO_2 uptake (almost double in case of full wetted sample) (Figure 38), and this correlates to the increasing the CO_2 solubility in the wet condition, and this an important result to consider as many porous materials exhibited a significant decrease its CO_2 capacity in presence of water[103–107], while few examples retain their uptake else[108,109]. The KFUPM-2 material was regenerated under mild condition by the humid N_2 flow at ambient temperature. This regeneration process reflects the capability of the KFUPM-2 material for a pressure swing adsorption (PSA) which is used for industrial scale flue gas as energy efficient method.

Table 4. Dynamic CO_2 capture properties under wet conditions for KFUPM-2 in comparison with similarly related high-performing adsorbents.

Material	SA_{BET} ($m^2\ g^{-1}$)	CO_2 Uptake ($cm^3\ g^{-1}$)[a]	CO_2/N_2 Selectivity[b]	Dynamic CO_2 Uptake Capacity – Dry ($cm^3\ g^{-1}$)[c]	Dynamic CO_2 Uptake Capacity - **Wet** ($cm^3\ g^{-1}$)[c]	Regeneration Temp.	Ref.
KFUPM-2	352	23.3	64	9.7	32.2	298	This work
KFUPM-1	305	23.4	141	8.5	15.1	298	[96]
NUT-6	1138	83.5	338	—	—	333	[94]
NUT-10	100[d]	40.2	159	—	—	333	[93]
PAF-26-COOH	717	31.3	29	—	—	—	[111]
PPN-6-SO_3NH4	593	81	196	25.8[h]	—	363	[95]
CTF-FUM-350	230	57.2	102	11.4	—	—	[84]
CTF-DCN-500	735	38.4	37	8.3	—	—	[84]
LZU-301	654	35.6	—	4.9	8.2	373	[86]
[HO_2C]100%-H2P-COF	364	76	77	16.4	—	353[e]	[47]
FCTF-1	662	72	31	16.1	14.2	298[f]	[28]
Azo-COP-1	635	32	96	—	—	298	[71]
BPL Carbon	1210	47	—	6.0	4.2	—	[89]
Carbon Monolith (HCM-DAH-1)	670	58.2	28	20.9	20.3	298	[110]

[a]At 298 K and 760 Torr. [b]Calculated by Ideal Adsorbed Solution Theory at 298 K and 1 bar. [c]Calculated from dynamic breakthrough experiments. [d]Calculated from CO_2 isotherms at 273K, [e]Regenerated under vacuum. [f]At 313 K. Those properties that were not reported are identified with '—'.

CHAPTER FIVE

MELAMINE-PYRROLE CROSSLINKED POLYMER FOR CARBON DIOXIDE AND HYDROGEN SULFIDE REMOVAL FROM NATURAL GAS

5.1 Introduction

Selective removal of the acidic gases carbon dioxide and hydrogen sulfide from gas mixtures such as natural gas and syngas has attracted a great research interests due to the energy demand associated short-lived oil reserves and environmental concerns. In presence of water, H_2S will form an acidic solution causing corrosion of the storage tanks and pipelines. Furthermore, combustion of fuel gas containing H_2S will produce sulfur oxides, leading to environmental problems. The sweetening of the natural gas and syngas gas to reasonable pure components with needful specification for transport and storage necessitate the development of new complex technology for removal of CO_2 and H_2S.

The natural gas sweetening process mainly relied on the conventional energy consuming chemical absorption using liquid amine solution in a gas-liquid processes. Recently, adsorption-based separation on solid sorbents is supposed to be more energy effective and beneficial than the chemical absorption processes [4,111,112]. Metal-oxide sorbents is another commercial method used to selectively adsorb H_2S forming metal sulfides. A wide varieties of metal oxide had been used such as zinc oxides (ZnO)[114], ferric oxyhydroxides (FeOOH)[115], iron-zinc and iron-cobalt mixed oxides[116], and Ti-Zn based oxides[117], However these metal oxides sorbents require high regeneration temperatures (>400 °C) and cannot be used for simultaneous removal of CO_2 and H_2S.

Porous materials such as metal organic frameworks (MOFs) have been reported for selective capture of H_2S such as HKUST-1[118], MIL-53(Cr, Al)[118–120], Uio-66[122], Mg-MOF-74[122], Ce-BTC[122] and ZIF-8[122]. These materials have the ability to capture H_2S by physisorption mechanism, but with high temperature of regeneration (200 °C) while others like MIL-100(Cr)[120], MIL-53(Fe)[120], IRMOF-3[123], and MOF-5[122] have irreversible adsorption of H_2S forming metal-sulfide bonds leading to structure collapse and lack recyclability.

The development of new porous sorbents that can be more effective and selective for simultaneous CO_2 and H_2S capture is a promising practical solution. Moreover, the design of such sorbents that can resist the corrosion of H_2S (physical adsorption) and can be regenerated at ambient condition is challenge. In our recent work[96], we discover new hypercrosslinked organic porous polymers that can selectively capture CO_2 in presence of water with via physical adsorption mechanism and can be regenerated at room temperature due to their unique physicochemical stability that's inspire us to discover new porous organic polymer that can selectively capture both CO_2 and H_2S at ambient condition. To the best of our knowledge, no porous organic polymer was reported up to date for H_2S/CH_4 and $H_2S/CH_4/CO_2$ separations.

In addition to the synthesis and design of high surface area, narrow pores size distribution and low density microporous polymers, the presence of high nitrogen content within the polymer network is considered a good strategy to enhance carbon dioxide capture due to strengthen of the local dipole-quadrupole interactions between the acidic CO_2 molecules the basic amine groups of the polymer skeleton[53,100], similar trend due to the acid properties of H_2S using the same concept of introducing melamine **(M)** moieties in porous

polymers has attracted great interest due to its high basic nitrogen content that results in greater affinity to CO_2 molecules[123–125], but unfortunately, most of the reported melamine-based materials exhibited low surface area.

Herein, we report a strategy to introduce more rigidity within the melamine-formaldehyde networks using pyrrole (**Py**) as more rigid building block. The resulting copolymer **MPy** exhibited permanent microporosity (400 m^2 g^{-1}) and high affinity to CO_2 with excellent dynamic separation of CO_2 from N_2 under humid conditions (91% relative humidity) and more interestingly it can simultaneously capture CO_2 and H_2S with high capacity.

5.2 Experimental section

Materials and Methods.

Pyrrole (Py, 98% purity), melamine (M, 99% purity) and ammonium hydroxide (28-30 *w*/*w*%) were purchased from Alfa Aser. Methanol (99.9% purity), N,N-dimethylformamide (99% purity), and concentrated hydrochloric Acid (HCl, 37%) were purchased from Sigma Aldrich Co.. Paraformaldehyde (≥99% purity) was purchased from Fluka. All the chemicals were used without further purification unless pyrrole was distilled under N_2 flow at 145 °C prior to use. For gas sorption measurements, ultrahigh purity grade nitrogen (99.999%), helium (99.999%), methane (99.999%), and high purity CO_2 (99.99%) were obtained from Abdullah Hashem Industrial Co., Dammam, Saudi Arabia.

Synthesis of Melamine-Pyrrole (MPy) polymer.

Melamine (M, 1.26 g, 10.0 mmol) and *p*-formaldehyde (2.10 g, 70.0 mmol) were added with 50 mL DMF in a 125 mL round bottom flask and stirred at room temperature for 5 min. Then, pyrrole (2.00 g, 30.0 mmol) was added into the reaction mixture and stirred for an additional 5 min. Then hydrochloric acid chloride (HCl, 1.00 g, 10 mmol) was added and subsequently, the flask was sealed with a rubber septum. The flask was transferred into a preheated oil bath at 90 °C and continuously vigorously stirred for 24 h with a rate of 700 rpm (a black solid was formed after 5 min). The resulting solid was washed with 60 mL of methanol followed by sonication for 30 min. The solid was continuously washed with methanol for three days (3*100 mL, per day) with stirring at which time a clear filtrate solution was obtained. Then the solid was immersed in an ammonia solution (25% *w*/*w*) for 2 h, filtered, washed by 150 mL distilled water and then continue soaking in water (150 mL) for 24 h, after that solvent exchanged and washing by methanol for one day (3*100 mL) with stirring. Finally, the product was dried at 80 °C in an oven for 12 h. The final yield (4.34 g) was 99.5% based on the monomers weights (after excluding the equivalent amount of water as by product), over calculated yield may be due to the material not completely dry (hydrophilic material); EA: calculated C, 63.14, H 5.29, N 31.56, (C/N = 2.00); Found C, 48.24; H, 4.00; N, 23.34; (C/N = 2.06); FT-IR (KBr, cm^{-1}) 3406 (br), 3238 (br), 2918 (m), 2850 (w), 1624 (m), 1564 (m), 1466 (w), 1338 (w), 814 (m).

Yield calculation:

% yield = (experimental weight/ (total monomers weights-weight of the H_2O by product)) * 100

= 4.34 / (1.26 + 2.1+ 2.0 – (44 mmol * 18)) = 4.34/ 4.36 = 99.5%

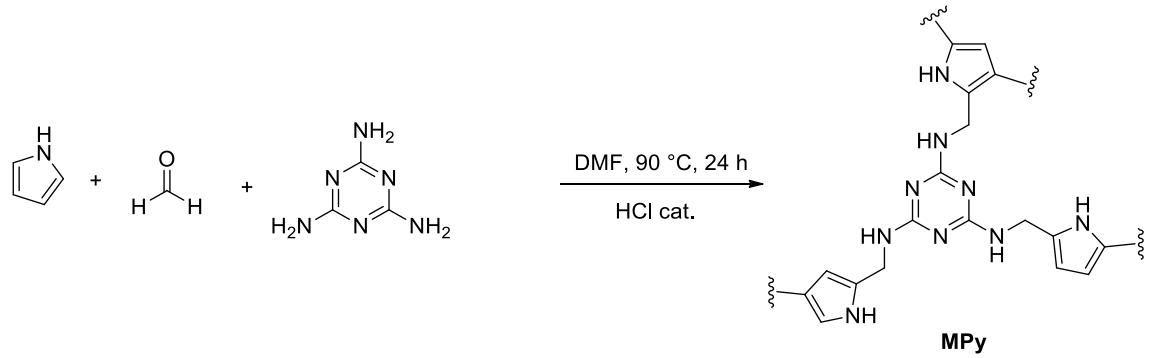

Scheme 14 General synthetic scheme of MPy copolymer.

Breakthrough measurements.

(A) Experimental procedure of breakthrough tests for CO_2/N_2 gas mixture.

The schematic for the homemade breakthrough system set-up is shown in Figure 7. The column was packed with MPy powder (1.0 g) and the sample was activated at 373 K under vacuum for 24 hours prior to carrying out the breakthrough measurements. The breakthrough experiments were conducted under ambient conditions (298 K and 1 bar) with a 10 sccm flowrate of CO_2:N_2 (20:80 *v*/*v*) feed mixture. For the measurements under humid conditions, the sample bed was subjected to a stream of wet N_2 gas (91% relative humidity, RH), in which the water level in the gas stream was monitored until saturation was obtained as detected by mass spectrometry. After that, dry CO_2 was introduced into the wet N_2 stream with the same flowrate as the dry conditions noted above. The full breakthrough capacity of CO_2 was measured by evaluating the ratio of compositions of the downstream gas and the feed gas. The regeneration of the sample was done by the flow of pure wet N_2 through the sample bed at room temperature for 5-6 h.

(B) Experimental procedure of breakthrough tests for H_2S gas mixtures.

The H_2S adsorption tests were performed at room temperature by packing the novel polymers into columns with an inner diameter of ~2 mm and length of 200 mm, as shown in the figure. The quartz was used in both column-ends to maintain the polymer inside the column. The gas containing 2% H_2S was passed through the column of adsorbent at 10 mL min^{-1}. The outlet H_2S was determined by gas chromatography. The excess of the gas was allowed to be adsorbed in NaOH solution for safety. The regeneration was performed using nitrogen gas which was flowed through the spent polymer at 60 °C.

5.3 Characterization

Solid state ^{13}C nuclear magnetic resonance (NMR) spectroscopy measurements were measured on a Bruker 400 MHz spectrometer operating at 125.65 MHz (11.74 T) and at ambient temperature (298 K). Samples were packed into 4 mm ZrO_2 rotors and cross-polarization magic angle spinning (CP-MAS) was employed with a magic angle spinning rate of 14 kHz. Fourier transform infrared (FT-IR) spectroscopy measurements were performed on a PerkinElmer 16 PC spectrometer from KBr pellets. The spectra were recorded over 4000 – 600 cm^{-1} in transmission mode and the output signals were described as follows: s, strong; m, medium; w, weak; and br, broad. CHN analysis was carried out at PerkinElmer (EA-2400) elemental analyzer. Thermal gravimetric analysis (TGA) was run on a TA Q-500 instrument with a platinum pan sample holder under. About 10 mg of sample were heated under air flow with heating rate 10 °C per min. Powder X-ray diffraction (PXRD) measurements were recorded on a Rigaku MiniFlex II X-ray diffractometer with Cu K_α radiation (λ = 1.54178 Å). Field emission scanning electron

microscope (FE-SEM) images were taken on a Tescan LYRA3 Dual Beam microscope at an acceleration voltage of 14 kV. Low-pressure nitrogen sorption isotherms were undertaken using a Quantachrome QUADRASOROB *evo* instrument. A liquid nitrogen bath was used for the measurements at 77 K. CO_2 sorption isotherms were measured on an Autosorb iQ2 volumetric gas adsorption analyser. The measurement temperatures at 273 and 298 K were controlled with a water circulator.

5.4 Results and Discussion

5.4.1 Synthesis strategy

This study was targeted to synthesize a nitrogen rich porous crosslinked polymer from inexpensive aromatic amines that can simultaneously selectively separate acidic gases (CO_2 and H_2S) from natural gas streams. As such, melamine unit with polar aromatic amine moieties (six nitrogen atoms compared to three carbons) was selected to be copolymerized with pyrrole in order to yield a final nitrogen-rich rigid porous network (known to have interaction with acid gases)[53], in addition to the fact that they are in expensive and commercially available. The polymer network was subsequently purified after the synthesis by washing with methanol and water to remove any unreacted starting materials. And after that, the synthesized polymer was dried at 65 °C for 12 h in a vacuum oven prior to use in any further characterization.

5.4.2 Structural characterization.

Solid-state Nuclear Magnetic Resonance (^{13}C-NMR)

The successful construction of the melamine-pyrrole copolymer was proved using a combination of the ^{13}C -solid state NMR and FT-IR spectroscopies as well as elemental analysis. Therefore, ^{13}C - NMR spectra (Figure 39) revealed the characteristic peaks for both melamine and pyrrole moieties crosslinked with the methylene group as follows; peak at δ = 26.7 ppm which can be assigned to the chemical shift of the aliphatic CH2 group linking two pyrrole moieties, peak centered at δ = 40.3 ppm was assigned to the chemical shift of CH2 between the α-carbon of the pyrrole and NH from the melamine, while, peak at δ = 51.6 ppm was assigned to the chemical shift of CH_2 linking the β-carbon of the pyrrole with the NH from the melamine, and additional lower intensity peak at δ = 60.4 ppm was assigned to the chemical shift of carbon of terminal CH_2-OH group from the formaldehyde. A broad peak at δ = 131.9 ppm was assigned to the chemical shift of the aromatic carbon atoms from the pyrrole. A sharp peak at δ = 165.3 ppm is characteristic chemical shift for the triazine ring of the melamine. The quantitative NMR of the peaks of the melamine and the pyrrole further confirms that both melamine and pyrrole incorporated quantitively as the designed precursors ratios.

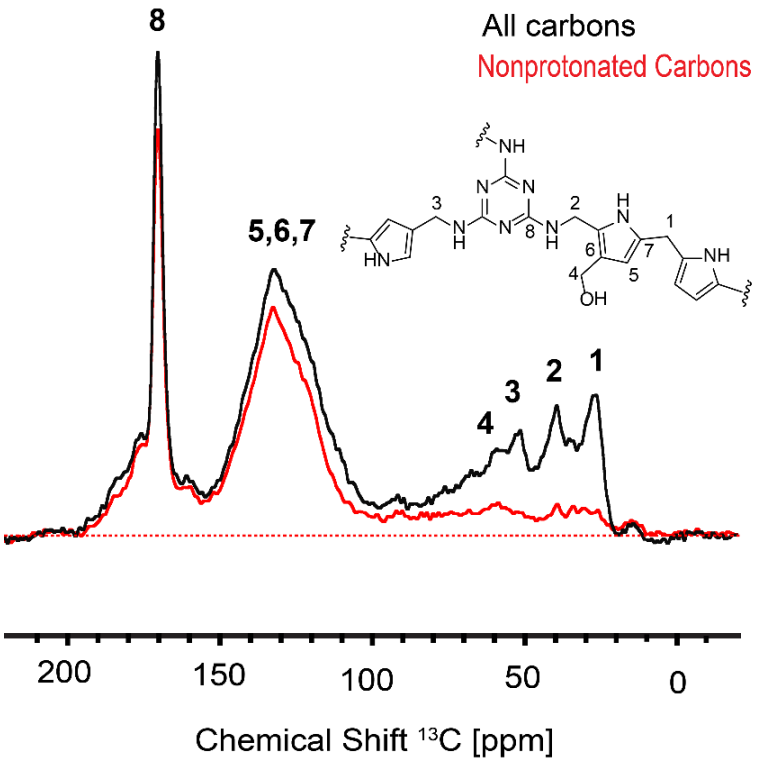

Figure 39 Cross polarization-magic angle spinning solid state nuclear magnetic resonance (CP-MAS ^{13}C-NMR) spectrum at 14 KHz, with the corresponding peak assignments. Inset: The core structure of MPy fragment is provided for peak assignment.

Fourier Transform Infrared Spectroscopy (FTIR)

To further support the ^{13}C NMR data, FT-IR spectra of the monomers and MPy polymers (Figure 40) is supporting the expected structure. The spectral band at 3406 cm^{-1} can be assigned to the stretching vibration of the N—H for both the pyrrole and of the MPy. The appearance of new bands around 2918 cm^{-1} assigned to methylene C-H stretch specific for CH_2 linkage not present in the melamine or the pyrrole monomers. Two strong bands at 1560 and 1336 cm^{-1} characteristic for the C-N stretching and breathing modes of melamine triazine ring, respectively. Furthermore, the C=C stretching vibrations at 1643 cm^{-1} are characteristic band for pyrrole.

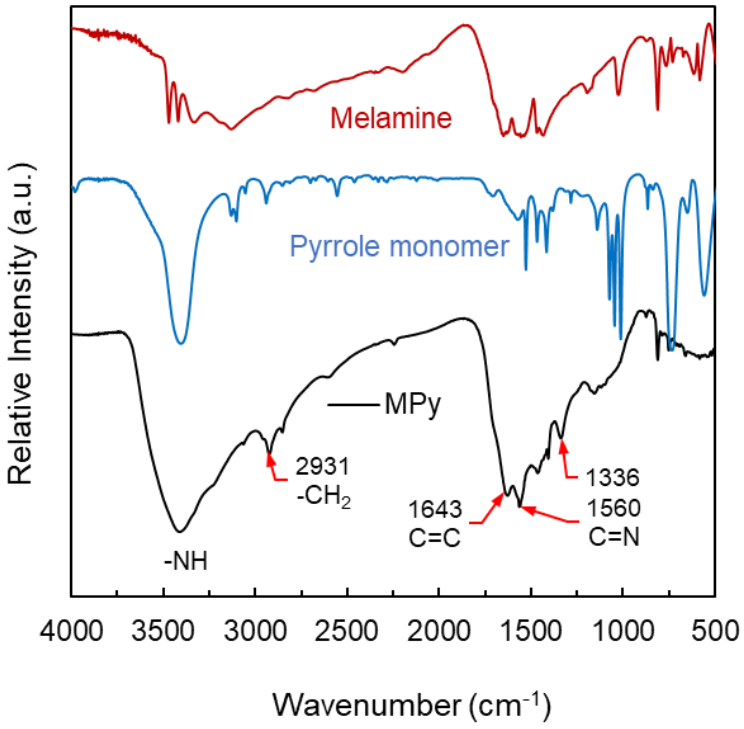

Figure 40 Fourier transform-infrared spectroscopy (FT-IR) analysis of MPy (black) in comparison to pure melamine (red) and pure pyrrole (blue). Those absorption bands directly related to the characteristic functionalities of MPy are highlighted.

Elemental composition

Elemental analysis of the MPy polymers was carried out to support the structural composition of the polymers. The mole C/N ratio of the synthesized MPy polymers is matching the theoretical values predicted from the precursors, with some deviation for the particular elemental analysis (EA: calculated C, 63.14, H 5.29, N 31.56, (C/N = 2.00); Found C, 48.24; H, 4.00; N, 23.34; (C/N=2.06)).This deviation between theoretical and experimental values can be attributed to incomplete combustion during analysis, trapped adsorbate species (*i.e.* gases and water vapors), as well as irregularity of the polymer structure itself and this behavior, is found in other reported porous polymers[53,96,97].

Thermal Gravimetric Analysis (TGA)

The thermal stability of the polymers was examined by TGA measurement under air flow. The TGA of the polymers (Figure 41) reveals that the MPy show a gradual weight loss after 220 °C, indicating high thermal stability of the polymer network. The first derivative (Δweight loss / Δtemperature) (DTG) was obtained from the TGA curves using the TA Instruments Thermal Solution Software package. The peak areas in the DTG curve related to the decomposition of specific chemical bond. The small beak before 220 °C can be attributed to the water molecules trapped in the pores of the MPy while the second sharp peak after 220 °C up to 335 °C can be reflecting the decomposition of the melamine - methylene ($NH\text{-}CH_2\text{-}$) linkage. In addition, the third peak at higher temperature above 330 °C was attributed to the decomposition of the aromatic rings of the pyrrole and melamine.

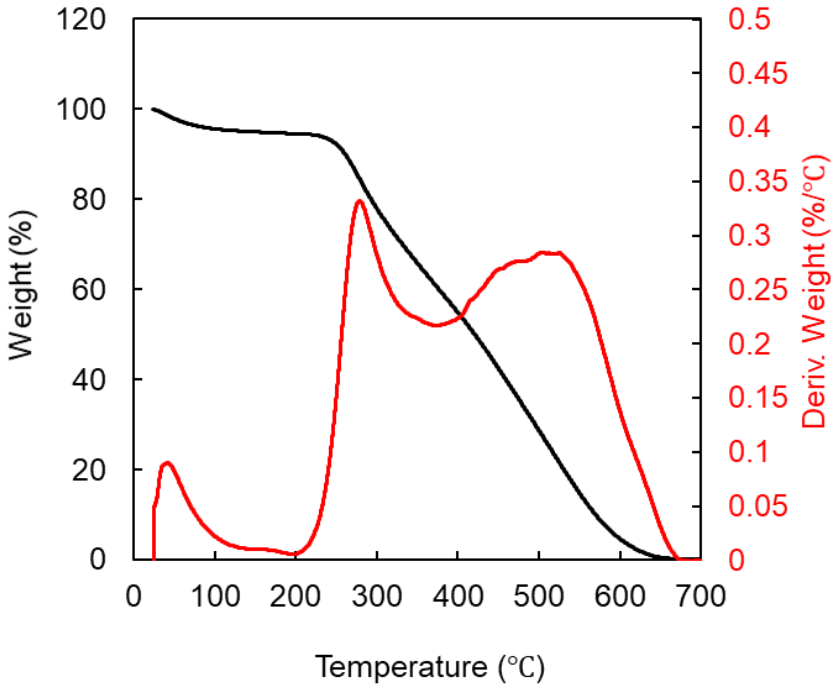

Figure 41 Thermogravimetric analysis of the MPy polymer network, measured under air (black) and first derivative with the temperature (red).

Powder X-Ray Diffraction (PXRD)

Powder X-ray diffraction was done for the polymer to evaluate the crystallinity of the materials. The data was obtained in the range of 5 to 40 degrees with a rate of 2 degrees/min. From the data obtained and presented in (Figure 42), it can be clearly stated that the synthesized polymer is amorphous in nature.

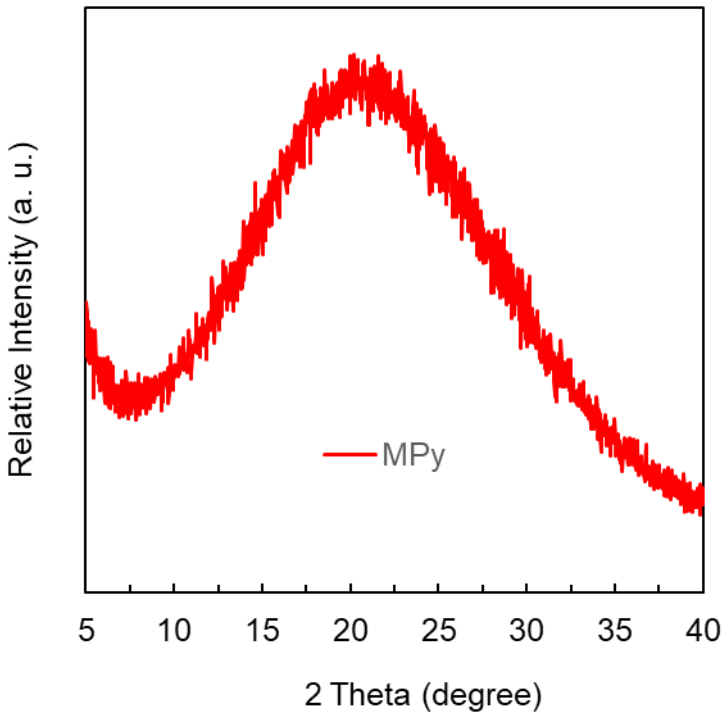

Figure 42 Powder X-ray diffraction of MPy.

5.4.3 Textural properties and Porosity characterization

The textural properties of the activated MPy polymer was determined from N_2 sorption measurements at 77 K (Figure 43A). The N_2 isotherms for polymer network shows a sharp uptake at low relative pressure ($P/P_0 < 0.001$) indicating the predominant microspore nature of the network that resembles Type-I isotherms according to the IUPAC classification[26, 76]. A steep rise in the uptake at higher relative pressure ($P/P_0 > 0.5$) indicating the capillary

condensation of N_2 molecules in a mesopores and the inter-particle condensation that is also in agreement with the pore size distribution curve (Figure 43B) shown the presence of micro and mesopores in the structure. The isotherm showed a hysteresis during the desorption up to the low pressure region as indication of elastic deformation or swelling after gas desorption[81]. The BET surface area (at P/P_0 = 0.01-0.3) is 399 $m^2 g^{-1}$.

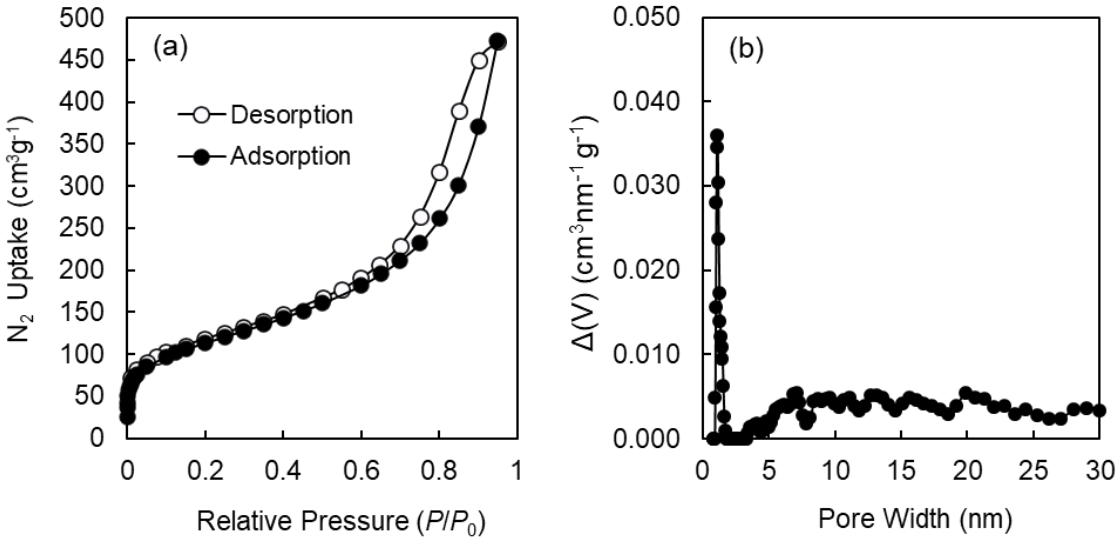

Figure 43 (a) N_2 isotherms measured at 77 K, Full symbols characterize adsorption isotherms, hollow symbols the corresponding desorption curve, (b) pore size distributions calculated by QSDFT adsorption branch kernel for slit, cylindrical, and sphere pores in carbon-based materials.

5.4.4 Gas Adsorption Studies

Thermodynamic Uptake Capacity. The nitrogen rich network on of synthesized crosslinked Mpy, good surface area and the intrinsic microporosity, encouraged us to test the materials for CO_2 capture and separation. Accordingly, the thermodynamic gas adsorption properties were assessed for the MPy polymer network at 273 and 298 K (Figure 44). The isotherms exhibit a reversible adsorption and desorption indicating the physical adsorption of the CO_2 with the material. MPy exhibited high CO_2 uptake capacity of 39.0 cm^3 g^{-1} at 273 K and 760 Torr and 26.0 cm^3 g^{-1} at 298K and 760 Torr. While low CH_4 and N_2 uptake capacities were found under the same experimental conditions to be for N_2 (1.8 and 1.6 cm^3 g^{-1} at 273

and 298 K, respectively, and 760 Torr) and for CH_4 (10.1 and 6.0 cm^3 g^{-1} at 273 and 298 K, respectively, and 760 Torr). It clearly seen that the initial slopes of the CO_2 isotherms were sharper than that of the N_2, reflecting the higher affinity of the material toward CO_2 compared to the N_2 and CH_4, which advance the potential use of MPy as an adsorbent for selective CO_2 capture from different gas streams. The CO_2 uptake capacity of MPy at 273 K is comparable of or higher than those of reported crystalline covalent frameworks COFs (COF-5 29.9 cm^3 g^{-1}, COF-8 32.0 cm^3 g^{-1},and COF-10 27.0 cm^3 g^{-1})[45] and comparable with other porous organic polymers such as KFUPM-1(36.8 cm^3 g^{-1}), NUT-1 (36.8 cm^3 g^{-1})[94], CMP-1 (29.6 cm^3 g^{-1})[10], and PPN-6-CH_2Cl (28.6 cm^3 g^{-1})[83].

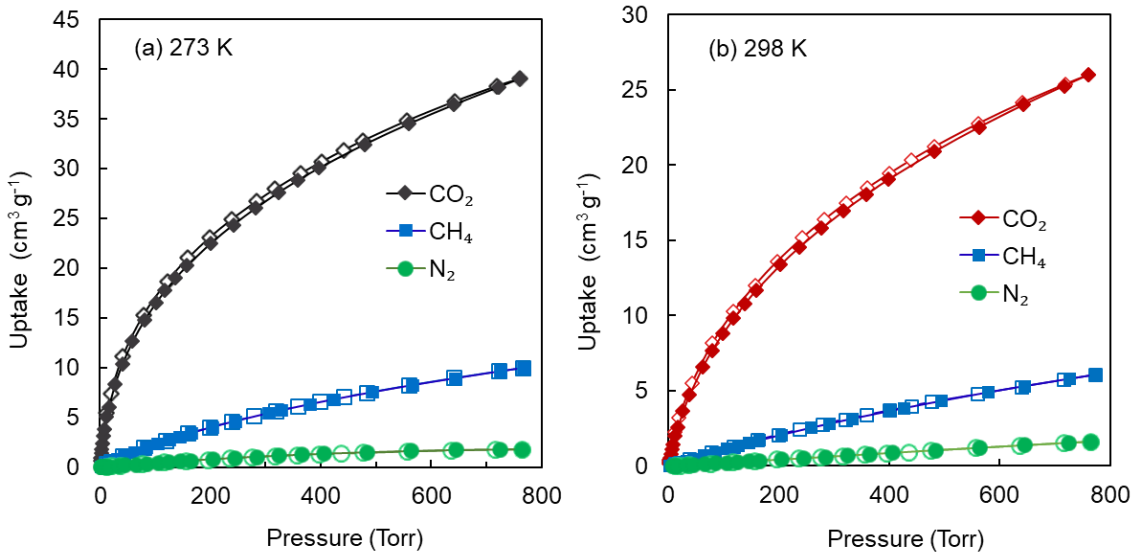

Figure 44 (a) and (b) Gas adsorption properties, CO_2 (blue triangle) and N_2 (red circle) adsorption isotherms for MPy at 273 and 298 K respectively. Filled and open symbols represent adsorption and desorption branches, respectively. The connecting lines serve as a guide to the eye.

5.4.5 Coverage Dependent Enthalpy of Adsorption (Q_{st}) and CO_2/N_2 selectivity.

Coverage Dependent Enthalpy of Adsorption (Q_{st})

Coverage-Dependent Enthalpy of Adsorption and CO_2/N_2 Selectivity. Encouraged with good the thermodynamic gas results, we pursued to better understand the interaction behavior of MPY with CO_2 gas and other gas mixture components. Therefore, the coverage-dependent enthalpy of adsorption (Q_{st}) for CO_2 and N_2 and CH_4 were estimated using the virial-type expansion equation to fit the isotherms collected at 273 and 298 K (Appendix C). Notably, the initial heat of adsorption at zero coverage for CO_2 was found to be 35 kJ mol^{-1}, whereas 22 and 17 kJ mol^{-1} for CH_4 and N_2, respectively, reflecting the material's strong affinity for CO_2 compared to CH_4 and N_2.

The Q_{st} value is moderately high for physisorption-driven materials as compared to the related materials: BILP-1 (26.5 kJ mol^{-1}) [89], Azo-COP-1 (29.3 kJ mol^{-1}) [71], and With these results, the high Q_{st} values comes in the favorable range for strong enough and reversible adsorption-desorption for efficient CO_2 separation, which lands squarely in the physisorption range[24,73]. This clearly indicates that MPy works as physisorption material and can be simply regenerated at mild conditions. The CO_2/N_2 selectivity of the MPy was then estimated using Henry's model. KFUPM-2 shows remarkably good CO_2/N_2 of CO_2/CH_4 selectivity of 12.

5.4.6 Dynamic CO_2 Capture by Breakthrough Experiments

The dynamic breakthrough experiments were conducted for MPy to prove that the MPy material could effectively separate CO_2 in a practical industrial condition. A homemade breakthrough setup was used as shown in the introduction chapter (Figure 7) Firstly, the

activated dry sample of MPy was tested in a dry gas mixture stream of 20% (*v*/*v*) CO_2 and 80% (*v*/*v*) N_2. The experimental breakthrough curves (Figure 45A) shows that CO_2 was retained while N_2 passed through the bed that reflecting the selectivity of MPy polymer for CO_2 over N_2. The calculated CO_2 capacity from the breakthrough curve was estimated to be about 12.1 $cm^3\ g^{-1}$ for the dry CO_2/N_2 mixture and this value are higher than other porous polymers with higher surface area (CTF-FUM-350 & CTF-DCN-500 are 11.4 and 8.3 $cm^3\ g^{-1}$ respectively)[84] and also greater than some other COFs (LZU-301, 4.9 $cm^3\ g^{-1}$)[86] , and commercially BPL Carbon (6.0 $cm^3\ g^{-1}$)[103].

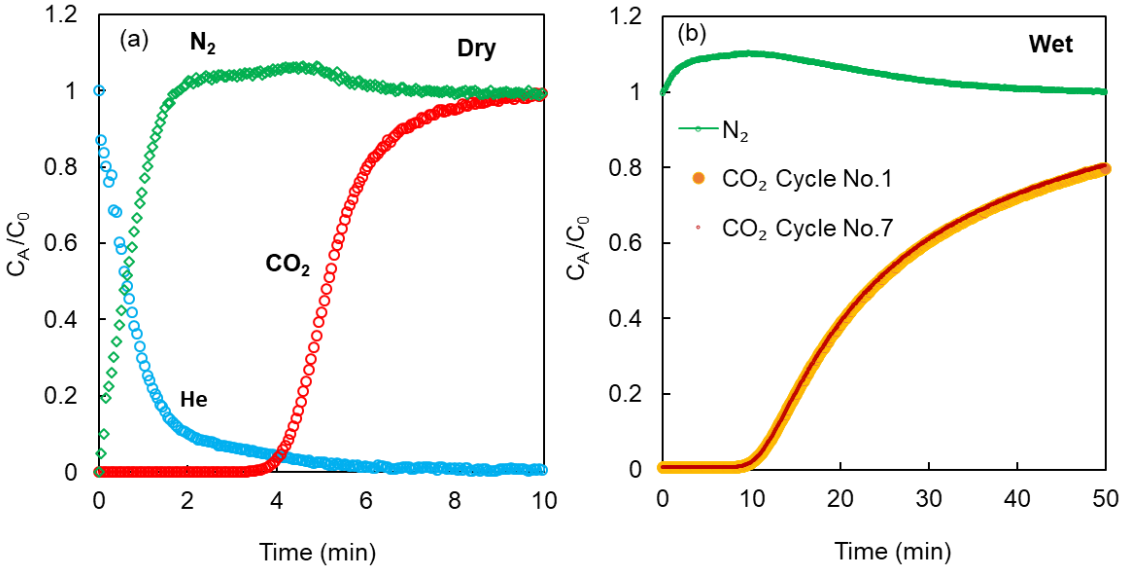

Figure 45 A 20:80 gas mixture containing CO_2 and N_2, respectively, was flown through a fixed bed of MPy at 298 K and 1 bar (a) under dry conditions (b) under wet conditions (91% relative humidity). There is no loss in dynamic adsorption capacity over 7 consecutive breakthrough measurements (b).

Tanking in consideration that industrial flue gas contains significant amount of moisture (5-7%)[18], the sorbent materials should demonstrate their effectiveness to mitigate the effect of water. Accordingly, we tested the MPy material for its stability and recyclability for separating CO_2 in presence of water through multicycle continuous breakthrough experiments (7 cycles) at 298 K. The MPy material is exposed firstly to N_2 stream with 91

% Relative humidity (2.7 wt% as detected by the mass spectrometry) until saturation of the MPy bed. At this point, a dry CO_2 stream is passed with the dual mixture (N_2 and H_2O) and this process was repeated for 7 cycles through which, the material showed an excellent recycling stability with the interesting improvement in CO_2 uptake (Figure 45), and this correlates to the increasing the CO_2 solubility in the wet condition, and this an important result to consider as many porous materials exhibited a significant decrease its CO_2 capacity in presence of water[103–107], while few examples retain their uptake else [108,109]. The MPy material was regenerated under mild condition by the humid N_2 flow at ambient temperature.

Encouraged by the breakthrough results of CO_2/N_2 separation and in order to assess the potential use of MPy material for natural gas purification, similar protocol for H_2S adsorption tests were evaluated by the breakthrough column experiments using a simulated natural gas (0.5% H_2S / 89% CH_4). A homemade setup as shown in Figure 46 in the introduction chapter was used. The gas mixture containing 2% H_2S balanced with methane was controlled by gas flow meter passed through the column containing 0.5 g of MPy material. The outlet gas was detected using gas chromatography (GC Shimadzu, GC2010) equipped with a flame photometry detector (FPD). The hydrogen sulfide dynamic capacity Q_{BT} was estimated from breakthrough time (*i.e.*, the time of H_2S appearance at the sorbent column outlet with the concentration of 5 ppm or 5% of initial concentration, in case of low ppm H_2S). The experimental breakthrough curves (Figure 47) shows that H_2S was retained for 122 min and the calculated H_2S capacity from the breakthrough curve was estimated to be about 48.8 $cm^3\ g^{-1}$. This result among the top performing materials reported as shown in Table 5.

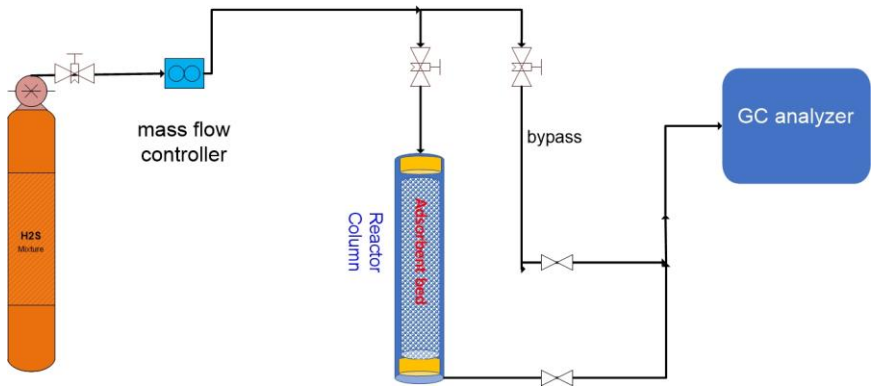

Figure 46 Schematic representation of the home-made breakthrough system for dynamic H_2S separation.

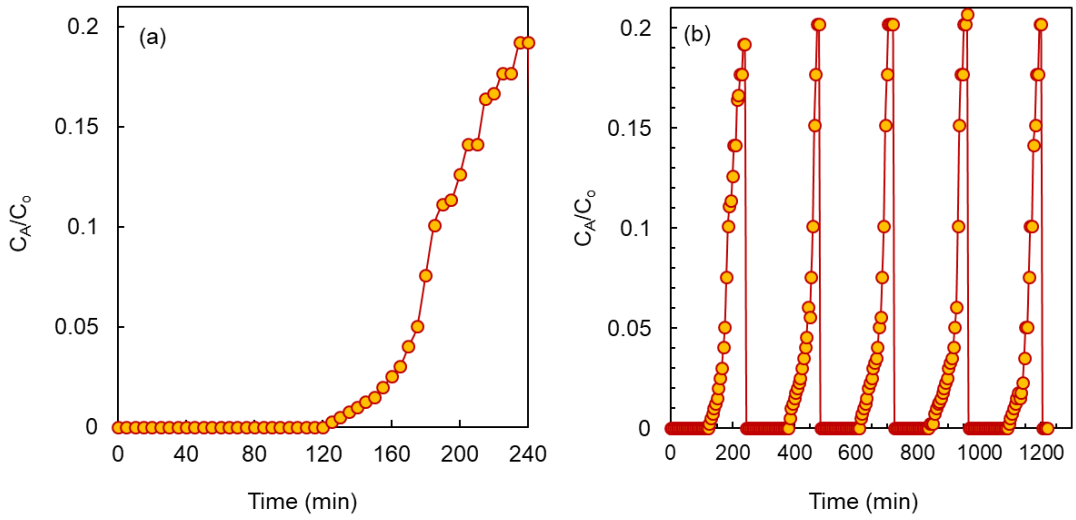

Figure 47 Experimental breakthrough curves of gas mixture containing 2% H_2S in methane (a). A multi cycles experiments shown that there is no loss in the dynamic capacity of the H_2S through five consecutive cycles (b).

Table 5 Dynamic breakthrough capacities of CO_2 and H_2S KFUPM-3 in comparison with other reported adsorbents.

Material	SA_{BET} ($m^2\ g^{-1}$)	Dynamic H_2S Uptake Capacity ($cm^3\ g^{-1}$)[a]	Regeneration Temp. (°C)	Ref.
MPy	399	48.8[b]	60	This work
Commercial ZnO-C50	---	22	---	[115]
FeOOH	214	69.1[c]/105.8[d]	XX	[115]
Zeolite NaY	---	0.64	120	[127]
CA NaY-fiber	---	0.44	120	[127]
Mg-MOF-74	1244	5.3	200	[122]
MIL-101(Cr)	3203	8.9	200	[122]
UiO-66	1322	5.2	200	[122]
ZIF-8	1602	1.1	200	[122]
Ce-BTC	930	2.8	200	[122]
Y-FTZB-fcu-MOF	1310	20.1	50	[128]
Y-fum-fcu-MOF	691	24.6	25	[128]
Y-1,4-NDC-fcu-MOF	546	33.6	25	[128]
Ga-soc-MOF-1a	1350	20	50	[129]
SBA-15_ DMAPS	454	1.2	---	[130]
Desorex K43-Na (AC)	815	102.5[b]	---	[131]

[a]Calculated from dynamic breakthrough experiments. [b]Calculated from H_2S/CH_4 mixture, [c] at 273 K, [d]at 301 K Those properties that were not reported are identified with '—'.

CHAPTER SIX

STUDY OF THE EFFECT OF NITROGEN CONTENT ON THE CARBON DIOXIDE CAPTURE OF 1,3,5-BENZENETRIAIME-PYRROLE CROSSLINKED POLYMER

6.1 Introduction

Introducing polar functional groups has been proven effective to enhance the CO_2 capacity and selectivity by increasing the dipole interaction with the CO_2 gas. Aromatic amine group (-NH) is considered as a promising function group to enhance the capacity and selectivity of porous materials toward CO_2 over N_2. Therefore, combining the chemistry of incorporating aromatic amine group with the water and chemical stability of hyper-crosslinked polymers expected to design promising materials for selective capture of CO_2 in presence of water. Although there are many studies for synthesis and designing porous organic polymers for CO_2 separation and storage application, very few materials showed their capabilities for the CO_2 capture in humid Flue gas condition[79,89,95,131–133], Moreover, the stability of the of any solid sorbent in the adsorption-desorption cycles is a critical concern should be desired for construction of such porous materials.

Here, we demonstrate the selective separation of CO_2 from the humid CO_2/N_2 mixture using novel hypercrosslinked microporous polymers, by incorporation of aromatic amine motifs through one-step reaction of 1,3,5-benzenetriamine and 2,4,6-trimethylbenzene-1,3,5-triamine copolymerized with pyrrole using *p*-formaldehyde as external cross-linker.

We were successfully prepared the copolymer networks using concentrated HCl in a polar solvent (DMF). the design strategy of the copolymers is based on using aromatic amines monomers with similar geometry and expected reactivity, but with different C/N content in order to study the effect of the C/N ratio in the final polymer networks.

6.2 Experimental section

Materials and Methods.

Pyrrole (Py, 98% purity), 1,3,5-benzenetriamine trihydrochloride (**Tri**, 98% purity), 2,4,6-trimethylbenzene-1,3,5-triamine tri-hydrochloride (**TMT**, 98% purity), methanol (99.9% purity), N,N-dimethylformamide (99% purity), concentrated hydrochloric Acid (HCl, 37%) and ammonium hydroxide (28-30 *w*/*w*%) were purchased from Alfa Aser.Sigma Aldrich Co. Paraformaldehyde (≥99% purity) was purchased from Fluka. All the chemicals were used without further purification unless pyrrole was distilled under N_2 flow at 145 °C prior to use. For gas sorption measurements, ultrahigh purity grade nitrogen (99.999%), helium (99.999%), and high purity CO_2 (99.9%) were obtained from Abdullah Hashem Industrial Co., Dammam, Saudi Arabia.

Synthesis of TriPy.

1,3,5-Benzenetriamine trihydrochloride (Tri, 0.46 g, 2.00 mmol) and *p*-formaldehyde (0.42 g, 14.00 mmol) were added with 15 mL DMF in a 50 mL round bottom flask and stirred at room temperature for 5 min. Then, pyrrole (0.47 g, 7.00 mmol) was added to the reaction mixture and stirred for an additional 5 min. Then hydrochloric acid chloride (HCl, 0.12 g, 1.2 mmol) was added and subsequently, the flask was sealed with a rubber septum. The flask was transferred into a preheated oil bath at 90 °C and continuously stirred for 24 h with a rate of 500 rpm (a black solid was formed after 5 min). The resulting solid was washed with 30 mL of methanol followed by sonication for 30 min. The solid was continuously washed with methanol for three days (3*30 mL, per day) with stirring at which time a clear filtrate solution was obtained. Then the solid was immersed in an ammonia solution (25% *w*/*w*) for 2 h, filtered, washed by 60 mL distilled water and then continue soaking in water (40 mL) for 24 h after that solvent exchanged and washing by methanol for one day (3*30 mL) with stirring. Finally, the product was dried at 80 °C in an oven for 12 h. The final yield (0.91 g) was 83% based on the monomers weights (after excluding the equivalent amount of water as by-product); EA: Found C, 46.82; H, 3.11; N, 12.68; FT-IR (KBr, cm^{-1}) 3419 (br), 2924 (w), 2860 (w), 1622 (w), 1408 (w), 1117 (w).

Yield calculation:

% yield = (experimental weight/(total monomers weights-weight of the H_2O)) * 100

= 0.91 / (0.46 + 0.42+ 0.47– (0.014 mol * 18)) = 0.91/ 1.1 = 82%

Synthesis of TMTPy.

2,4,6-Trimethylbenzene-1,3,5-triamine tri-hydrochloride (TMT, 0.27 g, 1.00 mmol) and paraformaldehyde (0.21 g, 6.80 mmol) was added with 15 mL DMF in a 50 mL round

bottom flask and stirred at room temperature for 5 min. Then, pyrrole (0.23 g, 3.40 mmol) was added to the reaction mixture and stirred for an additional 5 min. Then hydrochloric acid chloride (HCl, 0.06 g, 0.68 mmol) was added and subsequently, the flask was sealed with a rubber septum. The flask was transferred into a preheated oil bath at 90 °C and continuously stirred for 24 h with a rate of 500 rpm (a black solid was formed after 5 min). The resulting solid was washed with 30 mL of methanol followed by sonication for 30 min. The solid was continuously washed with methanol for three days (3*30 mL, per day) with stirring at which time a clear filtrate solution was obtained. Then the solid was immersed in an ammonia solution (25% *w*/*w*) for 2 h, filtered, washed by 60 mL distilled water and then continue soaking in water (40 mL) for 24 h after that solvent exchanged and washing by methanol for one day (3*30 mL) with stirring. Finally, the product was dried at 80 °C in an oven for 12 h. The final yield (0.40 g) was 68% based on the monomers weights (after excluding the equivalent amount of water as by-product); EA: Found C, 38.74; H, 3.50; N, 10.94; FT-IR (KBr, cm^{-1}) 3412 (br), 3226 (br), 2920 (w), 2852 (w), 1647 (w), 1425 (w), 1119 (w).

Yield calculation:

% yield = (experimental weight/(total monomers weights-weight of the H_2O)) * 100

= 0.40 / (0.27 + 0.21+ 0.23– (0.0068 mol * 18)) = 0.40/ 0.59 = 68%

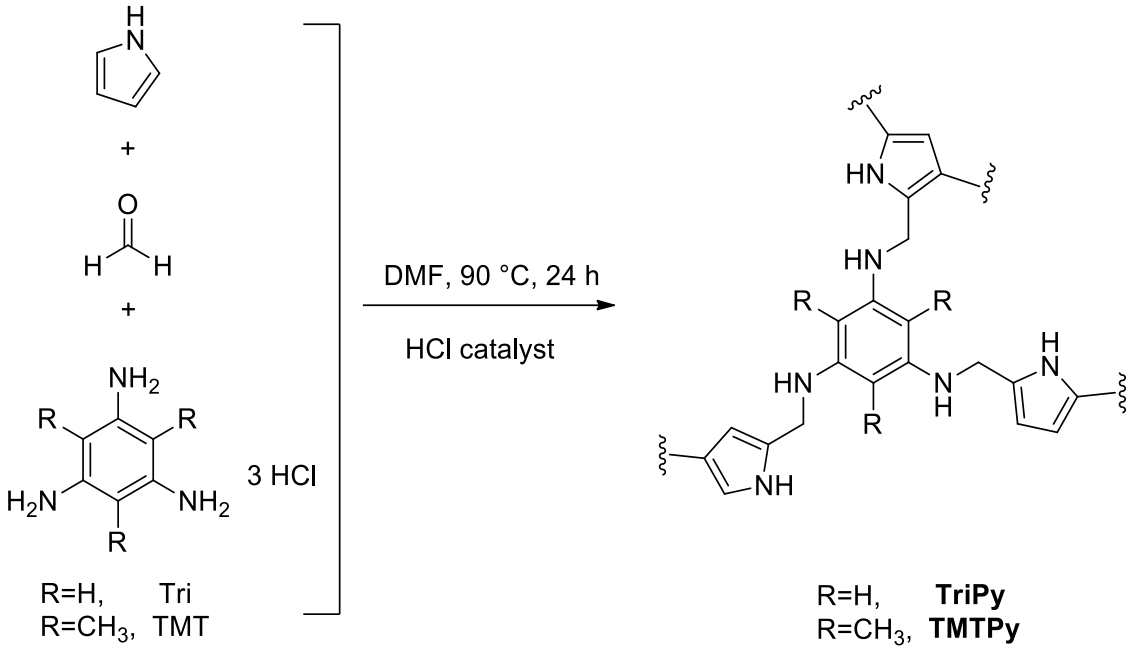

Scheme 15 General synthetic scheme of TriPy and TMTPy copolymers.

Breakthrough measurements.

(A)Experimental procedure of breakthrough tests for CO_2/N_2 gas mixture.

The schematic for the homemade breakthrough system set-up is shown in the introduction chapter (Figure 7). The column was packed with **TriPy** powder (0.3 g) and the sample was activated at 373 K under vacuum for 24 hours prior to carrying out the breakthrough measurements. The breakthrough experiments were conducted under ambient conditions (298 K and 1 bar) with a 10 sccm flowrate of CO_2:N_2 (20:80 *v*/*v*) feed mixture. For the measurements under humid conditions, the sample bed was subjected to a stream of wet N_2 gas (91% relative humidity, RH), in which the water level in the gas stream was monitored until saturation was obtained as detected by mass spectrometry. After that, dry CO_2 was introduced into the wet N_2 stream with the same flowrate as the dry conditions noted above. The full breakthrough capacity of CO_2 was measured by evaluating the ratio of compositions

of the downstream gas and the feed gas. The regeneration of the sample was done by the flow of pure wet N_2 through the sample bed at room temperature for 5-6 h.

6.3 Characterization

Solid state ^{13}C nuclear magnetic resonance (NMR) spectroscopy measurements were measured on a Bruker 400 MHz spectrometer operating at 125.65 MHz (11.74 T) and at ambient temperature (298 K). Samples were packed into 4 mm ZrO_2 rotors and cross-polarization magic angle spinning (CP-MAS) was employed with a magic angle spinning rate of 14 kHz. Fourier transform infrared (FT-IR) spectroscopy measurements were performed on a PerkinElmer 16 PC spectrometer from KBr pellets. The spectra were recorded over 4000 – 600 cm^{-1} in transmission mode and the output signals were described as follows: s, strong; m, medium; w, weak; and br, broad. CHN analysis was carried out at PerkinElmer (EA-2400) elemental analyzer. Thermal gravimetric analysis (TGA) was run on a TA Q-500 instrument with a platinum pan sample holder under. About 10 mg of sample were heated under air flow with heating rate 10 °C per min. Powder X-ray diffraction (PXRD) measurements were recorded on a Rigaku MiniFlex II X-ray diffractometer with Cu K_α radiation (λ = 1.54178 Å). Field emission scanning electron microscope (FE-SEM) images were taken on a Tescan LYRA3 Dual Beam microscope at an acceleration voltage of 10 kV. Low-pressure nitrogen sorption isotherms were undertaken using a Quantachrome QUADRASOROB *evo* instrument. A liquid nitrogen bath was used for the measurements at 77 K. CO_2 sorption isotherms were measured on an Autosorb iQ2 volumetric gas adsorption analyser. The measurement temperatures at 273 and 298 K were controlled with a water circulator.

6.4 Results and Discussion

6.4.1 Synthesis strategy

The aim of this study was to synthesize a porous crosslinked polymer with controlled structure and textural properties for selective CO_2 capture and separation as well as studying the effect of nitrogen content on the CO_2 selectivity over other gases. As such, pyrrole and trifunctional benzene moieties with different C/N ratios (1,3,5-triaminobenzene and 2,4,6-trimethyl 1,3,5-triaminobenzene) were selected since they have integrated polar aromatic amine moieties (known to be CO_2 philic functional groups) within their molecular structures[53], in addition to that, they have the same geometry and similar crosslinking possibilities. After synthesis, the polymer networks were thoroughly washed with methanol followed by soaking in a solution of ammonium hydroxide in order to remove any unreacted starting materials. Prior to use in any further characterization, the three synthesized polymers were dried at 353 K for 12 h.

6.4.2 Structural characterization.

Solid-state Nuclear Magnetic Resonance (^{13}C NMR)

The successful construction of the **TriPy** and **TMTPy** copolymer was proved using a combination of the ^{13}C solid state NMR and FT-IR spectroscopies as well as elemental analysis. Therefore, ^{13}C NMR spectra (Figure 48) revealed the characteristic peaks for both 1,3,5-triaminobenzene and pyrrole moieties crosslinked with the methylene group as follows; peak at δ = 26.0 ppm which can be assigned to the chemical shift of the aliphatic CH_2 group linking two pyrrole moieties, peak centered at δ = 36.5 ppm was assigned to the chemical shift of CH_2 between the pyrrole and NH from the 1,3,5-triaminobenzene. A shoulder peak at δ = 90 ppm was assigned for the aromatic carbon atom number (3) of the 1,3,5-triaminobenzene. A broad peak at δ = 133.3 ppm was assigned to the chemical shift of the aromatic α-carbon atoms from the pyrrole.

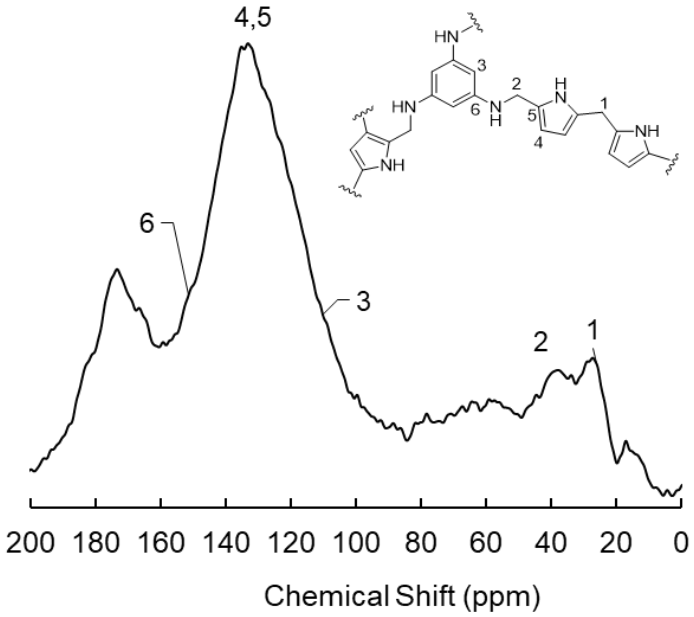

Figure 48 Cross polarization-magic angle spinning solid state nuclear magnetic resonance (CP-MAS ^{13}C-NMR) spectrum at 14 KHz, with the corresponding peak assignments. Inset: The core structure of TriPy fragment is provided for peak assignment.

Fourier Transform Infrared Spectroscopy (FTIR)

FT-IR spectra of the monomers and TriPy, and TMTPy polymers (Figure 49) is supporting the expected structure. For TriPy, the spectral band at 3419 cm^{-1} can be assigned to the stretching vibration of the N—H for both pyrrole and of the 1,2,3-triaminobenzene similar bands were found in TMTPy at 3021 cm^{-1}. The appearance of new bands around 2920 cm^{-1} assigned to methylene C-H stretch specific for CH_2 linkage not present in the 1,3-triaminobenzene or the pyrrole monomers.

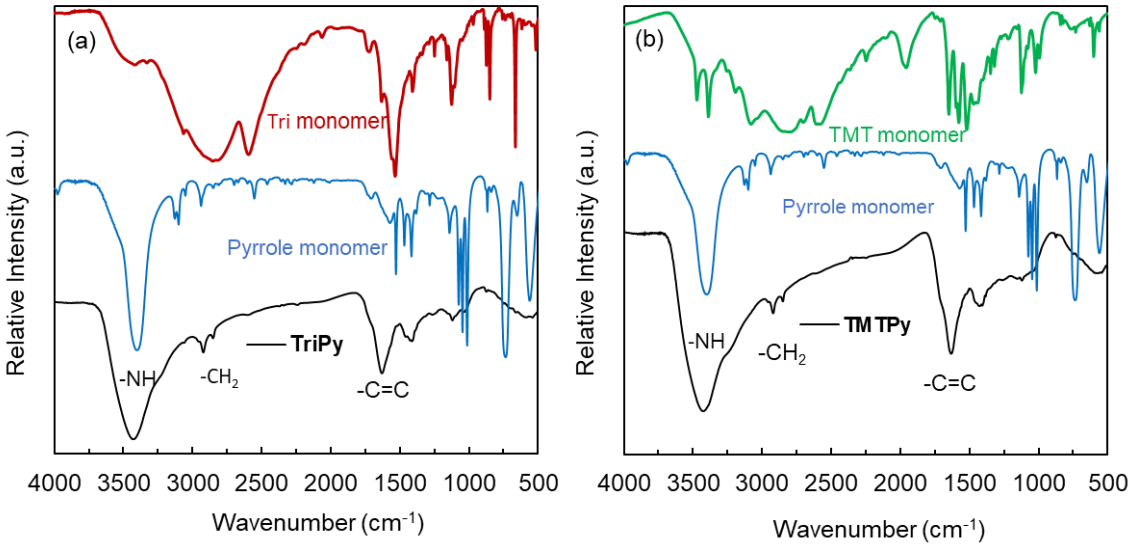

Figure 49 Fourier transform-infrared spectroscopy (FT-IR) analysis of TriPy and TMTPy (black) in comparison to pure monomers Tri and TMT (red) and pure pyrrole (blue). Those absorption bands directly related to the characteristic functionalities of the copolymers are highlighted.

Elemental composition

Elemental analysis of the TriPy and TMTPy polymers were carried out in order to support the structural composition of the polymers. As we discussed before in the previous chapters that the chemical formulation of porous polymers by elemental analysis is difficult. The deviation between theoretical and experimental values are observed in our samples, and this can be attributed to incomplete combustion during analysis, trapped adsorbate species

(*i.e.* gases and water vapors), as well as irregularity of the polymer structure itself and this behavior, is found in other reported porous polymers[53,96,97].

Table 6 CHN elemental composition it the synthesized TriPY and TMTPy polymers

Polymer	Elemental Analysis (Wt %)(found)			
	C	H	N	C/N ratio
TriPy	46.82	3.11	12.68	3.69
TMTPy	38.74	3.5	10.94	3.54

Thermal Gravimetric Analysis (TGA)

The thermal stability of the polymers was examined by TGA measurement in air. The TGA of the polymers (Figure 50) reveals that the **TriPy** and **TMTPy** show a gradual weight loss after 220 °C, indicating high thermal stability of the polymer networks.

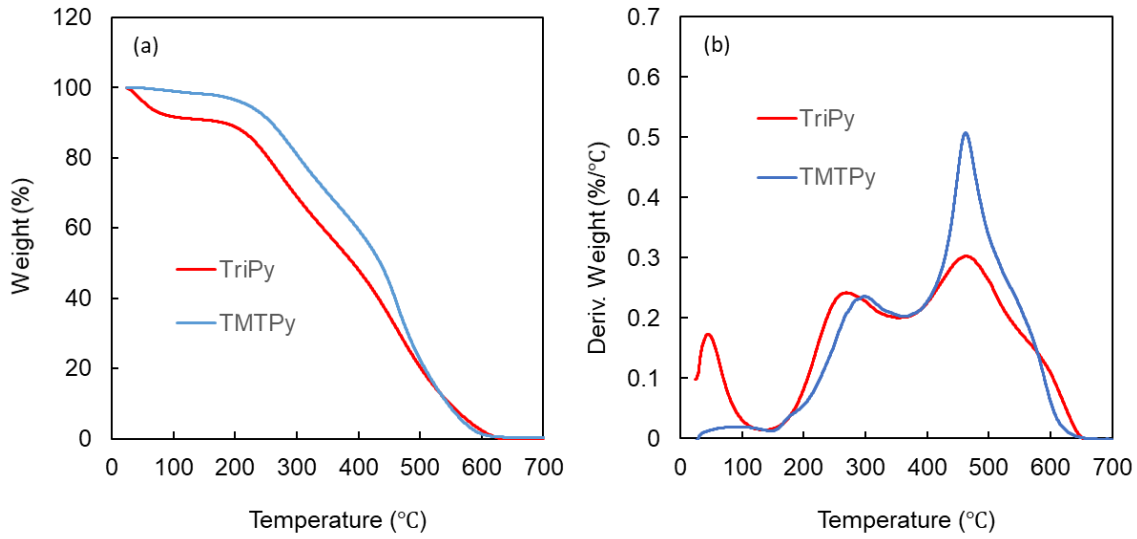

Figure 50 Thermogravimetric analysis (a) of the TriPy (red) and TMTPy (blue) polymer network, measured under air (black) and first derivative with the temperature (b).

Powder X-Ray Diffraction (PXRD)

Powder X-Ray Diffraction was done for the polymer to evaluate the crystallinity of the materials. The data was obtained in the range of 5 to 40 degrees with a rate of 2 degrees/min. From the data obtained and presented in (Figure 51), it confirms the amorphous nature of the synthesized polymers.

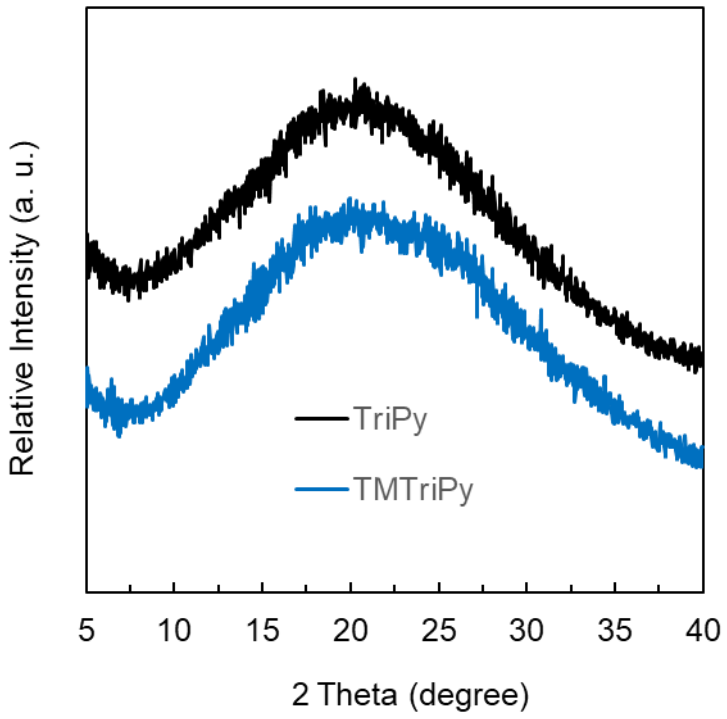

Figure 51 Powder X-ray diffraction of the copolymer networks TriPy (back), and TMTPy (blue).

6.4.3 Textural properties and Porosity characterization

The textural properties of all the activated TriPy and TMTPy polymers were determined from N_2 sorption measurements at 77 K (Figure 52). The N_2 isotherms for two polymer networks show a sharp uptake at low relative pressure (P/P_0 < 0.001) indicating the predominant microspore nature of the networks that resembles Type I isotherms according to the IUPAC classification[26,76]. A steep rise in the uptake at higher relative pressure

($P/P_0 > 0.5$) is found for the TriPy polymer, indicating the capillary condensation of N_2 molecules in a mesopores and the inter-particle condensation. The isotherms for the two polymers showed a hysteresis during the desorption up to the low pressure region indication elastic deformation or swelling after gas desorption[81]. The BET surface area (at P/P_0 = 0.01-0.3) were observed for TriPy and TMTPy are 625 and 447 $m^2\ g^{-1}$ respectively. Table 7 lists the surface area and pore properties calculated from N_2 adsorption isotherms at 77 K using BET and QSDFT models.

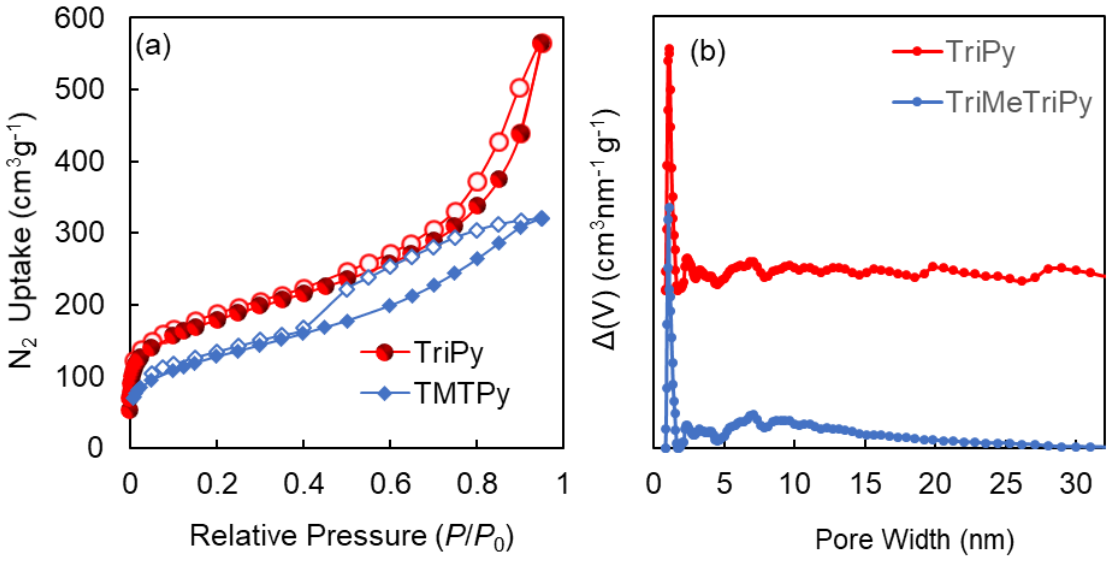

Figure 52 (a) N_2 adsorption isotherms TriPy (red), and TMTpy (blue) at 77 K. Filled and open symbols represent adsorption and desorption branches, respectively. The connecting lines serve as a guide to the eye. (b) Pore size distribution for TriPy (red) and TMTPy (blue) calculated by QSDFT method.

Table 7 Surface areas and pore volume determined from N_2 isotherms at 77 K by BET and DFT method.

Polymer	SA_{BET} ($m^2\ g^{-1}$)[a]	SA_{DFT} ($m^2\ g^{-1}$)[b]	$V_{tot,\ N_2,\ DFT}$ ($cm^3\ g^{-1}$)[c]	Pore width (nm)[b]
TriPy	630	596	0.821	1.05
TMTPy	447	375	0.473	1.10

[a]Calculated using BET model [d]Calculated using QSDFT for (slit/cylindrical/ sphere pores) in carbon-based materials for the adsorption branch.

6.4.4 Gas Adsorption Studies

Thermodynamic Uptake Capacity. Through previous studies, it has been proved that the CO_2 capture capability not only depend on the surface area or the pore nature but also on the functionality and active sites for the CO_2. Therefore, good surface area and the intrinsic microporosity of the synthesized crosslinked TriPy and TMTPy polymers as well as, the variation in nitrogen content in the final copolymer networks led us to study the effect of above-mentioned parameters on the CO_2 capture and separation. Accordingly, the thermodynamic gas adsorption properties were assessed for the two polymer networks at 273 and 298 K. The isotherms exhibit a reversible adsorption and desorption with small hysteresis indicating larger interaction of the CO_2 with the material. TriPy exhibited the highest CO_2 uptake capacity of 51.8 $cm^3\ g^{-1}$ at 273 K and 760 Torr and 32.8 $cm^3\ g^{-1}$ at 298K and 760 Torr (Figure 53). While TMTPy exhibited the lower CO_2 uptake capacity of 40.3 $cm^3\ g^{-1}$ at 273 K and 760 Torr and 26.3 $cm^3\ g^{-1}$ at 298K and 760 Torr (Figure 53). In contrast, low N_2 uptake capacities were found under the same experimental conditions for both TriPy and TMTPy, polymers. It clearly seen that the initial slopes of the CO_2 isotherms were sharper than that of the N_2, reflecting the higher affinity of the material toward CO_2 compared to the N_2, which advance the potential use of synthesized polymers as an adsorbent for selective CO_2 capture from flue gas. The CO_2 uptake capacity of the synthesized polymers at 273K is comparable of or higher than those of reported crystalline covalent frameworks COFs (COF-1 51.9 $cm^3\ g^{-1}$, COF-5 29.9 $cm^3\ g^{-1}$, COF-8 32.0 $cm^3\ g^{-1}$,and COF-10 27.0 $cm^3\ g^{-1}$)[45] and higher than other porous organic polymers such as NUT-1 (36.8 $cm^3\ g^{-1}$)[94] CMP-1 (29.6 $cm^3\ g^{-1}$)[10], and PPN-6-CH_2Cl (28.6 $cm^3\ g^{-1}$)[83].

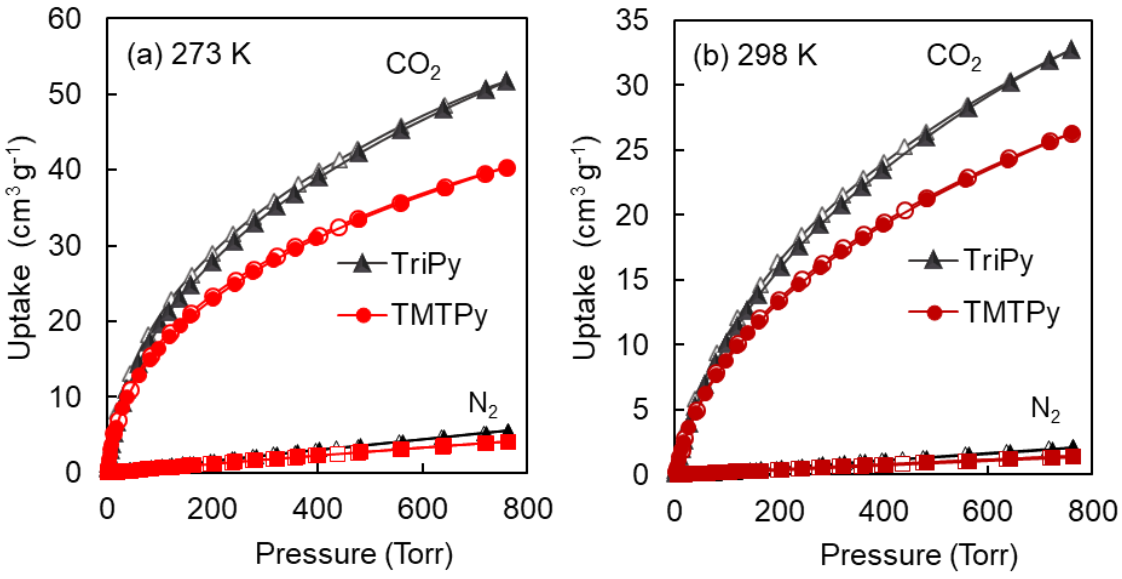

Figure 53 CO_2 and N_2 sorption isotherms for TriPy (Black) and TMTPy (red) (a) at 273 K (light colors) and (b) at 298 K (dark colors). Filled and open symbols represent adsorption and desorption branches, respectively. The connecting lines serve as a guide to the eye.

6.4.5 Coverage Dependent Enthalpy of Adsorption (Q_{st}) and CO_2/N_2 selectivity.

Coverage Dependent Enthalpy of Adsorption (Q_{st})

Coverage-Dependent Enthalpy of Adsorption and CO_2/N_2 Selectivity. After getting the thermodynamic CO_2 and N_2 adsorption measurement results, we were encouraged to understand more the structure relationship between the polymers and CO_2. Therefore, the coverage-dependent enthalpy of adsorption (Q_{st}) for CO_2 was estimated by fitting the isotherms collected at 273 and 298 K with a virial-type expansion equation. The resulting initial Q_{st} value was calculated to be 33 and 35 kJ mol^{-1} for TriPy and TMTPy respectively. These Q_{st} values quantifiably reflect the strong binding affinity of the Three materials to CO_2. The Q_{st} value is moderately high for physisorption-driven materials as compared to the related materials: BILP-1 (26.5 kJ mol^{-1})[82], Azo-COP-1 (29.3 kJ mol^{-1})[71], and PAF-1 (15.6 kJ mol^{-1})[135]. With these results, the high Q_{st} values come in the favorable range for strong enough and reversible adsorption-desorption for efficient CO_2 separation,

which lands squarely in the physisorption range[24,73]. This clearly indicates that TriPy and TMTPy work as physisorption materials and can be simply regenerated at mild conditions. Although the difference in the N_2 content of the TriPy and TMTPy they demonstrated similar Q_{st} values. With these results, the CO_2/N_2 selectivity was then estimated based on Henry's law. TriPy demonstrated a high CO_2/N_2 selectivity of 88 and 79 at 273 and 298 K, respectively. While TMTPy showed higher selectivity of 121 and 103 at 273 and 298 K. These values were corroborated by applying Ideal Adsorbed Solution Theory (IAST), which provided information about selectivity with pressure as a consideration (Figure 54). These selectivity results may be attributed to the higher majority of micropores of TMTPy than that of TriPy as shown in the pore size distribution (Figure 52b).

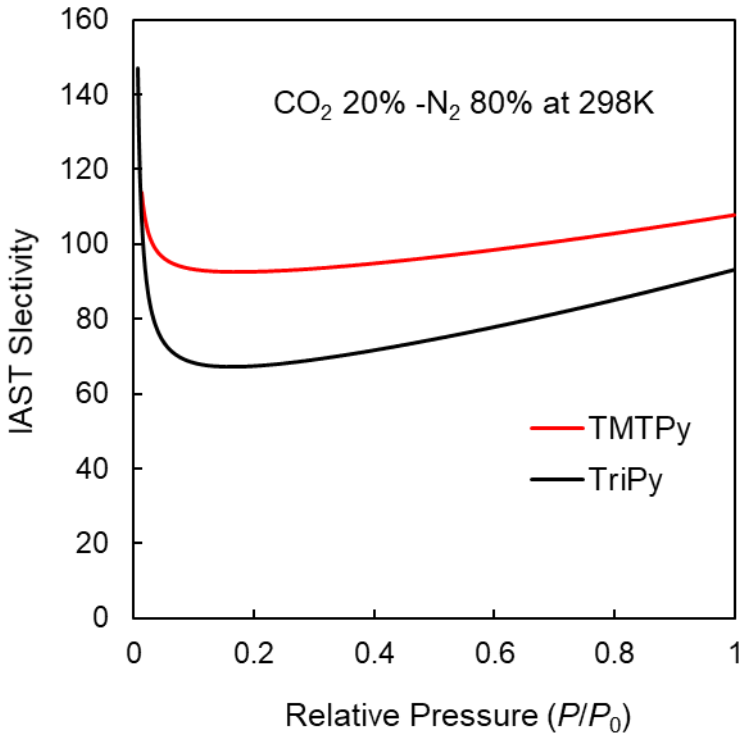

Figure 54 CO_2/N_2 IAST selectivity of TriPy (black) and TMTPy (red) at 298 K for mixture composition of 20% CO_2 and 80% N_2.

6.4.6 Dynamic CO_2 Capture by Breakthrough Experiments

The dynamic breakthrough experiments were carried out for **TriPy** in order to fortify that the **TriPy** material could efficiently separate CO_2 in a practical industrial gas mixture. Firstly, the activated dry sample of **TriPy** was exposed to a dry gas mixture stream of 20% (*v*/*v*) CO_2 and 80% (*v*/*v*) N_2. The experimental breakthrough curves (Figure 55) shows that CO_2 was retained while N_2 passed through the bed that clearly indicating the selectivity and the N_2 affinity of **TriPy** polymer for CO_2 over N_2. The CO_2 capacity calculated from the respective breakthrough curve was estimated to be about 12.1 $cm^3\ g^{-1}$ for dry CO_2/N_2 mixture and this value are higher than other porous polymers with higher surface area (CTF-FUM-350 & CTF-DCN-500 are 11.4 and 8.3 $cm^3\ g^{-1}$ respectively)[84] and also greater than some other COFs (LZU-301, 4.9 $cm^3\ g^{-1}$)[86], and commercially BPL Carbon (6.0 $cm^3\ g^{-1}$)[103].

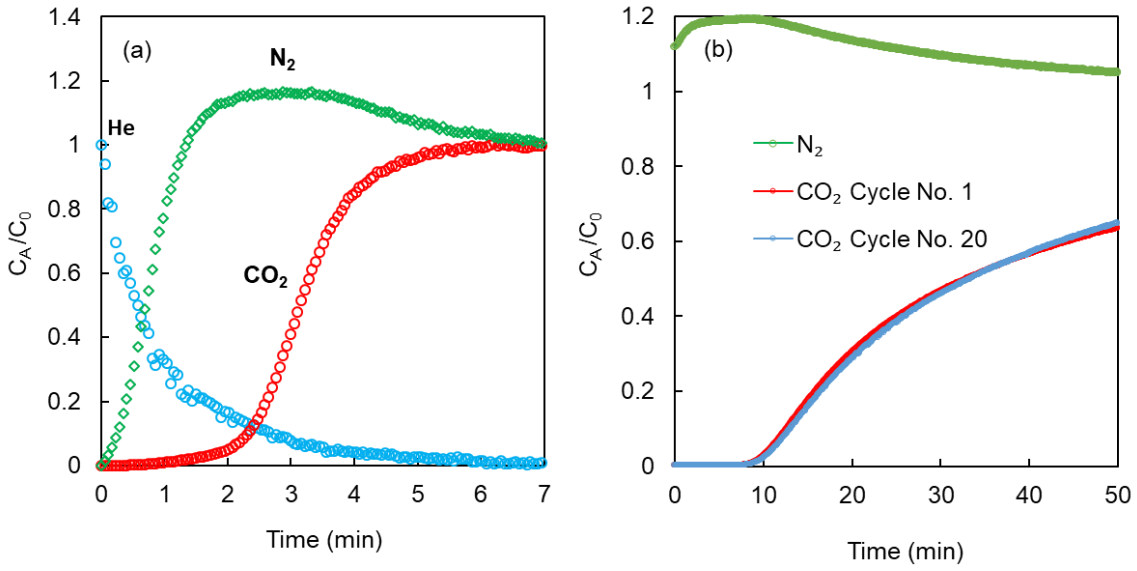

Figure 55 (a) A 20:80 gas mixture containing CO_2 (blue) and N_2 (red) was flown through a fixed bed of TriPy under dry conditions at 298 K and 1 bar, (b) under wet conditions. There is no loss in dynamic adsorption capacity over 10 consecutive breakthrough measurements.

Considering the fact that industrial flue gas contains a significant amount of moisture (5-7%)[18], the sorbent material should demonstrate their effectiveness to tolerant the effect of water. Accordingly, we tested the TriPy material for its stability and recyclability for separating CO_2 in wet condition through multicycle continuous breakthrough experiments (20 cycles) at 298 K. The TriPy material is exposed firstly to N_2 stream with 91% relative humidity (2.7 wt% as detected by the mass spectrometry) until saturation of the TriPy bed. Then, a dry CO_2 stream is passed with the dual mixture (N_2 and H_2O) and this process was repeated for 20 cycles through which, the material showed an excellent recycling stability with the interesting improvement in CO_2 uptake up to 60.6 $cm^3\ g^{-1}$ in case of full wetted sample (Figure 55), and this may due to the increasing the CO_2 solubility in the wet condition as well as swelling of the material, and this an important result to consider as many porous materials exhibited a significant decrease its CO_2 capacity in presence of water[103–107], while few examples retain their uptake else[108,109]. The TriPy material was regenerated under mild condition by the humid N_2 flow at ambient temperature. This regeneration process reflects the capability of the TriPy material for a pressure swing adsorption (PSA) which is used for industrial scale flue gas as energy efficient method.

6.5 Study on the structure relationship with the CO_2 uptake capacity

Figure 56, shows the CO_2 uptake of TriPy, TMTPy, and MPy polymers at 298 K.

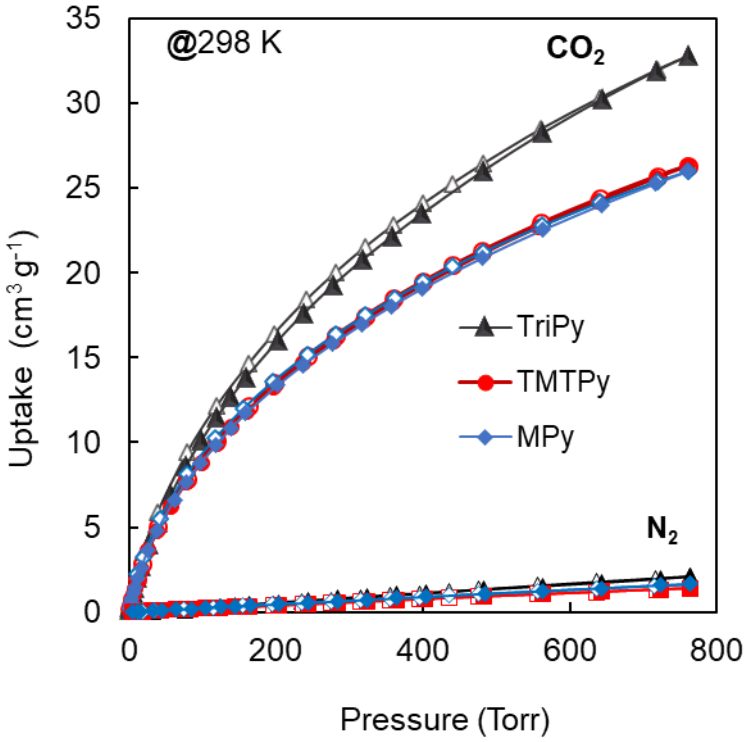

Figure 56 Comparison of CO_2 sorption isotherms for TriPy (black triangle, TMTPy (red circle), and MPy (blue rhombus) at 298 K. Filled and open symbols represent adsorption and desorption branches, respectively. The connecting lines serve as a guide to the eye.

CHAPTER SIVEN

CONCLUSION AND PERSPECTIVES

By developing a new synthetic strategy based on the acid catalyzed polycondensation of amine base aromatic monomers with *p*-formaldehyde, a series of novel inexpensive, robust, and CO_2-phillic porous polymer, KFUPM-1, KFUPM-2, **MPy TriPy**, and **TMTPy** were realized. Taking stock of the synthesized crosslinked polymer's properties and performance in light of the criteria needed for developing an effective adsorbent material for post-combustion CO_2 capture, we quickly observe new materials whose performance stands out in an otherwise crowded field for this particular application. Indeed, the synthesized polymers are among the highest performing (or, alternatively, most well-rounded) materials for CO_2 capture under industrially-relevant, practical conditions. With respect to this work, we demonstrated that the structure connectivity's of the constituents comprising the copolymers were successfully determined via CP-MAS ^{13}C NMR and FT-IR spectroscopies and the permanent porosity was proven (up to 620 m^2 g^{-1}, for **TriPy**). The porous material, with its high density of polar, aromatic amines, displayed relatively high CO_2 uptake capacity (from 23.4 cm^3 g^{-1} for KFUPM-1 to 32.8 for **TriPy**) at 298 K along with a moderately high coverage-dependent enthalpy of adsorption (Q_{st} around 34 kJ mol^{-1} for all the polymers). The effect of the nitrogen content in the polymers networks is studied along with pore properties of the polymer as in Chapter 5 that proves that the CO_2 capture not only depend on the amine functionality of the porous polymers but also the micropore character of the material. When comparing the CO_2 uptake with that of N_2,

a CO_2/N_2 selectivity of 249 at 273 K and 141 at 298 K was recorded of KFUPM-1. These selectivity values are among the highest reported for a porous polymer. With these results in hand, the synthesized polymers (KFUPM-1, KFUPM-2, **TriPy**, and **MPy**) were explored for its ability to selectively capture CO_2 from a binary (CO_2/N_2) and ternary ($CO_2/N_2/H_2O$) gas mixture via breakthrough measurements. Accordingly, KFUPM-1 demonstrated dynamic CO_2 uptake capacities under dry and wet conditions of 8.6 and 15.1 $cm^3\ g^{-1}$, respectively while **TriPy** recorded exceptional dynamic CO_2 capacities of 60 $cm^3\ g^{-1}$ under wet conditions. Furthermore, a multicycle continuous breakthrough measurement, whereby the regeneration of the synthesized polymers between each cycle was energy efficient, demonstrated that our materials was able to selectively capture CO_2 from a wet N_2 stream over long periods of time without significant loss in performance. The findings studied herein highlight a strategy for progressing porous polymers as potential and rationale adsorbent materials for industrially-relevant, practical gas separation processes.

Perspectives:

1) Study and optimize the use of different catalysts for the synthesis of Amine base hypercrosslinked polymers such as different Lewis acids such as $AlCl_3$, $ZnCl_2$, and CuCl and different protonic acid such as H_2SO4, H_3PO_4, F_3C-COOH.
2) Synthesis of hypercrosslinked polymers from 3D monomers such as tetrahedral structures and pyrene rings that can lead for porous polymers with very high surface areas for gas storage and separation.

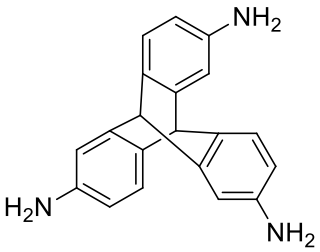

9,10-dihydro-9,10-[1,2]benzenoanthracene-2,6,14-triamine

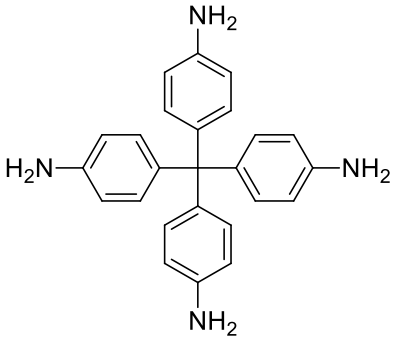

4,4',4",4'"-methanetetrayltetraaniline

3) Study the effect of different water concentrations (different humidity ratios) on the CO_2 separation.
4) Study the kinetic of the CO_2 adsorption on the new synthesized polymers.
5) Test the H_2S separation capacities for the other synthesize polymers and study the structure relationship with the H_2S capacity.

APPENDICES

Appendix A: Supporting Information for Chapter two

Table 8 Optimization conditions for KFUPM-1 synthesis.

Condition No.	Linker	Solvent	Catalyst	Catalyst mol %	Temperature (K)	Remarks
1	*p*-formaldehyde dimethyl acetal	1,2-dichloroethane	$FeCl_3$	10[b]	323 -353	Nonporous material
2	*p*-formaldehyde dimethyl acetal	1,2-dichloroethane	$FeCl_3$	100[b]	323 -353	Nonporous material
3	*p*-formaldehyde	DMSO	$FeCl_3$	10[b]	363	Low yield
4	*p*-formaldehyde	DMSO	Conc. HCl	27[a]	363	Low yield
5	*p*-formaldehyde	DMF	Conc. HCl	27[a]	363	Micropore with good CO_2 uptake
6	*p*-formaldehyde	DMF	$FeCl_3$	10[b]	363	Low CO_2 uptake
7	*p*-formaldehyde	DMF	CuCl	10[b]	263	High Cu content in final product

[a]mol% of all the monomers, [b]mol% of linker

Synthesis of model polymer.

Paraformaldehyde (0.60 g, 20 mmol) and 1,4-benzenediamine (0.60 g, 5.5 mmol) were added with 20 mL DMF to a 50 mL round bottom flask. This mixture was stirred for 15 min., at which time 0.4 mL conc. HCl (12 M) was added. The round bottom flask was sealed with a rubber septum and heated at 323 K for 15 h and at 363 K for 9 h with a stirring rate of 200 rpm. After this time elapsed, a yellow precipitate was observed and isolated by centrifugation. This solid was then washed with 20 mL of methanol. The yellow product was filtered and washed with 20 mL of methanol per d for 3 d with continuous stirring. Finally, the product was dried at 348 K under vacuum (<0.1 bar) for 15 h. The final yield (0.65 g) was 77% based on the 1,4-benzenedaimine monomer. FT-IR (KBr, cm^{-1}) 3379 (br), 3217 (w), 2916 (w), 2850 (w), 1651 (s), 1604 (w), 1512 (m), 1385 (w), 1130 (w), 822 (w).

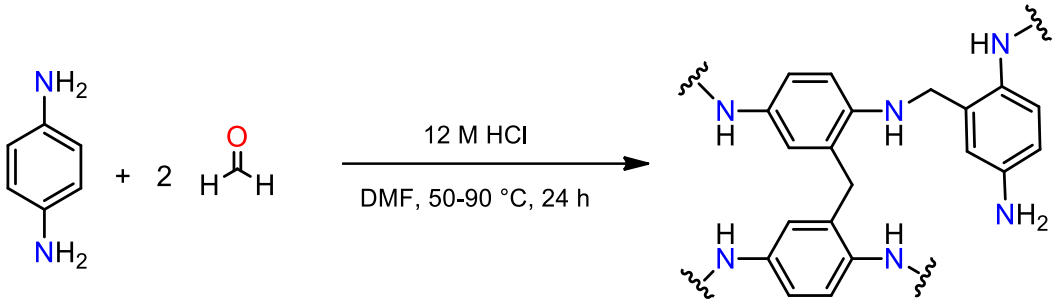

Scheme 16 Synthetic scheme of model polymer.

Synthesis of KFUPM-1/$FeCl_3$.

1,4-Benzenediamine (0.27 g, 2.5 mmol) and *p*-formaldehyde (0.30 g, 10 mmol) were added with 20 mL DMF to a 50 mL round bottom flask and stirred at room temperature for 5 min. After this, pyrrole (0.36 g, 5.4 mmol) was added into the reaction mixture and continuously stirred for an additional 5 min. and then the flask was purged with N_2 for 2-3 min and

subsequently iron (III) chloride ($FeCl_3$, 0.16 g, 1 mmol) was added under inert atmosphere and the flask was sealed with a rubber septum. The mixture was heated at 363 K in an oil bath for 24 h with continuous stirring at a rate of 200 rpm. After this time elapsed, a black solid was isolated by centrifugation and filtration. The solid was washed with 40 mL of methanol followed by sonication for 30 min. The solid was filtered and immersed in an ammonia solution (25% *w*/*w*) for 24 h, 40 mL distilled water for 24 h, and 60 mL of methanol per d for 3 d with stirring, at which time a clear filtrate solution was obtained. Finally, the product was dried at 348 K under vacuum (<0.1 bar) for 20 h. The final yield (0.59 g) was 78% based on the monomers weights. FT-IR (KBr, cm^{-1}) 3431 (br), 3267 (br), 2927 (w), 2868 (w), 1612 (w), 1512 (w), 1433 (w), 1120 (w), 673 (m).

Synthesis of KFUPM-1/CuCl.

1,4-Benzenediamine (1.08 g, 10.0 mmol) and paraformaldehyde (1.20 g, 40.0 mmol) were added with 60 mL DMF to 100 mL round bottom flask and stirred at room temperature for 5 min. After this pyrrole (1.34 g, 20.0 mmol) was added into the reaction mixture and continuously stirred for 5 min. and then the flask was purged with N_2 for 2-3 min and subsequently copper (I) chloride (CuCl, 0.39 g, 4.0 mmol) was added under inert atmosphere and the flask was sealed with a rubber septum. The mixture was heated at 363 K in an oil bath for 24 h with continuous stirring at a rate of 200 rpm. After this time elapsed, a black solid was isolated by centrifugation and filtration. The solid was washed with 40 mL of methanol followed by sonication for 30 min. The solid was filtered and immersed in an ammonia solution (25% *w*/*w*) for 24 h, 40 mL distilled water for 24 h, and 60 mL of methanol per d for 3 d with stirring, at which time a clear filtrate solution was obtained. Finally, the product was dried at 348 K under vacuum (<0.1 bar) for 20 h. The

final yield (3.00 g) was 100% based on the monomers weights. FT-IR (KBr, cm^{-1}) 3406 (br), 3236 (br), 2920 (w), 2848 (w), 1614 (w), 1510 (w), 1107 (w), 827 (m).

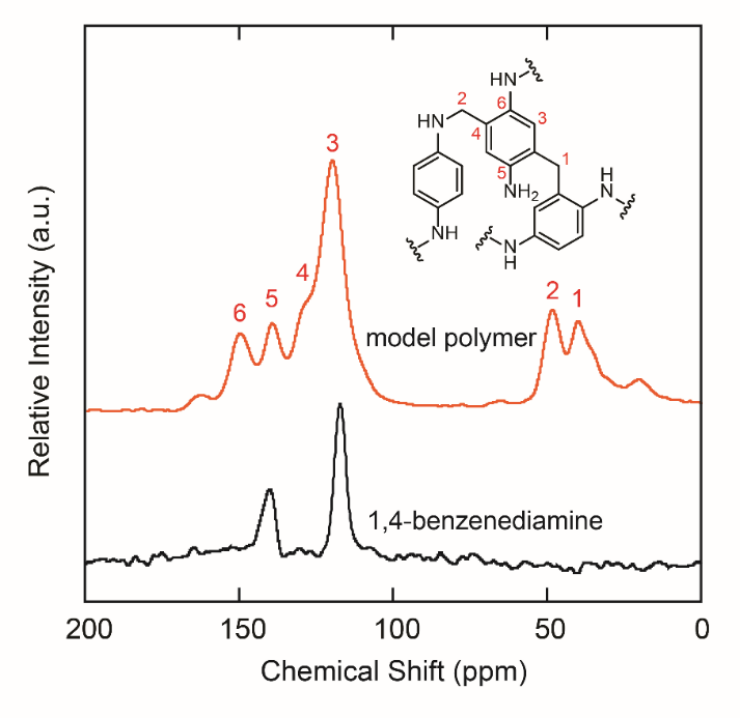

Figure 57 Solid state CP-MAS 13C-NMR stack mode of the model polymer and the 1,4-benzenediamine monomer at 10 KHz with the corresponding core structure of model polymer provided in the inset for peak assignment.

Table 9 Assignment of the ^{13}C NMR spectrum peaks of the model polymer.

Peaks (ppm)	Peak No.	Assignment of the characteristic peaks in the structure
39	1	Aliphatic CH_2 linkage between aromatic C atoms form two phenylene rings
48	2	Aliphatic CH_2 linkage between aromatic C atom NH group of another molecule
119	3	Non-substituted aromatic C
129	4	Substituted aromatic C
138	5	Quaternary carbon attached to free amine group
149	6	Quaternary carbon attached to linked amine group

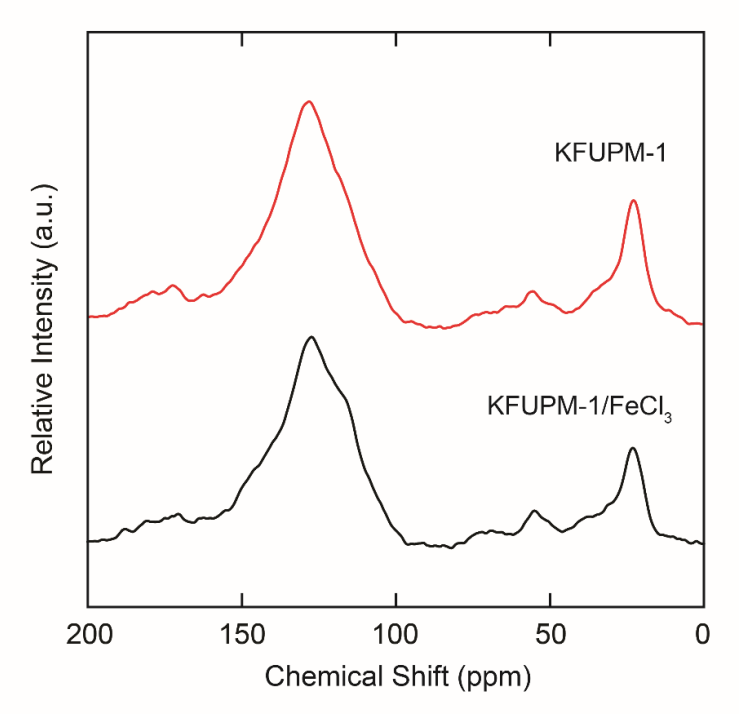

Figure 58 ^{13}C CP-MAS NMR spectra of KFUPM-1 and KFUPM-1/$FeCl_3$ at 14 KHz.

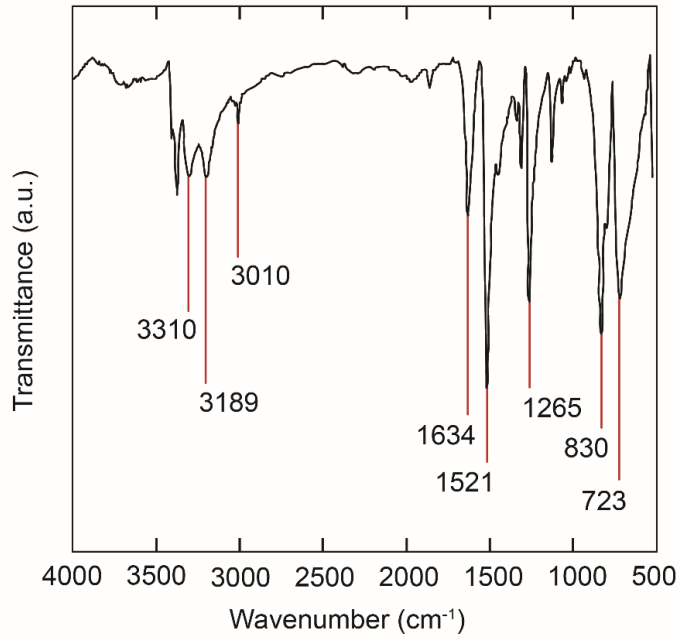

Figure 59 FT-IR spectrum of 1,4-benzenediamine monomer.

Table 10 Assignment of the FT-IR spectrum peaks of the 1,4-benzenediamine monomer.

Band Position (cm^{-1})	Band Assignments & Description
3310 (m) & 3189 (m)	NH_2 stretch (asymmetric, higher frequency, and symmetric)
3010 (w)	Aromatic C—H stretch
1634 (m)	Aromatic C=C vibration mode for aromatic ring
1521 (s)	Phenyl ring C=C vibration mode
1265 (s)	Can be assigned to the C—N stretch
830 (s)	C-H bending
723 (s)	NH_2 wagging

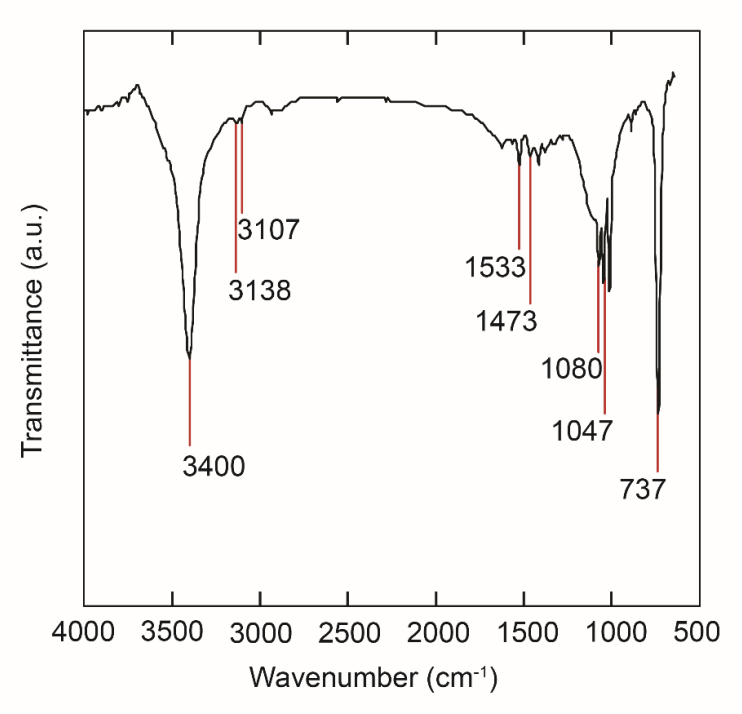

Figure 60 FT-IR spectrum of pyrrole monomer.

Table 11 Assignment of the FT-IR spectrum bands of the pyrrole monomer.

Band Position (cm^{-1})	Band Assignments & Notes
3400 (s)	NH stretching from the pyrrole ring
3138 (w)	Aromatic =C-H stretching from the pyrrole ring
3107 (w)	Aromatic =C-H stretching from the pyrrole ring
1533 (w)	Aromatic ring stretching
1473 (w)	Aromatic ring stretching
1080 (m)	Aromatic C-H bending
737 (s)	NH wagging (H-bonded)

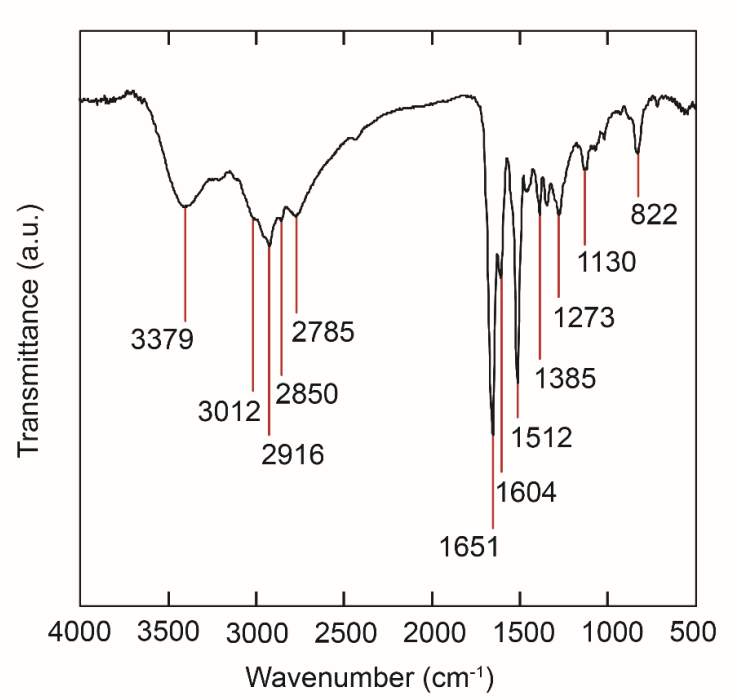

Figure 61 FT-IR spectrum of model polymer.

Table 12 Assignment of the FT-IR spectrum bands of the synthesized model polymer.

Band Position (cm^{-1})	Band Assignments & Description
3379 (br)	2^{ry} amine N-H stretching, is considered as an evidence for the methylene linkage from the formaldehyde at the NH_2
3012 (w) & 2916 (w)	Aromatic C-H stretching from the phenyl ring
2850 (w)	Methylene C-H stretch specific for CH_2 linkage for the polymer NOT present in the benzenediamine ring
1651 (s)	Aromatic C=C vibration mode
1512 (s)	Phenyl ring C=C vibration mode
1385 (m)	Can be assigned CH_2 deformation band
1130 (w)	C-N stretching
822 (w)	NH_2 wagging

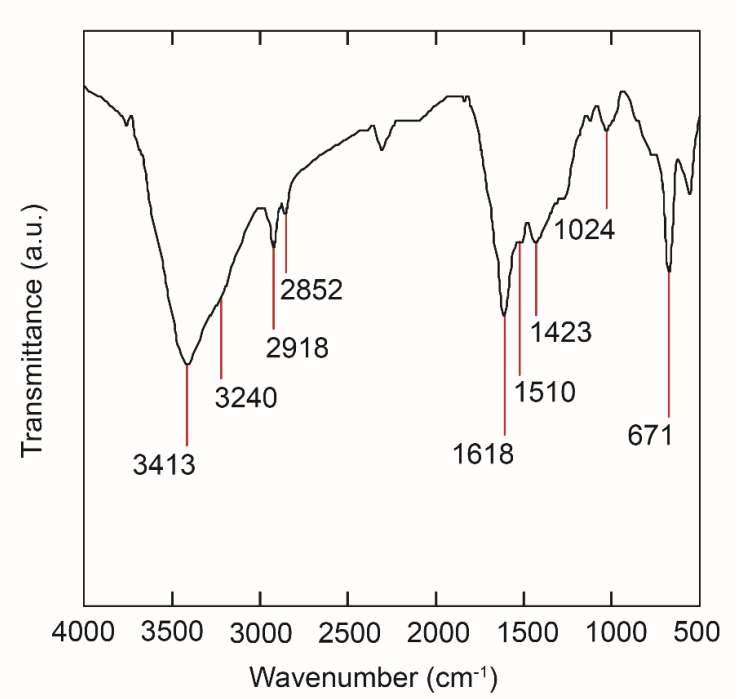

Figure 62 FT-IR spectrum of KFUPM-1

Table 13 Assignment of the FT-IR spectrum bands of the synthesized KFUPM-1.

Band Position (cm^{-1})	Band Assignments & Description
3413 (br)	N-H stretch from both pyrrole & benzenediamine moieties overlap with O-H stretch of terminal groups
3240 (w)	Can be assigned to NH_2 stretches of 1,4-benzenediamine moiety
2918 (w)	Aliphatic C-H stretch of CH_2 linkage, NOT present in neither benzenediamine nor pyrrole monomers
1618 (m)	Aromatic C=C vibration mode for the Asymmetric aromatic rings
1510 (w)	Phenyl ring C=C vibration mode, characteristic band, proves the presence of the benzenediamine moiety in the copolymer
1423 (w)	Can be assigned to the phenyl C=C vibrational mode
1124 (w)	C-N stretch in both benzenediamine & pyrrole moieties
671 (w)	NH_2 wagging

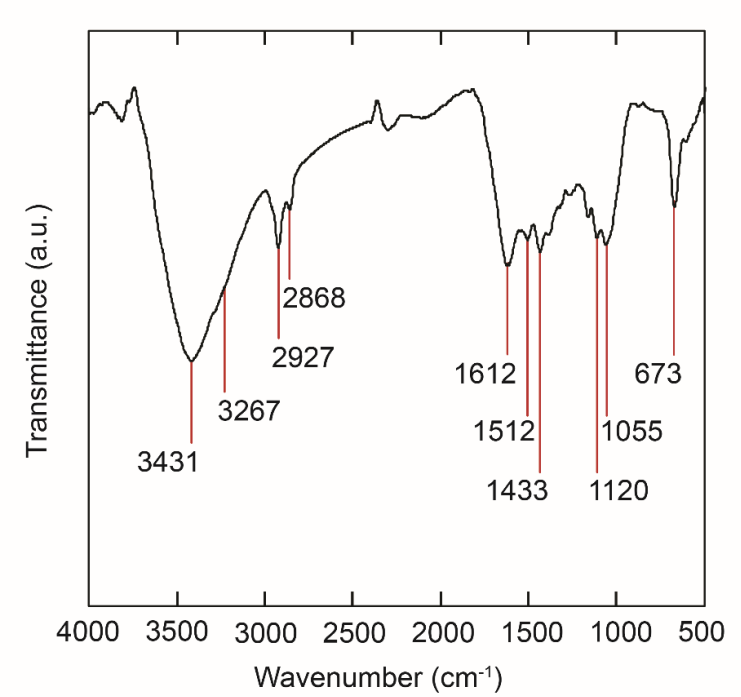

Figure 63 FT-IR spectrum of KFUPM-1/$FeCl_3$.

Table 14 Assignment of the FT-IR spectrum peaks of the synthesized KFUPM-1/$FeCl_3$.

Band Position (cm-1)	Band Assignments & Description
3431 (br)	N-H stretch from both pyrrole & benzenediamine moieties overlap with O-H stretch of terminal groups
3267 (w)	Can be assigned to NH_2 stretches of 1,4-benzenediamine moiety
2927 (m)	Aliphatic C-H stretch of CH_2 linkage, NOT present in neither benzenediamine nor pyrrole monomers
1612 (m)	Aromatic C=C vibration mode for the Asymmetric aromatic rings in the copolymer
1512 (w)	Phenyl ring C=C vibration mode, characteristic band, proves the presence of the benzenediamine moiety in the copolymer
1433 (w)	Can be assigned to the phenyl C=C vibrational mode
1120 (w)	C-N stretch in both the benzenediamine and pyrrole moieties in the polymer
673 (m)	NH_2 wagging

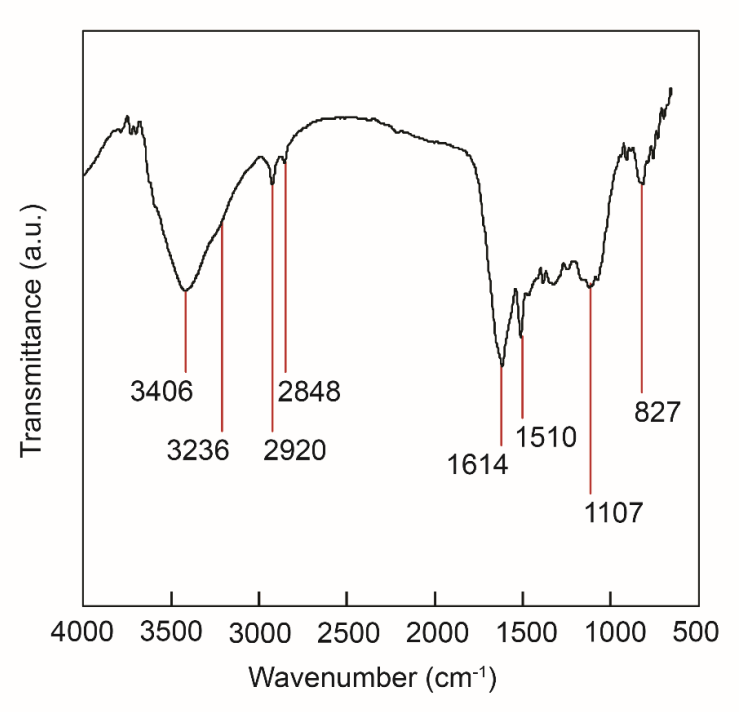

Figure 64 FT-IR spectrum of KFUPM-1/CuCl.

Table 15 Assignment of the FT-IR spectrum peaks of the synthesized KFUPM-1/CuCl.

Band Position (cm^{-1})	Band Assignments & Description
3406 (br)	N-H stretch for the pyrrole as well as the benzenediamine moieties overlap with O-H stretch, terminal OH
3236 (w)	Can be assigned to NH_2 group for the 1,4-benzenediamine moieties.
2920 (w)	Aliphatic C-H stretch of CH_2 linkage, NOT present in neither benzenediamine nor pyrrole monomers
1614 (m)	Aromatic C=C vibration mode for the Asymmetric aromatic rings in the copolymer and phenyl ring C=C vibration mode
1423 (w)	Can be assigned to the phenyl C=C vibrational mode
1107 (w)	C-N stretch in both the benzenediamine and pyrrole moieties in the polymer
827 (w)	NH_2 wagging

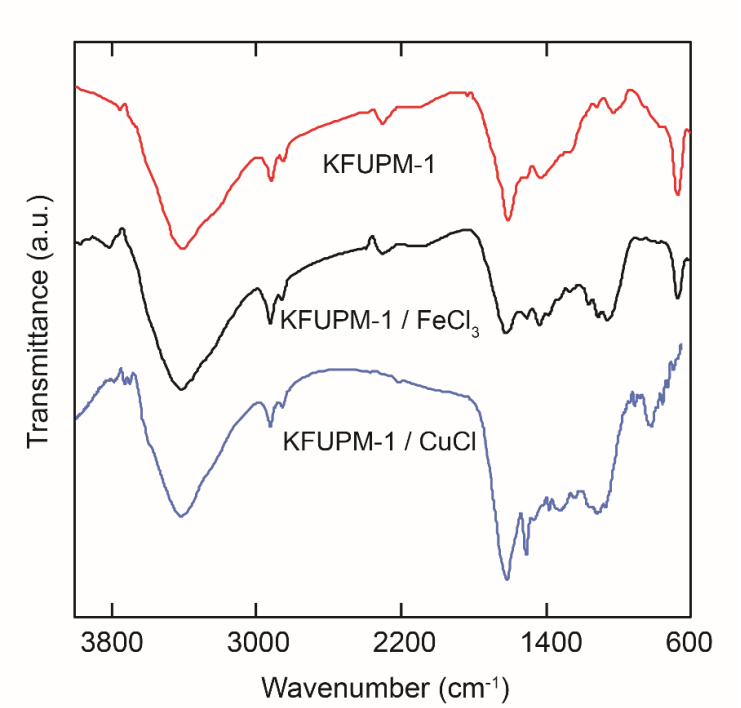

Figure 65 Stack mode of the FT-IR spectra of the polymers KFUPM-1 (red), KFUPM-1/$FeCl_3$ (black), and KFUPM-1/CuCl (blue).

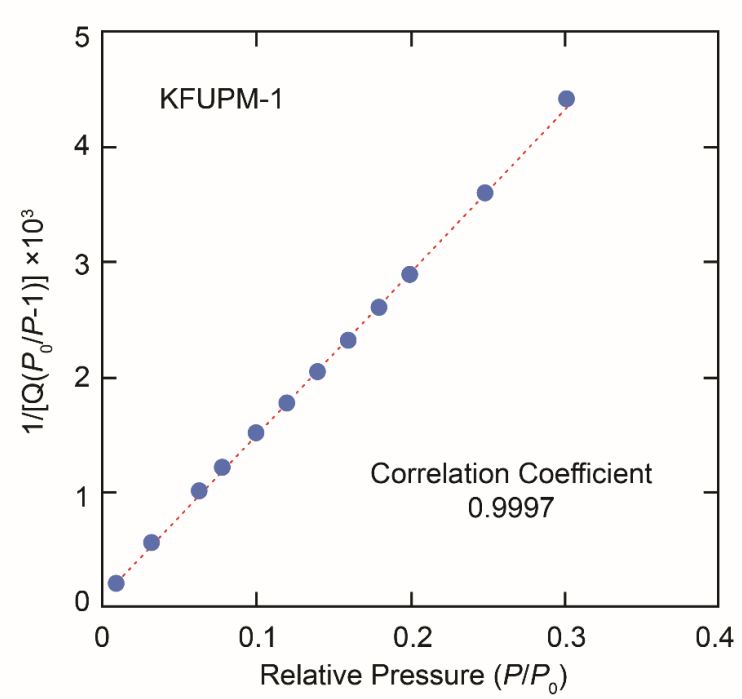

Figure 66 BET plot of KFUPM-1 from experimental nitrogen adsorption isotherm at 77 K within low relative pressure showing data points (blue circle), and the trend line (red dashed line).

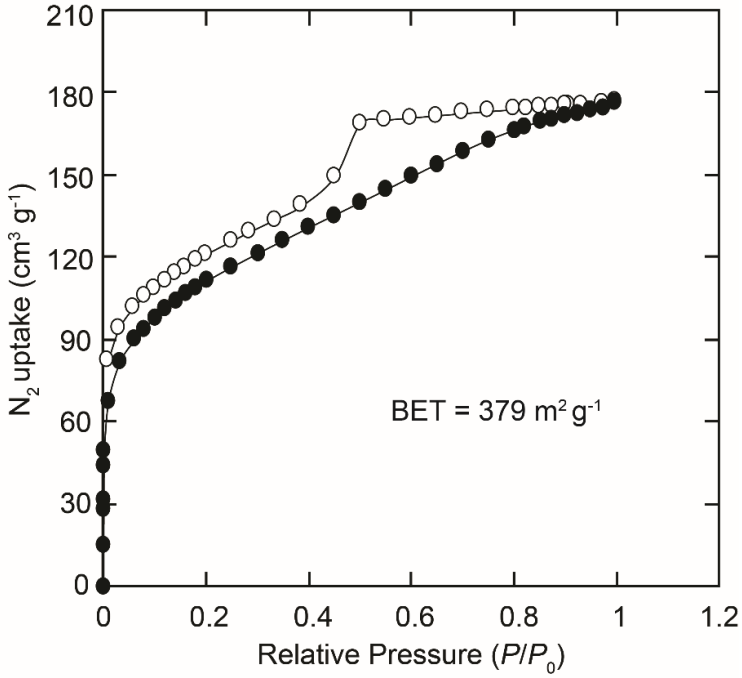

Figure 67 N_2 adsorption isotherm at 77 K for KFUPM-1/$FeCl_3$. Filled and open symbols represent adsorption and desorption branches, respectively. The connecting lines serve as a guide to the eye.

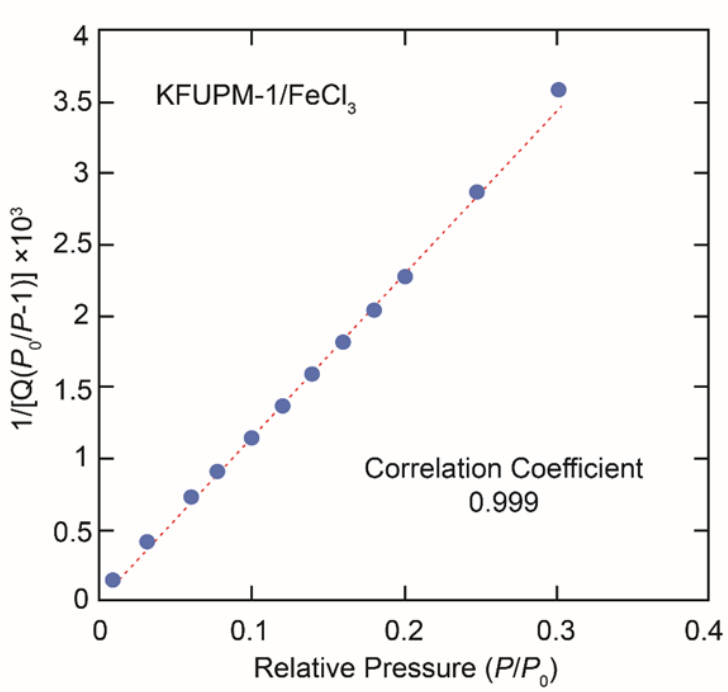

Figure 68 BET plot of KFUPM-1/$FeCl_3$ from experimental nitrogen adsorption isotherm at 77 K within low relative pressure showing data points (blue circle), and the trend line (red dashed line).

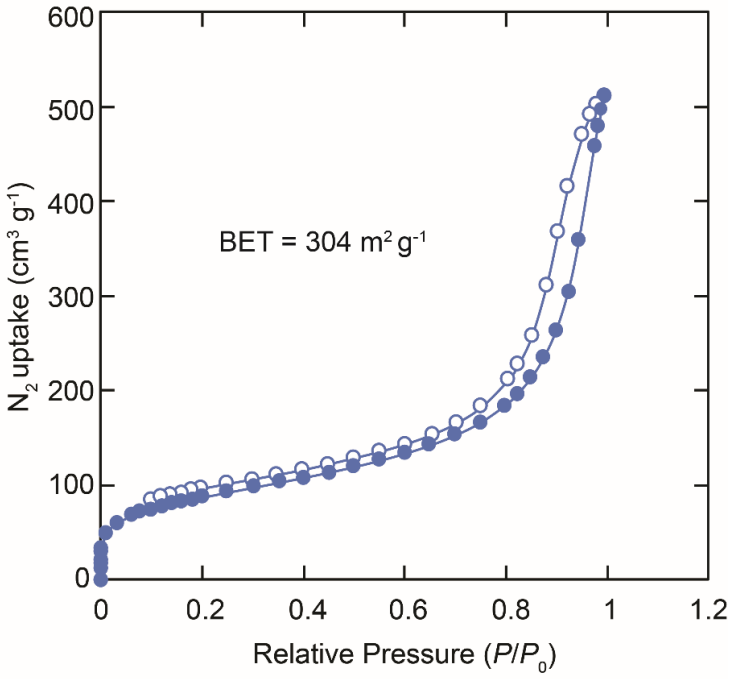

Figure 69 N_2 adsorption isotherm at 77 K for KFUPM-1/CuCl. Filled and open symbols represent adsorption and desorption branches, respectively. The connecting lines serve as a guide to the eye.

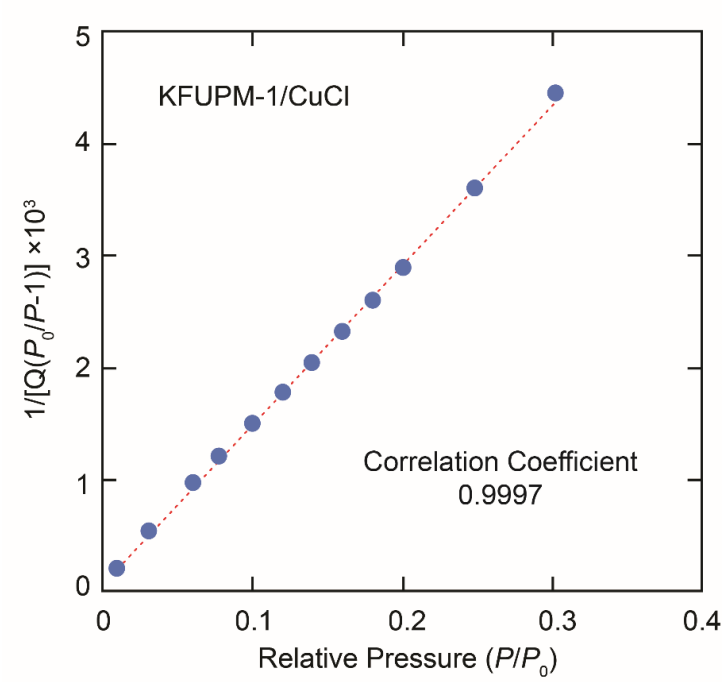

Figure 70 BET plot of KFUPM-1/CuCl from experimental nitrogen adsorption isotherm at 77 K within low relative pressure showing data points (blue circle), and the trend line (red dashed line).

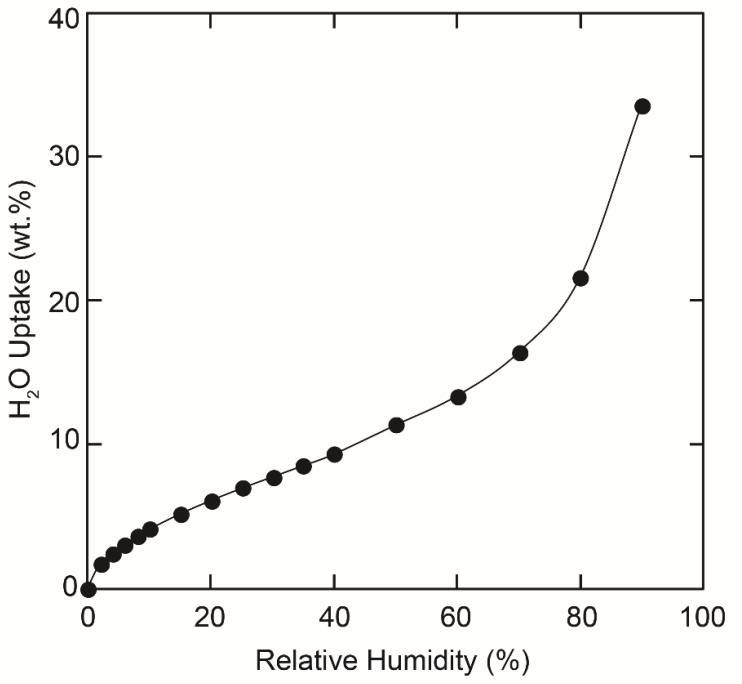

Figure 71 Water isotherm of KFUPM-1 at 298 K.

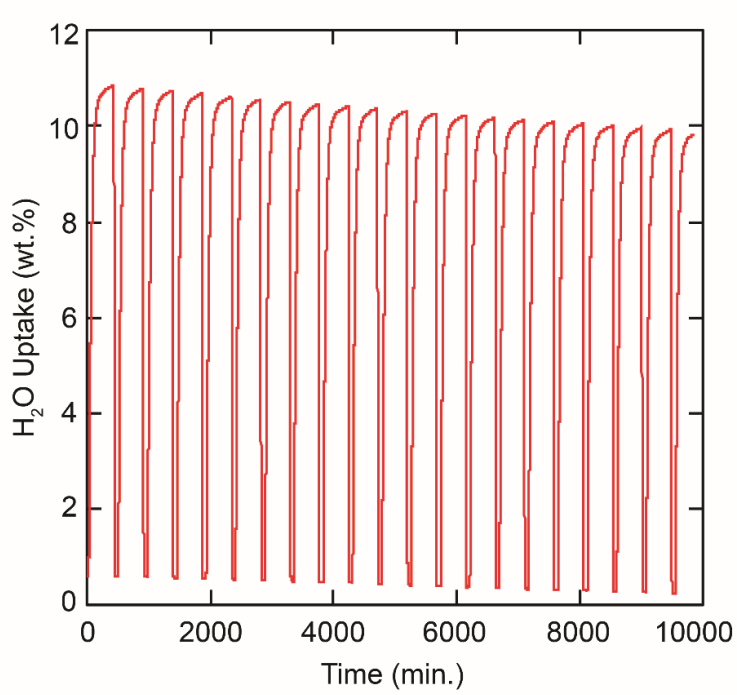

Figure 72 Water adsorption cycles at 313 K and 76% RH. Activation between cycles was carried out at 383 K under vacuum.

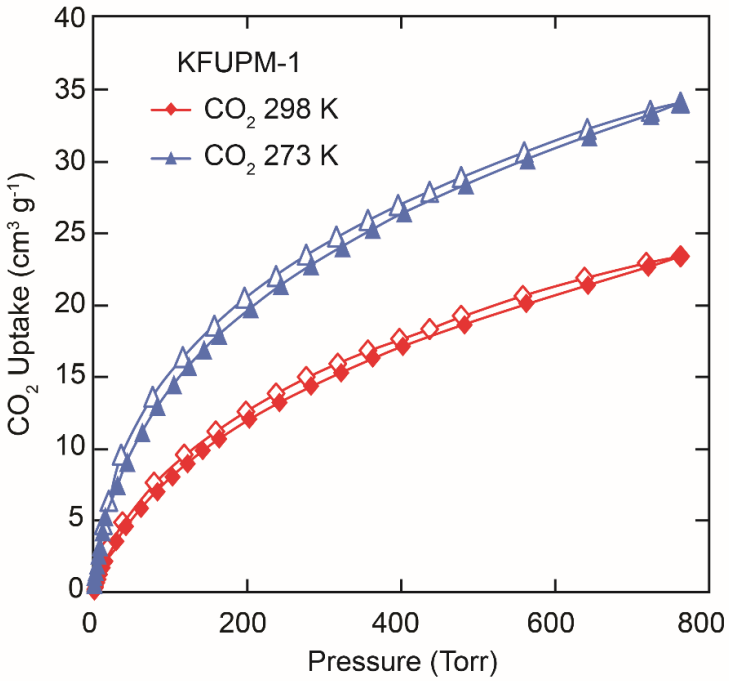

Figure 73 CO_2 sorption isotherms for KFUPM-1 at 273 K (triangle) and 298 K (diamond). Filled and open symbols represent adsorption and desorption branches, respectively. The connecting lines serve as a guide to the eye.

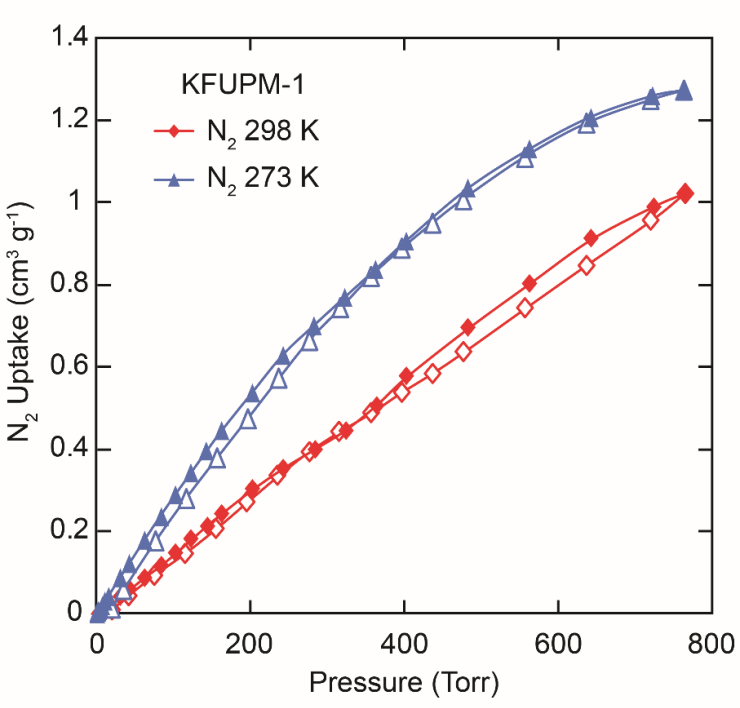

Figure 74 N_2 sorption isotherms for KFUPM-1 at 273 K (triangle) and 298 K (diamond). Filled and open symbols represent adsorption and desorption branches, respectively. The connecting lines serve as a guide to the eye.

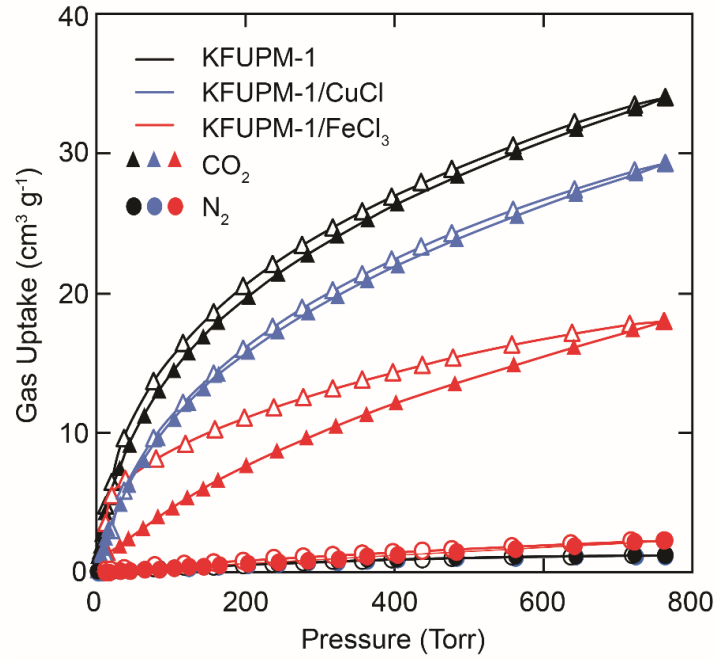

Figure 75 CO_2 (triangle) and N_2 (circle) sorption isotherms for KFUPM-1 (black), KFUPM-1/CuCl (blue), and KFUPM-1/$FeCl_3$ (red) at 273 K. Filled and open symbols represent adsorption and desorption branches, respectively. The connecting lines serve as a guide to the eye.

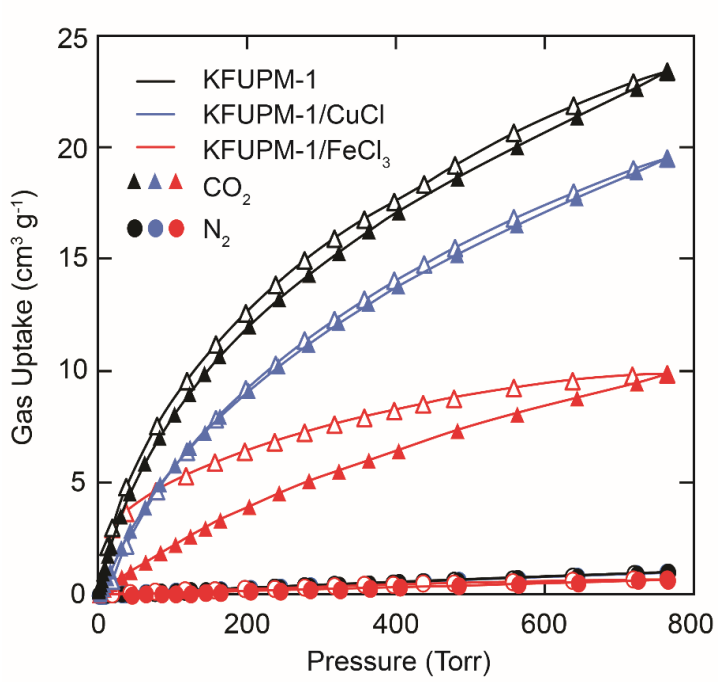

Figure 76 CO_2 (triangle) and N_2 (circle) sorption isotherms for KFUPM-1 (black), KFUPM-1/CuCl (blue), and KFUPM-1/$FeCl_3$ (red) at 298 K. Filled and open symbols represent adsorption and desorption branches, respectively. The connecting lines serve as a guide to the eye.

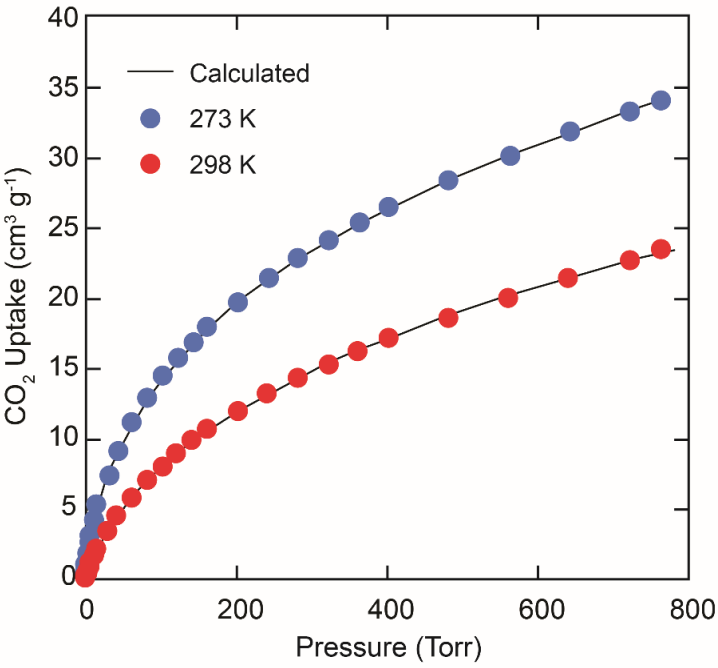

Figure 77 Virial-type equation fitting (black line) of experimental CO_2 adsorption data for KFUPM-1 at 273 K (blue circle) and 298 K (red circle).

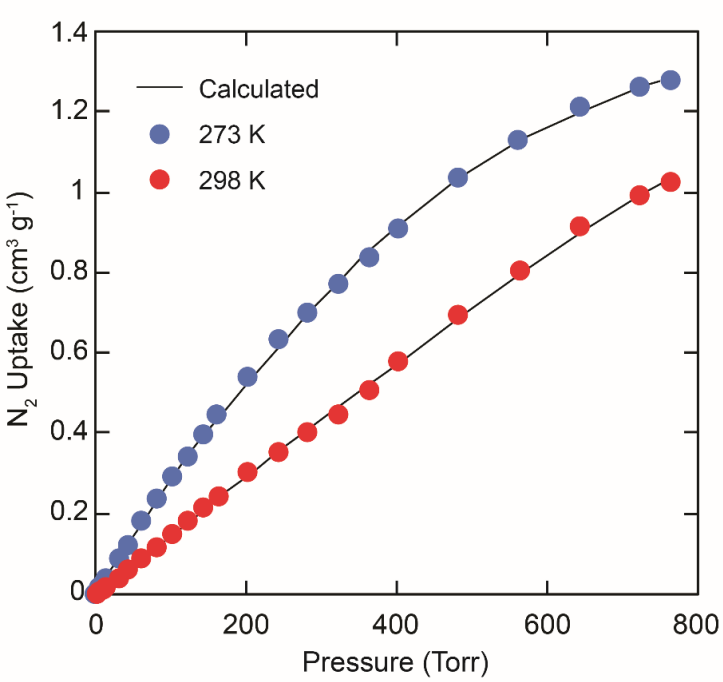

Figure 78 Virial-type equation fitting (black line) of experimental N_2 adsorption data for KFUPM-1 at 273 K (blue circle) and 298 K (red circle).

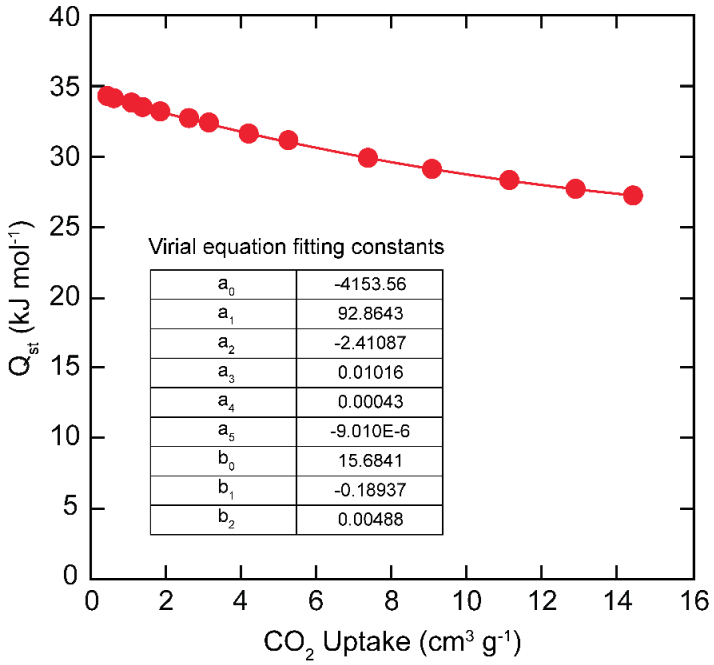

Figure 79 Calculated enthalpy of adsorption (Q_{st}) of CO_2 gas for KFUPM-1. Inset provides the constants used for the fitting of 273 K and 298 K CO_2 adsorption isotherms using virial-type equation.

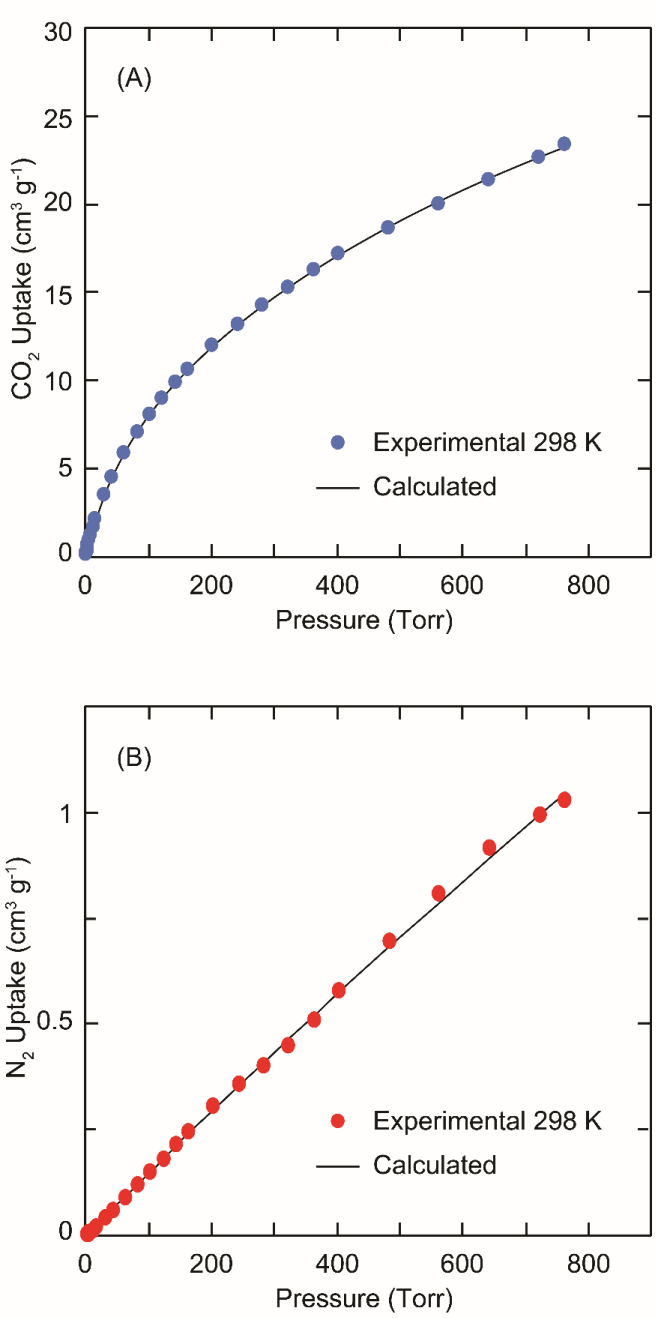

Figure 80 Dual-site Langmuir fitting of experimental isotherms at 298 K for (A) CO_2 (blue circle), and (B) N_2 (red circle).

Table 16 Dual site Langmuir fitting parameters for CO_2 and N_2 adsorption at 298K for KFUPM-1 used for calculating the IAST selectivity.

CO_2		N_2	
$qmax_1$	8.4790391724590	**$qmax_1$**	10.1700610532542
K_1	0.0146335714423	**K_1**	0.0001509288138
$qmax_2$	42.4294292028068	**$qmax_2$**	-0.0066302405165
K_2	0.0007526233526	**K_2**	-30.0495872907169

Appendix B: Supporting Information for Chapter three

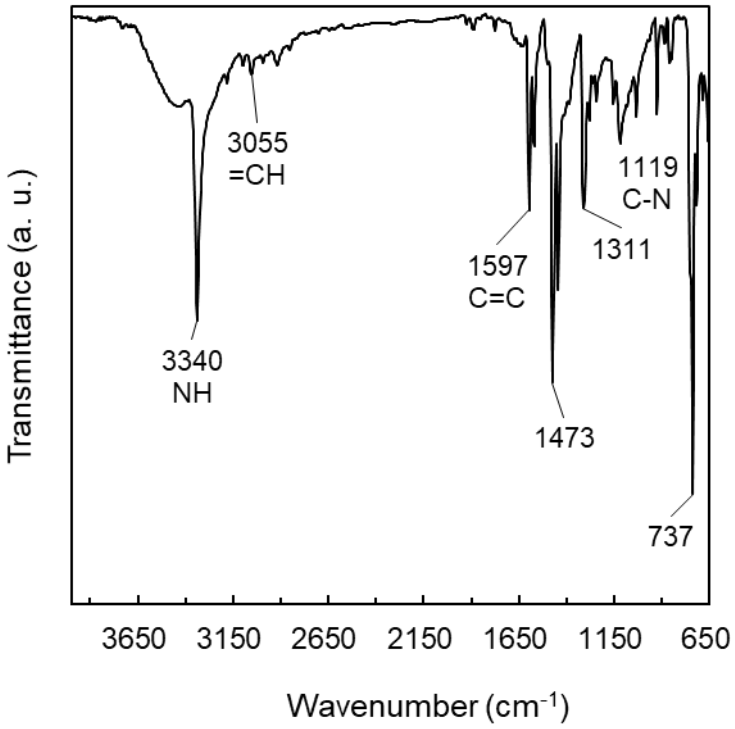

Figure 81 FT-IR spectrum of Phenothiazine monomer.

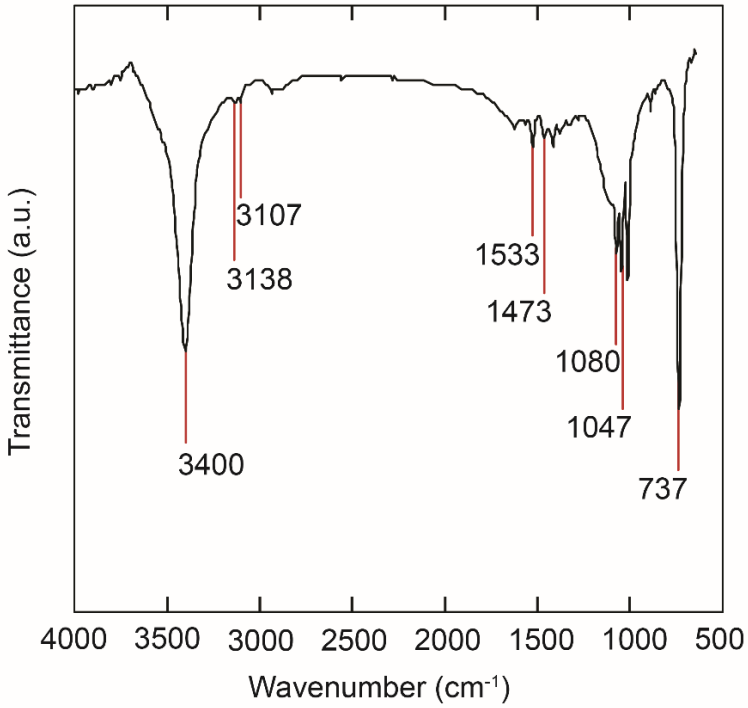

Figure 82 FT-IR spectrum of pyrrole monomer.

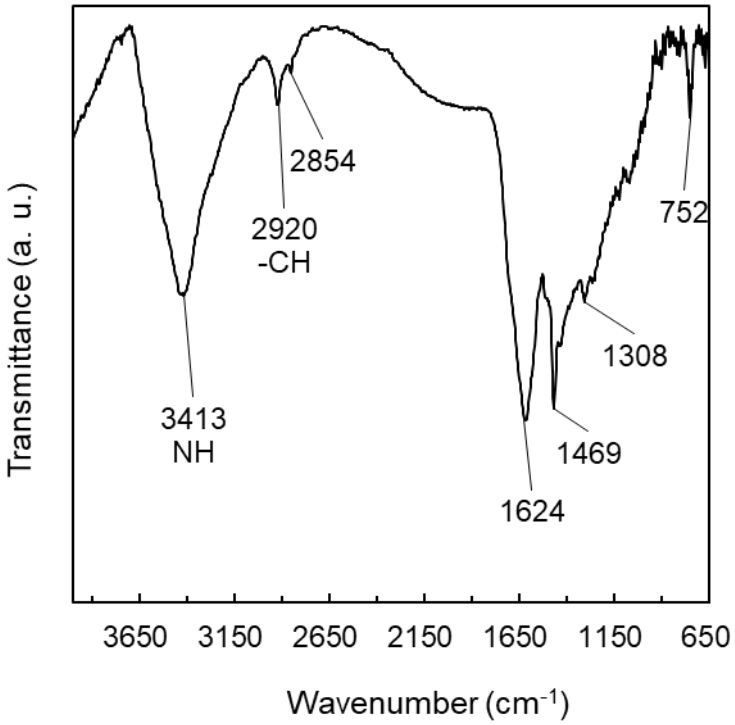

Figure 83 FT-IR spectrum of PhzPy-1

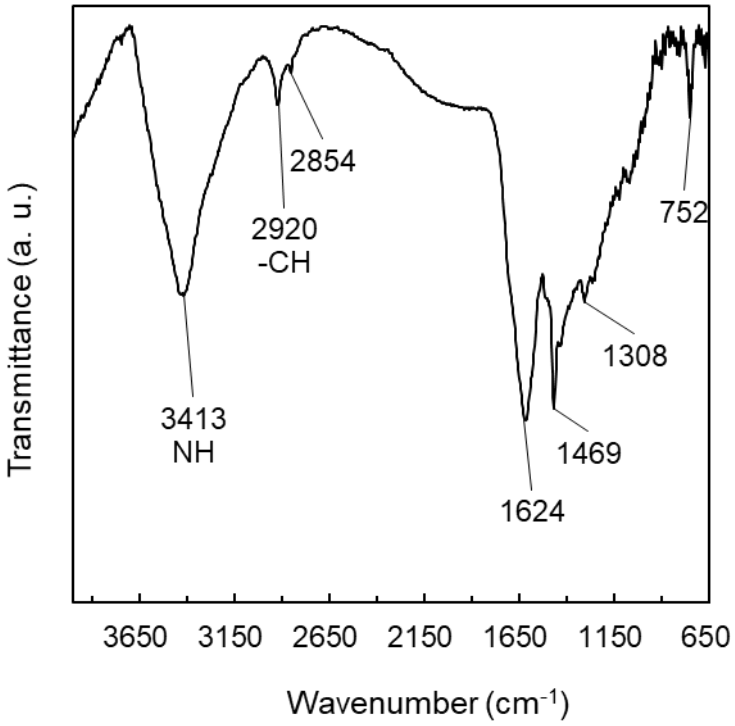

Figure 84 FT-IR spectrum of PhzPy-2

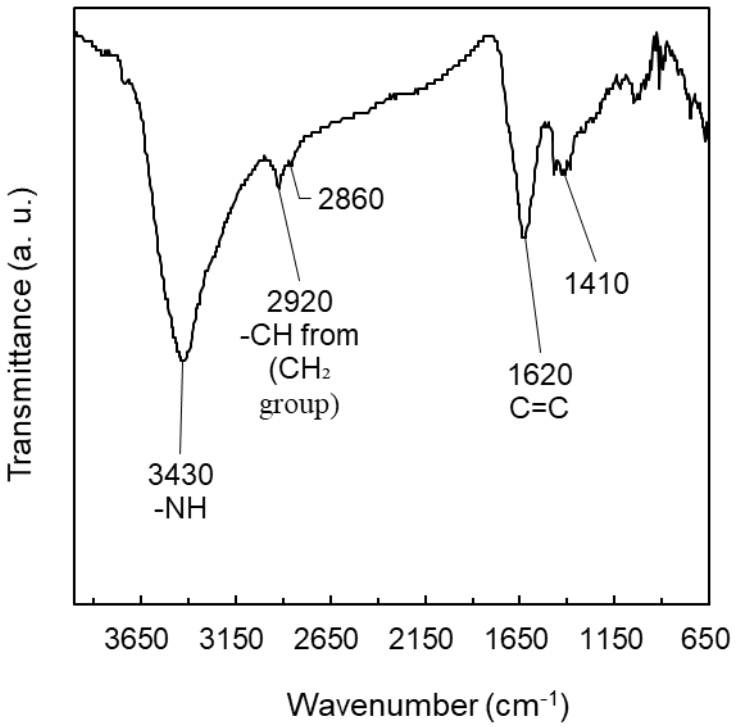

Figure 85 FT-IR spectrum of (PhzPy-3) KFUPM-2

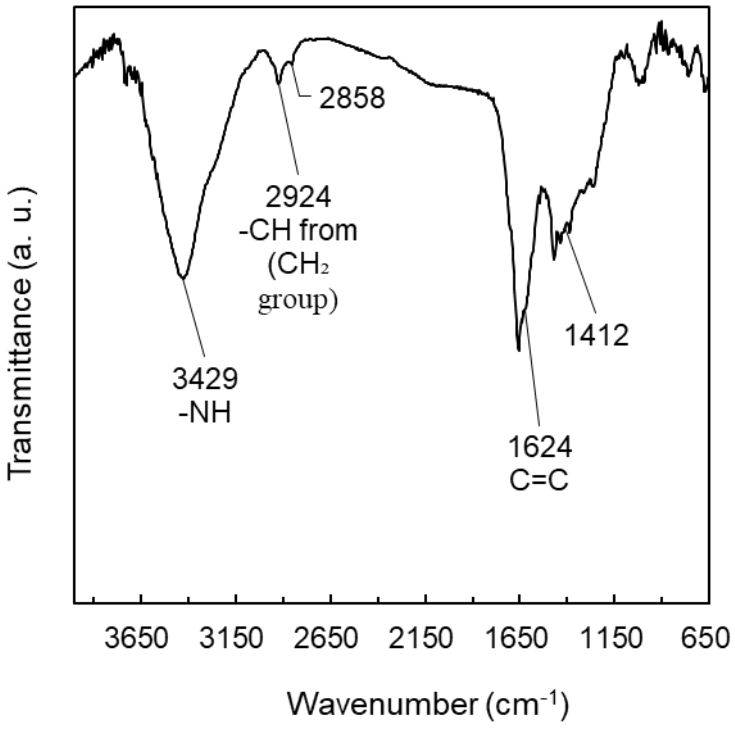

Figure 86 FT-IR spectrum of PhzPy-4

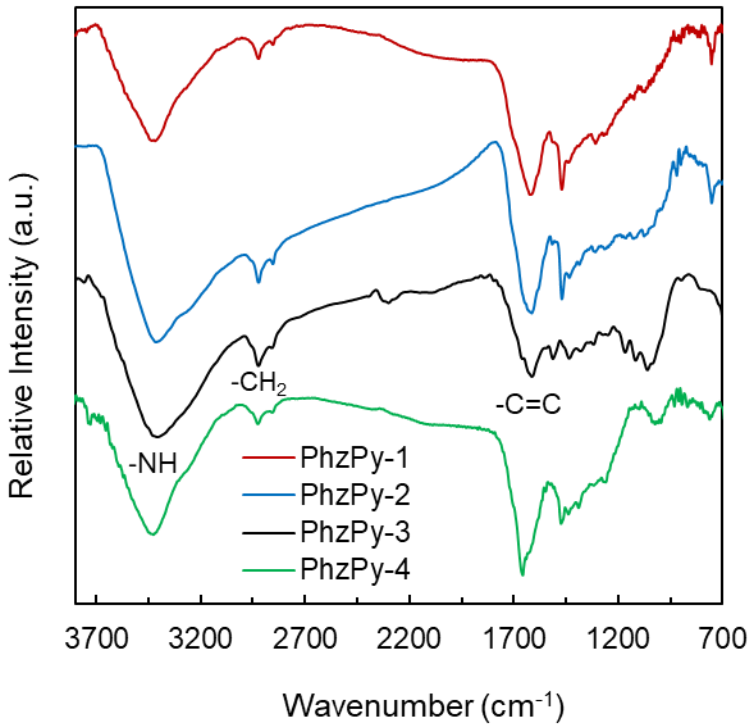

Figure 87 Stack mode of the FT-IR spectra of the polymers PhzPy-1 (red), PhzPy-2 (blue), PhzPy-3 (KFUPM-2) (black), and PhzPy-4 (green).

Gas sorption properties

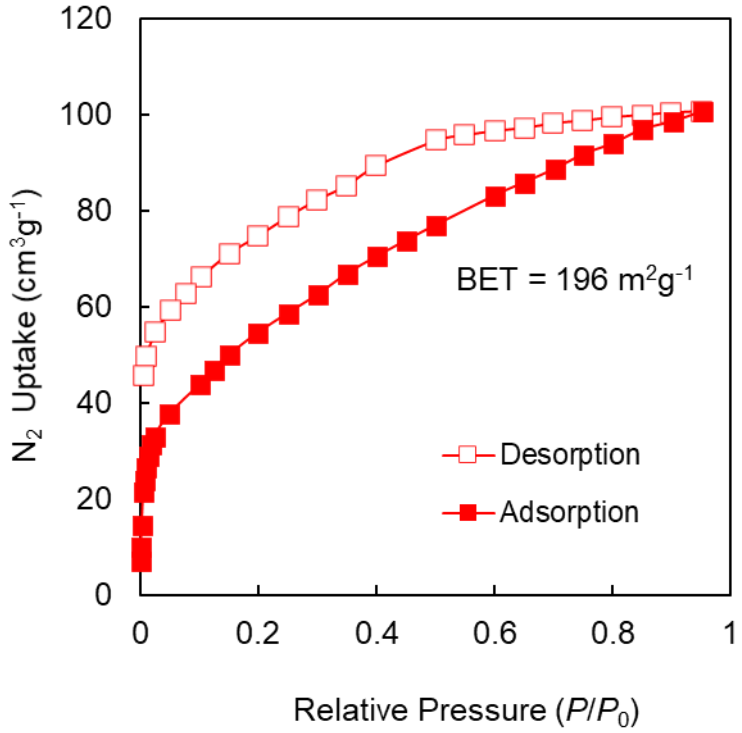

Figure 88 N_2 adsorption isotherm at 77 K for PhzPy-1. Filled and open symbols represent adsorption and desorption branches, respectively. The connecting lines serve as a guide to the eye.

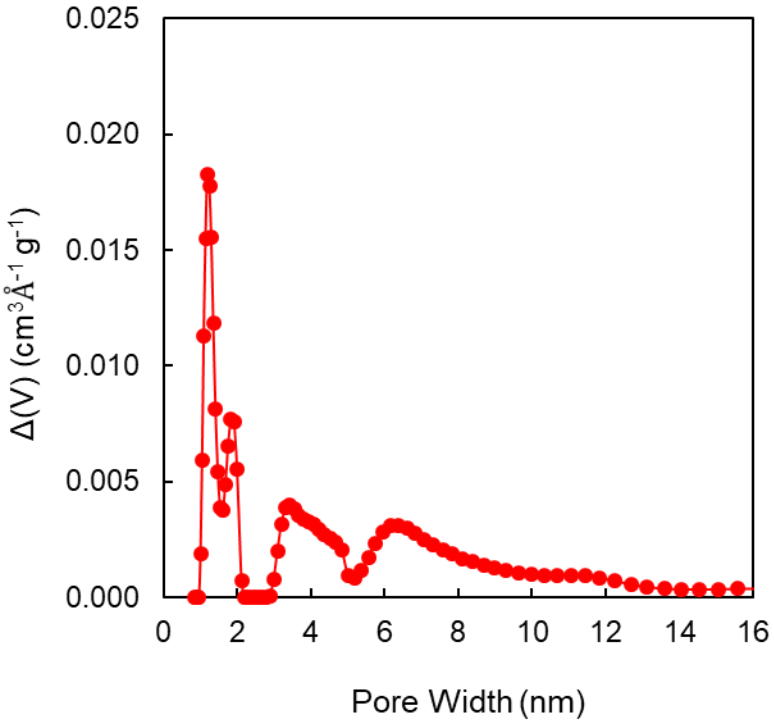

Figure 89 Pore size distribution of PhzPy-1 calculated by QSDFT model.

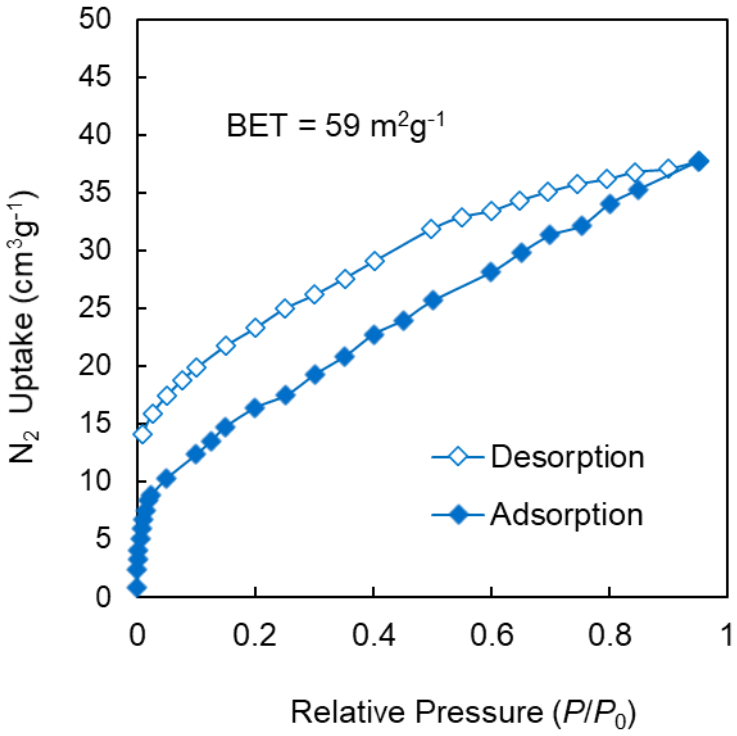

Figure 90 N_2 adsorption isotherm at 77 K for PhzPy-2. Filled and open symbols represent adsorption and desorption branches, respectively. The connecting lines serve as a guide to the eye.

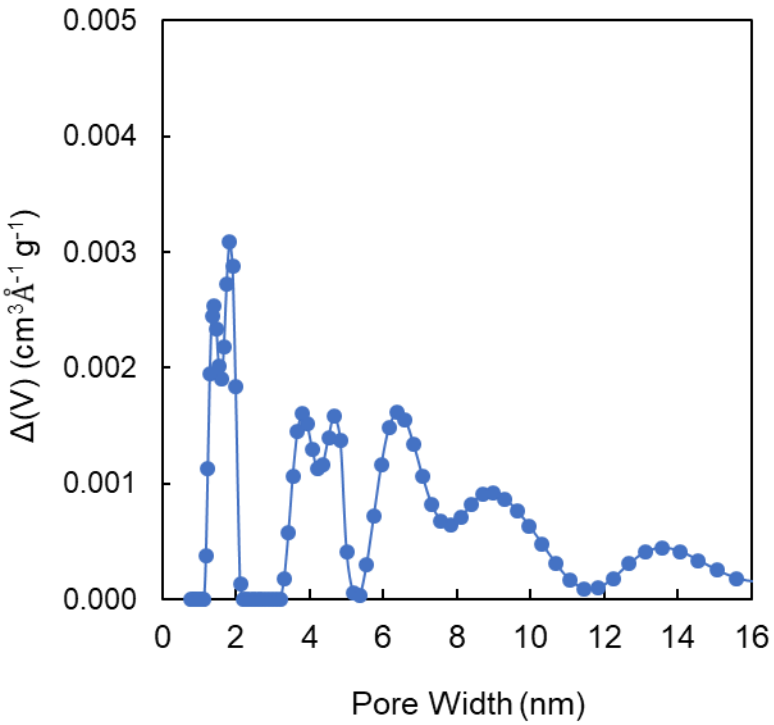

Figure 91 Pore size distribution of PhzPy-2 calculated by QSDFT model.

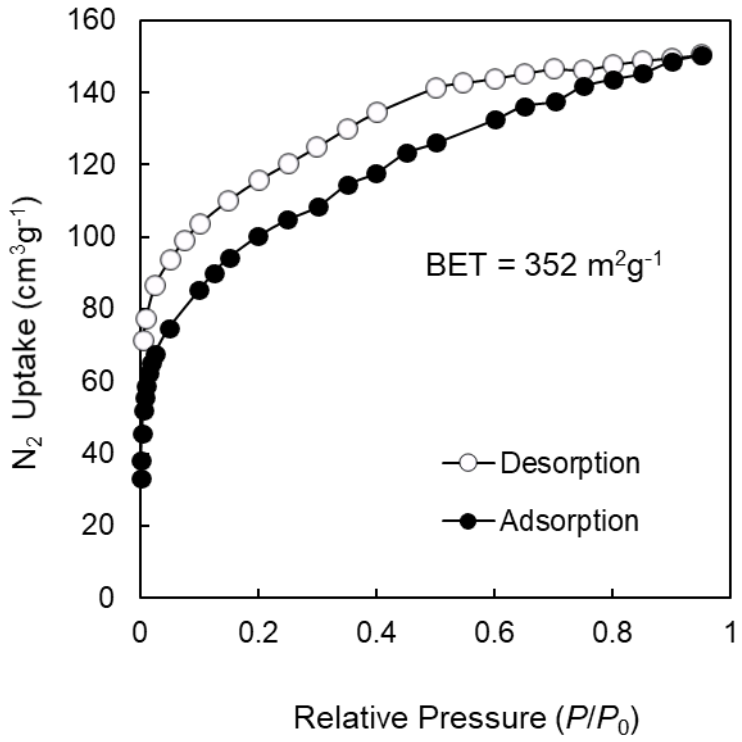

Figure 92 N_2 adsorption isotherm at 77 K for PhzPy-3 (KFUPM-2). Filled and open symbols represent adsorption and desorption branches, respectively. The connecting lines serve as a guide to the eye.

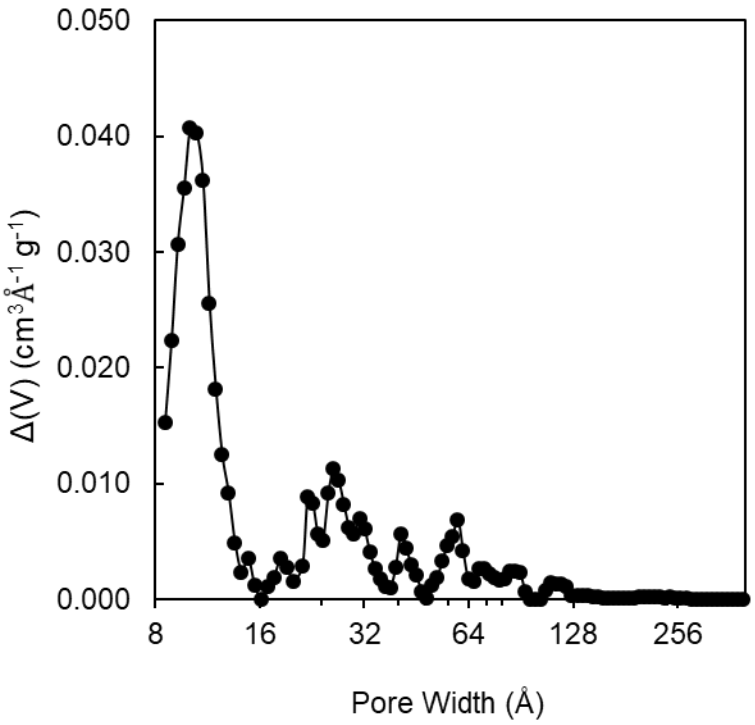

Figure 93 Pore size distribution of PhzPy-3 (KFUPM-2) calculated by QSDFT model.

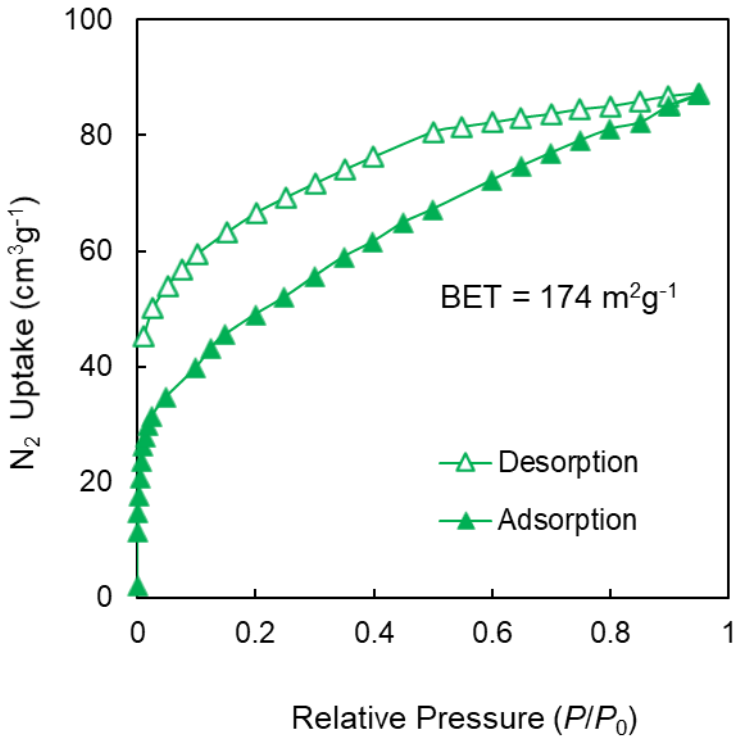

Figure 94 N_2 adsorption isotherm at 77 K for PhzPy-4. Filled and open symbols represent adsorption and desorption branches, respectively. The connecting lines serve as a guide to the eye.

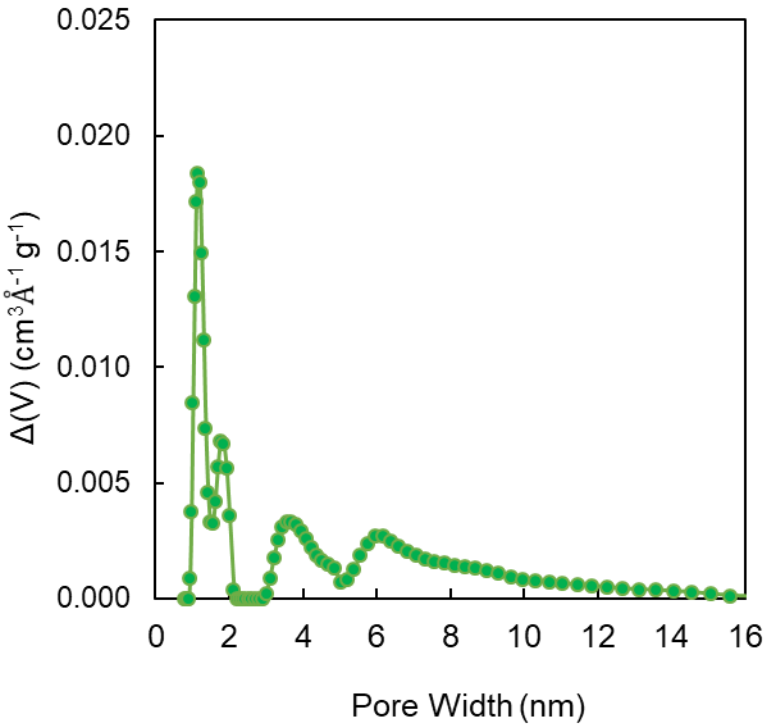

Figure 95 Pore size distribution of PhzPy-4 calculated by QSDFT model.

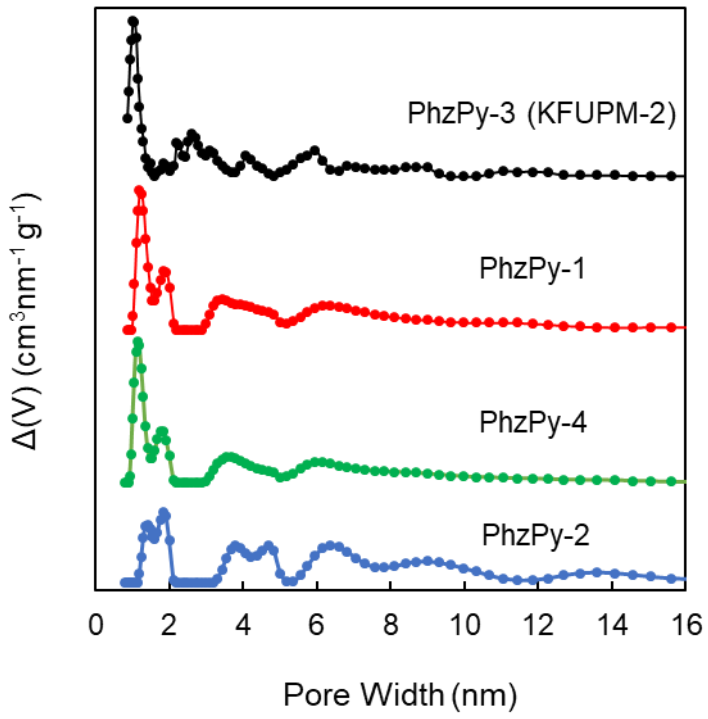

Figure 96 Stack graph of the Pore size distribution (PSD) of the polymers PhzPy-1 (red), PhzPy-2 (blue), PhzPy-3 (KFUPM-2) (black), and PhzPy-4 (green).

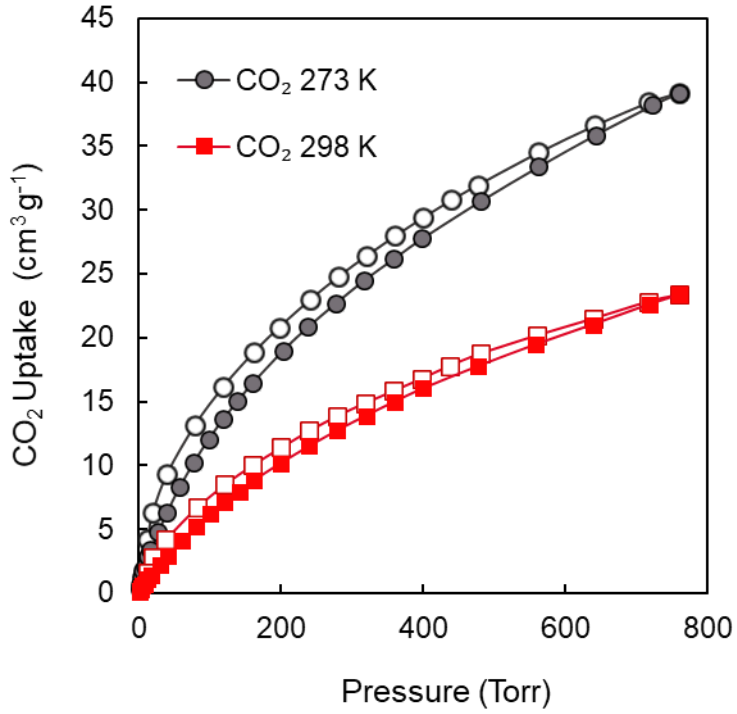

Figure 97 CO_2 sorption isotherms for PhzPy-3 (KFUPM-2) at 273 K (gray circle) and 298 K (red cube). Filled and open symbols represent adsorption and desorption branches, respectively. The connecting lines serve as a guide to the eye.

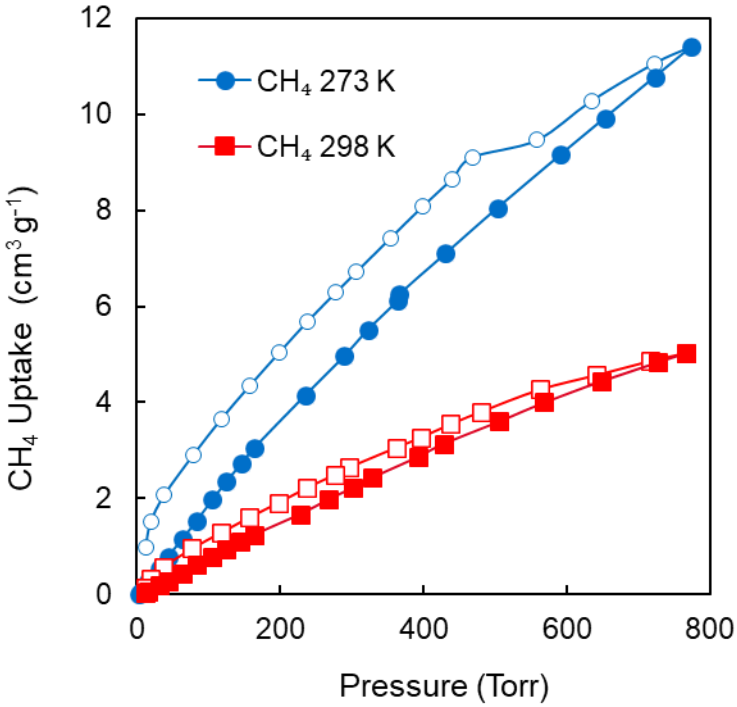

Figure 98 CH_4 sorption isotherms for PhzPy-3 (KFUPM-2) at 273 K (blue circle) and 298 K (red cube). Filled and open symbols represent adsorption and desorption branches, respectively. The connecting lines serve as a guide to the eye.

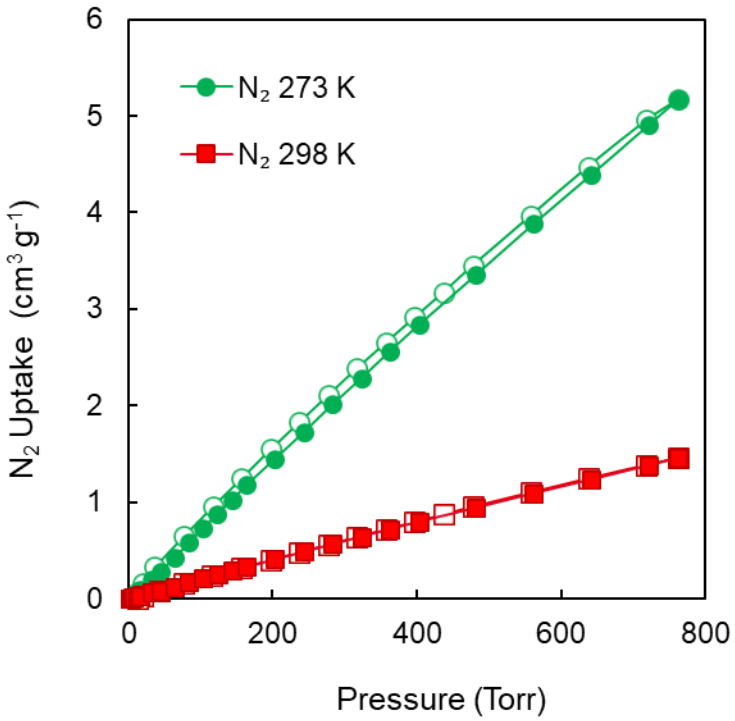

Figure 99 N_2 sorption isotherms for PhzPy-3 (KFUPM-2) at 273 K (green ball) and 298 K (red cube). Filled and open symbols represent adsorption and desorption branches, respectively. The connecting lines serve as a guide to the eye.

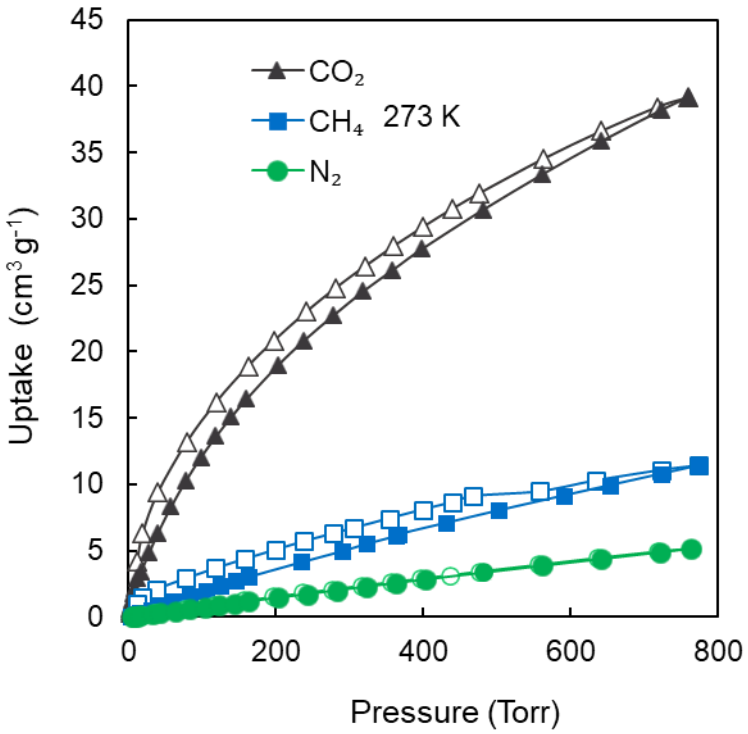

Figure 100 CO_2 (triangle), CH_4 (cube) and N_2 (circle) sorption isotherms for PhzPy-3 at 273 K. Filled and open symbols represent adsorption and desorption branches, respectively. The connecting lines serve as a guide to the eye.

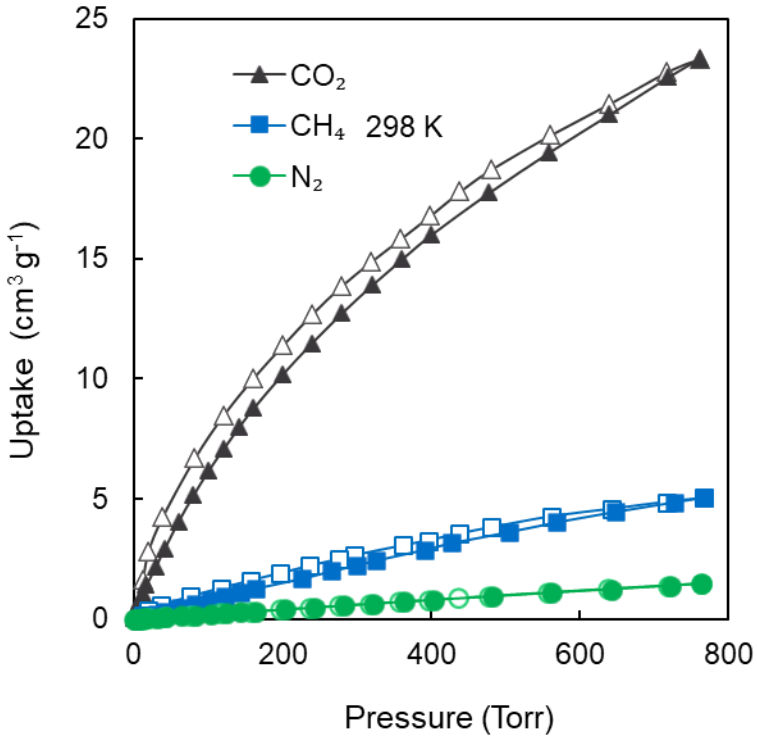

Figure 101 CO_2 (triangle) CH_4 (cube) and N_2 (circle) sorption isotherms for PhzPy-3 (KFUPM-2) at 298 K. Filled and open symbols represent adsorption and desorption branches, respectively. The connecting lines serve as a guide to the eye.

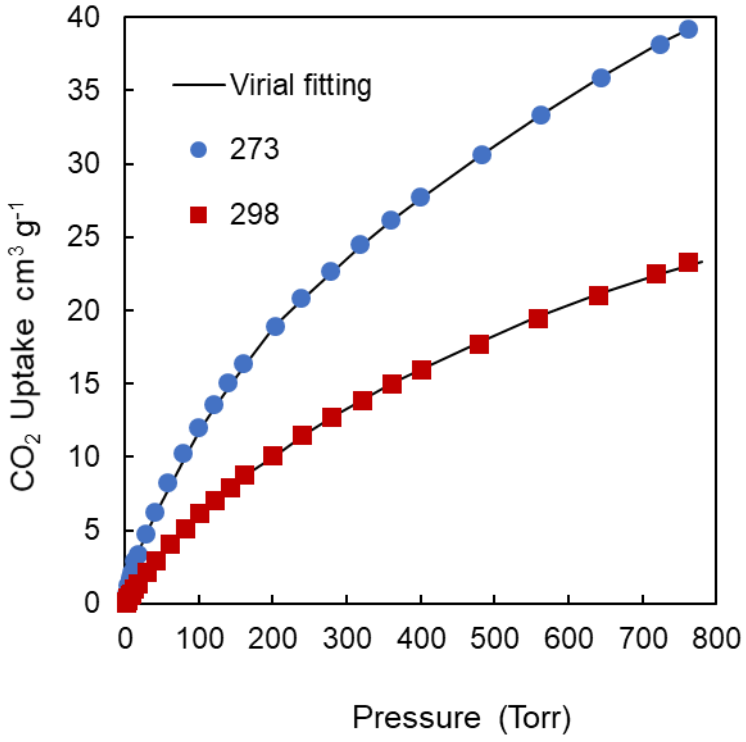

Figure 102 Virial-type equation fitting (black line) of experimental CO_2 adsorption data for PhzPy-3 (KFUPM-2) at 273 K (blue circle) and 298 K (red cube).

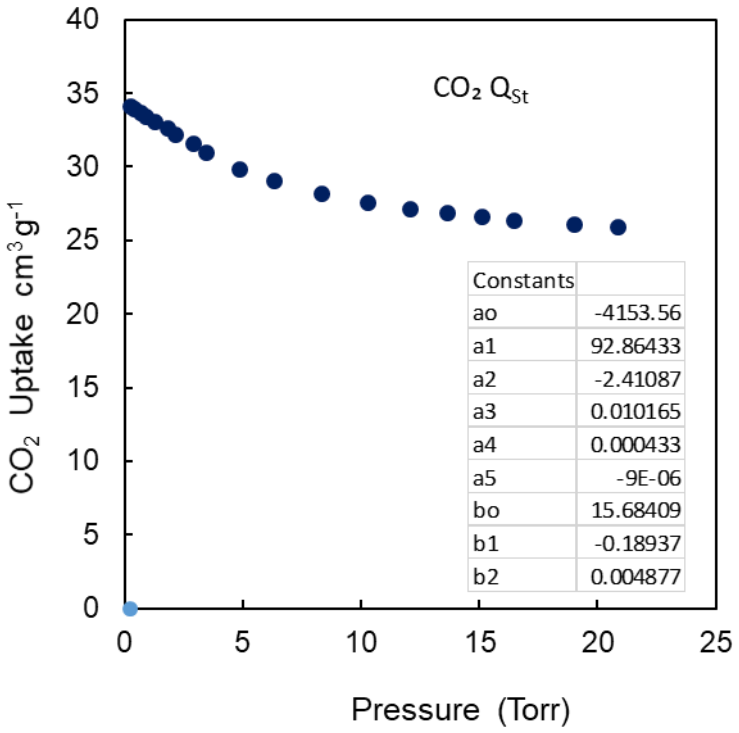

Figure 103 Calculated enthalpy of adsorption (Q_{st}) of CO_2 gas for PhzPy-3 (KFUPM-2). Inset provides the constants used for the fitting of 273 K and 298 K CO_2 adsorption isotherms using virial-type equation.

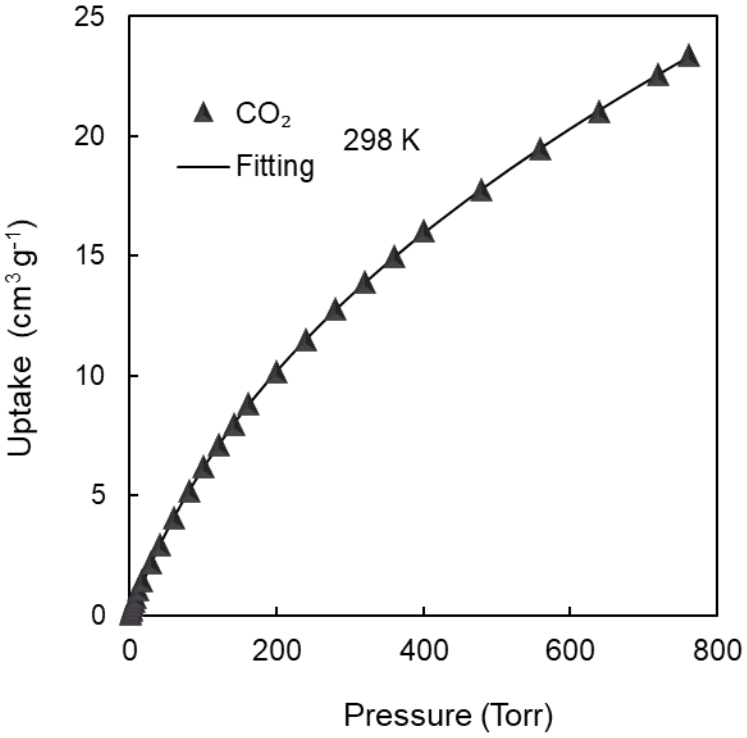

Figure 104 Dual site Langmuir fitting (black line) of experimental CO_2 adsorption data for PhzPy-3 (KFUPM-2) at 298 K (black triangle).

Appendix C: Supporting Information for Chapters four and five

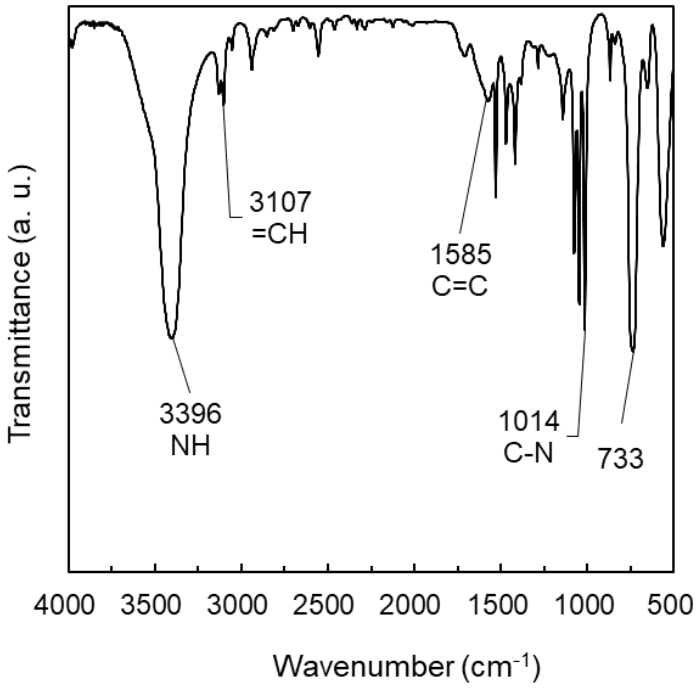

Figure 105 FT-IR spectrum of pyrrole monomer.

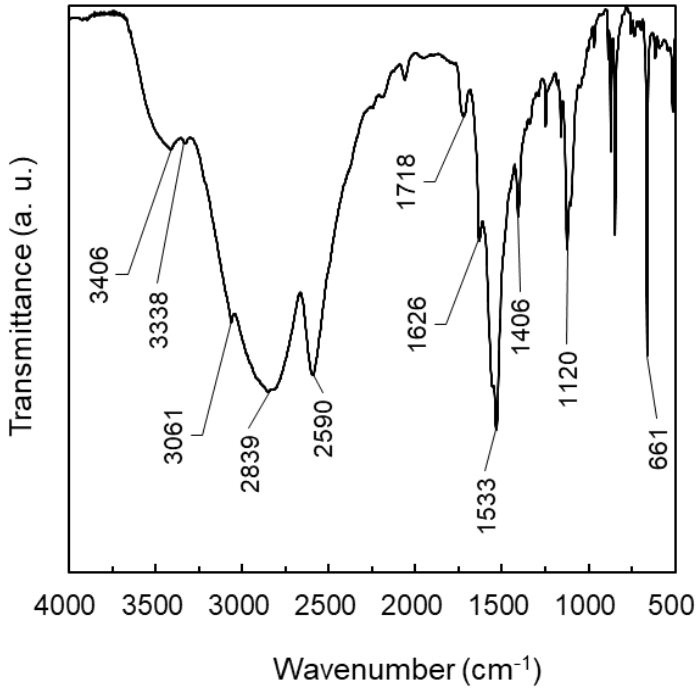

Figure 106 FT-IR spectrum of 1,3,5-triaminobenzene tri-hydrochloride (Tri) monomer.

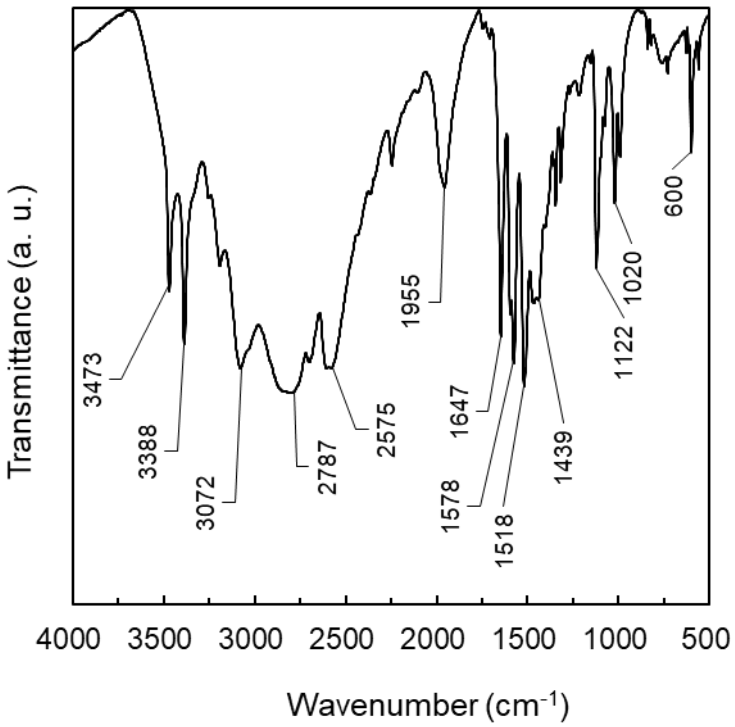

Figure S107 FT-IR spectrum of 2,4,6-trimethyl-benzene-1,3,5-triamine tri-hydrochloride (TMT) monomer.

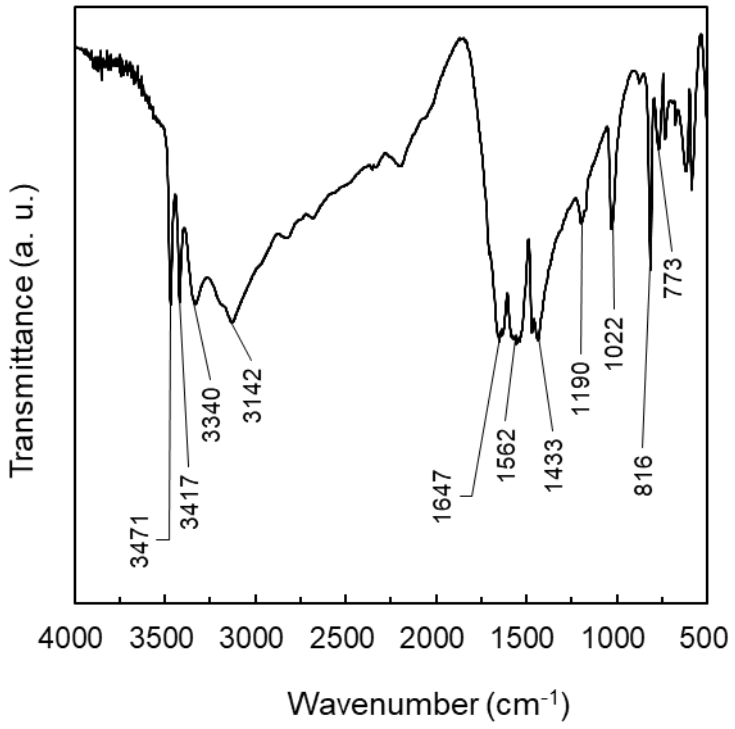

Figure 108 FT-IR spectrum of melamine (M) monomer.

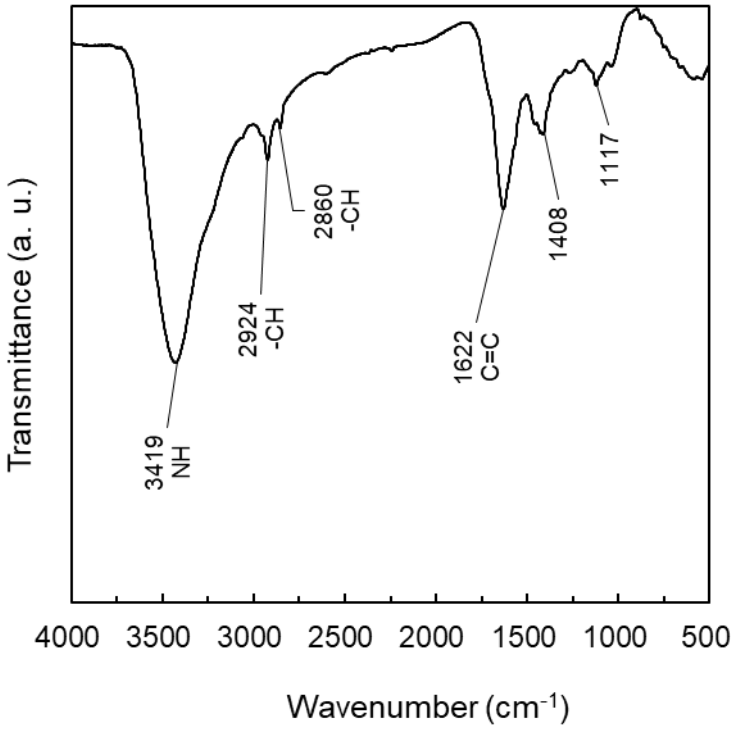

Figure 109 FT-IR spectrum of TriPy copolymer.

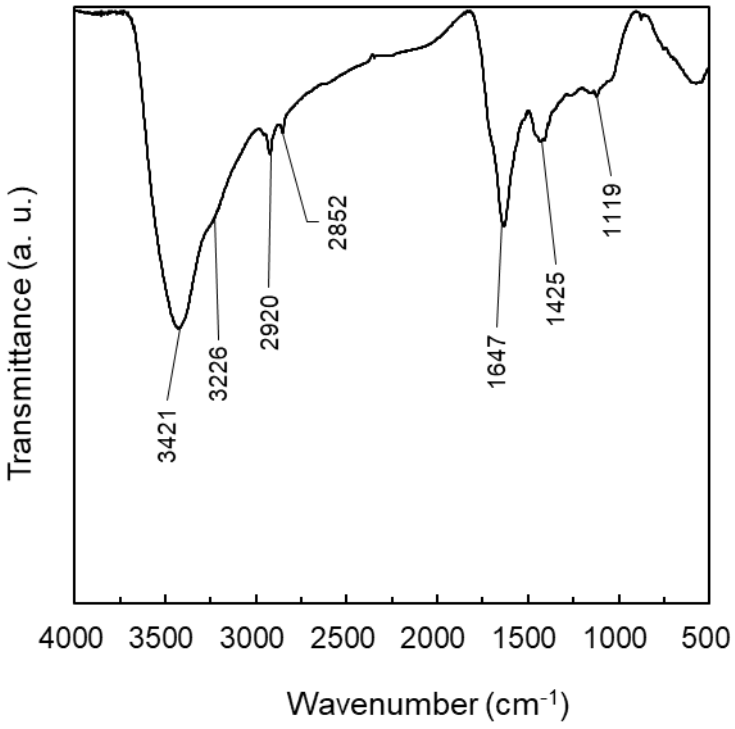

Figure 110 FT-IR spectrum of TMTPy copolymer.

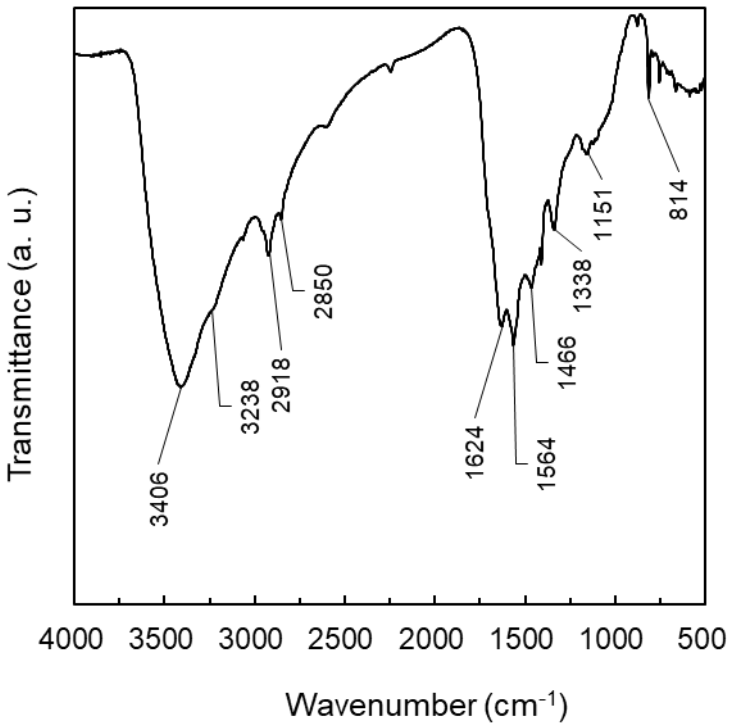

Figure 111 FT-IR spectrum of MPy copolymer.

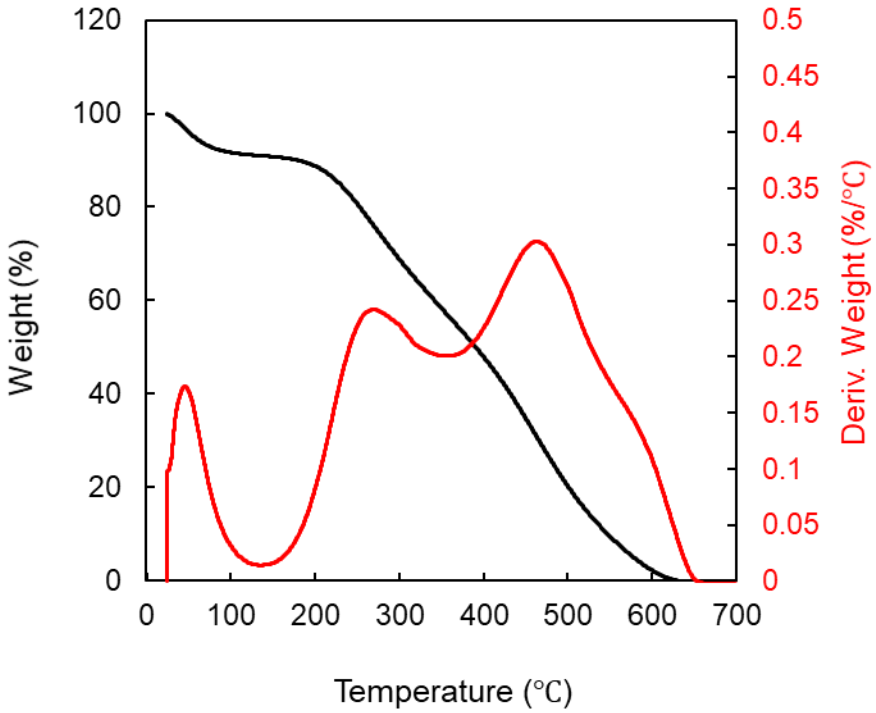

Figure 112 Thermogravimetric analysis of the TriPy copolymer network, measured under air (black) and first derivative with the temperature (red).

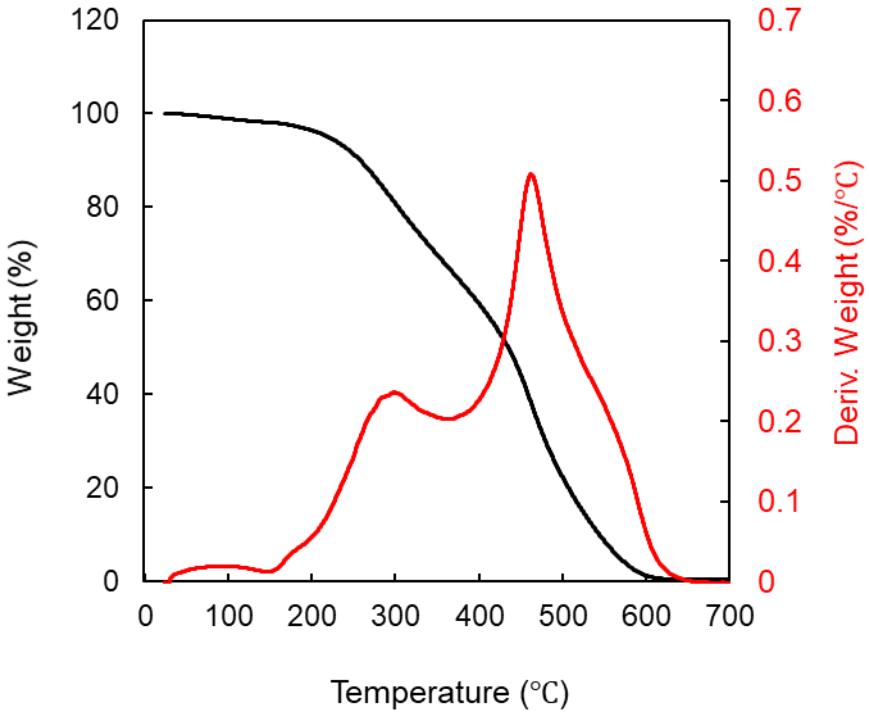

Figure 113 Thermogravimetric analysis of the TMTPy copolymer network, measured under air (black) and first derivative with the temperature (red).

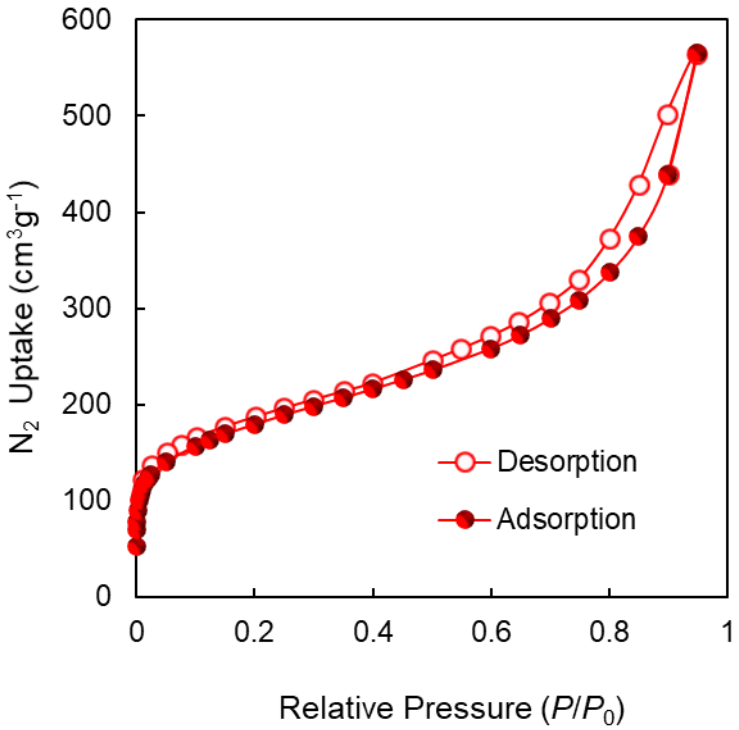

Figure 114 N_2 adsorption isotherm at 77 K for TriPy copolymer. Filled and open symbols represent adsorption and desorption branches, respectively. The connecting lines serve as a guide to the eye.

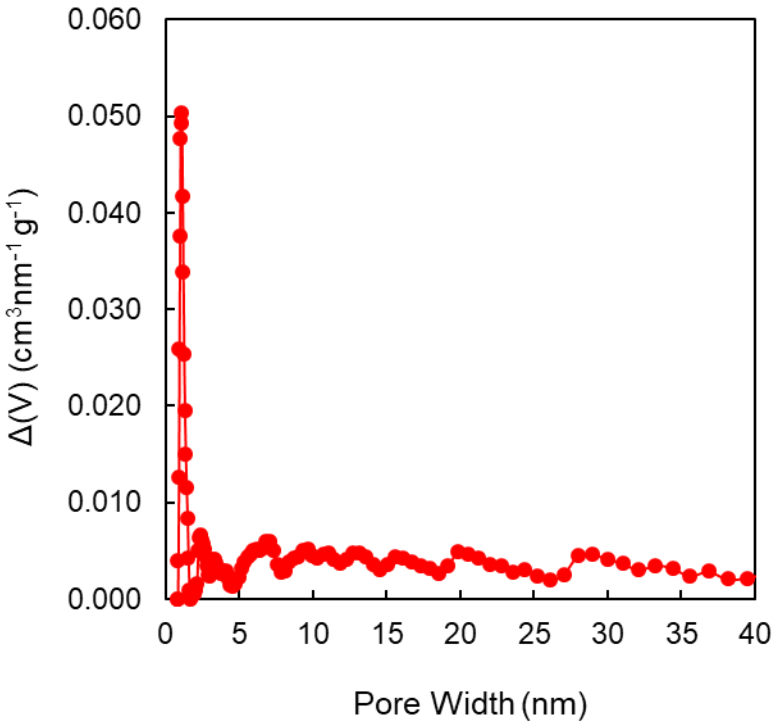

Figure 115 Pore size distribution of TriPy calculated by QSDFT model.

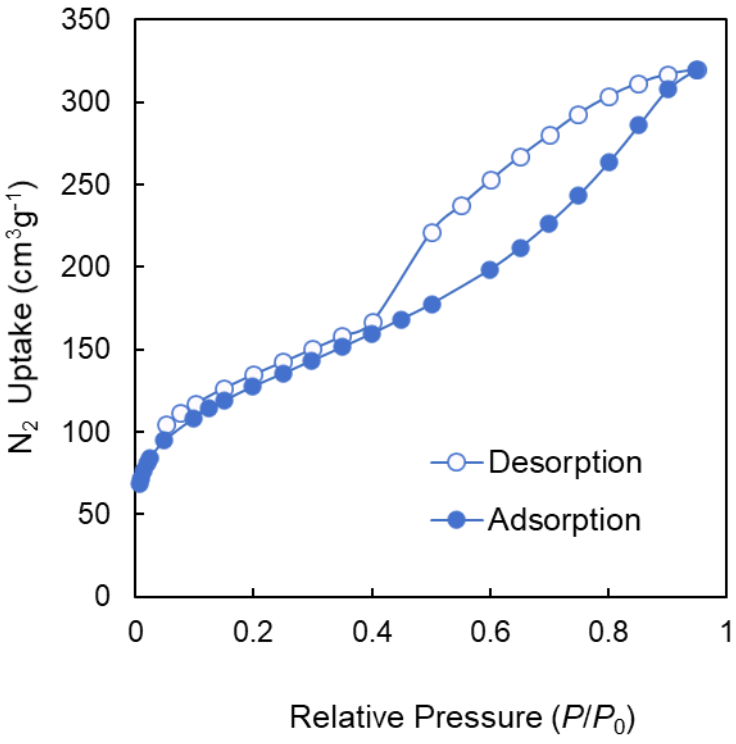

Figure 116 N_2 adsorption isotherm at 77 K for TMTPy. Filled and open symbols represent adsorption and desorption branches, respectively. The connecting lines serve as a guide to the eye.

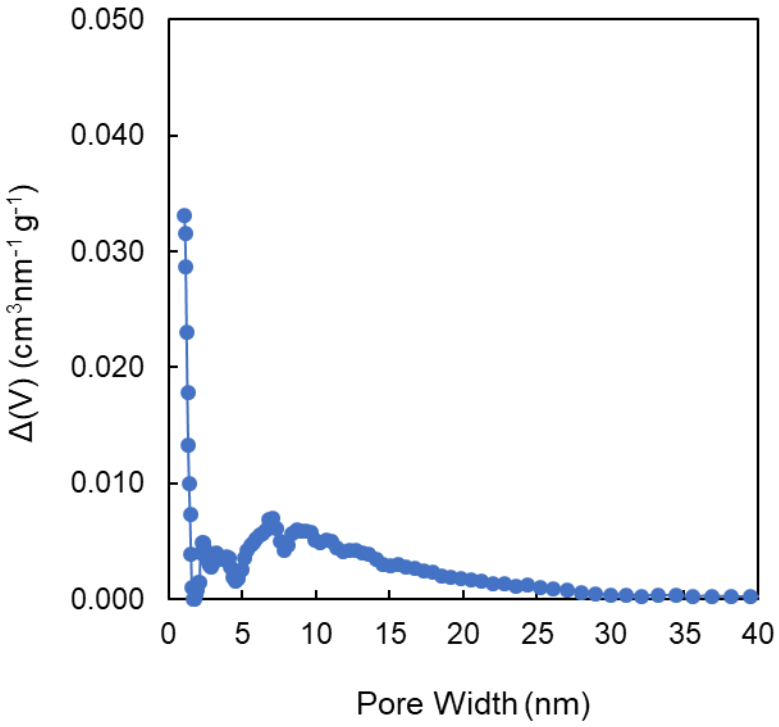

Figure 117 Pore size distribution of TMTPy calculated by QSDFT model.

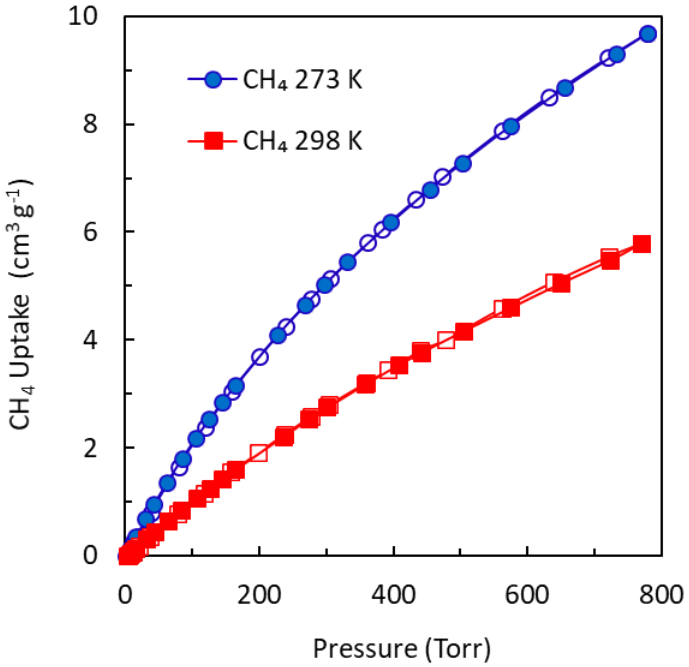

Figure 118 CH_4 sorption isotherms for TMTPy at 273 K (blue circle) and 298 K (red square). Filled and open symbols represent adsorption and desorption branches, respectively. The connecting lines serve as a guide to the eye.

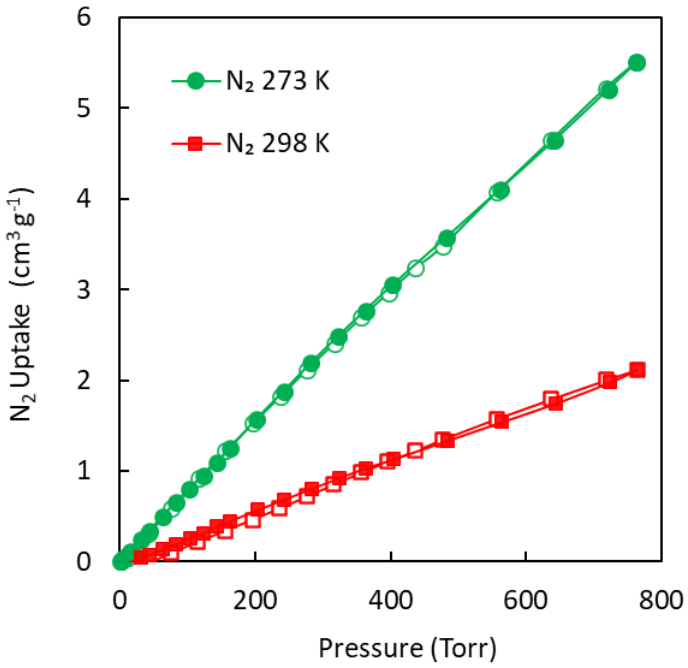

Figure 119 N_2 sorption isotherms for TMTPy at 273 K (green circle) and 298 K (red square). Filled and open symbols represent adsorption and desorption branches, respectively. The connecting lines serve as a guide to the eye.

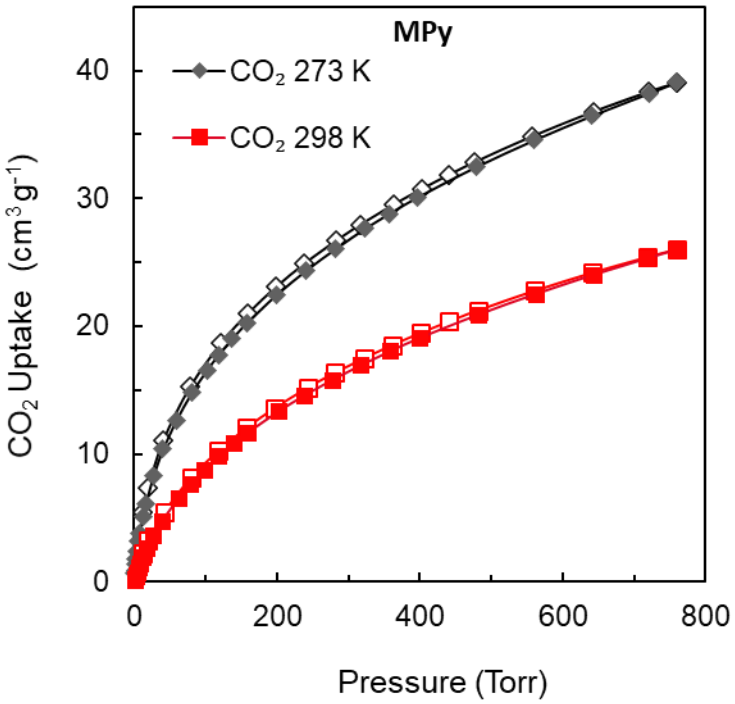

Figure 120 CO_2 sorption isotherms for MPy at 273 K (black rhombus) and 298 K (red square). Filled and open symbols represent adsorption and desorption branches, respectively. The connecting lines serve as a guide to the eye.

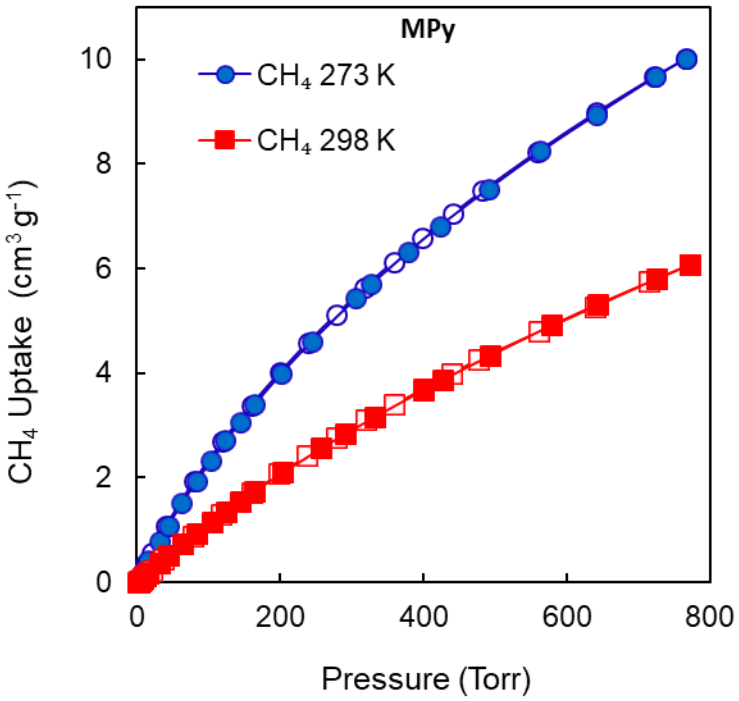

Figure 121 CH_4 sorption isotherms for MPy at 273 K (blue circle) and 298 K (red square). Filled and open symbols represent adsorption and desorption branches, respectively. The connecting lines serve as a guide to the eye.

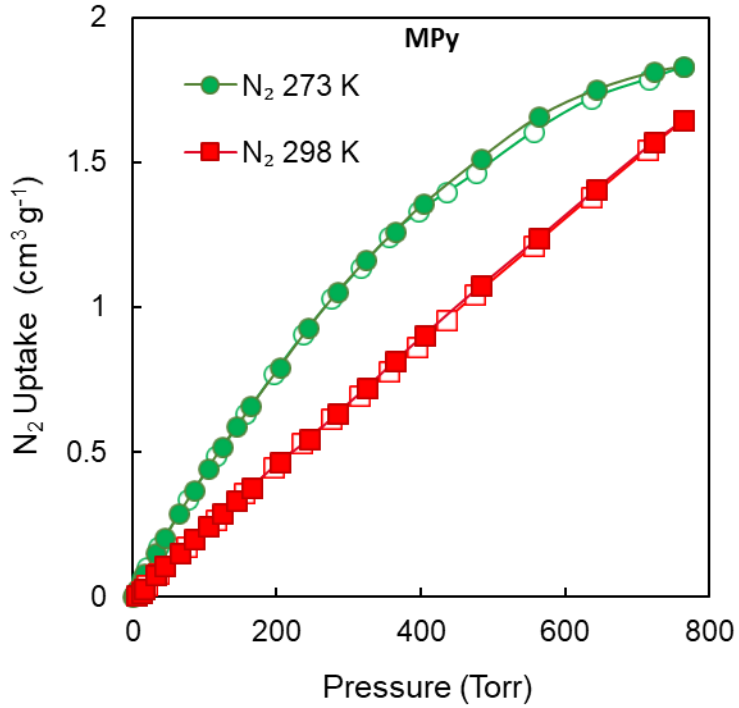

Figure 122 N_2 sorption isotherms for MPy at 273 K (green circle) and 298 K (red square). Filled and open symbols represent adsorption and desorption branches, respectively. The connecting lines serve as a guide to the eye. Coverage dependent enthalpy of adsorption (Q_{st}) and CO_2/N_2 selectivity.

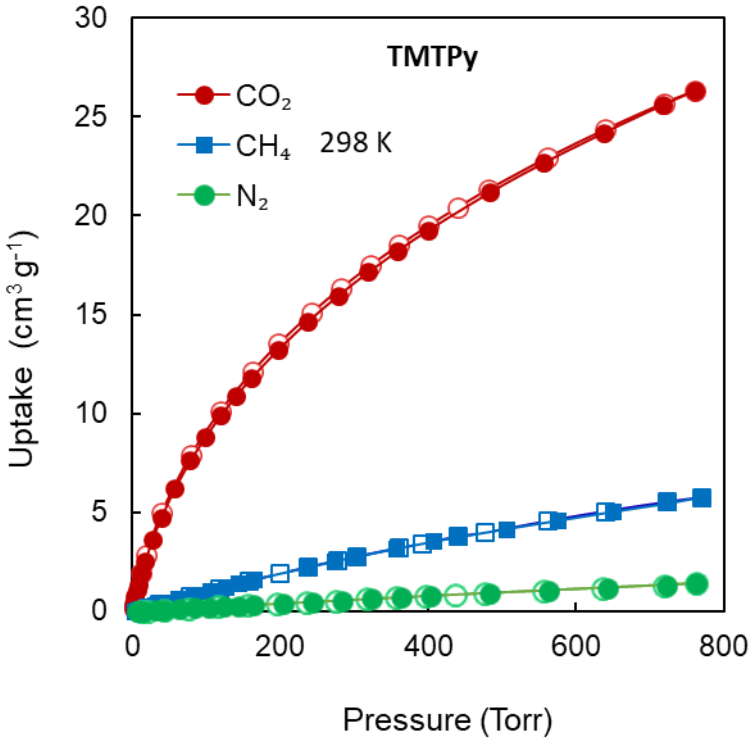

Figure 123 CO_2 (red circle), CH_4 (blue square) and N_2 (green circle) sorption isotherms for TMTPy at 273 K. Filled and open symbols represent adsorption and desorption branches, respectively. The connecting lines serve as a guide to the eye. Coverage-Dependent Enthalpy of Adsorption

Q_{st} and selectivity calculation

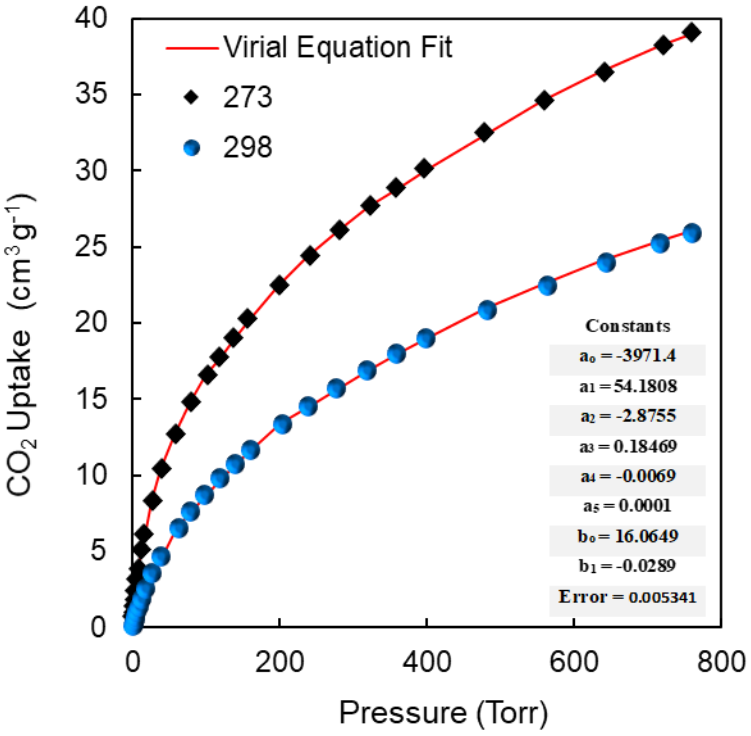

Figure 124 Virial-type equation fitting (red line) of experimental CO_2 adsorption data for MPy at 273 K (black rhombus) and 298 K (blue ball). Inset provides the constants used for the fitting of 273 K and 298 K CO_2 adsorption isotherms using virial-type equation.

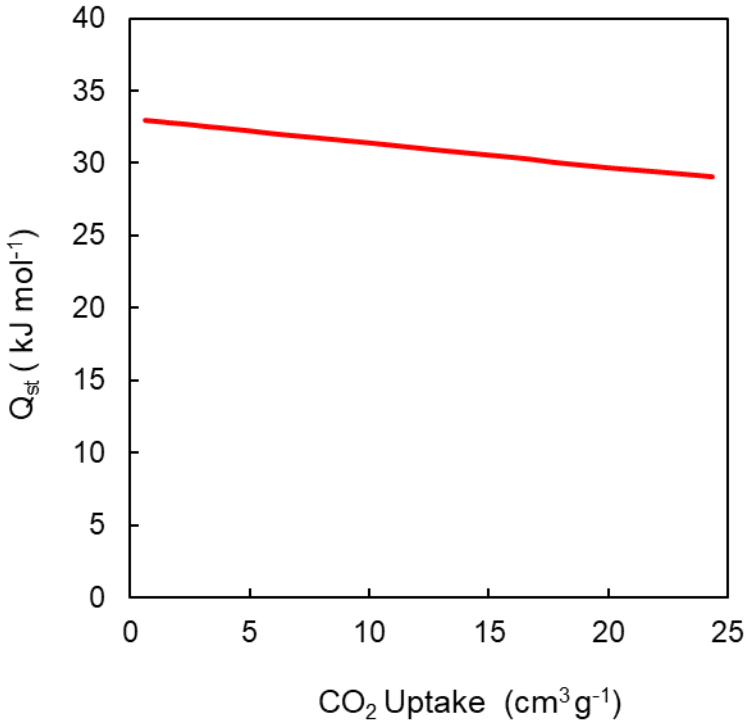

Figure 125 Calculated enthalpy of adsorption (Q_{st}) of CO_2 gas for MPy.

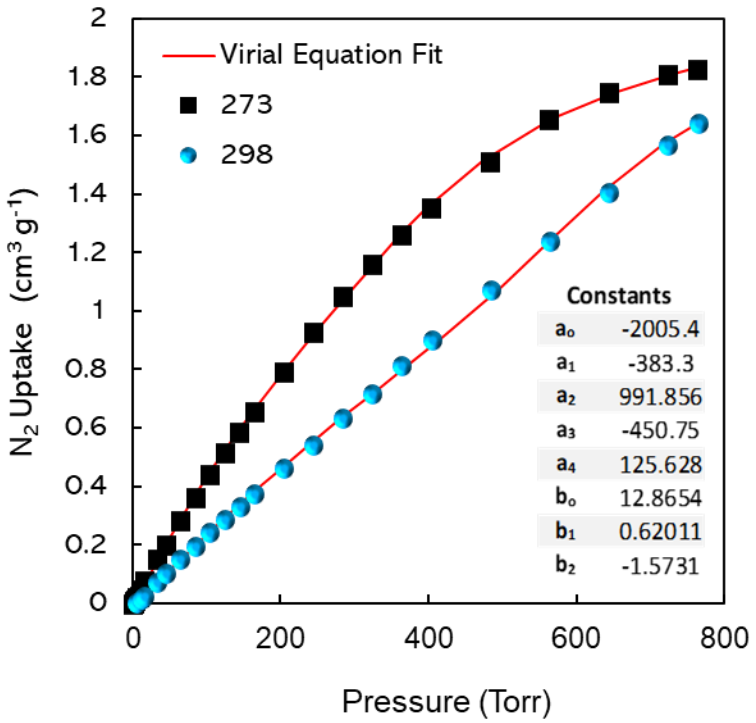

Figure 126 Virial-type equation fitting (red line) of experimental N_2 adsorption data for MPy at 273 K (black square) and 298 K (blue ball). Inset provides the constants used for the fitting of 273 K and 298 K CO_2 adsorption isotherms using virial-type equation.

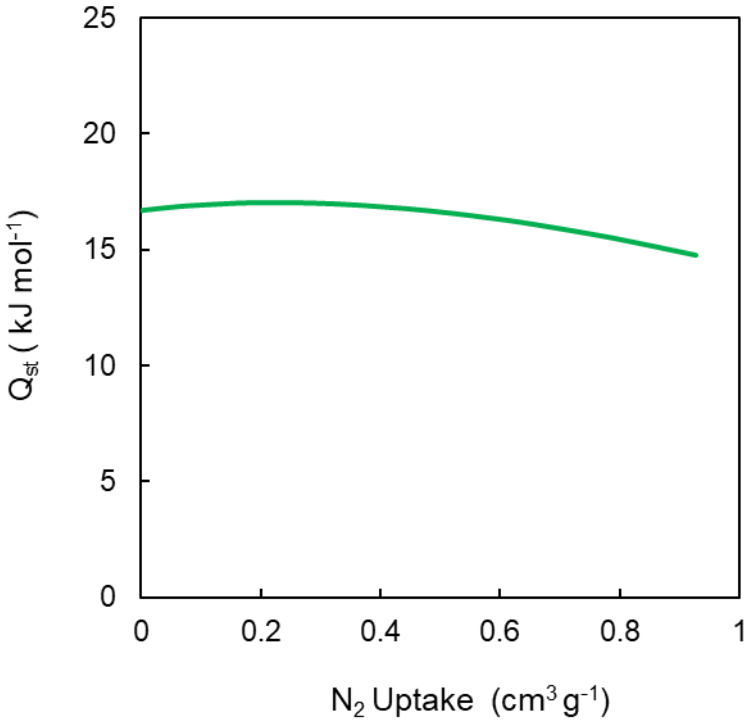

Figure 127 Calculated enthalpy of adsorption (Q_{st}) of N_2 gas for MPy.

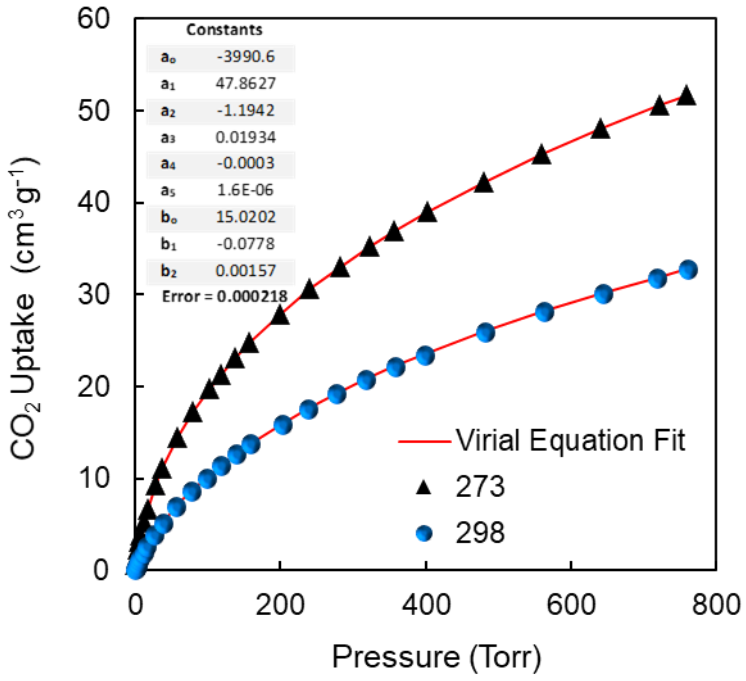

Figure 128 Virial-type equation fitting (red line) of experimental CO_2 adsorption data for TriPy at 273 K (black triangle) and 298 K (blue ball). Inset provides the constants used for the fitting of 273 K and 298 K CO_2 adsorption isotherms using virial-type equation.

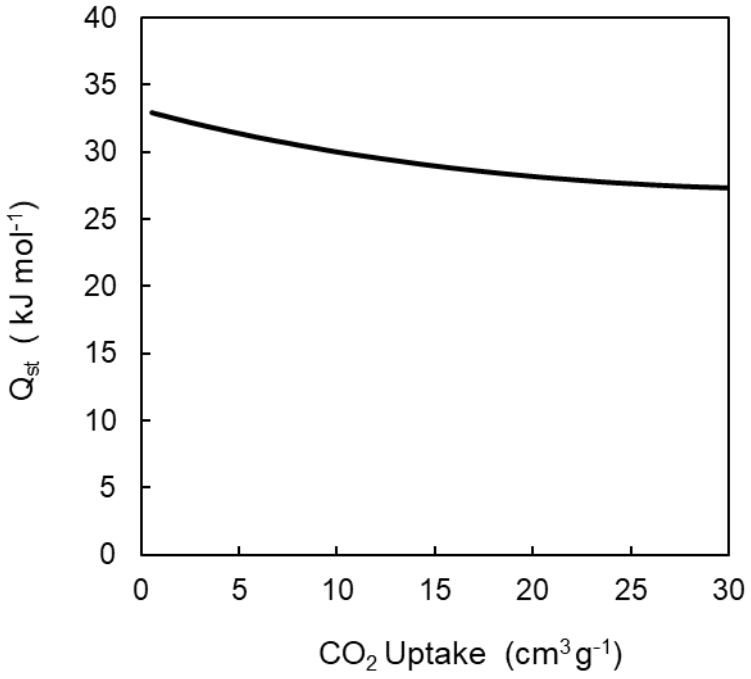

Figure 129 Calculated enthalpy of adsorption (Q_{st}) of CO_2 gas for TriPy.

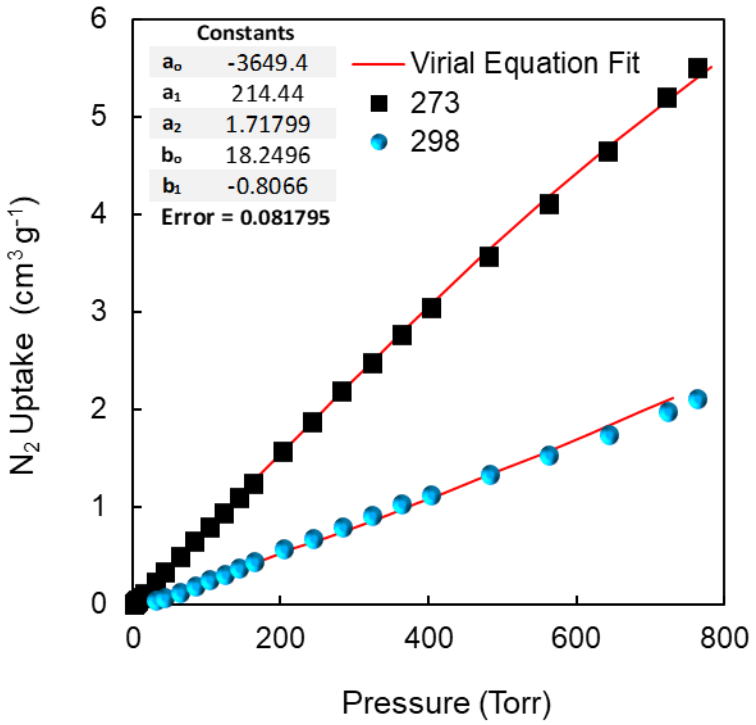

Figure 130 Virial-type equation fitting (red line) of experimental N_2 adsorption data for TriPy at 273 K (black square) and 298 K (blue ball). Inset provides the constants used for the fitting of 273 K and 298 K N_2 adsorption isotherms using virial-type equation.

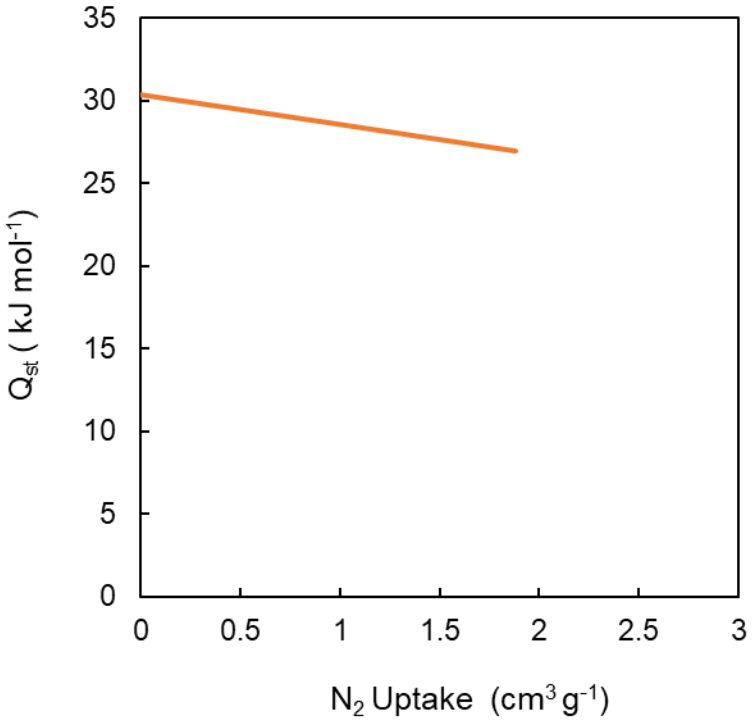

Figure 131 Calculated enthalpy of adsorption (Q_{st}) of N_2 gas for TriPy.

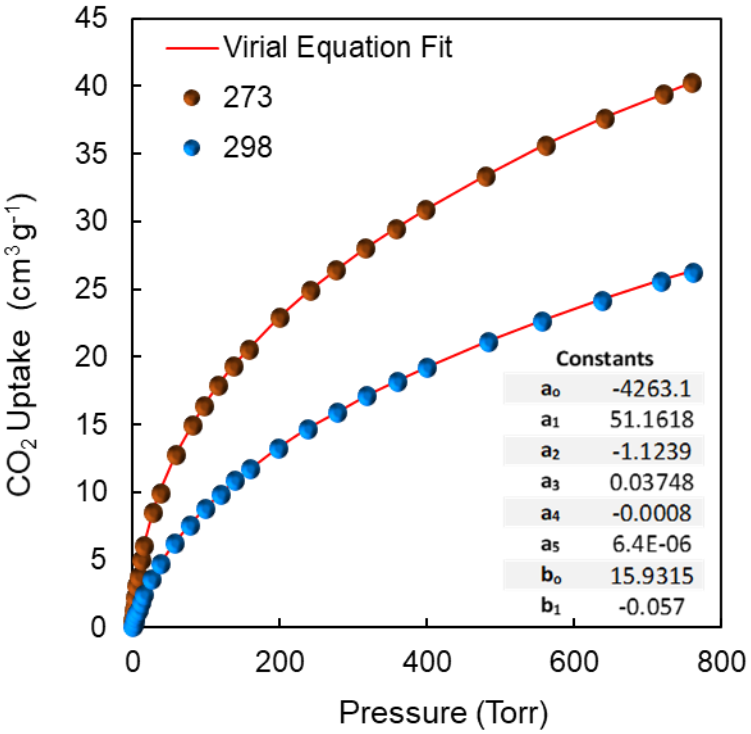

Figure 132 Virial-type equation fitting (red line) of experimental CO2 adsorption data for TMTPy at 273 K (brown ball) and 298 K (blue ball). Inset provides the constants used for the fitting of 273 K and 298 K CO_2 adsorption isotherms using virial-type equation.

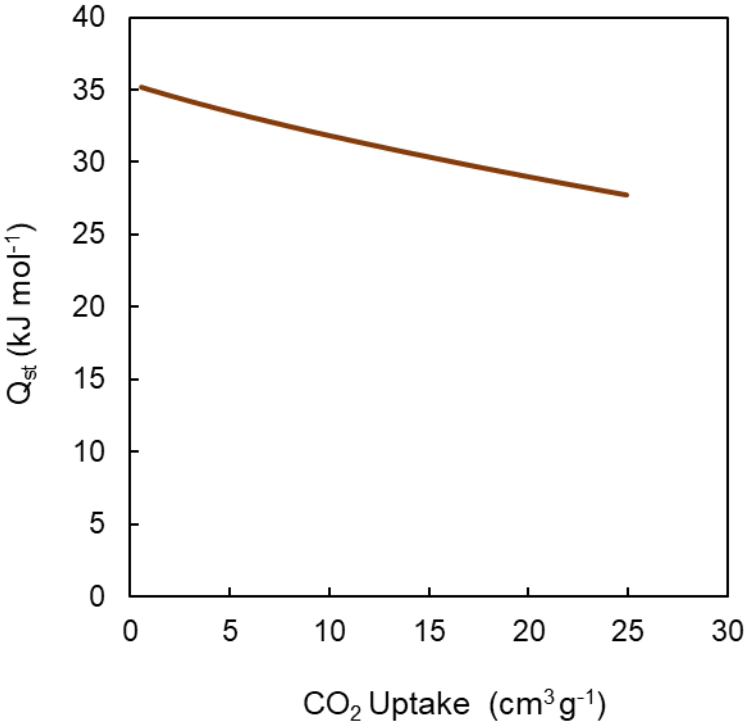

Figure 133 Calculated enthalpy of adsorption (Q_{st}) of CO_2 gas for TMTPy.

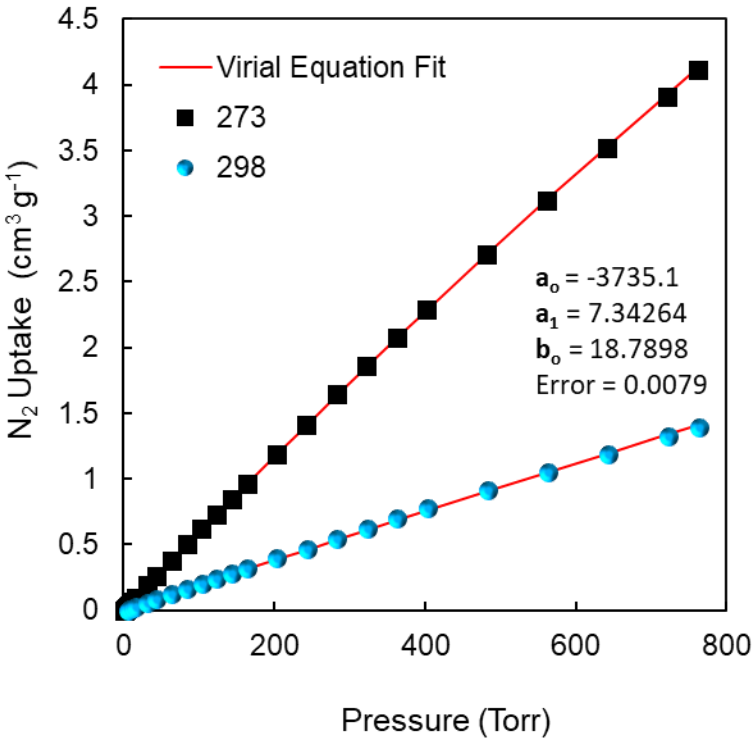

Figure 134 Virial-type equation fitting (red line) of experimental N_2 adsorption data for TMTPy at 273 K (black square) and 298 K (blue ball). Inset provides the constants used for the fitting of 273 K and 298 K N_2 adsorption isotherms using virial-type equation.

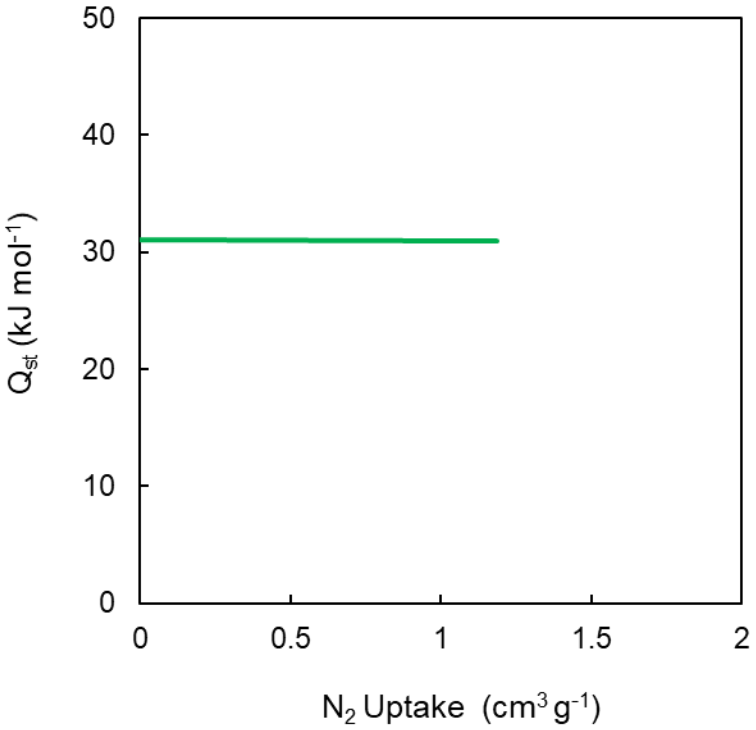

Figure 135 Calculated enthalpy of adsorption (Q_{st}) of N_2 gas for TMTPy.

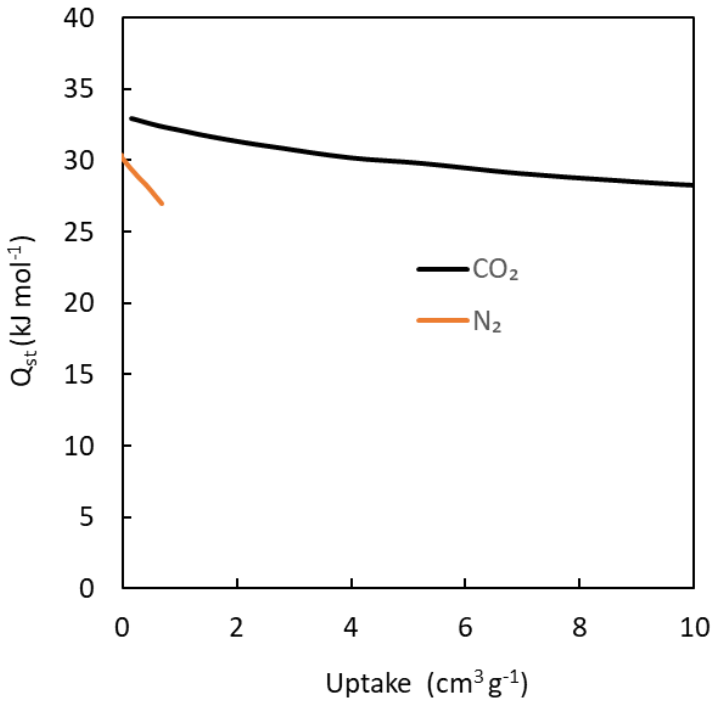

Figure 136 Calculated enthalpy of adsorption (Q_{st}) of CO_2 (black line) and N_2 (orange line) for TriPy.

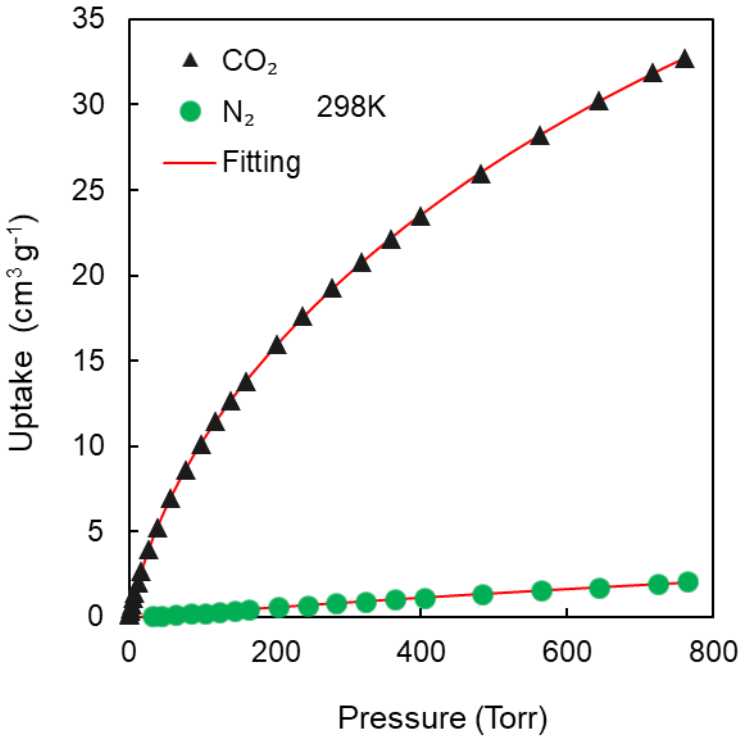

Figure 137 Dual site Langmuir fitting (red line) of experimental CO_2 (black triangle) and N_2 (green circle) adsorption data for TriPy at 298 K.

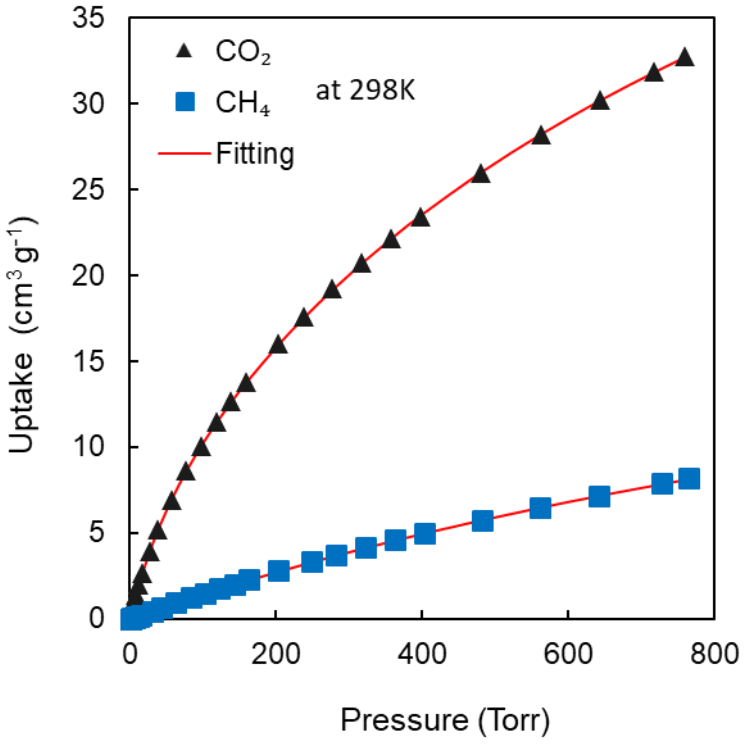

Figure 138 Dual site Langmuir fitting (red line) of experimental CO_2 (black triangle) and CH_4 (blue square) adsorption data for TriPy at 298 K.

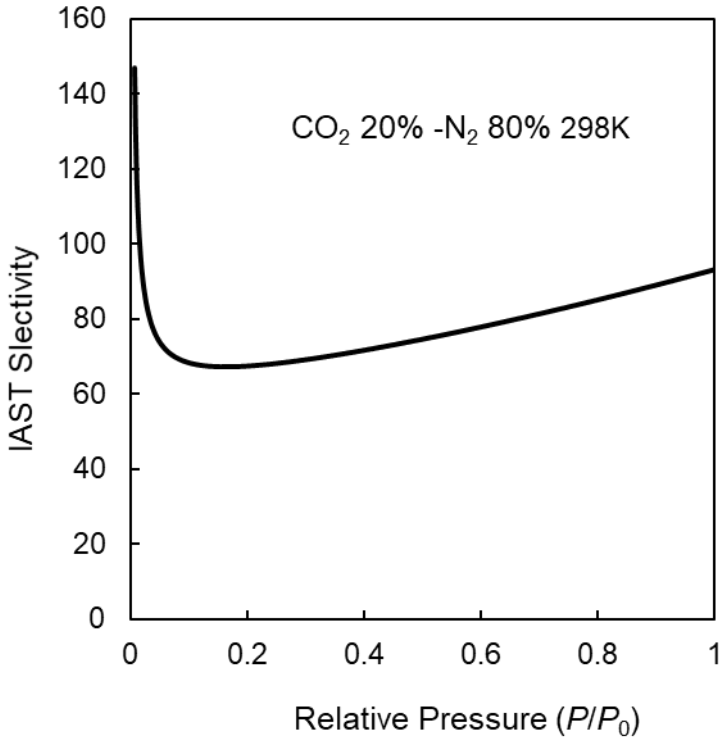

Figure 139 Calculated IAST selectivity of CO_2 over N_2 for TriPy.

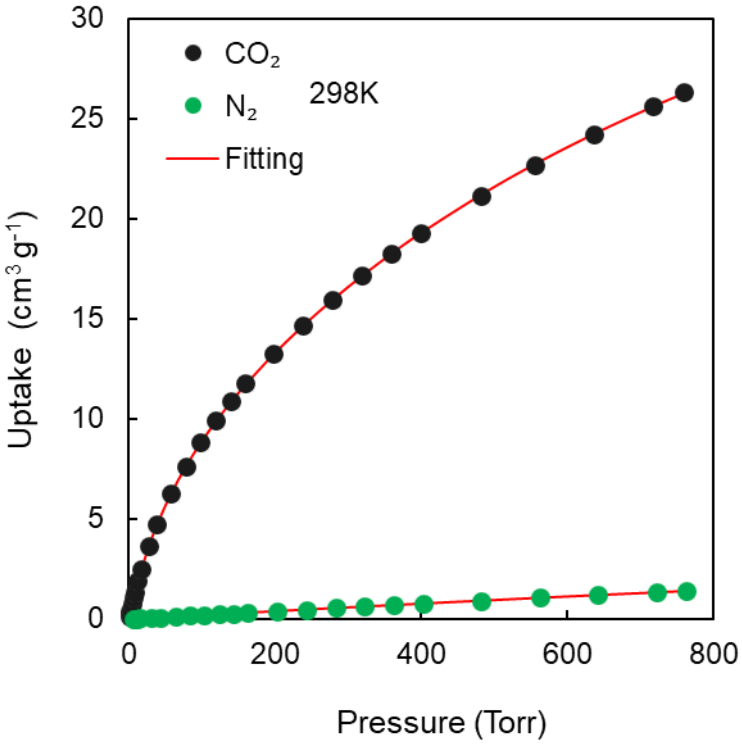

Figure 140 Dual site Langmuir fitting (red line) of experimental CO_2 (black circle) and N_2 (green circle) adsorption data for TMTPy at 298 K.

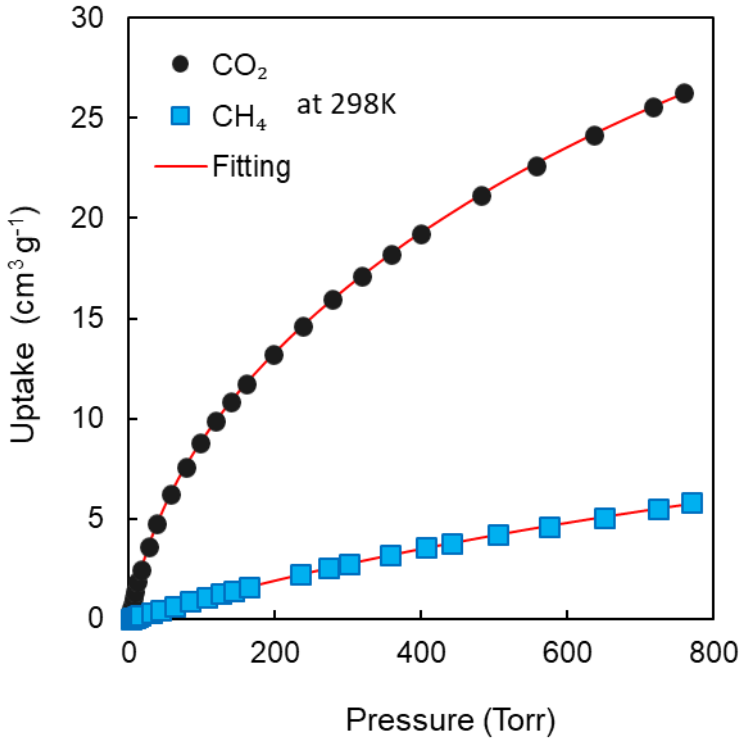

Figure 141 Dual site Langmuir fitting (red line) of experimental CO_2 (black circle) and CH_4 (blue square) adsorption data for TMTPy at 298 K.

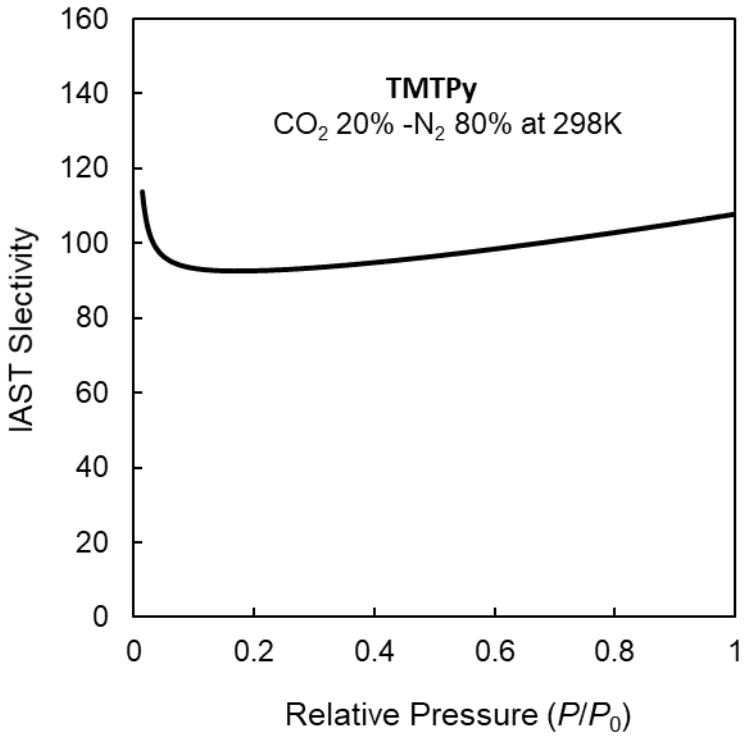

Figure 142 Calculated IAST selectivity of CO_2 over N_2 for TMTPy.

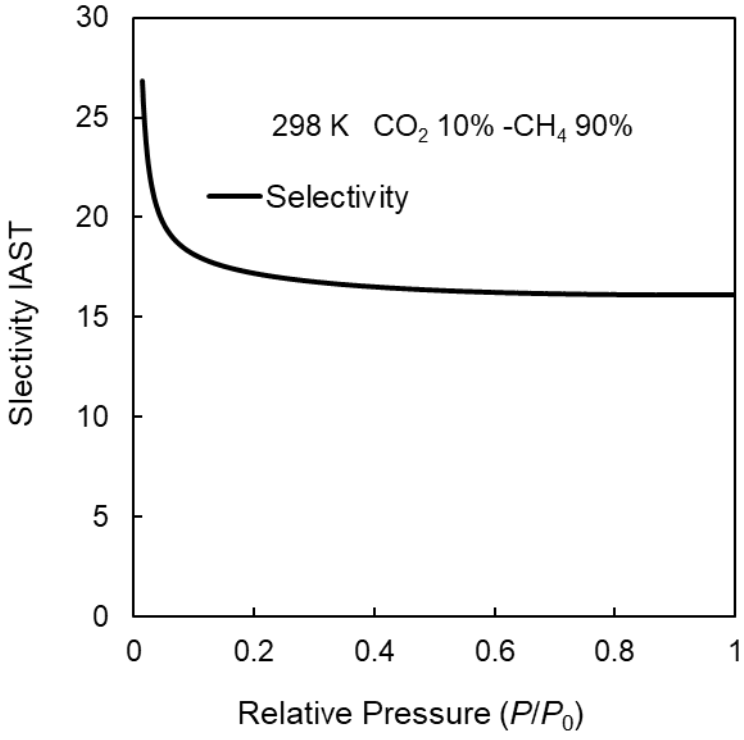

Figure 143 Calculated IAST selectivity of CO_2 over CH_4 for TMTPy.

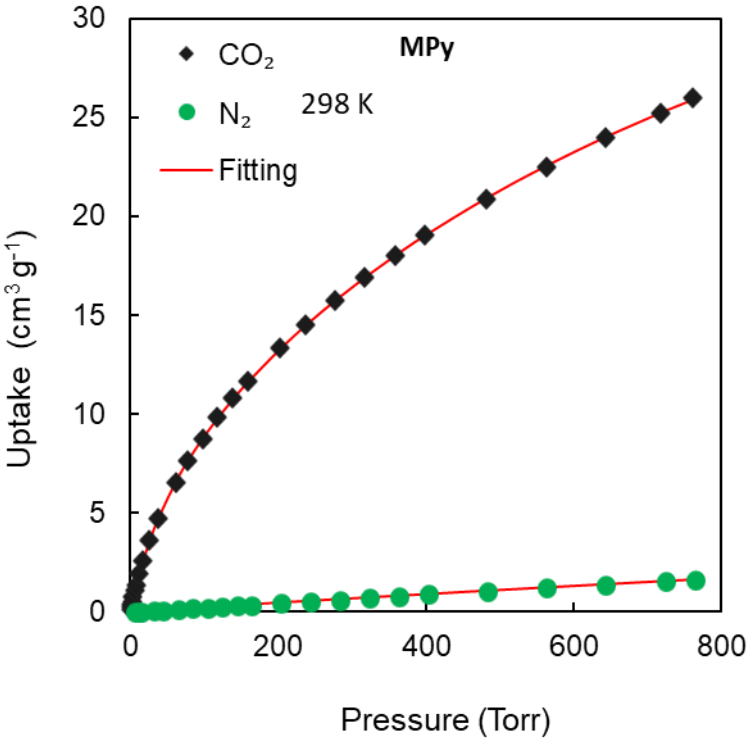

Figure 144 Dual site Langmuir fitting (red line) of experimental CO_2 (black rhombus) and N_2 (green circle) adsorption data for MPy at 298 K.

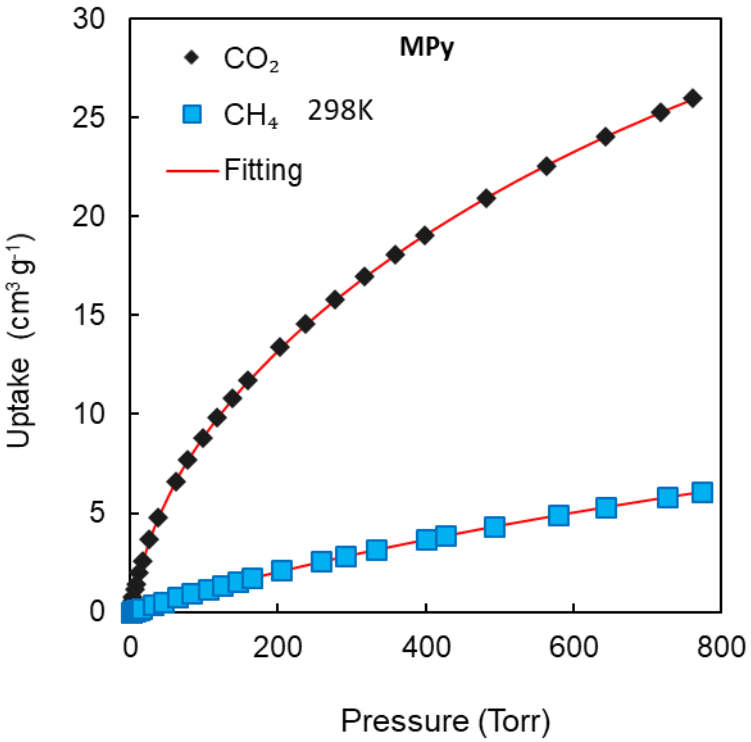

Figure 145 Dual site Langmuir fitting (red line) of experimental CO_2 (black rhombus) and CH_4 (blue square) adsorption data for MPy at 298 K.

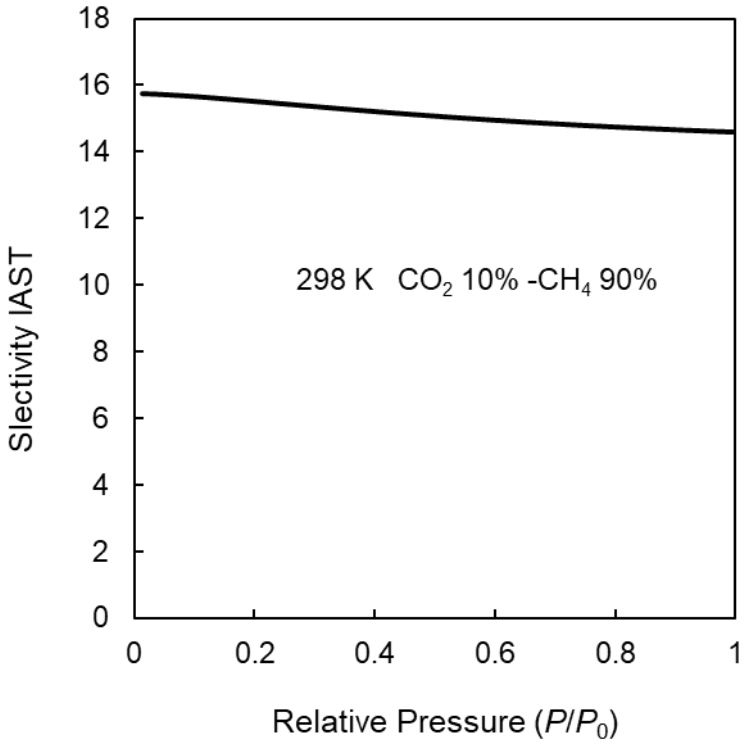

Figure 146 Calculated IAST selectivity of CO_2 over CH_4 for MPy.

References

[1] R. K. Pachauri *et al.*, “Climate Change 2014: Synthesis Report. Contribution of Working Groups I, II and III to the Fifth Assessment Report of the Intergovernmental Panel on Climate Change.” IPCC, 08-Mar-2014.

[2] C. Song, “Global challenges and strategies for control, conversion and utilization of CO_2 for sustainable development involving energy, catalysis, adsorption and chemical processing,” *Catal. Today*, vol. 115, no. 1–4, pp. 2–32, Jun. 2006.

[3] A. Najam, A. A. Rahman, S. Huq, and Y. Sokona, “Integrating sustainable development into the Fourth Assessment Report of the Intergovernmental Panel on Climate Change,” *Clim. Policy*, vol. 3, pp. S9–S17, Nov. 2003.

[4] G. T. Rochelle, “Amine scrubbing for CO_2 capture.,” *Science*, vol. 325, no. 5948, pp. 1652–4, Sep. 2009.

[5] A. N. M. Peeters, A. P. C. Faaij, and W. C. Turkenburg, “Techno-economic analysis of natural gas combined cycles with post-combustion CO_2 absorption, including a detailed evaluation of the development potential,” *Int. J. Greenh. Gas Control*, vol. 1, no. 4, pp. 396–417, Oct. 2007.

[6] K. Sumida *et al.*, “Carbon dioxide capture in metal-organic frameworks.,” *Chem. Rev.*, vol. 112, no. 2, pp. 724–81, Feb. 2012.

[7] G. T. Rochelle, “Amine scrubbing for CO_2 capture.,” *Science*, vol. 325, no. 5948, pp. 1652–4, Sep. 2009.

[8] D. M. D’Alessandro, B. Smit, and J. R. Long, “Carbon dioxide capture: Prospects for new materials,” *Angewandte Chemie - International Edition*, vol. 49, no. 35. pp. 6058–6082, 2010.

[9] J. Hennessy, "CO_2 capture: Bespoke zeolites," *Nat. Mater.*, vol. 14, no. 9, pp. 857–857, Aug. 2015.

[10] R. Dawson, E. Stöckel, J. R. Holst, D. J. Adams, and A. I. Cooper, "Microporous organic polymers for carbon dioxide capture," *Energy Environ. Sci.*, vol. 4, no. 10, p. 4239, Sep. 2011.

[11] H. Gao, L. Ding, W. Li, G. Ma, H. Bai, and L. Li, "Hyper-Cross-Linked Organic Microporous Polymers Based on Alternating Copolymerization of Bismaleimide," *ACS Macro Lett.*, vol. 5, no. 3, pp. 377–381, Feb. 2016.

[12] H. Li, X. Ding, Y.-C. Zhao, and B.-H. Han, "Preparation of mannitol-based ketal-linked porous organic polymers and their application for selective capture of carbon dioxide," *Polymer (Guildf).*, vol. 89, pp. 112–118, Apr. 2016.

[13] A. Schoedel, Z. Ji, and O. M. Yaghi, "The role of metal–organic frameworks in a carbon-neutral energy cycle," *Nat. Energy*, vol. 1, no. 4, p. 16034, Apr. 2016.

[14] A. M. Fracaroli *et al.*, "Metal-organic frameworks with precisely designed interior for carbon dioxide capture in the presence of water.," *J. Am. Chem. Soc.*, vol. 136, no. 25, pp. 8863–6, Jun. 2014.

[15] D. J. Fauth, M. L. Gray, H. W. Pennline, H. M. Krutka, S. Sjostrom, and A. M. Ault, "Investigation of Porous Silica Supported Mixed-Amine Sorbents for Post-Combustion CO_2 Capture," *Energy & Fuels*, vol. 26, no. 4, pp. 2483–2496, Apr. 2012.

[16] R. Serna-Guerrero, Y. Belmabkhout, and A. Sayari, "Triamine-grafted pore-expanded mesoporous silica for CO_2 capture: Effect of moisture and adsorbent regeneration strategies," *Adsorption*, vol. 16, no. 6, pp. 567–575, Aug. 2010.

[17] A. Sayari, Y. Belmabkhout, and R. Serna-Guerrero, “Flue gas treatment via CO_2 adsorption,” *Chem. Eng. J.*, vol. 171, no. 3, pp. 760–774, Jul. 2011.

[18] E. J. Granite and H. W. Pennline, “Photochemical removal of mercury from flue gas,” *Ind. Eng. Chem. Res.*, vol. 41, no. 22, pp. 5470–5476, 2002.

[19] M. T. Ho, G. W. Allinson, and D. E. Wiley, “Reducing the cost of CO_2 capture from flue gases using pressure swing adsorption,” *Ind. Eng. Chem. Res.*, vol. 47, no. 14, pp. 4883–4890, Jul. 2008.

[20] W. Lu, W. M. Verdegaal, J. Yu, P. B. Balbuena, H.-K. Jeong, and H.-C. Zhou, “Building multiple adsorption sites in porous polymer networks for carbon capture applications,” *Energy Environ. Sci.*, vol. 6, no. 12, p. 3559, Nov. 2013.

[21] R. S. Haszeldine, “Carbon capture and storage: how green can black be?,” *Science*, vol. 325, no. 5948, pp. 1647–52, Sep. 2009.

[22] C. A. Trickett, A. Helal, B. A. Al-Maythalony, Z. H. Yamani, K. E. Cordova, and O. M. Yaghi, “The chemistry of metal–organic frameworks for CO_2 capture, regeneration and conversion,” *Nat. Rev. Mater.*, vol. 2, no. 8, p. 17045, Jul. 2017.

[23] P. J. Milner *et al.*, “A Diaminopropane-Appended Metal–Organic Framework Enabling Efficient CO_2 Capture from Coal Flue Gas via a Mixed Adsorption Mechanism,” *J. Am. Chem. Soc.*, vol. 139, no. 38, pp. 13541–13553, Sep. 2017.

[24] L. Zou *et al.*, “Porous Organic Polymers for Post-Combustion Carbon Capture,” *Adv. Mater.*, p. 1700229, Jul. 2017.

[25] R. Dawson *et al.*, “Microporous organic polymers for carbon dioxide capture,” *Energy Environ. Sci.*, vol. 4, no. 10, p. 4239, 2011.

[26] S. Dey *et al.*, “Covalent triazine-based frameworks (CTFs) from triptycene and

fluorene motifs for CO_2 adsorption," *J. Mater. Chem. A*, vol. 4, no. 17, pp. 6259–6263, 2016.

[27] R. T. Woodward *et al.*, "Swellable, Water- and Acid-Tolerant Polymer Sponges for Chemoselective Carbon Dioxide Capture," *J. Am. Chem. Soc.*, vol. 136, no. 25, pp. 9028–9035, Jun. 2014.

[28] Y. Zhao, K. X. Yao, B. Teng, T. Zhang, and Y. Han, "A perfluorinated covalent triazine-based framework for highly selective and water–tolerant CO_2 capture," *Energy Environ. Sci.*, vol. 6, no. 12, p. 3684, 2013.

[29] G.-P. Hao *et al.*, "Structurally Designed Synthesis of Mechanically Stable Poly(benzoxazine-co-resol)-Based Porous Carbon Monoliths and Their Application as High-Performance CO_2 Capture Sorbents," *J. Am. Chem. Soc.*, vol. 133, no. 29, pp. 11378–11388, Jul. 2011.

[30] H. Li, M. Eddaoudi, M. O'Keeffe, and O. M. Yaghi, "Design and synthesis of an exceptionally stable and highly porous metal-organic framework," vol. 402, no. 6759, pp. 276–279, Nov. 1999.

[31] H. Furukawa, K. E. Cordova, M. O'Keeffe, and O. M. Yaghi, "The chemistry and applications of metal-organic frameworks.," *Science*, vol. 341, no. 6149, p. 1230444, Aug. 2013.

[32] A. C.-H. Sue *et al.*, "Heterogeneity of functional groups in a metal-organic framework displays magic number ratios.," *Proc. Natl. Acad. Sci. U. S. A.*, vol. 112, no. 18, pp. 5591–6, May 2015.

[33] C. Le Calvez, M. Zouboulaki, C. Petit, L. Peeva, and N. Shirshova, "One step synthesis of MOF–polymer composites," *RSC Adv.*, vol. 6, no. 21, pp. 17314–

17317, Feb. 2016.

[34] Q.-L. Zhu and Q. Xu, “Metal-organic framework composites.,” *Chem. Soc. Rev.*, vol. 43, no. 16, pp. 5468–512, Aug. 2014.

[35] N. Stock and S. Biswas, “Synthesis of metal-organic frameworks (MOFs): routes to various MOF topologies, morphologies, and composites.,” *Chem. Rev.*, vol. 112, no. 2, pp. 933–69, Feb. 2012.

[36] V. Stavila, A. A. Talin, and M. D. Allendorf, “MOF-based electronic and opto-electronic devices.,” *Chem. Soc. Rev.*, vol. 43, no. 16, pp. 5994–6010, Aug. 2014.

[37] Y. Liu, Z. U. Wang, and H.-C. Zhou, “Recent advances in carbon dioxide capture with metal-organic frameworks,” *Greenh. Gases Sci. Technol.*, vol. 2, no. 4, pp. 239–259, Aug. 2012.

[38] F. Raganati, V. Gargiulo, P. Ammendola, M. Alfe, and R. Chirone, “CO_2 capture performance of HKUST-1 in a sound assisted fluidized bed,” *Chem. Eng. J.*, vol. 239, pp. 75–86, Mar. 2014.

[39] S. T. Meek, J. A. Greathouse, and M. D. Allendorf, “Metal-organic frameworks: a rapidly growing class of versatile nanoporous materials.,” *Adv. Mater.*, vol. 23, no. 2, pp. 249–67, Jan. 2011.

[40] Z. Xiang, X. Peng, X. Cheng, X. Li, and D. Cao, “CNT@$Cu_3(BTC)_2$ and Metal–Organic Frameworks for Separation of CO_2 /CH_4 Mixture,” *J. Phys. Chem. C*, vol. 115, no. 40, pp. 19864–19871, Oct. 2011.

[41] J. L. C. Rowsell and O. M. Yaghi, “Effects of functionalization, catenation, and variation of the metal oxide and organic linking units on the low-pressure hydrogen adsorption properties of metal-organic frameworks.,” *J. Am. Chem. Soc.*, vol. 128,

no. 4, pp. 1304–15, Feb. 2006.

[42] D. Britt, H. Furukawa, B. Wang, T. G. Glover, and O. M. Yaghi, "Highly efficient separation of carbon dioxide by a metal-organic framework replete with open metal sites.," *Proc. Natl. Acad. Sci. U. S. A.*, vol. 106, no. 49, pp. 20637–40, Dec. 2009.

[43] Y. Jiao, C. R. Morelock, N. C. Burtch, W. P. Mounfield, J. T. Hungerford, and K. S. Walton, "Tuning the Kinetic Water Stability and Adsorption Interactions of Mg-MOF-74 by Partial Substitution with Co or Ni," *Ind. Eng. Chem. Res.*, vol. 54, no. 49, pp. 12408–12414, Dec. 2015.

[44] A. P. Côté, A. I. Benin, N. W. Ockwig, M. O'Keeffe, A. J. Matzger, and O. M. Yaghi, "Porous, crystalline, covalent organic frameworks.," *Science*, vol. 310, no. 5751, pp. 1166–70, Nov. 2005.

[45] H. Furukawa and O. M. Yaghi, "Storage of Hydrogen, Methane, and Carbon Dioxide in Highly Porous Covalent Organic Frameworks for Clean Energy Applications," *J. Am. Chem. Soc.*, vol. 131, no. 25, pp. 8875–8883, Jul. 2009.

[46] Y. Zeng, R. Zou, and Y. Zhao, "Covalent organic frameworks for CO_2 capture," *Adv. Mater.*, vol. 28, no. 15, pp. 2855–2873, Feb. 2016.

[47] N. Huang, X. Chen, R. Krishna, and D. Jiang, "Two-dimensional covalent organic frameworks for carbon dioxide capture through channel-wall functionalization.," *Angew. Chem. Int. Ed. Engl.*, vol. 54, no. 10, pp. 2986–90, Mar. 2015.

[48] R. Dawson, D. J. Adams, and A. I. Cooper, "Chemical tuning of CO_2 sorption in robust nanoporous organic polymers," *Chem. Sci.*, vol. 2, no. 6, p. 1173, Jun. 2011.

[49] H. Gao, L. Ding, W. Li, G. Ma, H. Bai, and L. Li, "Hyper-Cross-Linked Organic Microporous Polymers Based on Alternating Copolymerization of Bismaleimide,"

ACS Macro Lett., vol. 5, no. 3, pp. 377–381, Mar. 2016.

[50] C. Klumpen, M. Breunig, T. Homburg, N. Stock, and J. Senker, "Microporous Organic Polyimides for CO_2 and H_2O Capture and Separation from CH_4 and N_2 Mixtures: Interplay between Porosity and Chemical Function," *Chem. Mater.*, vol. 28, no. 15, pp. 5461–5470, Aug. 2016.

[51] G. Liu *et al.*, "A facile synthesis of microporous organic polymers for efficient gas storage and separation," *J. Mater. Chem. A*, vol. 3, no. 6, pp. 3051–3058, 2015.

[52] H. Xu, J. Gao, and D. Jiang, "Stable, crystalline, porous, covalent organic frameworks as a platform for chiral organocatalysts.," *Nat. Chem.*, vol. 7, no. 11, pp. 905–12, Nov. 2015.

[53] Y. Luo, B. Li, W. Wang, K. Wu, and B. Tan, "Hypercrosslinked aromatic heterocyclic microporous polymers: a new class of highly selective CO_2 capturing materials.," *Adv. Mater.*, vol. 24, no. 42, pp. 5703–7, Nov. 2012.

[54] L. Hu *et al.*, "Hypercrosslinked polymers incorporated with imidazolium salts for enhancing CO_2 capture," *Polym. Eng. Sci.*, vol. 56, no. 5, pp. 573–582, Jan. 2016.

[55] L. Tan *et al.*, "Hypercrosslinked porous polymer materials: design, synthesis, and applications," *Chem. Soc. Rev.*, vol. 203, pp. 752–758, 2017.

[56] S. Hug, L. Stegbauer, H. Oh, M. Hirscher, and B. V. Lotsch, "Nitrogen-Rich Covalent Triazine Frameworks as High-Performance Platforms for Selective Carbon Capture and Storage," *Chem. Mater.*, vol. 27, no. 23, pp. 8001–8010, Dec. 2015.

[57] U. Díaz and A. Corma, "Ordered covalent organic frameworks, COFs and PAFs. From preparation to application," *Coord. Chem. Rev.*, vol. 311, pp. 85–124, Mar.

2016.

[58] P. Kuhn, M. Antonietti, and A. Thomas, “Porous, Covalent Triazine-Based Frameworks Prepared by Ionothermal Synthesis,” *Angew. Chemie Int. Ed.*, vol. 47, no. 18, pp. 3450–3453, Apr. 2008.

[59] R. Dawson *et al.*, “Impact of water coadsorption for carbon dioxide capture in microporous polymer sorbents,” *J. Am. Chem. Soc.*, vol. 134, no. 26, pp. 10741–10744, 2012.

[60] M. Seo, S. Kim, J. Oh, S.-J. Kim, and M. A. Hillmyer, “Hierarchically porous polymers from hyper-cross-linked block polymer precursors.,” *J. Am. Chem. Soc.*, vol. 137, no. 2, pp. 600–3, Jan. 2015.

[61] M. . Tsyurupa and V. . Davankov, “Hypercrosslinked polymers: basic principle of preparing the new class of polymeric materials,” *React. Funct. Polym.*, vol. 53, no. 2–3, pp. 193–203, Dec. 2002.

[62] B. Li *et al.*, “A New Strategy to Microporous Polymers: Knitting Rigid Aromatic Building Blocks by External Cross-Linker,” *Macromolecules*, vol. 44, no. 8, pp. 2410–2414, Apr. 2011.

[63] C. Zhang *et al.*, “Triptycene-Based Hyper-Cross-Linked Polymer Sponge for Gas Storage and Water Treatment,” *Macromolecules*, vol. 48, no. 23, pp. 8509–8514, Dec. 2015.

[64] S. Yao *et al.*, “High surface area hypercrosslinked microporous organic polymer networks based on tetraphenylethylene for CO_2 capture,” *J. Mater. Chem. A*, vol. 2, no. 21, p. 8054, 2014.

[65] X. Zhu *et al.*, “Efficient CO_2 capture by a task-specific porous organic polymer

bifunctionalized with carbazole and triazine groups," *Chem. Commun.*, vol. 50, no. 59, p. 7933, Jun. 2014.

[66] R. Dawson *et al.*, "Microporous copolymers for increased gas selectivity," *Polym. Chem.*, vol. 3, no. 8, p. 2034, 2012.

[67] P. A. Kumar, M. Ray, and S. Chakraborty, "Hexavalent chromium removal from wastewater using aniline formaldehyde condensate coated silica gel," *J. Hazard. Mater.*, vol. 143, no. 1–2, pp. 24–32, 2007.

[68] G. Liu and M. S. Freund, "New Approach for the Controlled Cross-Linking of Polyaniline : Synthesis and Characterization," *Macromolecules*, vol. 9297, no. 97, pp. 5660–5665, 1997.

[69] Y.-Q. Shi, J. Zhu, X.-Q. Liu, J.-C. Geng, and L.-B. Sun, "Molecular template-directed synthesis of microporous polymer networks for highly selective CO_2 capture.," *ACS Appl. Mater. Interfaces*, vol. 6, no. 22, pp. 20340–9, Nov. 2014.

[70] D. Lee, C. Zhang, and H. Gao, "Amine-Functionalized Porous Polymer Network for Highly Selective Absorption of CO_2 Over N_2," *Macromol. Chem. Phys.*, vol. 216, no. 5, pp. 489–494, Mar. 2015.

[71] H. A. Patel *et al.*, "Unprecedented high-temperature CO_2 selectivity in N_2-phobic nanoporous covalent organic polymers.," *Nat. Commun.*, vol. 4, p. 1357, Jan. 2013.

[72] L. Czepirski and J. JagieŁŁo, "Virial-type thermal equation of gas—solid adsorption," *Chem. Eng. Sci.*, vol. 44, no. 4, pp. 797–801, 1989.

[73] S.-C. Xiang *et al.*, "Rationally tuned micropores within enantiopure metal-organic frameworks for highly selective separation of acetylene and ethylene," *Nat. Commun.*, vol. 2, p. 204, Feb. 2011.

[74] P. Nugent *et al.*, “Porous materials with optimal adsorption thermodynamics and kinetics for CO_2 separation,” *Nature*, vol. 495, no. 7439, pp. 80–84, Feb. 2013.

[75] H. Deng *et al.*, “Large-pore apertures in a series of metal-organic frameworks.,” *Science*, vol. 336, no. 6084, pp. 1018–23, May 2012.

[76] J. S. Yeon *et al.*, “Homodiamine-functionalized metal–organic frameworks with a MOF-74-type extended structure for superior selectivity of CO_2 over N_2,” *J. Mater. Chem. A*, vol. 3, no. 37, pp. 19177–19185, Sep. 2015.

[77] M. Thommes *et al.*, “Physisorption of gases, with special reference to the evaluation of surface area and pore size distribution (IUPAC Technical Report),” *Pure Appl. Chem.*, vol. 87, no. 9–10, pp. 1051–1069, Jan. 2015.

[78] L.-B. Sun *et al.*, “Facile fabrication of cost-effective porous polymer networks for highly selective CO_2 capture,” *J. Mater. Chem. A*, vol. 3, no. 7, pp. 3252–3256, Feb. 2015.

[79] P. Puthiaraj and W.-S. Ahn, “CO_2 Capture by Porous Hyper-Cross-Linked Aromatic Polymers Synthesized Using Tetrahedral Precursors,” *Ind. Eng. Chem. Res.*, vol. 55, no. 29, pp. 7917–7923, Jul. 2016.

[80] J. Han, Z. Du, W. Zou, H. Li, and C. Zhang, “Moisture-Responsive Hydrogel Impregnated in Porous Polymer Foam as CO_2 Adsorbent in High-Humidity Flue Gas,” *Ind. Eng. Chem. Res.*, vol. 54, no. 31, pp. 7623–7631, Aug. 2015.

[81] J. Weber, M. Antonietti, and A. Thomas, “Microporous Networks of High-Performance Polymers: Elastic Deformations and Gas Sorption Properties,” *Macromolecules*, vol. 41, no. 8, pp. 2880–2885, Apr. 2008.

[82] M. G. Rabbani and H. M. El-Kaderi, “Synthesis and Characterization of Porous

Benzimidazole-Linked Polymers and Their Performance in Small Gas Storage and Selective Uptake," *Chem. Mater.*, vol. 24, no. 8, pp. 1511–1517, Apr. 2012.

[83] W. Lu, J. P. Sculley, D. Yuan, R. Krishna, Z. Wei, and H.-C. Zhou, "Polyamine-Tethered Porous Polymer Networks for Carbon Dioxide Capture from Flue Gas," *Angew. Chemie Int. Ed.*, vol. 51, no. 30, pp. 7480–7484, Jul. 2012.

[84] K. Wang, H. Huang, D. Liu, C. Wang, J. Li, and C. Zhong, "Covalent Triazine-Based Frameworks with Ultramicropores and High Nitrogen Contents for Highly Selective CO_2 Capture," *Environ. Sci. Technol.*, vol. 50, no. 9, pp. 4869–4876, May 2016.

[85] N. Huang, X. Chen, R. Krishna, and D. Jiang, "Two-Dimensional Covalent Organic Frameworks for Carbon Dioxide Capture through Channel-Wall Functionalization," *Angew. Chemie Int. Ed.*, vol. 54, no. 10, pp. 2986–2990, Mar. 2015.

[86] Y. X. Ma, Z. J. Li, L. Wei, S. Y. Ding, Y. B. Zhang, and W. Wang, "A Dynamic Three-Dimensional Covalent Organic Framework," *J. Am. Chem. Soc.*, vol. 139, no. 14, pp. 4995–4998, Mar. 2017.

[87] S. Choi, J. H. Drese, and C. W. Jones, "Adsorbent Materials for Carbon Dioxide Capture from Large Anthropogenic Point Sources," *ChemSusChem*, vol. 2, no. 9, pp. 796–854, Sep. 2009.

[88] K. E. Cordova and O. M. Yaghi, "The 'folklore' and reality of reticular chemistry," *Mater. Chem. Front.*, vol. 1, no. 7, pp. 1304–1309, Jun. 2017.

[89] N. T. T. Nguyen *et al.*, "Mixed-Metal Zeolitic Imidazolate Frameworks and their Selective Capture of Wet Carbon Dioxide over Methane," *Inorg. Chem.*, vol. 55, no. 12, pp. 6201–6207, Jun. 2016.

[90] S. J. Datta *et al.*, "CO_2 capture from humid flue gases and humid atmosphere using a microporous coppersilicate.," *Science*, vol. 350, no. 6258, pp. 302–6, Oct. 2015.

[91] A. O. Yazaydın *et al.*, "Enhanced CO_2 Adsorption in Metal-Organic Frameworks via Occupation of Open-Metal Sites by Coordinated Water Molecules," *Chem. Mater.*, vol. 21, no. 8, pp. 1425–1430, Apr. 2009.

[92] J. Byun, S.-H. Je, H. A. Patel, A. Coskun, and C. T. Yavuz, "Nanoporous covalent organic polymers incorporating Tröger's base functionalities for enhanced CO_2 capture," *J. Mater. Chem. A*, vol. 2, no. 31, p. 12507, Jun. 2014.

[93] S. Mane, Z.-Y. Gao, Y.-X. Li, X.-Q. Liu, and L.-B. Sun, "Rational Fabrication of Polyethylenimine-Linked Microbeads for Selective CO_2 Capture," *Ind. Eng. Chem. Res.*, vol. 57, no. 1, pp. 250–258, Jan. 2018.

[94] S. Mane, Z.-Y. Gao, Y.-X. Li, D.-M. Xue, X.-Q. Liu, and L.-B. Sun, "Fabrication of microporous polymers for selective CO_2 capture: the significant role of crosslinking and crosslinker length," *J. Mater. Chem. A*, vol. 5, no. 44, pp. 23310–23318, Nov. 2017.

[95] W. Lu, W. M. Verdegaal, J. Yu, P. B. Balbuena, H.-K. Jeong, and H.-C. Zhou, "Building multiple adsorption sites in porous polymer networks for carbon capture applications," *Energy Environ. Sci.*, vol. 6, no. 12, p. 3559, Nov. 2013.

[96] M. M. Abdelnaby *et al.*, "Carbon dioxide capture in the presence of water by an amine-based crosslinked porous polymer," *J. Mater. Chem. A*, vol. 6, no. 15, pp. 6455–6462, 2018.

[97] S. Ren *et al.*, "Porous, Fluorescent, Covalent Triazine-Based Frameworks Via Room-Temperature and Microwave-Assisted Synthesis," *Adv. Mater.*, vol. 24, no.

17, pp. 2357–2361, May 2012.

[98] Y. Xu, L. Chen, Z. Guo, A. Nagai, and D. Jiang, “Light-Emitting Conjugated Polymers with Microporous Network Architecture: Interweaving Scaffold Promotes Electronic Conjugation, Facilitates Exciton Migration, and Improves Luminescence,” *J. Am. Chem. Soc.*, vol. 133, no. 44, pp. 17622–17625, Nov. 2011.

[99] M. Sevilla *et al.*, “Sustainable porous carbons with a superior performance for CO_2 capture,” *Energy Environ. Sci.*, vol. 4, no. 5, p. 1765, 2011.

[100] S. Bhunia, P. Bhanja, S. K. Das, T. Sen, and A. Bhaumik, “Triazine containing N-rich microporous organic polymers for CO_2 capture and unprecedented CO_2/N_2 selectivity,” *J. Solid State Chem.*, vol. 247, pp. 113–119, Mar. 2017.

[101] S. K. Kundu and A. Bhaumik, “Novel Nitrogen and Sulfur Rich Hyper-Cross-Linked Microporous Poly-Triazine-Thiophene Copolymer for Superior CO_2 Capture,” *ACS Sustain. Chem. Eng.*, vol. 4, no. 7, pp. 3697–3703, Jul. 2016.

[102] S. Wang *et al.*, “A novel metalporphyrin-based microporous organic polymer with high CO_2 uptake and efficient chemical conversion of CO_2 under ambient conditions,” *J. Mater. Chem. A*, vol. 5, no. 4, pp. 1509–1515, 2017.

[103] N. T. T. Nguyen *et al.*, “Mixed-Metal Zeolitic Imidazolate Frameworks and their Selective Capture of Wet Carbon Dioxide over Methane,” *Inorg. Chem.*, vol. 55, no. 12, pp. 6201–6207, Jun. 2016.

[104] Z. Liang, M. Marshall, and A. L. Chaffee, “CO_2 Adsorption-Based Separation by Metal Organic Framework (Cu-BTC) versus Zeolite (13X),” *Energy & Fuels*, vol. 23, no. 5, pp. 2785–2789, May 2009.

[105] Y. Wang, Y. Zhou, C. Liu, and L. Zhou, “Comparative studies of CO_2 and CH_4

sorption on activated carbon in presence of water," *Colloids Surfaces A Physicochem. Eng. Asp.*, vol. 322, no. 1, pp. 14–18, 2008.

[106] J. Liu, Y. Wang, A. I. Benin, P. Jakubczak, R. R. Willis, and M. D. LeVan, "CO_2 /H_2O Adsorption Equilibrium and Rates on Metal−Organic Frameworks: HKUST-1 and Ni/DOBDC," *Langmuir*, vol. 26, no. 17, pp. 14301–14307, Sep. 2010.

[107] F. Brandani and D. M. Ruthven, "The Effect of Water on the Adsorption of CO_2 and C_3H_8 on Type X Zeolites," *Ind. Eng. Chem. Res.*, vol. 43, no. 26, pp. 8339–8344, 2004.

[108] A. C. Kizzie, A. G. Wong-Foy, and A. J. Matzger, "Effect of humidity on the performance of microporous coordination polymers as adsorbents for CO_2 capture.," *Langmuir*, vol. 27, no. 10, pp. 6368–73, May 2011.

[109] D. Li, H. Furukawa, H. Deng, C. Liu, O. M. Yaghi, and D. S. Eisenberg, "Designed amyloid fibers as materials for selective carbon dioxide capture.," *Proc. Natl. Acad. Sci. U. S. A.*, vol. 111, no. 1, pp. 191–6, Jan. 2014.

[110] G.-P. Hao *et al.*, "Structurally Designed Synthesis of Mechanically Stable Poly(benzoxazine-co-resol)-Based Porous Carbon Monoliths and Their Application as High-Performance CO_2 Capture Sorbents," *J. Am. Chem. Soc.*, vol. 133, no. 29, pp. 11378–11388, Jul. 2011.

[111] H. Ma, H. Ren, X. Zou, S. Meng, F. Sun, and G. Zhu, "Post-metalation of porous aromatic frameworks for highly efficient carbon capture from CO_2 + N_2 and CH_4 + N_2 mixtures," *Polym. Chem.*, vol. 5, no. 1, pp. 144–152, Nov. 2014.

[112] J. Kobayashi, B. Vannachone, Y. Sato, K. Manivong, S. Nambanya, and S. Inthakone, "An epidemiological study on Opisthorchis viverrini infection in Lao

villages," *Southeast Asian J. Trop. Med. Public Health*, vol. 31, no. 1, pp. 128–132, May 2000.

[113] A. Samanta, A. Zhao, G. K. H. Shimizu, P. Sarkar, and R. Gupta, "Post-Combustion CO_2 Capture Using Solid Sorbents: A Review," *Ind. Eng. Chem. Res.*, vol. 51, no. 4, pp. 1438–1463, Feb. 2012.

[114] J. M. Davidson, C. H. Lawrie, and K. Sohail, "Kinetics of the absorption of hydrogen sulfide by high purity and doped high surface area zinc oxide," *Ind. Eng. Chem. Res.*, vol. 34, no. 9, pp. 2981–2989, Sep. 1995.

[115] T. Yamamoto, M. Tayakout-Fayolle, and C. Geantet, "Gas-phase removal of hydrogen sulfide using iron oxyhydroxide at low temperature: Measurement of breakthrough curve and modeling of sulfidation mechanism," *Chem. Eng. J.*, vol. 262, pp. 702–709, Feb. 2015.

[116] T. Baird *et al.*, "Mixed cobalt–iron oxide absorbents for low-temperature gas desulfurisation," *J. Mater. Chem.*, vol. 13, no. 9, pp. 2341–2347, Aug. 2003.

[117] K. Polychronopoulou, J. L. G. Fierro, and A. M. Efstathiou, "Novel Zn–Ti-based mixed metal oxides for low-temperature adsorption of H_2S from industrial gas streams," *Appl. Catal. B Environ.*, vol. 57, no. 2, pp. 125–137, Apr. 2005.

[118] B. Supronowicz, A. Mavrandonakis, and T. Heine, "Interaction of Small Gases with the Unsaturated Metal Centers of the HKUST-1 Metal Organic Framework," *J. Phys. Chem. C*, vol. 117, no. 28, pp. 14570–14578, Jul. 2013.

[119] L. Hamon *et al.*, "Molecular Insight into the Adsorption of H_2S in the Flexible MIL-53(Cr) and Rigid MIL-47(V) MOFs: Infrared Spectroscopy Combined to Molecular Simulations," *J. Phys. Chem. C*, vol. 115, no. 5, pp. 2047–2056, Feb. 2011.

[120] L. Hamon *et al.*, "Comparative Study of Hydrogen Sulfide Adsorption in the MIL-53(Al, Cr, Fe), MIL-47(V), MIL-100(Cr), and MIL-101(Cr) Metal−Organic Frameworks at Room Temperature," *J. Am. Chem. Soc.*, vol. 131, no. 25, pp. 8775–8777, Jul. 2009.

[121] N. Heymans, S. Vaesen, and G. De Weireld, "A complete procedure for acidic gas separation by adsorption on MIL-53 (Al)," *Microporous Mesoporous Mater.*, vol. 154, pp. 93–99, May 2012.

[122] J. Liu, Y. Wei, P. Li, Y. Zhao, and R. Zou, "Selective H_2S/CO_2 Separation by Metal–Organic Frameworks Based on Chemical-Physical Adsorption," *J. Phys. Chem. C*, vol. 121, no. 24, pp. 13249–13255, Jun. 2017.

[123] X.-L. Wang, H.-L. Fan, Z. Tian, E.-Y. He, Y. Li, and J. Shangguan, "Adsorptive removal of sulfur compounds using IRMOF-3 at ambient temperature," *Appl. Surf. Sci.*, vol. 289, pp. 107–113, Jan. 2014.

[124] J.-X. Hu *et al.*, "Highly Enhanced Selectivity and Easy Regeneration for the Separation of CO_2 over N_2 on Melamine-Based Microporous Organic Polymers," *Ind. Eng. Chem. Res.*, vol. 53, no. 29, pp. 11828–11837, Jul. 2014.

[125] S. Zulfiqar, M. I. Sarwar, and C. T. Yavuz, "Melamine based porous organic amide polymers for CO_2 capture," *RSC Adv.*, vol. 4, no. 94, pp. 52263–52269, 2014.

[126] S. Y. Kim *et al.*, "Template-free synthesis of high surface area nitrogen-rich carbon microporous spheres and their hydrogen uptake capacity," *J. Mater. Chem. A*, vol. 2, no. 7, pp. 2227–2232, Jan. 2014.

[127] D. A. Bhandari, N. Bessho, and W. J. Koros, "Hollow Fiber Sorbents for Desulfurization of Natural Gas," *Ind. Eng. Chem. Res.*, vol. 49, no. 23, pp. 12038–

12050, Dec. 2010.

[128] P. M. Bhatt *et al.*, "Isoreticular rare earth fcu-MOFs for the selective removal of H2S from CO_2 containing gases," *Chem. Eng. J.*, vol. 324, pp. 392–396, Sep. 2017.

[129] Y. Belmabkhout *et al.*, "Metal-organic frameworks to satisfy gas upgrading demands: fine-tuning the soc-MOF platform for the operative removal of H_2S," *J. Mater. Chem. A*, vol. 5, no. 7, pp. 3293–3303, Feb. 2017.

[130] C. N. Okonkwo, C. Okolie, A. Sujan, G. Zhu, and C. W. Jones, "Role of Amine Structure on Hydrogen Sulfide Capture from Dilute Gas Streams Using Solid Adsorbents," *Energy & Fuels*, vol. 32, no. 6, pp. 6926–6933, Jun. 2018.

[131] M. C. Castrillon *et al.*, "CO_2 and H_2S Removal from CH_4 -Rich Streams by Adsorption on Activated Carbons Modified with K_2CO_3 , NaOH, or Fe_2O_3," *Energy & Fuels*, vol. 30, no. 11, pp. 9596–9604, Nov. 2016.

[132] A. C. Kizzie, A. G. Wong-Foy, and A. J. Matzger, "Effect of humidity on the performance of microporous coordination polymers as adsorbents for CO_2 capture.," *Langmuir*, vol. 27, no. 10, pp. 6368–73, May 2011.

[133] P.-Q. Liao *et al.*, "Monodentate hydroxide as a super strong yet reversible active site for CO_2 capture from high-humidity flue gas," *Energy Environ. Sci.*, vol. 8, no. 3, pp. 2308–2322, 2015.

[134] S. Nandi, U. Werner-Zwanziger, and R. Vaidhyanathan, "A triazine–resorcinol based porous polymer with polar pores and exceptional surface hydrophobicity showing CO_2 uptake under humid conditions," *J. Mater. Chem. A*, vol. 3, no. 42, pp. 21116–21122, Oct. 2015.

[135] W. Lu, J. P. Sculley, D. Yuan, R. Krishna, and H.-C. Zhou, "Carbon Dioxide

Capture from Air Using Amine-Grafted Porous Polymer Networks," *J. Phys. Chem. C*, vol. 117, no. 8, pp. 4057–4061, Feb. 2013.

Vitae

Mahmoud Mohamed Abdelnaby

King Fahd University of Petroleum & Minerals (KFUPM),

Dhahran 31261, Saudi Arabia

Phone +966580011307

E-MAIL: mahmoudm@kfupm.edu.sa;

mlimoud.mm@gmail.com

Personal information

Nationality	: Egyptian
Date of Birth	:3/27/1987
Address	: Sahad Zaghlol street, Awseem, Giza, Egypt
Academic Background	: Chemistry

EDUCATION

January 2014- (expected November. 2018)	Ph.D. Student, Chemistry, Department, KFUPM, Dhahran, Saudi Arabia. Thesis title "Synthesis and characterization of porous polymers and metal organic frameworks (MOF)/polymer composites for carbon dioxide capture" Advisor: ***Prof. Omar M. Yaghi***
July 2013	M. Sc. in Cairo University joint with Egyptian Petroleum Research Institute (EPRI) Thesis title "Synthesis and biological activity of nanometal based cationic Schiff base surfactants as sulfate-reducing bacteria (SRB) inhibitors" Advisor: ***Prof. Abdelfattah M.Badawi, D.Sc***
June 2008	B.Sc., Cairo University, Egypt (Distinction with honor).

PROFESSIONAL EXPERIENCES AND POSITIONS

Jan. 2014 –Now	**Lecturer-B (Safety officer):** Center Of Research Excellence in Nanotechnology (CENT)-Research Institute, KFUPM, Saudi Arabia
Jan. 2011–Jan. 2014	**Research Assistant** Egyptian Petroleum Research Institute (EPRI), Nasir City, Egypt
May 2012–Sep. 2013	**Teaching Assistant,** Helwan University, Egypt
Feb. 2009-Jan. 2014	**Research Engineer**, Chemicals Services & Development Center**,** Egyptian Petroleum Research Institute (EPRI), Nasr City, Egypt

AREAS OF INTEREST

- Synthesis of porous materials such as porous polymers, MOFs, ZIFs, and COFs, and their characterization and application in carbon dioxide capture and conversion
- Environmental and Chemical Safety

RESEARCH AND HAND-ON EXPERIENCE

- **Excellent experience in material characterization** using techniques such as but not limited to:
  - Nuclear magnetic resonance (NMR) spectroscopy
  - Fourier transform infrared (FT-IR) spectroscopy
  - Powder X-ray diffraction (PXRD),
  - Thermal Analysis (TGA-DSC-MS)

  Good Experience on:
  - Electron microscopy
  - Gas and vapor adsorption
  - Gas and liquid separation (GC-LC)
  - UV-Vis spectroscopy

- Gas sensors

❖ **Excellent experience in chemical lab safety; working three years as safety officer;**

- One-week training course by Lab safety institute (LSI) conducted by Dr James A. Kaufman, Ph.D.
- Three days' workshop on "Reputable Chemical Supplier" supported by KFUPM-Lab Technical Support Office (LTSO) in collaboration with Chemical Security Program (CSP) & Sandia National Laboratories (SNL).

❖ Good Experience in production of petroleum chemicals (Corrosion Inhibitors and H_2S Scavenger and de-emulsifier) as industrial scale for petroleum companies

PUBLICATION

Peer reviewed journal publications:

1. **Abdelnaby, M. M**.; Alloush, A. M.; Qasem, N. A. A.; Al-Maythalony, B. A.; Mansour, R. B.; Cordova, K. E.; Al Hamouz, O. C. S. Carbon Dioxide Capture in the Presence of Water by an Amine-Based Crosslinked Porous Polymer. **J. Mater. Chem. A** 2018. (DOI: 10.1039/c8ta00012c)
2. Albakri, M. A.; **Abdelnaby, M. M.**; Saleh, T. A.; Al Hamouz, O. C. S. New Series of Benzene-1,3,5-Triamine Based Cross-Linked Polyamines and polyamine/CNT Composites for Lead Ion Removal from Aqueous Solutions. **Chem. Eng. J**. 2018, 333, 76–84. (https://doi.org/10.1016/j.cej.2017.09.152)

Ready for submission (in the pipeline)

- Mahmoud M. Abdelnaby, Naef A. A. Qasem, Bassem A. Al-Maythalony, Rached B. Mansour, Kyle E. Cordova, Othman Charles S. Al-Hamouz, * "Tuning the Textural Properties of Porous Crosslinked Polymers for Selective Carbon Dioxide Capture under Humid Condition"
- Mahmoud M. Abdelnaby, Naef A. A. Qasem, Bassem A. Al-Maythalony, Rached B. Mansour, Kyle E. Cordova, Othman Charles S. Al-Hamouz "benzene-triamine pyrrole crosslinked polymer for outstanding Carbon dioxide capture in humid conditions"

- Mahmoud M. Abdelnaby, Naef A. A. Qasem, Bassem A. Al-Maythalony, Kyle E. Cordova, Othman Charles S. Al-Hamouz "Melamine based crosslinked polymer for Carbon dioxide and Hydrogen sulfide capture"
- Mahmoud M. Abdelnaby, Muhammed Usman, Bassem A. Al-Maythalony* Metal Organic Framework (MOF-74)/polyimide MMM for selective Hydrogen separation.

PATENTS

Abdelnaby, M. M. and Al Hamouz, O. C. S. Carbon Dioxide Capture in the Presence of Water by an Amine-Based Crosslinked Porous Polymer. (submitted KFUPM, Ref. No. 2018-035)

Abdelnaby, M. M. and Al Hamouz, O. C. S. Phenothiazine Based Crosslinked Porous Polymer for CO_2 capture. (submitted KFUPM,)

Conference

- *Mohamed. F. Zaky*, A. M. Badawi*, Hamed A. Ead** and Mahmoud M. Abdelnabi** Synthesis and biological activity of silver nanoparticles self-assembled and stabilized by cationic surfactants**,** 16th International conference on Petroleum, Mineral Resources and Development (PMRD), EGYPT, 10-12 Feb. 2013.

TEACHING

Courses taught in Helwan University, Egypt

Organic chemistry lab.

Graduate Courses Taken at KFUPM (Ph.D. program) (GPA =3.73)

Advanced Organic Chemistry

1. Synthetic Organic Chemistry
2. Polymer Chemistry
3. Advanced Analytical Chemistry
4. Spectroscopic Identification of Organic Compounds
5. Organometallic Chemistry
6. Heterogeneous Catalysis (engineering course)

7. Physics and Chemistry of Nano materials
8. Separation Methods
9. Industrial water treatment

Graduate Courses Taken at Cairo University (GPA = 3.5)

1. Advanced Applied Spectroscopy
2. Introduction to green Chemistry –Bioorganic Chemistry
3. Applied Organic Chemistry
4. Advanced Physical Organic Chemistry
5. Structural Dynamic and Macro-Molecular Chemistry
6. Chemotherapy Organic Design
7. Organometallic Compounds –Catalysis in Organic Chemistry
8. PhotoChemistry –Precyclic Reactions -Chemistry of Organic Laser

SOFTWARE

Origin, Chem. Draw, Mendeley, Mercury, and Material studio.

RESEARCH PROJECTS

1. Synthesis of Metal Organic Frameworks (MOFs) for Carbone capture and separation, under supervision of prof. Omar M. Yaghi –sponsored by KFUPM and Saudi Aramco, (S. Aramco Chair program, project code: ORCP2390)
2. Synthesis of porous polymer for carbon dioxide capture (DSR, IN161034)
3. Synthesis of Schiff base Organic Compounds as Biocide for SRB “Sulphate Reducing Bacteria” in Petroleum Production (Master degree_asrt-Fund, Egypt)

REFERENCES

Prof. Omar M. Yaghi	James and Neeltje Tretter Chair Professor of Chemistry, UC Berkeley 602 Latimer Hall Berkeley, CA 94720 Ph: 510-643-5507 yaghi@berkeley.edu Chair Professor Chemistry Department, KFUPM, Dhahran 31261, Saudi Arabia yaghi@kfupm.edu.sa
Prof. Othman C. S. Al Hamouz	Department of Chemistry, King Fahd University of Petroleum and Minerals (KFUPM), Dhahran 31261, Saudi Arabia othmanc@kfupm.edu.sa
Dr. Nasiruzzaman Shaikh M	CENT lab Manger CENT, KFUPM, Dhahran 31261, Saudi Arabia mnshaikh@kfupm.edu.sa
Prof. Abdelfattah M.Badawi	Prof. Abdelfattah M.Badawi, D.Sc Prof. of Applied Chemistry Egyptian Petroleum E-mail: badawi8@Yahoo.com Address: Heliopolis, P.O.Box 5015,Cairo 11771, EGYPT Mobile: 002 0111 6749248

My URLs:

https://www.researchgate.net/profile/Mahmoud_Abdelnabi3

https://scholar.google.com/citations?user=BLMFawMAAAAJ&hl=en

https://globalscience.berkeley.edu/centers/KFUPM-members